

**Characterization of Neurofibromatosis 2 (NF2) Tumor  
Suppressor Binding Proteins**

**Dissertation**

zur

Erlangung des Doktorgrades

(Dr. rer. nat.)

der

Mathematisch-Naturwissenschaftlichen Fakultät

der

Rheinischen Friedrich-Wilhelms-Universität Bonn

Vorgelegt von  
Thorsten Wiederhold

aus  
Neustadt an der Weinstrasse

Boston & Bonn (Dezember) 2001

Angefertigt mit Genehmigung der Mathematisch-Naturwissenschaftlichen Fakultät der  
Rheinischen Friedrich-Wilhelms-Universität Bonn

Die vorliegende Arbeit wurde in der „Molecular Neurogenetics Unit,  
Massachusetts General Hospital and Harvard Medical School, Boston“  
durchgeführt.

1. Referent: Dr. Vijaya Ramesh, Associate Professor, Harvard Medical School
2. Referent: Prof. Dr. Karl Heinz Scheidtmann

Tag der Promotion: 15.04.2002

## Table of Contents

<b>1. INTRODUCTION.....</b>	<b>9</b>
<b>1.1 Neurofibromatosis .....</b>	<b>9</b>
<b>1.2 NF2, the Genetic Disease.....</b>	<b>10</b>
1.2.1 Definition.....	10
1.2.2 Neuropathology.....	11
<b>1.3 NF2, the Gene.....</b>	<b>13</b>
1.3.1 Identification of the Gene.....	13
1.3.2 The Gene Structure.....	14
1.3.3 Mutations in NF2.....	14
<b>1.4 NF2, the Protein (Merlin).....</b>	<b>16</b>
1.4.1 Merlin and its Family Members.....	16
1.4.2 Possible Functions of Merlin and ERM Proteins .....	17
1.4.3 Merlin and ERM Interacting Proteins .....	20
<b>1.5 Specific Aims .....</b>	<b>23</b>
<b>2. MATERIALS AND METHODS.....</b>	<b>25</b>
<b>2.1 Materials .....</b>	<b>25</b>
<b>2.2 Molecular Biological Methods .....</b>	<b>31</b>
<b>2.3 Biochemical and Cell Biological Methods.....</b>	<b>38</b>
<b>3. RESULTS.....</b>	<b>55</b>
<b>3.1 Characterization of the Interaction of NHE-RF with Merlin Isoform 1 and 2.....</b>	<b>55</b>
3.1.1 NHE-RF Binds Differentially to Merlin Isoform 1 and 2.....	55
3.1.2 Phospholipids Enhance the Binding of NHE-RF to Merlin Isoform 1 .....	58
<b>3.2 Isolation and Characterization of NHE-RF Binding Proteins.....</b>	<b>61</b>
3.2.1 NHE-RF Co-localizes with the H <sup>+</sup> ATPase.....	63
3.2.2 Soluble H <sup>+</sup> ATPase Complexes bind to NHE-RF <i>In Vitro</i> .....	65
3.2.3 NHE-RF and the H <sup>+</sup> ATPase Associate <i>In Vivo</i> .....	66
<b>3.3 Examination of NHE-RF in Human Cancer .....</b>	<b>69</b>
3.3.1 Expression of NHE-RF is Upregulated in a Subset of Breast Cancer Cell Lines .....	69
3.3.2 NHE-RF Expression is Regulated Through the Estrogen Receptor.....	72
3.3.3 Expression of NHE-RF in Primary Breast Tumors .....	75
<b>3.4 Isolation and Characterization of Novel Merlin Binding Proteins.....</b>	<b>77</b>
3.4.1 Identification of Merlin Binding Proteins by a Yeast Two-Hybrid Screen.....	77
3.4.2 DNA Sequence Analysis and Isolation of a Full-length MerintA cDNA .....	79
3.4.3 MerintA is Widely Expressed in Cells and Tissues.....	82
3.4.4 Merlin but not Moesin binds to MerintA <i>In Vitro</i> and <i>In Vivo</i> .....	87
3.4.5 MerintA Localization and Co-localization with Merlin.....	91
3.4.6 MerintA Associates with the Actin Cytoskeleton .....	93
3.4.7 MerintA Binds to Grb2.....	99

<b>4.</b>	<b>DISCUSSION .....</b>	<b>104</b>
<b>4.1</b>	<b>Characterization of the Interaction of Merlin Isoform 1 and 2 with NHE-RF .....</b>	<b>104</b>
<b>4.2</b>	<b>NHE-RF Binding Proteins.....</b>	<b>108</b>
<b>4.3</b>	<b>The Potential Role of NHE-RF in Cancer.....</b>	<b>113</b>
4.3.1	NHE-RF Expression is Regulated by Estrogen in Breast Cancer Cells.....	113
4.3.2	The Role of Estrogen and NHE-RF in Breast Cancer .....	114
4.3.3	The Role of NHE-RF in the Organization of Microvilli .....	115
<b>4.4</b>	<b>Merlin Binding Proteins.....</b>	<b>118</b>
4.4.1	Identification of Merlin Binding Proteins.....	118
4.4.2	The Interaction of MerintA with Merlin .....	119
4.4.3	Characterization of MerintA.....	120
4.4.4	MerintA and the Actin Cytoskeleton .....	123
4.4.5	The Association of MerintA with the Adaptor Protein Grb2.....	125
<b>4.5</b>	<b>Possible Biological Functions of Merlin.....</b>	<b>130</b>
<b>5.</b>	<b>SUMMARY .....</b>	<b>132</b>
<b>6.</b>	<b>ACKNOWLEDGEMENTS.....</b>	<b>135</b>
<b>7.</b>	<b>REFERENCES .....</b>	<b>136</b>
<b>8.</b>	<b>APPENDIX .....</b>	<b>149</b>

## Table of Figures

Figure 1. MRI Scans of Bilateral Vestibular Schwannomas and Multiple Meningiomas in Patients with NF2.....	12
Figure 2. Merlin and its Related ERM Proteins. ....	17
Figure 3. An Intramolecular Head-to-Tail Association Model for the Activation of ERM Proteins.....	19
Figure 4. Simplified Structure of NHE-RF containing PDZ-Domains. ....	22
Figure 5. Binding of NHE-RF to Merlin Isoforms. ....	56
Figure 6. Binding of Merlin Isoforms 1 and 2 to NHE-RF.....	57
Figure 7. PIP <sub>2</sub> Enhances Binding of NHE-RF to Merlin Isoform 1.....	59
Figure 8. Diagram of H <sup>+</sup> ATPase. ....	62
Figure 9. NHE-RF (A and C) and the E (31kD) Subunit of the H <sup>+</sup> ATPase (B and D) Colocalize in Double Stained Sections of Rat Kidney Cortex. ....	64
Figure 10. NHE-RF Binds to the H <sup>+</sup> ATPase <i>in vitro</i> and <i>in vivo</i> . ....	67
Figure 11. Western Blot Analysis of Various Mammary Epithelial and Breast Cancer Cell Lines. ....	70
Figure 12. Northern Blot Analysis of Various Mammary Epithelial and Breast Cancer Cell Lines. ....	71
Figure 13. Expression of NHE-RF is Induced by $\beta$ -Estradiol in MCF-7 cell line. ....	73
Figure 14. Visualization of NHE-RF by Immunocytochemistry in $\beta$ -Estradiol Induced Cells.....	75
Figure 15. Expression of NHE-RF in ER-positive and ER-negative breast carcinomas by immunohistochemistry. ....	76
Figure 16. Isolation of Merlin Binding Proteins Using the Yeast-Two Hybrid System. ....	78
Figure 17. cDNA Sequence and Genomic Structure of the MerintA Gene. ....	80
Figure 18. Alignment on MerintA Orthologues.....	82
Figure 19. Characterization of MerintA Antibodies and HA-MerintA. ....	84
Figure 20. Expression of MerintA in Different Tissues and Cell Lines. ....	86
Figure 21. Binding of MerintA to Merlin but not to Moesin.....	89
Figure 22. MerintA Binds to Merlin <i>in vivo</i> . ....	90
Figure 23. Localization of GFP-Merlin and HA-tagged MerintA (A4). ....	92
Figure 24. Endogenous Localization of MerintA.....	93
Figure 25. Localization of HA-tagged MerintA (A4) and Actin. ....	94
Figure 26. Analysis of Merlin and MerintA Protein Solubility. ....	95
Figure 27. Localization of MerintA in a Neurite of a CAD Cell Determined by Electron Microscopy.....	96
Figure 28. Colocalization of MerintA and Merlin in the Cortex of a CAD Cell Determined by Electron Microscopy.....	98
Figure 29. MerintA Binds Grb2 <i>In Vitro</i> .....	101
Figure 30. MerintA Binds Directly to Grb2 <i>In Vitro</i> . ....	102
Figure 31. A Model of Merlin, NHE-RF and Their Binding Partner. ....	117
Figure 32. A Potential Model Connecting Merlin and MerintA to Signaling Pathways through Grb2.....	128

**List of Abbreviations**

aa:	amino acid
AE1:	anion exchanger 1 or band 3
AMP:	adenosine monophosphate
ATP:	adenosine triphosphate
bp:	base pair
BSA:	bovine serum albumin
C:	carboxy
cAMP:	cyclic AMP
cDNA:	complimentary DNA
d:	deoxy
dd:	dideoxy
DNA:	deoxyribonucleic acid
EGF:	epidermal growth factor
ELISA:	enzyme-linked immunosorbent assay
ER:	estrogen receptor
ERM:	ezrin, radixin and moesin
FERM:	4.1band, ezrin, radixin and moesin
FITC:	fluorescein isothiocyanate
GAPDH:	glyceraldehyde-3-phosphate dehydrogenase
Grb2:	growth factor receptor bound 2
GST:	glutathione <i>S</i> -transferase
HA:	hemagglutinin
HRP:	horseradish peroxidase
IgG:	immunoglobulin G
kb:	kilo base pair
kD:	kilo Dalton
MERM:	merlin, ezrin, radixin and moesin
N:	amino
N- and C-ERMADs:	amino- and carboxy- ERM association domains

---

NF2:	neurofibromatosis 2
NHE3:	Na <sup>+</sup> -H <sup>+</sup> exchanger 3
NHE-RF:	regulatory cofactor of Na <sup>+</sup> -H <sup>+</sup> exchanger
mRNA:	messenger RNA
PAGE:	polyacrylamide gel electrophoresis.
PBS:	phosphate-buffered saline
PCR:	polymmerase chain reaction
PDGF:	platelet-derived growth factor
PDGFR:	platelet-derived growth factor receptor
PIP <sub>2</sub> :	phosphatidylinositol 4,5-bisphosphate
PS:	phosphatidyl serine
RACE:	rapid amplification of cDNA ends
RNA:	ribonucleic acid
RTK:	receptor tyrosine kinase
SDS:	sodium dodecyl sulfate
SH2:	Src homology domain 2
SH3:	Src homology domain 3

**One and Three Letter Symbols for the Amino Acids<sup>a</sup>**

A	Ala	Alanine
C	Cys	Cysteine
D	Asp	Aspartic acid
E	Glu	Glutamic acid
F	Phe	Phenylalanine
G	Gly	Glycine
H	His	Histidine
I	Ile	Isoleucine
K	Lys	Lysine
L	Leu	Leucine
M	Met	Methionine
N	Asn	Asparagine
P	Pro	Proline
Q	Gln	Glutamine
R	Arg	Arginine
S	Ser	Serine
T	Thr	Threonine
V	Val	Valine
W	Trp	Tryptophan
Y	Tyr	Tyrosine

<sup>a</sup> X is the one letter symbol for an undetermined amino acid



## 1. Introduction

About one person in five, living in the western world, dies of cancer. Other health problems such as heart diseases cause more deaths in the world as a whole (Alberts *et al.*, 1994). However, cancer has a unique importance since one has to study fundamental functions of a cell in order to understand cancer. Furthermore, one has to investigate both the inner workings of cells such as their social interactions in the tissues of the body to ultimately understand the disease and to devise rational ways to treat it.

### 1.1 Neurofibromatosis

The term neurofibromatosis describes the two major human genetic disorders, neurofibromatosis type 1 (NF1) and neurofibromatosis type 2 (NF2). Both NF1 and NF2 display autosomal dominant inheritance and are tumors associated with the nervous system; however, they are distinct clinical and genetic entities (Mulvihill *et al.*, 1990). NF1, also known as von Recklinghausen neurofibromatosis or peripheral neurofibromatosis, is more common than NF2 with an incidence of 1 in 4,000. Neurofibromas, café-au lait macules, Lisch nodules of the iris, and a predisposition to certain malignant tumors are characteristics of neurofibromatosis 1 (Riccardi, 1981). The gene *NF1* has been mapped to chromosome 17 and has subsequently been isolated and characterized (Cawthon *et al.*, 1990; Viskochil *et al.*, 1990; Wallace *et al.*, 1990). The large protein product of the *NF1* gene has been named neurofibromin. It has a strong homology to the family of GTPase-activating proteins (GAP) and is involved in regulating Ras. The absence of neurofibromin leads to elevated basal levels of Ras-GTP in NF1-derived schwannomas and is thought to play a causal role in the etiology of these tumors (Ballester *et al.*, 1990; Basu *et al.*, 1992; Buchberg *et al.*, 1990; DeClue *et al.*, 1992; Xu *et al.*, 1990).

By contrast, neurofibromatosis 2 affects approximately 1 in 40,000 individuals and is characterized by bilateral vestibular schwannomas, which are benign, slow-growing tumors on the vestibular branch of the 8th cranial nerve. The exerting pressure of these tumors often results in deafness and balance disorders in early adulthood. In

few cases, onset occurs in childhood or in late adulthood. Although these tumors are benign, they are difficult to manage due to their anatomic location. Other brain-tumors such as meningiomas, gliomas, spinal schwannomas, and ependymomas are also common and are generally present in the affected young adult. In addition, the development of posterior capsular opacities has been observed in many patients. (Evans *et al.*, 1992; Martuza *et al.*, 1988; Kaiser-Kupfer *et al.*, 1989).

My “Dissertation” (PhD thesis) will focus on the characterization of Neurofibromatosis 2 (NF2) tumor suppressor binding proteins, and NF2 will be discussed in greater detail. The introduction will be subdivided into the following three sections:

- NF2, the genetic disease, including the definition and neuropathology.
- *NF2*, the gene, including the identification of the gene, the gene structure and mutations in NF2.
- NF2, the protein, including merlin and its family members; possible functions of merlin and ERM proteins and merlin/ERM interacting proteins

## **1.2 NF2, the Genetic Disease**

### **1.2.1 Definition**

Neurofibromatosis 2 is an uncommon disorder, and is also known as central neurofibromatosis or bilateral acoustic neurofibromatosis. The condition is inherited in an autosomal dominant manner with high penetrance. However, one half of the cases has no family history and therefore most likely represents new mutations. Patients with NF2 are genetically predisposed to a number of characteristic tumors, although some non-neoplastic conditions occur. Currently, diagnostic criteria for NF2 includes at least one of the following (Evans *et al.*, 1992; Huson *et al.*, 1994; Short *et al.*, 1994):

- Bilateral vestibular schwannomas.
- A first-degree relative with NF2, and either (A) a unilateral vestibular schwannoma or (B) two of the following: meningioma, schwannoma, glioma, neurofibroma, posterior subcapsular lens opacity, or cerebral calcification.
- Two of the following: (A) unilateral vestibular schwannoma or (B) multiple meningiomas or (C) either schwannoma, glioma, neurofibroma, posterior subcapsular lens opacity, or cerebral calcification.

### 1.2.2 Neuropathology

Both sporadic and familial NF2 can result in a number of different tumors. Following is a list of the most common tumors and abnormal cell proliferations:

- Vestibular schwannomas (primary hallmark of NF2)
- Peripheral (non-vestibular) schwannomas
- Cutaneous schwannomas
- Meningiomas (secondary hallmark of NF2)
- Meningioangiomatosis
- Gliomas
- Glial Hamartomas

Bilateral, vestibular schwannomas (Figure 1A+B) occur both in sporadic and in familial cases on the vestibular branch of the eighth cranial nerve and show the same preference for the internal acoustic meatus (Louis *et al.*, 1995). In sporadic schwannomas, the primary motor nerves are typically not affected as often as sensory nerves and roots (Evans *et al.*, 1992; Halliday *et al.*, 1991). In familial schwannomas (NF2), the tumors occur earlier in life, are multiple and may occur on any of the cranial and peripheral nerves. Also, three different variants of cutaneous schwannomas have been described in about half of NF2 patients (Evans *et al.*, 1992; Martuza *et al.*, 1988; Short *et al.*, 1994). The multiple peripheral (non-vestibular) schwannomas are currently studied in greater detail, and it remains to be determined whether these symptoms are variants of NF2 or a distinct disease. Therefore, the occurrence of peripheral schwannomas currently only

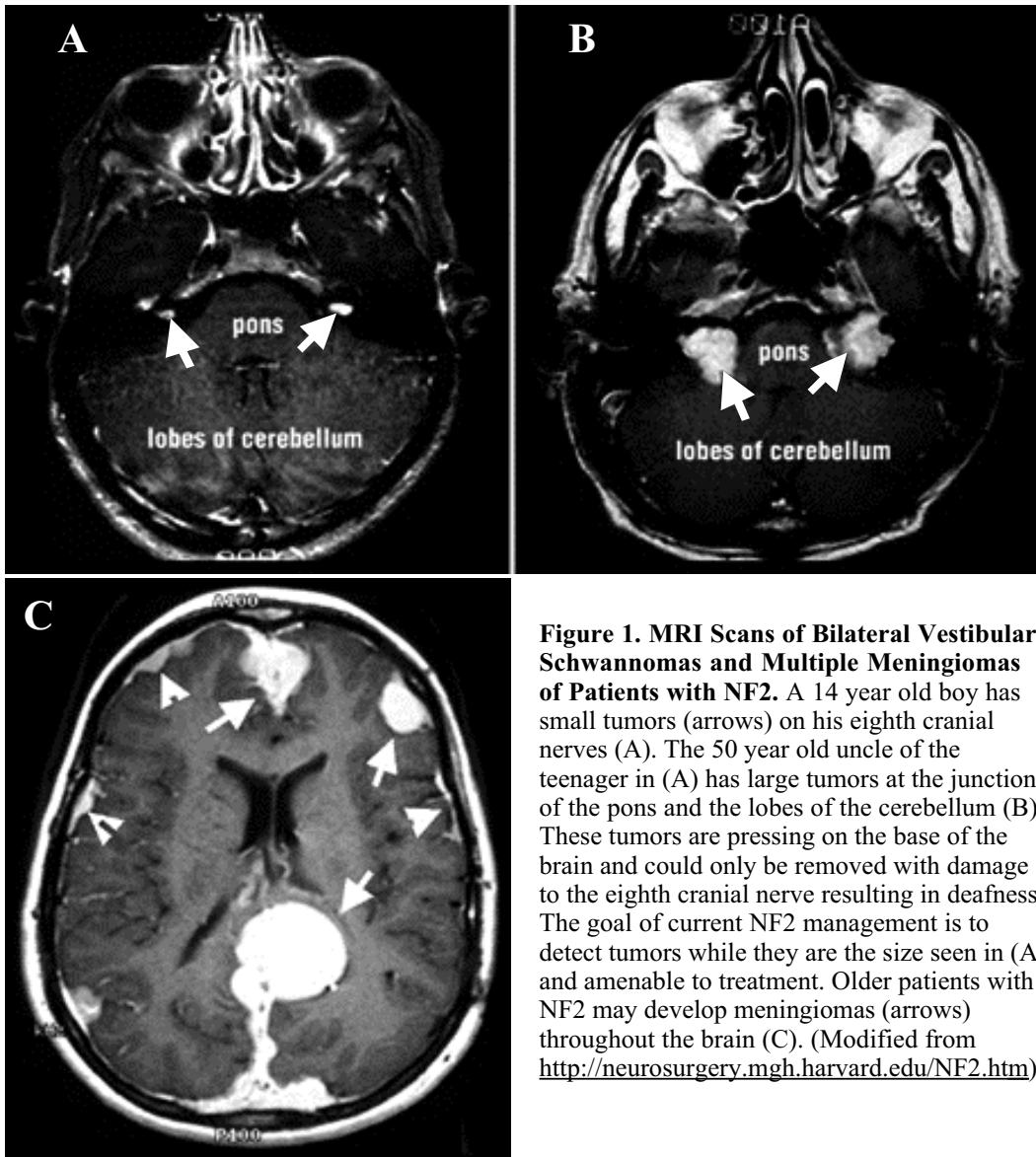


**Figure 1. MRI Scans of Bilateral Vestibular Schwannomas and Multiple Meningiomas of Patients with NF2.** A 14 year old boy has small tumors (arrows) on his eighth cranial nerves (A). The 50 year old uncle of the teenager in (A) has large tumors at the junction of the pons and the lobes of the cerebellum (B). These tumors are pressing on the base of the brain and could only be removed with damage to the eighth cranial nerve resulting in deafness. The goal of current NF2 management is to detect tumors while they are the size seen in (A) and amenable to treatment. Older patients with NF2 may develop meningiomas (arrows) throughout the brain (C). (Modified from <http://neurosurgery.mgh.harvard.edu/NF2.htm>).

defines a patient with a family history as having NF2. Schwannomas of NF2 patients are histologically very similar to their sporadic counterparts (Louis *et al.*, 1995).

Multiple meningiomas, the second hallmark of NF2, occur in the majority of NF2 patients, and they tend to occur earlier in life in these patients than in their sporadic counterparts (Figure 1C). However, multiple meningiomas alone do not characterize a patient as having NF2. Meningiomas that do occur in NF2 are usually histologically benign and of the fibroblastic type (Russell *et al.*, 1989; Schiffer *et al.*, 1993). A molecular genetic study of a family with cases that were diagnosed with multiple meningiomas, but no vestibular schwannomas, did not show linkage to the NF2 locus, suggesting a distinct gene responsible for these meningiomas (Pulst, *et al.*,

NF2 locus, suggesting a distinct gene responsible for these meningiomas (Pulst, *et al.*, 1993). Furthermore, there is evidence from this family that the potential non-NF2 meningioma locus is responsible for meningotheial meningiomas, as opposed to the fibroblastic type (Sieb *et al.*, 1992). This view is supported by sporadic meningiomas, where both chromosome 22q allelic loss and *NF2* gene mutations are more common in fibroblastic and transitional subtypes than in meningotheial forms (Wellenreuther *et al.*, 1995). Together, these kinds of studies have lead to the estimate that approximately 40% of all meningiomas have neither *NF2* gene mutations nor allelic loss of chromosome 22q, which implies that a gene other than the *NF2* gene is involved in the formation of some meningiomas. It is likely that this second gene is not on chromosome 22q, since *NF2* gene mutations in meningiomas correlate closely with chromosome 22q loss (Louis *et al.*, 1995).

### 1.3 NF2, the Gene

#### 1.3.1 Identification of the Gene

Genetic linkage studies and analysis of both sporadic and familial tumors led to the prediction that the *NF2* gene was located on chromosome 22 (Narod *et al.*, 1992; Rouleau *et al.*, 1987; Rouleau *et al.*, 1990; Wertelecki *et al.*, 1988). It was expected that the *NF2* gene functions as a tumor suppressor gene (Knudson, 1971) whose inactivation leads to tumor formation (Seizinger *et al.*, 1986, 1987a, 1987b). The evidence for this hypothesis was obtained from a family study of a single, extremely large, extended NF2 pedigree. In this family, irregularities on chromosome 22 could be tracked through multiple generations. The pattern of inheritance of the disorder was correlated with the inheritance of multiple polymorphic DNA markers on chromosome 22q12. Subsequent investigations of this and additional NF2 families gradually refined the localization of the genetic defect and underlined the single occurrence of the observed genetic defect for all cases of the disorder (Bijlsma *et al.*, 1992; Couturier *et al.*, 1990; Fiedler *et al.*, 1991; Fontaine *et al.*, 1991a, 1991b; Rouleau *et al.*, 1990; Wolff *et al.*, 1992). Finally, in 1993, the *NF2* tumor suppressor gene was identified by

Trofatter *et al.* (1993) using a positional cloning approach, and later that year it was confirmed by Rouleau *et al.* (1993). The isolation of this disease gene, based on its chromosomal location, was fundamental to then analyze the normal and defective versions of this culprit gene.

### 1.3.2 The Gene Structure

The *NF2* gene shows strong homology to a family of genes encoding proteins known as ERM (Ezrin, Radixin and Moesin), and it spans a region of 110kb, producing mRNAs of ~7kb, ~4.4kb, and ~2.6kb. These mRNAs encode at least two major alternative isoforms consisting of exons 1 through 15 and 17 or constitutive exons 1 through 16 (Bianchi *et al.*, 1994; Haase *et al.*, 1994; Pykett *et al.*, 1994; Trofatter *et al.*, 1993). Thus, the *NF2* gene products of these two isoforms differ from each other at the extreme carboxy-terminus. Alternative splicing of other exons in the *NF2* gene has been reported, but its physiological significance remains unclear (Arakawa *et al.*, 1994; Pykett *et al.*, 1994; Schmucker *et al.*, 1999). The *NF2* gene is expressed in most human tissues, including heart, lung, skeletal muscle, kidney, breast, ovary, placenta, brain, pancreas and liver (Rouleau *et al.*, 1993; Trofatter *et al.*, 1993). Once the gene was identified, it became possible to analyze germline and somatic mutations that are predicted to affect protein expression and thus lead to tumorigenesis.

### 1.3.3 Mutations in NF2

A large number of germline and somatic mutations have been found in *NF2* patients. Mainly inactivating genetic alterations, such as frameshift and nonsense mutations, have been identified, although rare missense mutations have also been discovered. Interestingly, germline mutations have been found to be different from those that occur on a somatic basis (Table 1). The most frequent type of germline mutations is point mutations that either alter splice junctions or create new stop codons. Small deletions or occasional insertions have mainly been found in somatic mutations. These alterations produce either a frameshift with a subsequent, premature stop codon, or alternatively

disrupt proper splicing. The current data proposes that mutations in schwannomas are observed throughout most of the coding sequence although no mutations have been found in the isoform defining exons 16 and 17 (Gusella *et al.*, 1999). Mutations in meningiomas have been mainly found in the first half of the gene, and one large study suggests that germline mutations preferentially occur in exons 1 through 8 (Louis *et al.*, 1995). Thus, the wide variety of inactivating mutations, most of which truncate the protein, supports the tumor suppressor model. Since no mutations have been reported in the isoform 1 and 2 defining exons 16 or 17, both merlin isoforms may be capable of fulfilling its tumor suppressor function (Gusella *et al.*, 1996).

	<b>Mutation</b>	<b>Types of mutation</b>	<b>Sites of mutation</b>
<b>NF2 patients</b>	Germline	Point mutations > deletions	Hot spots at Arg residues?
<b>Schwannomas</b>	Somatic	Deletions > Point mutations	None
<b>Meningiomas</b>	Somatic	Deletions > Point mutations	First half of coding sequence?

**Table 1. Trend in Mutational Spectra of the *NF2* gene.** (Modified from Louis *et al.*, 1995)

Non-*NF2* related tumors including colorectal tumors, melanomas and breast carcinomas were screened for mutations in the *NF2* gene. These studies suggest that the *NF2* gene is involved in few colorectal tumors although it is not critical in colon tumorigenesis (Rustgi *et al.*, 1995). Mutations in the *NF2* gene were also found in melanomas and breast carcinomas, and the importance of these findings with respect to tumorigenesis needs to be further addressed (Bianchi *et al.*, 1994). However, inactivating mutations of the *NF2* gene are frequent in malignant mesotheliomas (Bianchi *et al.*, 1995; Sekido *et al.*, 1995). Somatic mutations inactivating the *NF2* encoded protein in mesotheliomas appear to be a progression, rather than an initiation event, since *NF2* patients do not show a predisposition to this tumor type.

## 1.4 NF2, the Protein (Merlin)

### 1.4.1 Merlin and its Family Members

As mentioned above, the *NF2* gene has been isolated by a positional cloning strategy, and the identity of this novel tumor suppressor, which belongs to the 4.1 protein superfamily, has been discovered. The *NF2* gene encodes a 595 (isoform 1) or a 590 (isoform 2) amino acid protein named merlin. This protein was named merlin (**m**oesin, **e**zrin and **r**adixin **l**ike **p**rotein) because of its striking similarity to ezrin, radixin and moesin (ERM) (Trofatter *et al.*, 1993). It has also been named schwannomin for its role in preventing schwannoma formation (Rouleau *et al.*, 1993). Members of the protein 4.1 superfamily include protein 4.1, talin, ezrin, radixin, moesin, merlin and DAL-1 (**d**ifferentially expressed in **a**denocarcinoma of the **l**ung 1). Furthermore, several protein tyrosine phosphatases such as PTPH1 (**p**rotein-tyrosine **p**hosphatase-related cDNAs from a **H**eLa cell library), PTPMEG (**p**rotein-tyrosine **p**hosphatase of the human **m**egakaryoblastic cell line MEG-01) and pez (**p**hosphatase with **e**zrin domain) are members of the protein 4.1 superfamily (Gu *et al.*, 1991; Gusella *et al.*, 1996; Smith *et al.*, 1995; Tran *et al.*, 1999; Yang *et al.*, 1991). A homologous domain defines the members of this family with ~270 amino acids (FERM-domain) near the amino-terminus, which is followed by a long  $\alpha$ -helical domain and a charged carboxy-terminal domain. Overall, merlin is 45 to 47% identical to the ERM proteins and the amino-terminus is 63% identical to these family members (Figure 2) (Gusella *et al.*, 1999).

The strong similarity of merlin and the ERM proteins (MERM) has resulted in analogous research of these proteins and indeed many common features have been found. However, there is increasing evidence that merlin has unique functions. Merlin is detected with an apparent size of 66kD by Western blot analysis, close to that predicted from its actual sequence (Gonzalez-Agosti *et al.*, 1996), whereas, the ERM proteins migrate with an apparent molecular mass greater than predicted from their sequence. The anomalous migration has been ascribed to the structure of the carboxy-terminus and these observations suggest that merlin differs from its family members in the properties of this region (Gonzalez-Agosti *et al.*, 1996).



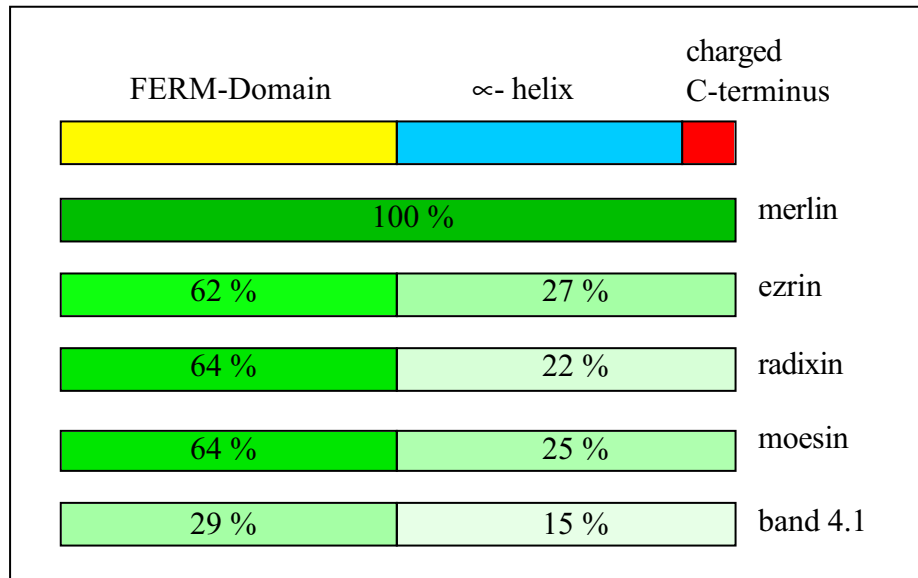


**Figure 2. Merlin and its Related ERM Proteins.** See text for details. (Modified from Gusella *et al.*, 1996).

#### 1.4.2 Possible Functions of Merlin and ERM Proteins

Localization studies demonstrate that merlin and the ERM proteins have not only common structural patterns but also share common cell distribution patterns. Using indirect immunofluorescence, endogenous merlin has been localized to the motile regions such as leading or ruffling edges in meningioma cells and human fibroblast. Furthermore, merlin co-localizes with F-actin in these motile regions in a serum or PDGF-dependent manner. However, unlike ezrin and moesin, merlin does not co-localize with F-actin at the stress fibers in human meningioma cells (Gonzalez-Agosti *et al.*, 1996; Ramesh V., pers. commun.). All three ERM proteins localize similarly to cortical actin structures near the plasma membrane such as microvilli, membrane ruffles and lamellipodia (Amieve *et al.*, 1994; Berryman *et al.*, 1993; den Bakker *et al.*, 1999; Franck *et al.*, 1993; Gonzalez-Agosti *et al.*, 1996; Goslin *et al.*, 1989; Henry *et al.*, 1995; Huynh *et al.*, 1996; Sato *et al.*, 1992; Stemmer-Rachamimov *et al.*, 1997a; Sainio *et al.*, 1997; Winckler *et al.*, 1994; Xu L. *et al.*, 1998). Thus, merlin and the ERM proteins have overlapping subcellular distributions.

Biochemical and structural investigations have unveiled similar conformational regulation of all MERM proteins. The amino-terminal ~300-amino acids of any ERM member can form an association with the carboxy-terminal ~100 residues of any member causing intra- and/or intermolecular head-to-tail associations. The regions that lead to these associations have been dubbed amino- and carboxy-ERM association domains respectively (N- and C-ERMADs) (Gary *et al.*, 1995; Magendantz *et al.*, 1995; Pearson *et al.*, 2000). Additionally, intermolecular head-to-tail association of ERM proteins have been detected *in vivo* such as ezrin-ezrin, ezrin-moesin and moesin-moesin dimers and oligomers (Berryman *et al.*, 1995; Bretscher *et al.*, 1995). How the different intermolecular and intramolecular associations of the ERM proteins contribute their activation *in vivo* remains to be determined. These studies lead to a model in which the inactive (closed) protein cannot associate with its binding partners including membrane-associated proteins and F-actin (Gary *et al.*, 1995; Pestonjamas *et al.*, 1995; Reczek *et al.*, 1998; Takahashi *et al.*, 1997; Turunen *et al.*, 1994). Phosphorylation of a carboxy-terminal threonine in conjunction with binding of specific phosphatidylinositides has been implicated in conformational regulation of the ERM proteins (Figure 3) (Matsui *et al.*, 1998; Matsui *et al.*, 1999; Nakamura *et al.*, 1995; Nakamura *et al.*, 1999; Pietromonaco *et al.*, 1998; Simons *et al.*, 1998). Testing this mode of regulation for merlin has been the subject of intensive research, and predictions were ambiguous since the carboxy-terminus of merlin shares only ~24% sequence identity with the ERM proteins over the critical region at the carboxy-terminus. Moreover, the sequence surrounding the threonine mentioned above, T558 in moesin, is well conserved in all three ERM proteins but it is quite distinct in merlin. This would suggest that phosphorylation of this particular threonine has no effect on merlin conformation.

Interestingly, merlin isoform 1 is regulated in a fashion similar to the ERM proteins; the carboxy-terminus of isoform 1 binds to the amino-terminus of merlin and moesin with comparable affinities. In contrast, merlin isoform 2 lacks the ability to form inter- and/or intramolecular head-to-tail associations (Gonzalez-Agosti *et al.*, 1999; Gronholm *et al.*, 1999; Huang *et al.*, 1998; Sherman *et al.*, 1997).

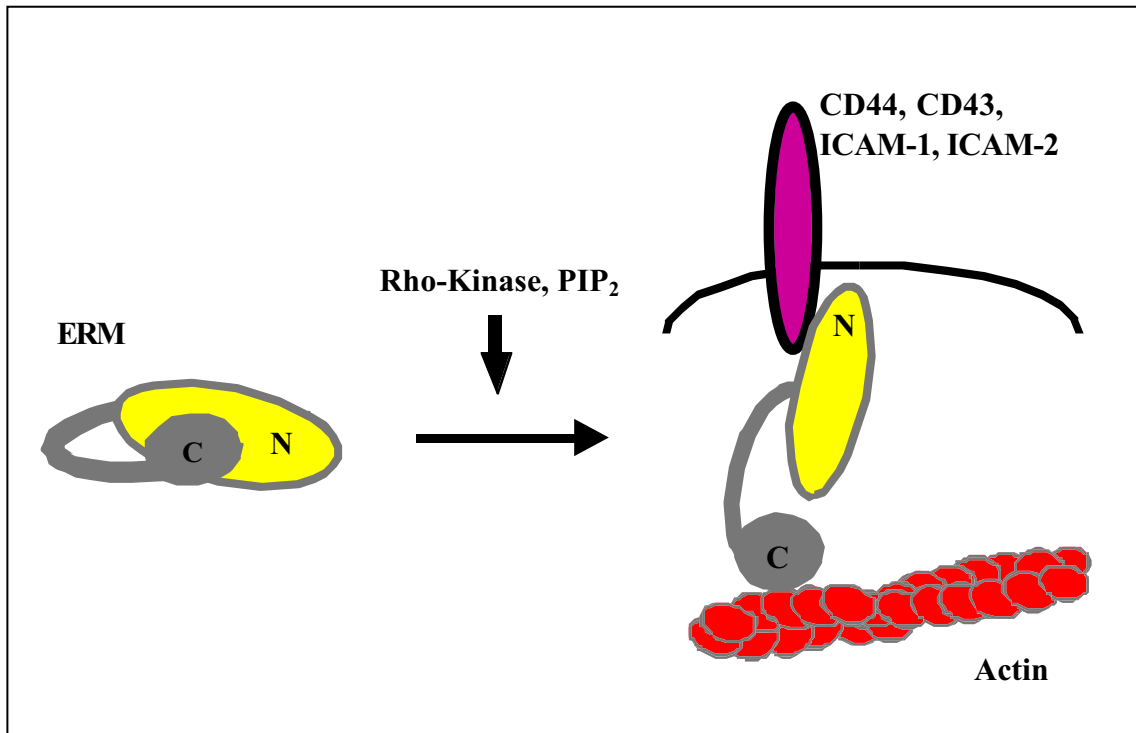


**Figure 3. An Intramolecular Head-to-Tail Association Model for the Activation of ERM Proteins.** The amino- and carboxy-terminal halves of native ERM proteins may mutually suppress their functions such as membrane- and actin binding respectively, through intramolecular head-to-tail association.

As mentioned above, mutational analysis of the *NF2* gene supports the hypothesis that both merlin isoforms may be capable of fulfilling its tumor suppressor function. In contrast, the ERM proteins are expressed in the *NF2* related tumors and have not been linked to tumor suppressor syndromes like *NF2* (Stemmer-Rachamimov *et al.*, 1997b). This argues that the critical signaling pathway disrupted by merlin deficiency is specific and not common to the ERM proteins. Overexpression of merlin isoform 1 in *NF2*-positive and *NF2*-negative primary human meningioma cells inhibits cell proliferation (Ikeda *et al.*, 1999). Introduction of merlin into cultured rat schwannoma cells suggests that merlin isoform 1 is the more potent tumor suppressor (Sherman *et al.*, 1997). However, this assay involves significant overexpression of merlin, and as the tumors involved did not arise due to merlin deficiency, it is possible that this growth suppression involves a different mechanism than *in vivo* tumor suppression. In fact, the growth of non-*NF2* tumor target cell types such as fibroblasts

can be altered by merlin overexpression (Lutchman *et al.*, 1995), illustrating the difficulty of directly equating growth suppression in cell culture with tumor suppression *in vivo*.

MacKay *et al.* (1997) have shown that the ERM proteins are essential participants in Rho- and Rac-mediated stress fiber assembly, cortical actin polymerization and focal complex formation. While some of these functions may be unique to the ERM proteins, there is increasing evidence that merlin also participates in a Rac-mediated pathway (MacKay *et al.*, 1997; Ramesh V., pers. commun.; Shaw *et al.*, 2001).

### 1.4.3 Merlin and ERM Interacting Proteins

Various avenues have been taken to study the function of merlin and to further compare merlin and the ERM proteins. These studies include the previously mentioned research on the conformation of ERM proteins, as well as studies involving fly and mouse models, cell culture investigations and the identification of ERM binding proteins. The ERM proteins have been demonstrated to bind to the integral membrane protein CD44, which is a receptor for hyaluronan (Tsukita *et al.*, 1994). However, full-length ERM proteins have very low affinity to the cytoplasmic domain of CD44 *in vitro*, whereas truncated amino-terminal halves of ERM proteins bind to CD44 with high affinity (Hirao *et al.*, 1996). In addition, significant amounts of monomeric ezrin can be detected as a soluble form in the cytoplasm (Berryman *et al.*, 1995; Bretscher *et al.*, 1995). These findings support the hypothesis of the intramolecular head-to-tail association model for ERM protein activation and inactivation (Figure 3) and show that the ERM proteins are connected directly to the plasma membrane through integral membrane proteins. Subsequent studies have shown that the ERM proteins can also bind through their FERM-domain to other membrane proteins including CD43, intercellular adhesion molecules 1 and 2 (ICAM1 and ICAM2) and layilin (Borowsky *et al.*, 1998; Heiska *et al.*, 1998; Legg *et al.*, 1998; Serrador *et al.*, 1998; Tsukita *et al.*, 1994; Yonemura *et al.*, 1999).

ERM proteins have a common carboxy-terminal actin binding side that is not present in either isoform of merlin. However, the association of merlin to actin has been characterized in detail, and this interaction is mediated through a different binding domain, which is also present in ezrin (James *et al.*, 2001; Xu H. *et al.*, 1998). CD44, NHE-RF and RhoGDI have also been shown to associate with the MERM proteins (Maeda *et al.*, 1999; Morrison *et al.*, 2001; Murthy *et al.*, 1998). Merlin binding proteins include schwannomin interacting protein (SCHIP-1), syntenin,  $\beta$ -fodrin,  $\beta$ 1-integrin,  $\beta$ II-spectrin and hepatocyte growth factor-regulated tyrosine kinase substrate (HRS) (Goutebroze *et al.*, 2000; Jannatipour *et al.*, 2001; Neill *et al.*, 2001; Obremski *et al.*, 1998; Scoles *et al.*, 1998, 2000). However not all of these proteins may have been tested for a possible interaction with the ERM proteins. It is of interest to note that merlin has been shown to bind to ERM family members *in vitro* and *in vivo* (Gonzalez-Agosti *et al.*, 1999; Gronholm *et al.*, 1999; Huang *et al.*, 1998). A recent study suggests furthermore that these interactions contribute to the regulation of these proteins (Morrison *et al.*, 2001). Thus, investigating MERM interacting proteins demonstrated further biochemical and cell biological mimicry between merlin and the ERM proteins.

The yeast two-hybrid system was employed in the Molecular Neurogenetics Unit at Massachusetts General Hospital and Harvard Medical School, Boston, to identify components that bind to merlin and the regulatory cofactor for  $\text{Na}^+/\text{H}^+$  exchanger (NHE-RF) was found to be a common interactor for the MERM proteins (Murthy *et al.*, 1998). Independently, a group of 50-55kD polypeptides that were specifically retained on beads containing immobilized amino-terminal domains of ezrin and moesin were also identified as NHE-RF (a.k.a. EBP50). These polypeptides were shown to be constitutively phosphorylated (Reczek *et al.*, 1997). Human NHE-RF is a 358 amino acid protein containing two PSD-95/DlgA/ZO-1 (PDZ-) domains that are known to mediate protein-protein interactions. It also possesses a MERM binding domain that encompasses the 30 most carboxy-terminal residues (Figure 4).

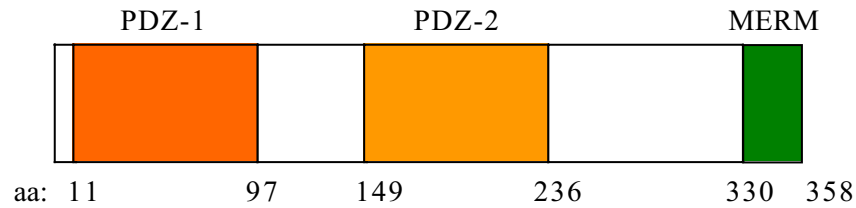


**Figure 4. Simplified Structure of NHE-RF containing PDZ-Domains.** Boxes show the coding region of NHE-RF. The orange areas represent PDZ-domains 1 and 2. The green area represents the MERM binding domain (Modified after Murthy *et al.*, 1998).

NHE-RF was originally identified in rabbit as a protein kinase A dependent regulator of the  $\text{Na}^+\text{-H}^+$  exchanger NHE3 to which it binds through the second PDZ-domain (Weinman *et al.*, 1995). The cytoplasmic protein, NHE-RF, has a family member called NHE-RF2 (a.k.a. E3KARP, SIP-1 and TKA-1) which also has two PDZ-domains, is 55% identical to NHE-RF and has been shown to bind to ezrin and merlin. NHE-RF2 was originally isolated through a yeast two-hybrid screen searching for proteins that interact with the cytoplasmic domain (aa 375-832) of the NHE3 (Hall *et al.*, 1998a; Nguyen *et al.*, 2001; Yun *et al.*, 1998). These studies provided evidence for the molecular linkage between MERM proteins and the cytoplasmic domain of NHE3 thus connecting the MERM proteins indirectly to the plasma membrane.

A number of studies have led to the identification of various proteins (mainly membrane proteins) that bind NHE-RF and NHE-RF2. In particular, mutagenesis studies of the cytoplasmic tail of the  $\beta$ 2-adrenergic receptor have revealed that the optimal binding motif to the first PDZ-domain of NHE-RF is DS/TXL (Hall *et al.*, 1998a). These authors further showed that co-expression of the  $\beta$ 2-adrenergic receptor with NHE3 resulted in inadequate regulation of exchanger activity by cAMP. However, normal regulation of NHE3 occurred when a mutant receptor with an additional alanine at the carboxy-terminus was co-transfected along with the exchanger (Hall *et al.*, 1998a; Hall *et al.*, 1998b). Searching databases for proteins with this binding cassette reveals many proteins with the PDZ-1 binding motif at the extreme carboxy-terminus. The identification of NHE-RF binding proteins is of great interest to further define the role of this adaptor protein, and various proteins that bind NHE-RF and/or NHE-RF2 have emerged out of a field of intensive study.

## 1.5 Specific Aims

Although progress was made over recent years, the physiological function of merlin is still the subject of many ongoing studies. Insights into possible roles of merlin have come in part from animal models (fly and mouse), and at the time this work began, limited information on merlin binding proteins was available. Several cellular proteins had been shown to interact with merlin *in vitro*; however, the identities of these proteins had not been revealed (Takeshima *et al.*, 1994). NHE-RF was one of the first merlin binding proteins that was also found binding to the ERM proteins (Murthy *et al.*, 1998; Rezek *et al.*, 1997). Therefore, it was and still remains of great interest to characterize further the interaction between merlin and NHE-RF.

Despite the existing similarities of the MERM proteins, merlin is predicted to have unique functions since only mutations in the *NF2* gene have been found in the tumor suppressor syndrome NF2. In contrast to merlin the ERM proteins are functionally expressed in these tumors. This observation suggests that the critical signaling pathway disrupted by the absence of merlin is unique and specific to this tumor suppressor protein and is not shared with the ERM proteins. To decipher this function, critical cellular target proteins that interact with merlin but not with the ERM proteins need to be discovered. The specific aims of this “Dissertation” (PhD thesis) were as follows:

- **Characterization of the interaction of NHE-RF with merlin isoform 1 and 2**  
Merlin isoform 1, but not isoform 2, has been shown to form intramolecular head-to-tail associations (Gonzalez-Agosti *et al.*, 1999; Gronholm *et al.*, 1999; Huang *et al.*, 1998; Sherman *et al.*, 1997). In this context, the relationship of NHE-RF to the isoforms of merlin and the influence of phospholipids was examined through *in vitro* binding studies.

- **Isolation and characterization of NHE-RF binding proteins**

During the course of this work, mutagenesis studies revealed that the optimal binding motif of the first PDZ-domain of NHE-RF is DS/TXL (Hall *et al.*, 1998a). The 56kD subunit of the H<sup>+</sup> ATPase has the carboxy-terminal motif DTAL. Thus, localization and binding studies (*in vitro* and *in vivo*) between NHE-RF and the H<sup>+</sup> ATPase were employed to test a possible interaction as well as the relevance of a possible interaction.

- **Examination of NHE-RF in human cancer**

The fact that *NF2* mutations are found in only approximately 60% of meningiomas implies that a gene other than the *NF2* gene is involved in the formation of some of these tumors (Louis *et al.*, 1995). Thus, a possible inactivation of the *NHE-RF* gene in meningiomas where no *NF2* mutations have been found was tested by molecular genetic analyses. Furthermore, the expression and localization of NHE-RF was investigated in meningiomas and tumors derived from other organs including colon, ovary and breast.

- **Characterization of novel merlin binding proteins**

To determine other functions of merlin, identifying additional merlin binding proteins is of great interest. Particular functions of merlin that are not shared with the ERM proteins may illuminate its role as a tumor suppressor protein. Two candidates, named merintA and merintB, were isolated in a yeast two-hybrid screen together with NHE-RF. Here, the significance of this interaction was analyzed *in vitro* and *in vivo* through binding studies, expression analysis and localization studies to address the functional importance of these potential interactions.

These experiments were designed to study functions of merlin and possibly to link this tumor suppressor protein to distinct signal transduction pathways in order to elucidate ultimately how merlin contributes to tumorigenesis.



## 2. Materials and Methods

### 2.1 Materials

#### Animals

- Female BALB/c mice for monoclonal antibody production (Massachusetts General Hospital animal facility)
- Male Harlan Sprague-Dawley rats for kidney lysates and NHE-RF/ H<sup>+</sup> ATPase staining (Massachusetts General Hospital animal facility)

#### Antibodies and Solutions for Immunofluorescence Analysis

##### Primary Antibodies

###### Commercial and Other Antibodies

- $\alpha$ -FLAG (M2, monoclonal antibody; Sigma)
- $\alpha$ -Grb2-C23 (sc-255, polyclonal rabbit IgG; Santa Cruz)
- $\alpha$ -GST-B14 (sc-138, monoclonal mouse IgG<sub>1</sub>; Santa Cruz)
- $\alpha$ -HA (hybridoma supernatant; kindly provided by Dr. Ed Harlow, Massachusetts General Hospital, Boston)
- $\alpha$ -HA (12CA5, monoclonal antibody; Roche)
- $\alpha$ -His-RGS (34610, monoclonal antibody, Qiagen)
- $\alpha$ -Merlin-A19 (sc-331, polyclonal rabbit IgG; Santa Cruz)
- $\alpha$ -phospho-tyrosine (4G10, monoclonal antibody; Upstate Biotechnology)
- $\alpha$ -phospho-tyrosine (pY20, monoclonal antibody; TaKaRa)

###### Merlin

- N21 (polyclonal rabbit serum; antigen: thrombin cleaved GST-merlin aa 1-332; Gonzalez-Agosti *et al.*, 1996)
- 1C4 (monoclonal mouse IgG<sub>1</sub>; antigen: thrombin cleaved GST-merlin aa 308-590; Gonzalez-Agosti *et al.*, 1996)

###### MerintA

- Tim3 (polyclonal anti-peptide serum; antigen: aa 165-178)
- 7E1 (monoclonal mouse IgG<sub>2b</sub>, antigen: GST-merintA aa 13-178)

### H<sup>+</sup> ATPase

- **B1-Subunit** (polyclonal, affinity-purified rabbit antibody; Breton *et al.*, 2000)
- **E-Subunit** (polyclonal, affinity-purified chicken antibody; Breton *et al.*, 2000)
- **E-Subunit E11** (monoclonal antibody; kindly provided by Dr. Steven Gluck, University of Florida, Gainesville)

### NHE-RF

- **IC270** (polyclonal rabbit serum; antigen: GST-NHE-RF aa 270-358; Gonzalez-Agosti *et al.*, 1999)
- **1D12** (monoclonal mouse IgG<sub>2a</sub>; antigen: GST-NHE-RF aa 270-358)

### Secondary Antibodies and Immunodetection Reagents

- Donkey  $\alpha$ -chicken-FITC (Jackson ImmunoResearch Laboratories)
- Goat  $\alpha$ -mouse-FITC (BioSource International)
- Goat  $\alpha$ -mouse-HRP (Amersham Pharmacia Biotech)
- Goat  $\alpha$ -mouse-Rhodamine (BioSource International)
- Goat  $\alpha$ -rabbit-biotin (Vector Laboratories)
- Goat  $\alpha$ -rabbit-FITC (BioSource International)
- Goat  $\alpha$ -rabbit-HRP (Amersham Pharmacia Biotech)
- Goat  $\alpha$ -rabbit-Rhodamine (BioSource International)
- Goat  $\alpha$ -rabbit-CY3 (Jackson ImmunoResearch Laboratories)
- Rabbit  $\alpha$ -chicken-HRP (Sigma)
- Streptavidin-HRP (Amersham Pharmacia Biotech)

### Solutions for Immunofluorescence Analysis

- Hoechst 33342, stains nuclei (B2261; Sigma)
- Mounting media (ProLong antifade kit, P-7481; Molecular Probes)
- Rhodamine phalloidin, stains F-actin specifically (R-415; Molecular Probes)

### Bacterial Strains

- **BL21** (B<sup>-</sup> F<sup>-</sup> *dcm ompT hsdS*(rB<sup>-</sup> mB<sup>-</sup>) gal; Stratagene)
- **DH5 $\alpha$**  (F<sup>-</sup>, *hsdR17*(rk<sup>-</sup>,mk<sup>-</sup>), *lambda*<sup>-</sup>, *supE44*, *endA1*, *thi1*, *gyrA96.relA1*; Hanahan, 1993)
- **M15** (K12-mutant with  $\Delta$ (*prolac*)*thi*,  $\Phi$ 80d, *ara-rspL*, *strr*, *lacZdel*; Qiagen)
- **NM522** (*supE thi-1*  $\Delta$  (*lac-proAB*),  $\Delta$  (*mcrB-hsdSM*)5, (rK<sup>-</sup> mK<sup>+</sup>), F'*proAB lacI* q $\Delta$ DM15; Stratagene)

### Commercial Grb2 GST-Fusion Proteins

- Full length protein (aa 1-217, sc-4015, Santa Cruz)

### Oligonucleotides

Oligonucleotides were obtained from GibcoBRL.

- **Cloning of A4:** aa 1-178 of merintA with 5' HA-tag in pcDNA3  
15S-*Bam*HI: GAT GGA TCC ATG TAC CCA TAC GAT GTT CCA GAT  
TAC GCT CTT ATG GCG GCT CCA CTA GGG GGT  
9AS-*Not*I: GGG GCG GCC GCT CAC GTT GGC TTC AG
- **Cloning of C35:** aa 340-590 (isoform 2) of merlin in pGEX-2T  
340S-*Bam*HI: GAT GGA TCC GCT CGA GAG AAG CAG ATG AGG  
5114-*Eco*RI: CCC GAA TTC TCA AAT GCA GAT AGG TCT TCT
- **Cloning of C36:** aa 340-579 (common to both isoforms) of merlin in pGEX-2T  
340S-*Bam*HI: GAT GGA TCC GCT CGA GAG AAG CAG ATG AGG  
579AS-*Eco*RI: CCC GAA TTC CTT TTT AAT GGT ATT GTG CTT
- **Cloning of GST-MerintA:** aa 13-178 of merintA in pGEX-4T1  
1S-*Bam*HI: GAT GGA TCC ACG AGG CGG CCA CCC  
9AS-*Not*I: GGG GCG GCC GCT CAC GTT GGC TTC AG
- **Cloning of His-MerintA:** aa 13-178 of merintA in pQE30  
1S-*Bam*HI: GAT GGA TCC ACG AGG CGG CCA CCC  
2AS-*Pst*I: GGG CTG CAG TCA CGT TGG CTT CAG
- **pcDNA3 primers:** Vector primers to PCR inserts and sequence  
3418: GCA GAG CTC TCT GGC TAA CT  
3419: TGG CAA CTA GAA GGC ACA GT

- **pGEX primers:** Vector primers to PCR inserts and sequence  
5' pGEX: GGG CTG GCA AGC CAC GTT TGG TG  
3' pGEX: CCG GGA GCT GCA TGT GTC AGA GG

### Plasmids and Expression Vectors

- pcDNA3 (Invitrogen)
- pcDNA3/5'F (Xu L. *et al.*, 1998)
- pEG202 (Gyuris *et al.*, 1993)
- pEGFP-N1 (Clontech)
- pGEX-2T and pGEX-4T1 (Amersham Pharmacia Biotech)
- pLexA (Gyuris *et al.*, 1993)
- pQE30 (Qiagen)

### List of Selected Materials

- **Antibiotics**

Ampicillin (50-100 $\mu$ g/ml final concentration)  
Kanamycin (25 $\mu$ g/ml final concentration)

- **Blot Buffer for Immunoblots**

192mM Glycine  
25mM Tris

- **DNA Loading Dye**

3mM EDTA  
50% Glycerol saturated with bromophenol blue  
0.1% SDS  
0.01M Tris pH 8.0

- **LB Broth**

10 g/l Bacto-tryptone  
5 g/l Bacto-yeast extract  
5 g/l NaCl

- **LB Agar**

LB broth (as described above)  
15 g/l Agar

- **Phosphate-Buffered Saline; PBS (pH 7.4)**

1mM  $\text{KH}_2\text{PO}_4$   
 155mM NaCl  
 3mM  $\text{Na}_2\text{HPO}_4 \cdot 7\text{-H}_2\text{O}$

- **Polyacrylamide Gels:**

<b>Separating Gels:</b>	<b>7.5%</b>	<b>10%</b>	<b>12%</b>
1.5M Tris-HCl (pH 8.8)	7.5ml	7.5ml	7.5ml
Distilled water	14.5ml	12ml	10ml
30% Acrylamide/bis (30:0.8)	7.5ml	10ml	12ml
10% SDS	300 $\mu$ l	300 $\mu$ l	300 $\mu$ l
10% Ammonium persulfate	100 $\mu$ l	100 $\mu$ l	100 $\mu$ l
TEMED	15 $\mu$ l	15 $\mu$ l	15 $\mu$ l

**Stacking Gel:**

0.5M Tris-HCl (pH 6.8)	2.5ml
Distilled water	6.1ml
30% Acrylamide/bis (30:0.8)	1.3ml
10% SDS	100 $\mu$ l
10% Ammonium persulfate	50 $\mu$ l
TEMED	10 $\mu$ l

- **Running Buffer for Polyacrylamide Gels**

250mM Glycine  
 0.1% SDS  
 25mM Tris

- **Sample Buffer (3x GSD)**

300mM DTT  
 33% Glycerol saturated with bromophenol blue  
 6% SDS

- **SSC (20x)**

3M NaCl  
 0.3M Sodium citrate 2- $\text{H}_2\text{O}$   
 Adjust to pH 7.0 with NaOH

- **TBE Buffer**

- 0.089M Boric acid
  - 2mM EDTA
  - 0.1M Tris

- **TBS Buffer**

- 150mM NaCl
  - 50mM Tris-HCl (pH 8.0)

- **TBST**

- TBS + 0.05% Tween-20

- **TE Buffer**

- 1mM EDTA
  - 10mM Tris-HCl (pH 8.0)

- **TE/RNase**

- TE buffer (as described above)
  - 0.05mg/ml RNase

## 2.2 Molecular Biological Methods

### DNA Mini- and Maxipreparation

Purification of plasmids from a culture of bacteria involves the following general strategy:

- Grow and harvest a culture of bacteria hosting the plasmid DNA of interest.
- Break cells to gain access to the plasmid DNA.
- Remove all components of the cell extract from the plasmid DNA.
- Concentrate the resulting plasmid DNA solution.

A single colony was chosen and grown under antibiotic selection in 5ml LB with the appropriate antibiotic (e.g. 50µg/ml ampicillin) at 37°C overnight to obtain a culture of cells containing the plasmid. Cells were pelleted by spinning them at room temperature for five minutes. In turn, cells were lysed by incubating them in ice-cold Solution 1 (10mM EDTA, 50mM Glucose, 25mM Tris) at room temperature for five minutes, and subsequently by incubating them in freshly prepared Solution 2 (200mM NaOH, 1% SDS) on ice for five minutes. Finally, ice-cold solution 3 (11.5% glacial acetic acid, 3M KAc) was added to the cell lysates and kept on ice for an additional five minutes. For minipreparations, cell debris and chromosomal DNA were pelleted by centrifugation at 14,000x g and 4°C for five minutes. The supernatant, containing the plasmid DNA, RNA and proteins, was extracted once with phenol-chloroform and once with chloroform alone. These organic solvents precipitate proteins but leave nucleic acids (DNA and RNA) in aqueous solution. The nucleic acids were precipitated in 100% ethanol before being pelleted by spinning at 14,000x g and room temperature for 15 minutes. Pellets were washed with 70% ethanol, air-dried and resuspended in TE/RNase. For maxipreparations, the plasmid DNA was purified in a cesium chloride column.

### Polymerase Chain Reaction

Polymerase chain reaction (PCR) is a technique that allows selective amplification of a chosen region of a DNA molecule. Two short oligonucleotides anneal to the DNA

molecule, one to each strand of the double helix, in order to carry out DNA amplification by PCR.

A basic protocol was performed for DNA amplification. The first step of this protocol is to denature the DNA at 94°C for four minutes followed by a second step consisting of 30 cycles with 3 substeps: denaturation, 94°C for 1 minute; annealing, 58-62°C for 1 to 2 minutes; and elongation, 72°C for 1 to 3 minutes. The third and final step allows completion of partial extended products at 72°C for 10 minutes. Primer stocks were diluted to 2ng of each primer per PCR reaction. A PCR-kit (Roche or GibcoBRL) supplied *Taq* polymerase, *Taq* polymerase buffer and dNTPs. Materials were adjusted to concentrations recommended by the manufacturer for each reaction. The annealing temperature was increased for more stringent conditions.

### **DNA Digest with Restriction Enzymes**

Purified restriction endonucleases (type II) cut DNA molecules in a precise manner. The enzyme *EcoR* I, for example, recognizes the hexanucleotide GAATTC. Some endonucleases (e.g. *Pvu* II or *Alu* I) make a simple double-stranded cut in the middle of the recognition site, resulting in a blunt-end, while others, cleavage is staggered, resulting in DNA fragments with short single-stranded overhangs at each end (so-called “sticky ends”). These “sticky ends” allow pairing between the bases with the result that the DNA molecules can “stick” back together. Typically, DNA was cut with 1 unit of restriction enzyme per µg DNA and incubated at 37°C for 1 to 16 hours. All restriction enzymes were obtained from New England Biolabs.

### **Dephosphorylation of Vector DNA**

Linearized vector DNA was dephosphorylated at its 5' ends to prevent religation. Calf intestine phosphatase (New England Biolabs) was used at 2 unit of enzyme per µg of DNA at 37°C for 1 to 2 hours. Adding 5mM EDTA and heat inactivating at 65°C for 15 minutes stopped the reaction. DNA was then purified by phenol-chloroform and chloroform extractions.



### **Agarose Gel Electrophoresis and Gel Extraction**

DNA can be separated according to size in an electrical field due to its negative charge. Agarose gels (1 or 1.2%) were poured and electrophoresis was performed at 100V in 1x TBE buffer for approximately 1 hour. Ethidium bromide was added to the gel at a concentration of 1µg/ml to visualize DNA under UV light.

A small DNA-gel piece was cut out of the gel if DNA was used for subcloning. Separation of the DNA from the gel and purification of the DNA was performed according to recommendations of the gel extraction kit, QiaexII (Qiagen).

### **Ligation**

T4 DNA ligase (GibcoBRL) catalyzes the formation of phosphodiester bonds in the presence of ATP between double-stranded DNAs with 3' hydroxyl- and 5' phosphate termini. A molar ratio of 3:1 to 10:1 of insert:vector was ligated in a total volume of 20µl. The ligation reaction was carried out at 20°C for 4 to 16 hours and subsequently transformed into bacteria.

### **Transformation**

Transformation is the introduction of DNA into living cells and antibiotic resistance monitors the uptake of plasmid DNA. Typically, the entire ligation reaction (20µl) was used to transform 100µl competent cells. The cell-DNA mixture was incubated on ice for 30 minutes and subsequently heat shocked at 37°C for five minutes to enable uptake of the recombinant vector by bacterial cells. Subsequently, cells were grown in LB at 37°C for one hour to allow expression of the resistance gene before being spun at 14,000x g and room temperature for five minutes. Cell pellets were resuspended in 100µl LB and plated on LB plates with the appropriate antibiotic. The plated cells were then incubated at 37°C overnight and the resulting colonies were screened for the presence of recombinant DNA by PCR.

### Double-Stranded DNA Sequencing

DNA sequencing enables to determine the precise order of nucleotides in a piece of DNA. The chain termination method (Sanger *et al.*, 1977) involves the synthesis of a DNA strand by elongating it from a primer that is annealed to the DNA template. Elongation is stopped by the four different ddNTPs.

An aliquot of 2-4µg of DNA to sequence, obtained by plasmid mini- or maxipreparation, was denatured by incubating in 0.2M NaOH and 0.2M EDTA at room temperature for five minutes. Subsequently, DNA was precipitated with 100% ethanol in the presence of 0.3M ammonium acetate (pH 4.5). The plasmid DNA was spun at 14,000x g and 4°C for 10 minutes, pellets were washed once with 70% ethanol and air-dried. The sequencing reactions were performed with a sequencing kit from United States Biochemical (USB). Briefly, plasmid DNA was resuspended in water and incubated at 37°C for 30 minutes with 0.02µg of the appropriate primer and recommended concentrations of reaction buffer (200mM Tris-HCl, pH 7.5, 100mM MgCl<sub>2</sub>, 250mM NaCl). In turn, 5.5µl of a master mix, prepared according to recommendations of the manufacture, was added to each sequencing reaction and incubated at room temperature for five minutes to allow incorporation of dNTPs and <sup>33</sup>P αATP by DNA polymerase (sequenase). Incubating this reaction mix with dideoxy nucleotide at 37°C for five minutes terminated the sequencing reaction. Finally, stop solution (USB) was added and the terminated sequencing reaction was denatured at 95°C before loaded on a polyacrylamide gel.

Ammonium Persulfate (0.1%) was added to the SequaGel-6 monomer solution (National Diagnostics) to pour 6% polyacrylamide gels. Electrophoresis was performed at 80W for one to three hours, and the gel was dried for one to two hours on a gel-dryer (BioRad) and exposed to X-Omat AR film (Kodak, Eastman Co.).

### **GenBank Analysis**

DNA and protein databases including GenBank, SwissProt and European Molecular Biology Laboratory databases were searched at the National Center of Biotechnology Information (<http://www.ncbi.nlm.nih.gov/BLAST>).

### **Northern Blot Analysis of Breast Cancer Cell Lines**

Isolation of total cellular RNA, electrophoresis, transfer and hybridization were performed as previously described (Ramesh *et al.*, 1986). Total RNA from breast cancer cell lines and normal mammary controls were isolated using the lithium-chloride/urea method. Thirty-five micrograms of the total RNA were separated on a 1% agarose-formaldehyde gel and blotted to nitrocellulose (Schleicher & Schuell). The DNA was labeled ( $\alpha$   $^{32}\text{P}$  dATP; 3,000 Ci/mmol, DuPont NEN; dCTP; dGTP; dTTP; Klenow, Roche) at 37°C for five hours and ultra-purified. For the purification, an Eppendorf tube with a hole in the bottom was packed with glass wool to the 50 $\mu\text{l}$  mark and filled 3/4 with Sepharose CL6b beads. The beads were washed three times with TNE (10mM Tris, 100mM NaCl, and 1mM EDTA, pH 8.0) and the probe was spun through. Membranes were probed with the  $^{32}\text{P}$ -labeled NHE-RF cDNA in hybridization solution (1x Denhardt's solution, 10% dextran sulfate, 45% formamide, 1M NaCl, 0.1% PyroPO<sub>4</sub>, 100 $\mu\text{g/ml}$  ssDNA, 50mM Tris) at 42°C for up to 48 hours. Next, the membranes were washed extensively: 1x with 2x SSC, 0.5% SDS, room temperature, 10 minutes; 5x with 2x SSC, 0.1% SDS, room temperature, 10 minutes; 1x with 1x SSC, 0.1% SDS, 52°C, 45 minutes; and 1x with 0.5x SSC, 0.1% SDS, 52°C, 45 minutes. Filters were then air-dried to dampness, wrapped in Saran-Wrap and exposed at -80°C to X-Omat AR film (Kodak Eastman Co.). Equal loading was confirmed by probing the stripped membranes with the GAPDH cDNA. Signal intensity was quantified by densitometric scanning of autoradiographs using transmittance analysis (Fluor-S, Multiimager, BioRad). Densitometric scanning was performed on bands that were not saturated. Thus, values obtained are in a linear range and reflect a true assessment.

### **Northern Blot Analysis of Multiple Tissue**

Commercially available human multiple tissue blots (Clontech) were obtained and probed with  $^{32}\text{P}$ -labeled DNA probes. The human multiple tissue blots were prehybridized in ExpressHyb solution (Clontech) at 42°C for five hours. The solution was replaced with fresh ExpressHyb solution containing the  $^{32}\text{P}$  labeled and ultra-purified  $\text{rDNA}$ . Blots were hybridized at 42°C for 16 hours, washed and exposed to X-Omat AR film (Kodak Eastman Co.).

### **cDNA Synthesis**

The SuperScript™ preamplification system (GibcoBRL) was used to synthesize first-strand cDNAs according to the recommendations of the manufacture. In summary, 2µg of total RNA were primed with oligo(dT) (0.5µg) and random hexamers (50ng), and denatured at 70°C for 10 minutes. SuperScriptII Reverse Transcriptase (GibcoBRL) synthesized the cDNA in the presence of dNTPs and reaction buffer (see GibcoBRL) at 42°C for 50 minutes.

The Marathon cDNA Amplification Kit (Clontech) was used to generate second-strand cDNA. Towards this end, the total amount of first-strand cDNA was incubated with dNTPs, second strand reaction buffer (see Clontech) and second-strand enzyme cocktail (Clontech) at 16°C for 90 minutes. Adding T4 DNA polymerase (Clontech) at 16°C for an additional 45 minutes completed the reaction. The second-strand cDNA was extracted once with phenol-chloroform and once with chloroform alone. The DNA was then precipitated in 100% ethanol before being pelleted by spinning at 14,000x g and room temperature for 20 minutes. Pellets were washed with 70% ethanol, air-dried and resuspended in H<sub>2</sub>O.

### **Rapid Amplification of cDNA Ends (5' RACE)**

The Marathon cDNA Amplification Kit (Clontech) provides a PCR-based method for selectively constructing cDNAs from specific RNAs. Specially designed adaptors (Marathon™) that significantly reduce background were employed. After second-strand cDNA synthesis from placenta and peripheral blood mononuclear cells (PBMC) RNA,

blunt ends were created and the Marathon adaptor was ligated to both ends of the double-stranded cDNA. Rapid amplification of cDNA ends was performed with the Marathon™ (sense) and gene specific primer (antisense) according to manufacture recommendations. Advantage 2 *Taq* polymerase (Clontech) was used for the PCR reaction and the products were subjected to sequence analysis.

### **Direct PCR Sequence Analysis**

5' RACE products were sequenced as previously described (Beauchamp *et al.*, 1998). In summary, PCR products (5µl) were incubated with 1U Exonuclease I (USB) and 2U shrimp alkaline phosphatase (SAP) (Amersham Pharmacia Biotech) at 37°C for 15 minutes, followed by 85°C for 15 minutes. Using the AmpliCycle Sequencing Kit (Perkin Elmer), 2µl of the Exonuclease I/SAP prepared PCR samples were sequenced with <sup>33</sup>P-dATP according to recommendations of the manufacturer. The sequencing reactions were performed for 26 PCR cycles (see Polymerase chain reaction) and the reactions were terminated with stop solution (95% formamide, 20mM EDTA, 0.05% bromophenol blue, and 0.05% xylene cyanol). Samples were analyzed on a 6% denaturing polyacrylamide gel, electrophoresed at 80W, which was dried and exposed to X-Omat AR film (Kodak, Eastman Co.).

### 2.3 Biochemical and Cell Biological Methods

#### Expression and Purification of GST-Fusion Proteins from Bacteria

The glutathione *S*-transferase (GST) expression system in bacteria allows expression of a foreign protein, and, thus, large amounts of the recombinant fusion protein can be purified with glutathione Sepharose beads. Full-length isoform 1 (F39: aa 1-595), full-length isoform 2 (F40: aa 1-590), amino-terminal (N21: aa 1-332), carboxy-terminal common to both isoforms (C26: aa 308-579) and carboxy-terminal isoform 1 (C34: aa 340-595) portions of merlin were cloned into pGEX-2T (Amersham Pharmacia Biotech). The bacterial host cells, BL21, transformed individually with the fusion constructs, were available in the laboratory. The carboxy-terminal isoform 2 (C35: aa 340-590) was PCR amplified, digested, ligated into pGEX-2T and transformed into BL21. The integrity of the entire sequence, including the junction region between the GST-epitope and the merlin coding sequence, was confirmed by DNA sequencing. The integrity of the protein was verified by Western blot analysis (see below) using GST-tag and merlin specific antibodies, and the expression of GST fusion proteins were analyzed by Coomassie staining (see below).

Expression and purification of GST-merlin fusion proteins was essentially performed as previously described (Gonzalez-Agosti *et al.*, 1996). In summary, 5ml of the appropriate BL21 clone was grown to mid-logarithm at 30°C and induced with 0.05M isopropyl  $\beta$ -D-thiogalactopyranoside (IPTG) at room temperature for 16 hours. The formation of inclusion bodies could be reduced significantly by inducing the fusion proteins at room temperature. The cells were pelleted, resuspended and incubated in PBS containing pefabloc (0.5mg/ml) and lysozyme (1.5mg/ml) at 4°C for 15 minutes. After freeze/thaw cycles (3x) and sonication (3x 30 seconds), debris was removed by centrifugation at 16,000x g and 4°C for 30 minutes. The soluble supernatant was collected and incubated with equilibrated glutathione Sepharose 4B beads (Amersham Pharmacia Biotech) at room temperature for 30 minutes. GST-merlin bound to beads was washed extensively with PBS containing pefabloc (0.5mg/ml), and eluted in either

sample buffer (1x GSD: 11% Glycerol, 2% SDS, 100mM DTT, 0.5% bromophenol blue) or glutathione buffer (20mM glutathione, 150mM NaCl, 50mM Tris, pH 8.0).

Full-length moesin (MFL: aa 1-577), amino-terminal (M5: aa 1-332) and carboxy-terminal (M3: aa 307-577) portions of moesin were expressed as GST fusion proteins in pGEX-4T1. Similarly, full-length NHE-RF (IFL: aa 1-358) was expressed as a GST fusion protein. Expression and purification of the GST-moesin and GST-NHE-RF were performed as previously described (Gonzalez-Agosti *et al.*, 1999) using standard methods.

MerintA (GST-merintA: aa 13-178) was PCR amplified, digested, ligated into pGEX-4T1 and transformed into BL21. The integrity of the entire sequence, including the junction region between the GST epitope and the merintA coding sequence, was confirmed by DNA sequencing. Expression and purification of the GST-merintA fusion protein was performed as described for merlin (see above). The integrity of the protein was verified by Western blot analysis (see below) using GST-tag and merintA specific antibodies, and the expression of GST fusion proteins were analyzed by Coomassie staining (see below).

### **Expression and Purification of 6xHis-Fusion Proteins from Bacteria**

The His-tag expression system in bacteria allows expression of a foreign protein similarly to the GST expression system. Large amounts of the recombinant fusion protein can be extracted under native or denaturing conditions and purified using nickel Sepharose beads. MerintA (His-merintA: aa 13-178) was cloned into pQE30 (Qiagen) and transformed into the bacterial host, M15. The His-tagged merintA construct was expressed and purified as recommended by the manufacture. Denaturing conditions were used since native conditions resulted in a very low yield. To produce the protein, a saturated culture was diluted 1:40 in 500ml of LB with 100µg/ml ampicillin and 25µg/ml kanamycin and grown at 37°C to mid-logarithm. The protein expression was induced by isopropyl-β-D-thiogalactopyranoside (IPTG) at a final concentration of 2mM and grown at 37°C for an additional 3 hours. Cells were collected by centrifugation, resuspended and lysed by stirring in buffer B (100mM NaH<sub>2</sub>PO<sub>4</sub>,

10mM Tris, 8M urea, pH 8.0) at room temperature for 1 hour. The supernatant was collected after high-speed centrifugation and incubated with equilibrated Ni-NTA Sepharose CL 6B resin (Qiagen) at room temperature for 45 minutes. Next, the beads were loaded into a 5ml column next and washed extensively with buffer C (100mM NaH<sub>2</sub>PO<sub>4</sub>, 10mM Tris and 8M urea, pH 6.3). His-merintA was eluted from the beads with buffer E (100mM NaH<sub>2</sub>PO<sub>4</sub>, 10mM Tris, 8M urea, pH 4.5) and the integrity of the protein was verified by Western blot analysis (see below) using His-tag and merintA specific antibodies, and the expression of His-merintA was analyzed by Coomassie staining (see below).

### **SDS-Polyacrylamide Gel Electrophoresis (SDS-PAGE)**

The SDS-polyacrylamide gel electrophoresis separates proteins under denaturing conditions, and according to an electric field, proteins will migrate at a rate dependent upon their size (Laemmli *et al*, 1970). The negatively charged detergent sodium dodecyl sulfate (SDS) is added to proteins, giving the solution and every individual protein a negative charge. The detergent binds to hydrophobic regions of the protein molecules, causing them to unfold into extended polypeptide chains. The proteins run through a stacking gel, which staggers the proteins in a tight band. In turn, the proteins are separated in a highly cross-linked resolving or separating gel. The electrophoresis was performed at 7mA overnight or 40mA during the day.

### **Coomassie Staining**

Large amounts of protein (>0.1µg) are stained and detected non-specifically with the dye Coomassie Brilliant Blue R-250. After separation of proteins by SDS-PAGE, gels were incubated in Coomassie blue staining solution (0.1% Coomassie Brilliant Blue R250, 25% methanol and 10% glacial acetic acid) at 20°C for 1 hour. Then, gels were incubated in destaining solution (25% methanol and 10% glacial acetic acid) to visualize proteins and dried on a gel-dryer (BioRad) for one hour.



### Western Blot Analysis (Immunoblotting)

Western blot analysis is performed to transfer proteins from a polyacrylamide gel to a nitrocellulose membrane. Subsequently, the transferred protein can be visualized by specific antibody binding and detection systems. Electroblooming of proteins to nitrocellulose (BioRad) was performed at 0.5A and 4°C for 1 to 3 hours. After the transfer, membranes were stained for total protein with 10% Ponceau-S (Sigma) for one minute. The membranes were then destained with distilled water until protein bands were visible. In turn, individual proteins were detected through specific protein-antibody interactions. To avoid non-specific binding of the used antibodies, the membranes were blocked in 5% milk/TBST at room temperature for 1 to 16 hours. The membranes were washed three times with TBST, five minutes each, before they were probed for one hour with primary antibodies. All polyclonal antibodies were diluted in TBST containing 1% milk, and monoclonal antibodies were diluted in TBST. Generally, merlin was detected with 1C4 (1:1,000), NHE-RF with IC270 (serum 1:1,000; affinity-eluted 1:50) or 1D12 (1:1,000) and merintA with 7E1 (1:500). The following antibodies were used for Western blot analysis of the H<sup>+</sup> ATPase: affinity-purified anti-E subunit (1:1,000) and affinity-purified anti-B1 subunit (1:1,000). The FLAG-tag antibody, M2, was diluted 1:2,000 and the HA-tag antibody, 12CA5, was diluted 1:4,000. The membranes were then washed again, three times, for five minutes with TBST, and incubated with the secondary antibody for one hour. Horseradish peroxidase conjugated secondary antibodies were diluted in TBST at the following dilutions: anti-rabbit (1:20,000), anti-mouse (1:10,000) and anti-chicken (1:4,000). The membranes were washed a final three times with TBST, incubated one minute in ECL 1 and 2 (Amersham Pharmacia Biotech) and exposed to X-Omat AR film (Kodak, Eastman Co.). Signal intensities were quantified at times (e.g. Figure 6) by densitometric scanning of autoradiographs using transmittance analysis (Fluor-S, Multiimager, BioRad). Densitometric scanning was performed on bands that were not saturated. Thus, values obtained are in a linear range and reflect a true assessment.

### **Blot Overlay Assay**

The direct interaction of merintA and Grb2 was confirmed by blot overlay assays. Purified His-merintA (3 $\mu$ g) or BSA (3 $\mu$ g) as a negative control was subjected to 10% SDS-gel electrophoresis and transferred to nitrocellulose membranes. After blocking membranes in 10% non-fat dry milk diluted in TBST, they were incubated with GST-Grb2 (3 $\mu$ g/ml in TBST) for 16 hours. Membranes were washed three times, incubated the anti-GST antibody B14 (1:1,000) for 1 hour, washed three more times and incubated with horseradish peroxidase anti-mouse antibodies (1:10,000) for 1 hour. The membranes were washed a final three times, incubated one minute in ECL 1 and 2 (Amersham Pharmacia Biotech) and exposed to X-Omat AR film (Kodak, Eastman Co.).

### **Generation of Polyclonal and Monoclonal Antibodies Against MerintA**

For polyclonal antibody production of Tim3, Research Genetics, Inc. performed the peptide synthesis (aa 165-178 of merintA: EQASANIPAPLKPT), coupling with KLH, immunization and bleeding of rabbits. Bleeds were then tested against merintA exogenously expressed in mammalian cells.

For monoclonal antibody production of 7E1, mice were injected six times every 14 days with approximately 50 $\mu$ g of GST purified and eluted protein. After a final boost the best responder was sacrificed, the spleen was removed and it was fused to SP2 myeloma cells. Ms. Nicole Smith carried out the fusion and the selection as previously described (Gonzalez-Agosti *et al.*, 1996). The class and subclass of the monoclonal, merintA specific antibody 7E1 were determined using an isotyping kit (Amersham Pharmacia Biotech). For preabsorption experiments, antibodies were incubated with 1-5 $\mu$ g of specific fusion protein or GST alone as a control.

### **Affinity Elution of Polyclonal Antibodies**

Naturally circulating antibodies in the collected serum of a rabbit produce background bands during Western blot analysis. To circumvent this problem, the specifically raised antibody can be purified by an affinity elution protocol. Bacterially expressed and

purified proteins or cell lysates that overexpress the antigen were run on a single-well comb polyacrylamide gel, blotted onto nitrocellulose and stained with 10% Ponceau-S (Sigma) for total protein. The protein band of interest was marked with a needle and the membrane was blocked with 3% BSA/PBS at room temperature for one hour. In turn, the membrane was hybridized overnight at room temperature with the anti-serum to be purified (e.g. Tim3), which was diluted 1:20 in 3% BSA/PBS. Membranes were then washed three times at room temperature for five minutes each with 3% BSA/PBS, 0.1% SDS, 0.05% NP40, two times with 3% BSA/PBS and once with PBS only. The part of the membrane containing the bound antibody of interest was cut into small pieces and washed twice with distilled water. The antibody was then eluted with 0.2M glycine-HCl (pH 2.8). Physiological conditions were reobtained by adding Tris-HCl (pH 8.0) to a final concentration of 0.15M. Membrane debris was removed by spinning the eluted antibody at 14,000x g and 4° C for 30 minutes before the affinity-eluted antibody was tested against an appropriate fusion construct or cell lysate by Western blot analysis.

### **Cell Culture of Mammalian Cells**

Mammalian cells were cultured at 37°C with a 10% CO<sub>2</sub>-concentration. Many cell lines, including Cos-7 (monkey kidney fibroblast), F293 (adult human fibroblast), G238 (glioma), H237 (glioma), HeLa (adenocarcinoma), Met5A (mesothelioma), RD135 (adult human fibroblast), MRC-5 (fetal human fibroblast) and 293T (embryonic kidney), were available in the laboratory and maintained in EMEM or DMEM (GibcoBRL) supplemented with 10% fetal calf serum (FCS) and 1% penicillin/streptomycin (GibcoBRL) as recommended by the American Type Culture Collection (ATCC). Breast cancer cell lines were obtained from the Cancer Center, Massachusetts General Hospital and normal breast epithelial cell lines were obtained from ATCC. These lines were maintained as described above. For induction experiments, MCF-7 and MCF-7-ADR cell lines were depleted of estrogen by maintenance in estrogen-free medium (phenol red deficient DMEM and 10% charcoal dextran treated fetal calf serum) for 3 days. Cells were then fed with estrogen-free medium supplemented with 10nM or 100nM  $\beta$ -estradiol (Sigma) and harvested at

various time points. For experiments with cycloheximide, cells were incubated with 10 $\mu$ g/ml cycloheximide (Calbiochem) for 30 minutes before inducing with  $\beta$ -estradiol.

Human primary meningioma cells were cultured as described (Gonzalez-Agosti *et al.*, 1996). CAD cells (mouse neural cells) were obtained from Dr. Xandra Breakefield, Massachusetts General Hospital, and cultured in DMEM-12F as described (Hewett *et al.*, 2000).

### **Transfection of Mammalian Cells**

To express FLAG-tagged merlin, the FLAG-tag (DYKDDDDK) was engineered into the expression vector pcDNA3 driven by the CMV promoter (Invitrogen) as previously described (Xu L. *et al.*, 1998). To generate 5'-tagged merlin expression constructs, full-length merlin isoforms 1 and 2 were PCR-amplified and ligated into the *Bam*HI and *Eco*RI sites of pcDNA3/5'F. The integrity of the entire sequence, including the junction region between the FLAG-epitope and the merlin coding sequence, was confirmed by DNA sequencing. Similarly, both isoforms of merlin were cloned into pEGFP-N1 (Clontech) and expressed as a GFP-fusion protein. All these expression constructs were available in the laboratory.

To express HA-tagged merintA (A4: aa 1-178), the full-length sequence was PCR-amplified and ligated into the *Bam*HI and *Not*I of pcDNA3 (no FLAG). The sense primer was engineered to have an HA-tag (YPYDVPDYA) between the *Bam*HI restriction site and the merintA. The integrity of the entire sequence, including the junction region between the HA-epitope and the merintA coding sequence, was confirmed by DNA sequencing.

CAD (Cath a-differentiated) cells, Cos-7 cells and 293T cells, were transfected using LipofectAMINE 2,000 (GibcoBRL) according to manufacture's recommendations. Small (immunocytochemistry), medium (e.g. cell fraction assay) and large scale (e.g. affinity binding assay) transfections were performed and the large-scale transfection is described here. Amounts of the reagents were adjusted according to scale. The day before transfection, cells were trypsinized, counted and seeded in a 15cm plate to obtain approximately 85% confluent cells on the day of transfection (approximately

40% in serum free media for cells subjected to immunocytochemistry). First, DNA (<10 $\mu$ g) and LipofectAMINE (<56 $\mu$ l) were diluted separately in 1.4ml media (without serum or antibiotics). Next, the two dilutions were combined and incubated at room temperature for 30 minutes to allow the formation of DNA-LipofectAMINE complexes. Meanwhile, the cells were washed with PBS and new media was added. The DNA-LipofectAMINE complexes were then slowly added to the cells and incubated for 12 to 48 hours.

### **Preparation of Cell Lysates from Mammalian Cells**

To make lysates, tissue cultured cells were washed twice in PBS, scraped and pelleted by centrifugation and cell pellets were resuspended in lysis buffer as indicated. After samples were lysed at 4°C for 30 minutes they were centrifuged at 14,000x g and 4°C for 30 minutes. Protein concentrations of the supernatants were measured using the DC protein assay system (BioRad). In this assay, the protein concentration is proportional to a color reaction that can be quantified by spectrometry.

### **Preparation of Rat Kidney Cytosol**

Inner stripe cytosol preparations of kidneys were performed as described (Breton *et al.*, 2000). Dr. Vladimir Marshansky anesthetized rats and perfused them with cold PBS for 2 minutes to remove blood. The inner stripe of the kidney was separated under a dissecting microscope, and pieces (approximately 0.4g) were homogenized in 2ml of buffer H (1mM EDTA, 0.25M sucrose, 10mM Tris, pH 7.4, protease inhibitor cocktail: 1x Complete™, Roche) using a Wheaton glass potter fitted with a Teflon pestle. The cytosol was obtained by centrifugation of the homogenate at 100,000x g for 1 hour and total protein concentration was determined with the Pierce BCA protein assay.

### **Affinity Precipitation Assays and Peptide Competition Assay**

This assay was performed under four different aspects: (A) Differential binding of merlin isoforms to NHE-RF was analyzed. (B) The interaction of NHE-RF, mediated by the PDZ-binding motif DTAL, to the H<sup>+</sup> ATPase was confirmed. (C) The

interaction of merlin and merintA, identified by the yeast two-hybrid system, was validated. (D) The predicted interaction of merintA and Grb2 was confirmed.

(A) *Differential binding of merlin isoforms to NHE-RF*. The breast cancer cells, ZR-75-B, were lysed in buffer Brij (1% Brij 96, 1mM EDTA, 30% glycerol, 150mM NaCl, 50mM Tris, pH 8.0 and protease inhibitor cocktail: 1x Complete™, Roche). The cell lysates were incubated with 600pmol of GST-merlin fusion proteins or GST alone immobilized on glutathione Sepharose 4B beads at 4°C for 16 hours. Subsequently, the beads were washed extensively with PBS containing pefabloc (0.5mg/ml) to remove proteins that bind non-specifically. Proteins were eluted with sample buffer (1x GSD), subjected to 10% SDS-gel electrophoresis and immunoblotted with IC270 serum (1:1,000). In some experiments, GST-merlin immobilized on beads was preincubated in buffer Brij with 50µg/ml phosphatidyl serine (Sigma) or in phosphatidylinositol 4,5-bisphosphate (Sigma) at 4°C for 1 hour. Then, GST-merlin was incubated with cell lysates including 50µg/ml phosphatidyl serine (Sigma) or in phosphatidylinositol 4,5-bisphosphate (Sigma) at 4°C for 16 hours. Each phospholipid was dissolved in distilled water to a final concentration of 1mg/ml and sonicated three times for 10 seconds.

Dr. C. Gonzalez-Agosti performed the reciprocal experiment in the absence of phospholipids. Cos-7 cells expressing FLAG-tagged merlin isoforms 1 or 2 were lysed in buffer NP40 (150mM NaCl, 0.5% Nonidet P40, United States Biochemical, 50mM Tris, pH 8.0, protease inhibitor cocktail: 1x Complete™, Roche). These lysates were incubated with 600pmol of GST-NHE-RF fusion protein or GST alone immobilized on glutathione Sepharose 4B beads at 4°C for 16 hours. The beads were washed and proteins were eluted as described above. SDS-gel electrophoresis (7.5%) separated the proteins that were immunoblotted with the anti-FLAG antibody M2 (1:2,000).

(B) *The interaction of NHE-RF, mediated by the PDZ-binding motif DTAL, to the H<sup>+</sup> ATPase*. Inner stripe cytosol of rat kidneys (0.4 mg of total protein) was incubated with 600pmol of GST-NHE-RF or GST alone bound to glutathione Sepharose 4B beads at 4°C for 16 hours. The beads were washed and proteins were eluted as described above. SDS-gel electrophoresis (12%) separated the proteins that were immunoblotted with either the B1 subunit or the E subunit antibodies of the H<sup>+</sup>

ATPase as described above (Western blot analysis). For the competition assay, peptides deriving from the B1 subunit (PQDTEADTAL) or the B2 subunit (EFYPRDSAKH) were dissolved in distilled water. Either peptide (300mg) was preincubated with the GST-NHE-RF bound to beads at 4°C for 1 hour. Then, the cytosol was supplemented with additional 300mg of peptide, added to the beads and incubated at 4°C for 16 hours. Proteins bound to beads were then handled as described above.

(C) *The interaction of merlin and merintA.* Cos-7 cells expressing HA-tagged merintA (aa 13-178) were lysed in buffer NP40 (150mM NaCl, 0.1% Nonidet P40, United States Biochemical, 50mM Tris, pH 8.0, protease inhibitor cocktail: 1x Complete™, Roche). These lysates were incubated with 600pmol of GST-merlin fusion proteins or GST alone immobilized on glutathione Sepharose 4B beads at 4°C for 16 hours. Beads were washed and proteins were eluted as described above. SDS-gel electrophoresis (10%) separated the proteins that were immunoblotted with an anti-HA antibody (1:35) kindly provided by Dr. Ed Harlow, Massachusetts General Hospital.

For the reciprocal experiment, 293T cells expressing FLAG-tagged merlin isoforms 1 or 2 were lysed in buffer NP40 (150mM NaCl, 0.5% Nonidet P40, United States Biochemical, 50mM Tris, pH 8.0, protease inhibitor cocktail: 1x Complete™, Roche). These lysates were incubated with 600pmol of GST-merintA or with GST alone immobilized on glutathione Sepharose 4B beads at 4°C for 16 hours. The beads were washed and proteins were eluted as described above. SDS-gel electrophoresis (7.5%) separated the proteins that were immunoblotted with the anti-FLAG antibody M2 (1:2,000).

(D) *The predicted interaction of merintA and Grb2.* CAD cells were lysed in buffer NP40 (150mM NaCl, 0.5% Nonidet P40, United States Biochemical, 50mM Tris, pH 8.0 with a protease inhibitor cocktail: 1x Complete™, Roche). These lysates were incubated with 600pmol of GST-merintA fusion proteins or GST alone immobilized on glutathione Sepharose 4B beads at 4°C for 16 hours. Beads were washed and proteins were eluted as described above. SDS-gel electrophoresis (12%) separated the proteins that were immunoblotted with the anti-Grb2 antibody sc-255 (1:1,000).

### Immunoprecipitation Assays

This assay was performed under three different aspects: (A) The interaction of NHE-RF, mediated by the PDZ-binding motif DTAL, to the H<sup>+</sup> ATPase was confirmed. (B) Antibodies against merintA were validated. (C) The interaction of merlin and merintA, identified by the yeast two-hybrid system, was validated.

(A) *The interaction of NHE-RF, mediated by the PDZ-binding motif DTAL, to the H<sup>+</sup> ATPase.* Rat kidney cytosol lysates were prepared as for affinity precipitation assays, except that the entire cortex and outer medulla was taken to obtain cytosol, which ensured adequate amounts of NHE-RF. To preclear samples, they were incubating with normal rabbit serum and protein A-agarose beads (Roche). NHE-RF was immunoprecipitated using IC270 serum and protein A-agarose beads. The samples were washed extensively with PBS containing pefabloc (0.5mg/ml) and eluted by boiling in sample buffer (1x GSD). The immunoprecipitates were subjected to SDS-polyacrylamide gel electrophoresis, blotted and probed with biotinylated IC270 (1:50) followed by horseradish peroxidase conjugated streptavidin (see biotinylation of antibodies and immunoblotting using biotinylated primary antibodies). The H<sup>+</sup> ATPase was detected with the monoclonal E subunit antibody (E11) as described above (Western blot analysis).

(B) *Validation of merintA antibodies.* CAD cells were lysed in buffer NP40 (150mM NaCl, 0.5% Nonidet P40, United States Biochemical, 50mM Tris, pH 8.0, protease inhibitor cocktail: 1x Complete™, Roche). To preclear lysates, they were incubating with normal rabbit serum and protein A-agarose beads (Roche). MerintA was immunoprecipitated using Tim3 serum and protein A-agarose beads. The samples were washed extensively with PBS containing pefabloc (0.5mg/ml) and eluted by boiling in sample buffer (1x GSD). The immunoprecipitates were subjected to SDS-polyacrylamide gel electrophoresis and immunoblotted with the anti-merintA antibody 7E1 (1:500).

(C) *The interaction of merlin and merintA.* CAD cells overexpressing FLAG-merlin isoform 2 were lysed in buffer NP40 (150mM NaCl, 0.5% Nonidet P40, United States Biochemical, 50mM Tris, pH 8.0, protease inhibitor cocktail: 1x Complete™,



Roche). To preclear lysates, they were incubated with normal rabbit serum and protein A-agarose beads (Roche). Merlin was immunoprecipitated using N21 serum and protein A-agarose beads. The samples were washed extensively with PBS containing pefabloc (0.5mg/ml) and eluted by boiling in sample buffer (1x GSD). The immunoprecipitates were subjected to SDS-polyacrylamide gel electrophoresis and immunoblotted with the anti-merlin antibody 1C4 (1:500) and the anti-merintA antibody 7E1 (1:500).

### **Biotinylation of Antibodies**

The polyclonal NHE-RF antibody, IC270, was biotinylated to detect the ~50kD protein NHE-RF in immunoprecipitates. Towards this end, IC270 serum was affinity-eluted as described above (affinity elution of polyclonal antibodies) and dialyzed against buffer NH (50mM NaCl, 50mM NaHCO<sub>3</sub>, pH 8.5) to remove free amines. A freshly prepared working stock of NHS-LC-biotin (Pierce, 10mg/ml in dH<sub>2</sub>O) was mixed with the dialyzed antibody at a final concentration of 0.1mg/ml and incubated at 4°C for 60 minutes. The reaction was quenched by adding 1/20th volume of buffer GT (1M glycine, 1M Tris, pH 6.8) to the sample. In a final step, the buffer was exchanged into PBS containing 0.02% NaN<sub>3</sub> using NAP 10 columns (Amersham Pharmacia Biotech).

### **Immunoblotting Using Biotinylated Primary Antibodies**

SDS-polyacrylamide gel electrophoresis separated immunoprecipitated antigens, which were then transferred to nitrocellulose membranes. After blocking membranes in 10% non-fat dry milk diluted in TBST, they were incubated with biotinylated primary antibody diluted in TBST containing 1% milk for 2 hours. After the membranes were washed, streptavidin-horseradish peroxidase (Amersham Pharmacia Biotech) was diluted 1:1,000 in TBST and applied for 1 hour. The membranes were washed again with TBST, incubated one minute in ECL 1 and 2 (Amersham Pharmacia Biotech) and exposed to X-Omat AR film (Kodak, Eastman Co.).

### **Soluble and Insoluble Cell Fraction Assay**

Cell fractionations were performed as previously described (Hartwig, 1992). Here, CAD cells were plated ( $1.75 \times 10^6$ /10cm plate), cultured for 16 hours and transfected with both full-length HA-merintA (A4) and full-length FLAG-merlin isoform 2. After 24 hours, cells were rinsed once with PBS and then incubated in 0.75% Triton X-100/PHEM buffer (60mM PIPES, 25mM HEPES, 2mM MgCl<sub>2</sub>, 10mM EGTA, pH 6.9 with 1 $\mu$ M phalloidin and a protease inhibitor cocktail: 1x Complete™, Roche) at 37°C for two minutes. Lysed cells were harvested with a rubber policeman and centrifuged 14,000x g and 4°C for 15 minutes to separate the soluble and insoluble fractions. The detergent-soluble material was precipitated with 85% acetone at -20°C for 16 hours and recovered by centrifugation at 14,000x g and 4°C for 15 minutes. Detergent-insoluble material was scraped in PBS containing protease inhibitors and centrifuged at 14,000x g and 4°C for 15 minutes. All samples were resuspended in the same volume of sample buffer (1x GSD), subjected to 12% SDS-polyacrylamide gel electrophoresis and examined by Western blot analysis.

### **Immunocytochemistry**

Immunofluorescence analysis of tissue culture cells was performed as previously described (Gonzalez-Agosti *et al.*, 1996). In summary, cells were grown on glass coverslips, fixed in 4% paraformaldehyde in PBS at 37°C for 15 minutes, washed three times with PBS and permeabilized with 0.1% NP40/PBS at room temperature for 15 minutes. To reduce background staining, cells were blocked with 10% normal goat serum (Vector Laboratories) in PBS at 37°C for 45 minutes. Primary antibodies were incubated at 37°C for 1 hour while secondary antibodies were incubated at 37°C for 30 minutes. All antibodies were diluted in 0.1% BSA/PBS. Coverslips were washed extensively between antibody incubations and mounted on glass slides using ProLong (Molecular Probes) as recommended by the manufacturer. Cells were examined on a Nikon fluorescence microscope using 40x 1.3 N.A. and 60x 1.4 N.A. objectives before images were recorded on Kodak Tri-X-Pan 400 (Kodak, Eastman Co.). Confocal images

were obtained with a Nikon TE 300 microscope and the BioRad MRC 100 laser confocal imaging system.

To stain NHE-RF in the breast cancer cells, MCF-7, the primary antibody IC270, was affinity-eluted and used at a dilution of 1:2. The secondary goat anti-rabbit antibody was FITC conjugated. CAD cells were transfected with full-length HA-merintA (A4) and GFP-merlin isoform 1 or 2, fixed, permeabilized and blocked as described above. As primary antibodies, 12CA5 (HA-tag, Roche) was used at a dilution of 1:200 to visualize exogenous merintA followed by the secondary rhodamine conjugated anti-mouse antibodies. Untransfected CAD cells were stained with the monoclonal antibody 7E1 at a dilution of 1:10 to visualize endogenous merintA. Secondary antibodies (rhodamine conjugated to goat anti-mouse antibodies) were used at dilutions recommended by the manufacturer. To visualize F-actin, rhodamine-coupled phalloidin (1:1,000) was incubated at 37°C for 30 minutes after the incubation of primary antibodies. To visualize nuclei, Hoechst 33342 (10µg/ml) was incubated at 37°C for 30 minutes after the incubation of primary antibodies or rhodamine-coupled phalloidin.

### **Immunostaining of NHE-RF and H<sup>+</sup> ATPase in the Kidney**

Rat kidney sections were stained for NHE-RF and the H<sup>+</sup> ATPase (Breton *et al.*, 2000). Male rats were anesthetized and kidneys were fixed by perfusion for 5 minutes through the abdominal aorta with a fixing solution (4% paraformaldehyde, 10mM sodium periodate, 70mM lysine (PLP) and 5% sucrose). Kidneys were separated from the animal, sliced and further fixed by immersion in fixing solution for 6 hours. For the preparation of 4µm sections, kidneys were washed in PBS and cryoprotected in 30% sucrose. Tissues were then sectioned with a Reichert Frigocut microtome using disposable knives. Kidney sections were then picked up on Fisher Superfrost Plus slides (Fisher Scientific), rinsed in PBS for 10 minutes and treated with 1% SDS for 5 minutes. The latter step augments antigenicity of many proteins as described previously (Brown *et al.*, 1996). After three additional washes in PBS, 5 minutes each, sections were incubated in 1% BSA/PBS for 20 minutes to reduce background staining.

The primary anti-NHE-RF antibody (affinity-eluted IC270; 1:4) was incubated at room temperature for 2 hours. After washing twice for 5 minutes in high salt PBS (PBS containing 2.7% NaCl) to reduce nonspecific staining and one further washing in normal PBS for 5 minutes, CY3 conjugated secondary anti-rabbit antibodies (1:800) were applied for 60 minutes. For double staining, sections were incubated for 2 hours with an affinity purified chicken polyclonal antibody against the E subunit of the H<sup>+</sup> ATPase (1:40). Next, samples were washed as before and FITC-coupled secondary anti-chicken antibodies (1:200) were applied for 60 minutes. Finally, sections were washed three more times and mounted with Vectashield anti-fading solution (Vector Labs). Control incubations were performed with IC270 that was preincubated with the GST-NHE-RF fusion protein (at a final concentration of 0.2 mg/ml) at room temperature for 1 hour. Samples were examined using a Nikon Eclipse 800 microscope equipped with specific CY3 and FITC filter combinations and images were captured on Ektachrome 400 Elite film (Kodak, Eastman Co.). CY3 emission appears yellow using the specific CY3 filter combination and analog photography (see Figure 9A and C).

### **Immunostaining of NHE-RF in Breast Carcinomas**

Formalin-fixed, paraffin-embedded sections of eighteen invasive breast carcinomas were retrieved from the files of the Department of Pathology, Massachusetts General Hospital, Boston. NHE-RF immunohistochemical staining was performed with the affinity-eluted IC270 antibody. In summary, 8 $\mu$ m thick sections of formalin-fixed, paraffin-embedded specimens were deparaffinized, rehydrated and immersed in 0.5% H<sub>2</sub>O<sub>2</sub>/methanol for 20 minutes. Sections were then rehydrated in graded ethanols and microwaved in 0.01M sodium citrate buffer (pH 6.0) for 15 minutes. To reduce non-specific staining, sections were blocked in 10% normal goat serum and 5% milk in 1% BSA/PBS solution. Samples were then incubated with the polyclonal antibody IC270 (affinity-eluted 1:100 in 1% BSA/PBS) at 4°C for 16 hours followed by incubation with biotinylated anti-rabbit secondary antibodies (1:500) at room temperature for 30 minutes. Finally, sections were subjected to standard avidin-biotin complex (ABC) process (Vectastain Elite ABC kit, Vector Laboratories). Diaminobenzidine (DAB) was

used as a chromogen, followed by counterstaining with hematoxylin. Formalin fixed, paraffin-embedded cell pellets from MCF-7 and MCF-7-ADR cell lines were used as controls. The primary antibody was omitted for negative controls. Ms. Tina Glyptis determined the status of primary breast for estrogen (ER) and progesterone (PR) receptors according to standard procedures. In summary, antigen retrieval was achieved by microwaving the sections in Tris buffer (pH 10) for 10 minutes, blocking with normal horse serum and incubating with ER antibodies (1:100; DAKO) or with PR antibodies (1:10; DAKO) at 4°C for 16 hours. Sections were incubated with secondary antibodies (1:200) at room temperature for 45 minutes followed by ABC reaction, visualized with DAB and counterstained with hematoxylin.

### **Electron Microscopy**

Immunogold labelling of merlin and merintA was conducted as previously described (James *et al.*, 2001). CAD cells were plated on coverslips, permeabilized in 0.75% Triton X-100/PHEM buffer (60mM PIPES, 25mM HEPES, 2mM MgCl<sub>2</sub>, 10mM EGTA, pH 6.9 with 1µM phalloidin and a protease inhibitor cocktail: 1x Complete™, Roche) for 2 minutes, and soluble proteins were removed with a PHEM buffer wash. Samples were fixed with 1% glutaraldehyde in PHEM buffer for 10 minutes and reactive aldehydes were blocked with 0.1% NaBH<sub>4</sub> in PHEM buffer. The coverslips containing residual, glass-adherent cytoskeletons were washed with PHEM buffer and treated with 0.1% SDS for 1 minute to augment antigenicity. Cytoskeletons were incubated with primary antibodies (merlin: A19, 1:10; merintA: 7E1, 1:10) in Tris buffer containing 1% BSA (150mM NaCl, 20mM Tris, pH 8.2) at 25°C for 1 hour. After washing three times, coverslips were incubated with goat anti-rabbit IgG-coated 5nm colloidal gold particles (1:20) for merlin staining and with goat anti-mouse IgG-coated 10nm colloidal gold particles (1:20) for merintA staining. Coverslips were washed three more times with 1% BSA in Tris buffer and before being fixed with 1% glutaraldehyde in Tris buffer for 10 minutes. Fixed cytoskeletons were washed extensively with distilled water, frozen rapidly, freeze-dried and rotary-coated with 1.2nm of tantalum-tungsten at 45° and 3.0nm of carbon at 90° without rotation.

Coverslips were analyzed and photographed in a Jeol 1200-EX electron microscope with 100kV accelerating voltage. No gold labelling was found when primary antibodies were omitted or when preimmune IgG was used as a control.

### 3. Results

#### 3.1 Characterization of the Interaction of NHE-RF with Merlin Isoform 1 and 2

The regulatory co-factor for the Na<sup>+</sup>-H<sup>+</sup> exchanger isoform 3 (NHE-RF) was identified as an interacting protein for merlin in the Molecular Neurogenetics Unit at Massachusetts General Hospital and Harvard Medical School, Boston. It was demonstrated that NHE-RF can bind to merlin, moesin and radixin via their conserved amino-terminal regions (Murthy *et al.*, 1998). Furthermore, a number of reports have shown that the binding of ERM proteins to their interactors is suppressed in the native full-length protein (Heiska *et al.*, 1998; Hirao *et al.*, 1996; Matsui *et al.*, 1998). This phenomenon can be explained by the interdomain interactions of the ERM proteins that compete with the ligand binding (Reczek *et al.*, 1998). Recent data from the laboratory of Dr. V. Ramesh demonstrated that merlin isoform 1 can form intra- and intermolecular head-to-tail associations similar to the ERM proteins. In contrast, merlin isoform 2 lacks this property due to the alternatively spliced carboxy-terminus (Gonzalez-Agosti *et al.*, 1999). Therefore, it was tested whether these different conformations of merlin isoforms 1 and 2 correlate with differences in binding with the ligand NHE-RF.

##### 3.1.1 NHE-RF Binds Differentially to Merlin Isoform 1 and 2

Affinity precipitation experiments were performed to investigate the binding of merlin isoforms to NHE-RF *in vitro*. Merlin full-length isoforms 1 and 2, the amino-terminal domain (aa 1-332) and the carboxy-terminal domains of both isoform 1 (aa 340-595) and 2 (aa 340-590) were expressed as GST fusion proteins. GST alone was included in these experiments as a negative control. Equal quantities of these proteins were bound to Sepharose beads and incubated with equal amounts of cell lysates. After extensive washes, the coupled proteins were removed from the beads by boiling in SDS sample buffer before being submitted to Western blot analysis. The membrane was incubated with a specific polyclonal antibody (IC270) to detect NHE-RF that bound to merlin fusion proteins. The results demonstrate that the amino-terminal domain and full-length

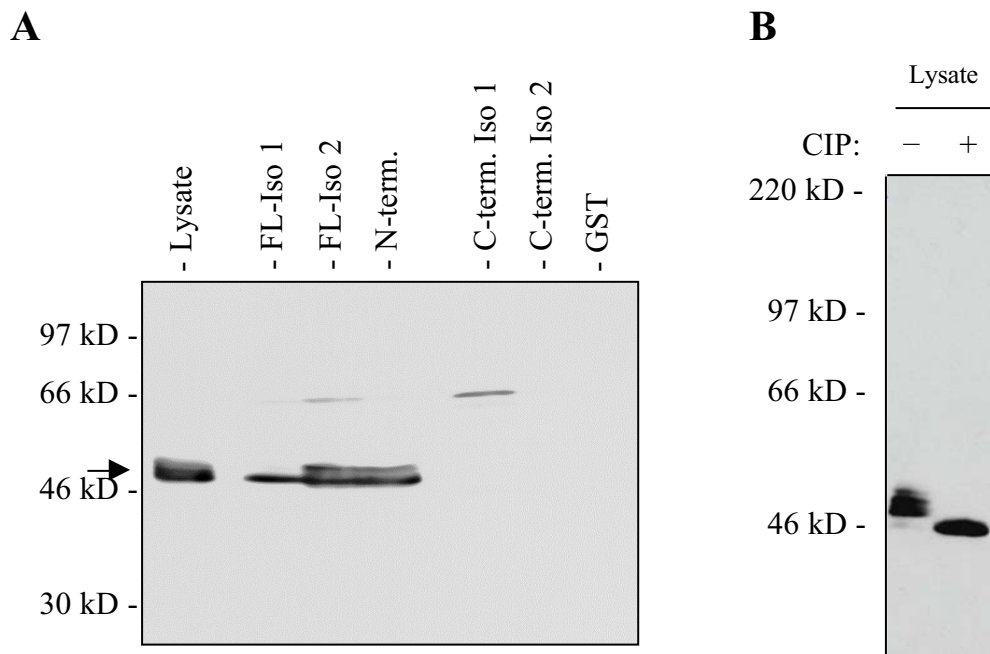


**Figure 5. Binding of NHE-RF to Merlin Isoforms.** Lysate from ZR-75-B cells were incubated with various GST-merlin fusion proteins immobilized on glutathione Sepharose 4B beads. The beads were extensively washed, bound proteins were separated on 10% SDS-PAGE and immunoblotted with an anti-NHE-RF antibody (IC270 serum). The arrow indicates NHE-RF at ~50kD (A). FL-iso 1, full-length isoform 1; FL-iso 2, full-length isoform 2. Lysates from ZR-75-B cells incubated with CIP show that NHE-RF migrates faster than from those not incubated with the phosphatase. Thus, NHE-RF is constitutively phosphorylated (B).

isoform 2 of merlin capture more NHE-RF than full-length isoform 1 of merlin. NHE-RF did not bind to the carboxy-terminal domain of either isoform of merlin or to the GST control protein (Figure 5A). Western blots were stained with Ponceau-S for total proteins before probing with the specific NHE-RF antibody. This staining confirmed that equal amounts of GST fusion proteins and GST alone were bound to the beads in the experiments (data not shown). It is known that NHE-RF is a constitutively phosphorylated protein (Reczek *et al.*, 1997). Treating cell lysates with calf intestinal alkaline phosphatase (CIP) shows that the multiple NHE-RF species collapse to a single band that migrates faster than the lowest species of untreated lysates (Figure 5B). Thus, hypophosphorylated NHE-RF shows no difference in binding to merlin isoforms in contrast to hyperphosphorylated NHE-RF that binds exclusively to merlin isoform 2 (Figure 5A). These results were confirmed by three independent experiments.



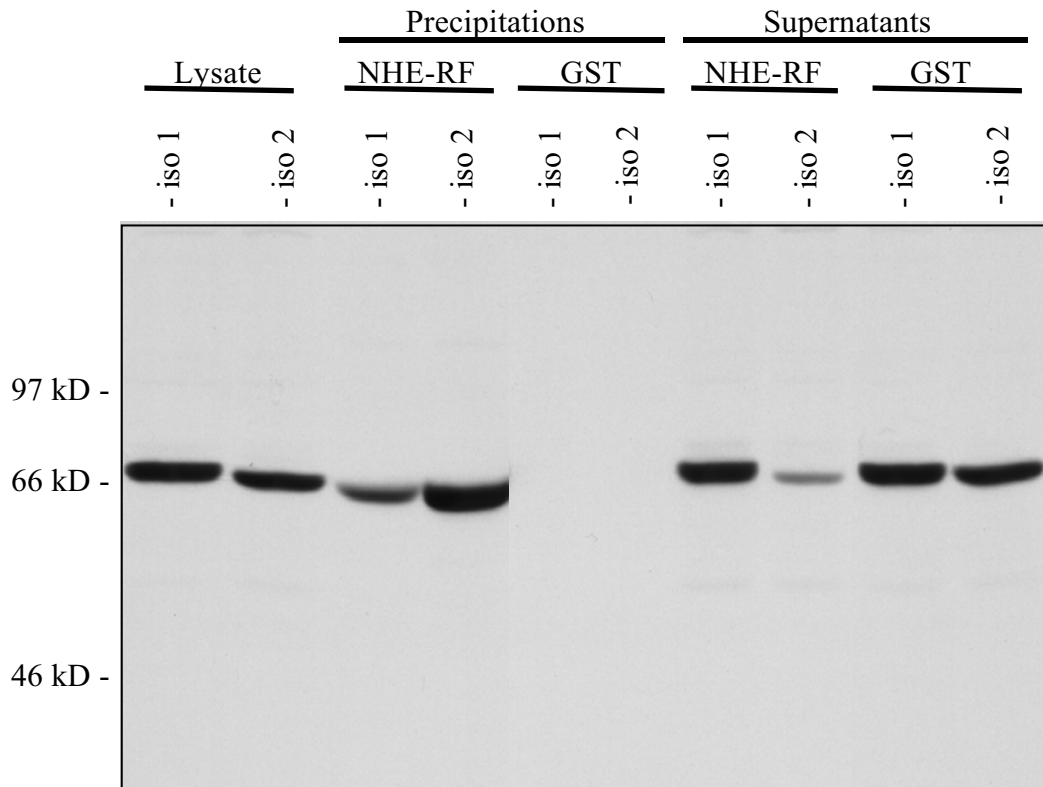


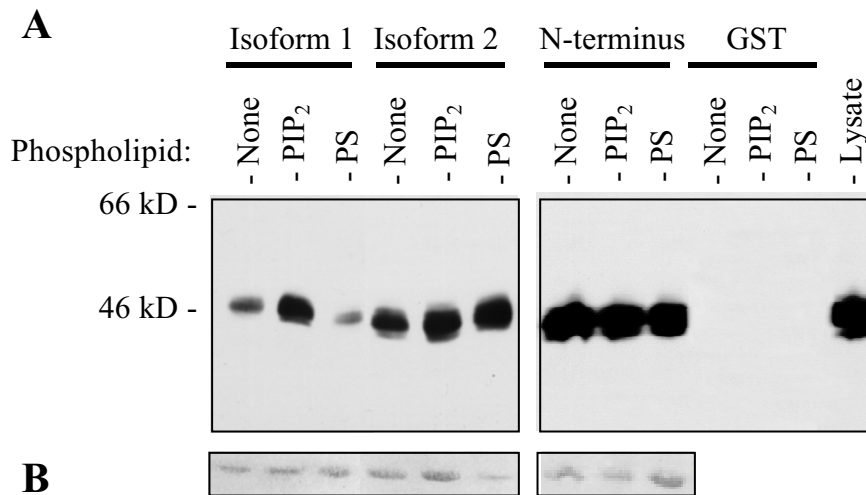
**Figure 6. Binding of Merlin Isoforms 1 and 2 to NHE-RF.** Cos-7 cell lysates expressing either FLAG-tagged merlin isoform 1 or merlin isoform 2 were incubated with GST-NHE-RF fusion protein or GST protein expressed alone (control) immobilized on glutathione Sepharose 4B beads. The beads were extensively washed, and bound proteins were separated on 7.5% SDS-PAGE and immunoblotted with the anti-FLAG monoclonal antibody M2. Lysates from Cos-7 cells expressing merlin isoforms are shown for protein expression level in transfected cells. The supernatants that were not bound to the beads are shown to point out that NHE-RF beads capture more merlin isoform 2 than merlin isoform 1 (From Gonzalez-Agosti *et al.*, 1999).

The reciprocal experiment was conducted in collaboration with Dr. C. Gonzalez-Agosti, a member of the Ramesh laboratory at the time. Here, merlin isoforms 1 and 2 were expressed as FLAG-tagged proteins in Cos-7 cells, which were then utilized in affinity binding assays with GST-NHE-RF fusion protein. The FLAG-tagged merlin isoform proteins were examined by Western blot analysis with an anti-FLAG antibody (M2, Sigma) prior to the affinity binding assay to ensure equal expression. Cell lysates, expressing approximately the same amount of merlin isoform 1 and 2, were then incubated with GST-NHE-RF or GST alone bound to beads. The proteins that precipitated with the beads were again analyzed by Western blot analysis for the presence of merlin with the M2 antibody. These experiments demonstrated that

merlin isoforms expressed in mammalian cells also bind differentially to NHE-RF (Figure 6). Analysis of the supernatants from the affinity binding assay clearly showed more depletion of merlin isoform 2 than isoform 1 confirming that more merlin isoform 2 was precipitated along with NHE-RF (Figure 6). A duplicate set of experiments demonstrated that NHE-RF captured ~4 fold more merlin isoform 2 than isoform 1 as determined by densitometric scanning of the autorads using transmittance analysis (Fluor-S, Multiimager, BioRad). Densitometric scanning was performed on bands deriving from merlin that were not saturated. Thus, values obtained are in a linear range and reflect true differences. Western blots were stained with Ponceau-S for total proteins before probing with the FLAG-antibody. This staining confirmed that equal amounts of GST fusion proteins and GST alone were bound to the beads in the experiments (data not shown). These data are consistent with the distinct intramolecular head-to-tail associations of merlin isoforms. The carboxy-terminus of merlin isoform 1 competes with NHE-RF for the amino-terminal binding site. On the other hand, merlin isoform 2 exists in a constitutively open conformation that allows the binding of the MERM binding protein NHE-RF without competition from the intramolecular association that occurs in merlin isoform 1.

### **3.1.2 Phospholipids Enhance the Binding of NHE-RF to Merlin Isoform 1**

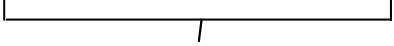
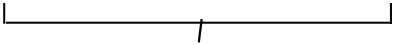
ERM proteins bind to the phospholipids phosphatidylinositol 4-phosphate (PIP) and phosphatidylinositol 4,5-bisphosphate (PIP<sub>2</sub>) (Niggli *et al.*, 1995), and it is believed that this binding evokes conformational changes in these proteins in a manner similar to the regulation of vinculin activity by PIP<sub>2</sub> (Gilmore *et al.*, 1996). Moreover, PIP and PIP<sub>2</sub> enhance the interaction of ERM proteins to their binding partners CD44, ICAM-1 and ICAM-2 while the phospholipids phosphatidyl choline (PC) and phosphatidyl serine (PS) have no effect (Heiska *et al.*, 1998; Hirao *et al.*, 1996). The affinity precipitation assay described above was performed to test if PIP<sub>2</sub> and PS influence the binding of NHE-RF to merlin isoforms. The amount of NHE-RF bound to merlin



**Figure 7. PIP<sub>2</sub> Enhances Binding of NHE-RF to Merlin Isoform 1.** GST-merlin fusion proteins or GST alone were bound to glutathione Sepharose 4B beads and incubated with ZR-75-B cell lysates. In addition, 50 $\mu$ g/ml phosphatidyl 4,5-bisphosphate (PIP<sub>2</sub>) or 50 $\mu$ g/ml phosphatidyl serine (PS) was added to the beads with the cell lysates. The eluted proteins were detected by Western blot analysis using IC270 serum (A). Ponceau-S staining of GST-merlin fusion proteins bound to the beads showing that equal amounts of GST-merlin fusion proteins bound to the beads (B).

isoform 1 significantly increased in the presence of PIP<sub>2</sub> but not in the presence of PS (Figure 7A). The intensity of the bands was quantified by densitometric scanning of the autorads using transmittance analysis (Fluor-S, Multiimager, BioRad). A three-fold increase ( $3.10 \pm 1.04$ ) in binding of NHE-RF to merlin isoform 1 was determined in the presence of PIP<sub>2</sub> compared to binding in the absence of PIP<sub>2</sub> (Table 2). In addition, hyperphosphorylated NHE-RF was captured by merlin isoform 1 in the presence of PIP<sub>2</sub> while this was not seen in the absence of PIP<sub>2</sub> (Figure 5A and 7A). The binding of NHE-RF to either the amino-terminal domain of merlin or merlin isoform 2 ( $1.07 \pm 0.45$ ) was not influenced by PIP<sub>2</sub> (Table 2). The control phospholipid, PS, did not enhance the NHE-RF binding to merlin isoform 1 and did not have an effect on the binding of hyperphosphorylated NHE-RF and merlin isoform 1 (Figure 7A). Western blots were stained again with Ponceau-S for total proteins before probing with the specific antibody and the staining confirmed that equal amounts of GST fusion proteins and GST alone were bound to the beads in the experiments (Figure 7B). These data are in agreement with the model worked out for the ERM proteins (Figure 3) and suggest that merlin isoform 1 may function similarly with respect to intramolecular head-to-tail

associations, its regulation by PIP<sub>2</sub> and the binding to some of its ligands including NHE-RF.

<b>Isoform 1</b>		1	2	3
Area (OD * mm)	without PIP <sub>2</sub>	0.50	0.07	0.54
	with PIP <sub>2</sub>	0.98	0.30	1.78
Increase of binding (ratio)		1.97	4.01	3.33
<b>Average of increase (ratio)</b>				
		<b>3.10</b>		
<b>Isoform 2</b>		1	2	3
Area (OD * mm)	without PIP <sub>2</sub>	1.69	2.56	1.63
	with PIP <sub>2</sub>	1.66	1.74	2.56
Increase of binding (ratio)		0.98	0.68	1.57
<b>Average of increase (ratio)</b>				
		<b>1.08</b>		

**Table 2. Merlin Isoform 1 Binding Increases in the Presence of PIP<sub>2</sub>.** NHE-RF was precipitated with merlin isoform 1 and 2 respectively in three individual experiments. Autorads obtained by Western blot analysis were examined by densitometric scanning using transmittance analysis to quantify the amount of NHE-RF that was recovered.

### 3.2 Isolation and Characterization of NHE-RF Binding Proteins

Defining functions of NHE-RF is/has been of great interest and NHE-RF binding proteins have been sought towards this end. Various proteins that bind NHE-RF and NHE-RF2 have emerged out of a field of intensive study. In particular, mutagenesis studies of the cytoplasmic tail of the  $\beta$ 2-adrenergic receptor have revealed that the optimal binding motif to the first PDZ-domain of NHE-RF is DS/TXL (Hall *et al.*, 1998a). Searching databases for proteins with this binding cassette reveals the three categories receptors, transporters and other proteins, and all of these proteins have the motif at the extreme carboxy-terminus of these proteins (Table 3).

<b>Potential NHE-RF (PDZ-1) Binding Proteins</b>	
<b>Receptors</b>	<b>C-terminal motif</b>
$\beta$ 2-adrenergic receptor	D-S-L-L
Purinerbic P2Y1 receptor	D-T-S-L
Platelet-derived growth factor receptor	D-S-F-L
<b>Transporters</b>	
Cystic fibrosis transmembrane regulator	D-T-R-L
Copper transporter (Menke's disease gene)	D-T-A-L
$H^+$ ATPase, B1 subunit	D-T-A-L
<b>Other Proteins</b>	
Phospholipase C- $\beta$ 1	D-T-P-L
Podocalyxin	D-T-H-L
Kunjin virus-specified protein	D-T-V-L

**Table 3. Potential NHE-RF Binding Proteins.** Database searches reveal a number of proteins that have the PDZ-1 binding cassette of NHE-RF. (Modified from Hall *et al.*, 1998a)

The B1 (56kD) subunit of the proton-pumping ATPase ( $H^+$  ATPase) has the PDZ-binding motif DTAL, which suggests it is a potential binding partner of NHE-RF. Most of the PDZ-1 binding proteins of NHE-RF are transmembrane proteins. In

contrast, the B1  $H^+$  ATPase subunit is part of the  $V_1$  portion of the holo-enzyme and has no membrane-spanning domain. However, it binds to other subunits including those that span the lipid bilayer of the plasma membrane. In addition, a direct binding between the E (31kD) and B1 subunit has been established (Figure 8). Multi-subunit complexes consisting of the  $V_1$  portion of the  $H^+$  ATPase can exist as free, cytosolic entities (Nelson *et al.*, 1999).

The B1 subunit of the  $H^+$  ATPase is expressed in several tissues and high levels are detected in specialized proton-translocating intercalated cells in the kidney. In contrast, the B2 (56kD) subunit, another isoform of the B1 subunit, is expressed in the proximal kidney tubules. Significantly, this B2 subunit has a carboxy-terminal truncation and lacks the terminal DTAL binding motif (Nelson *et al.*, 1992).

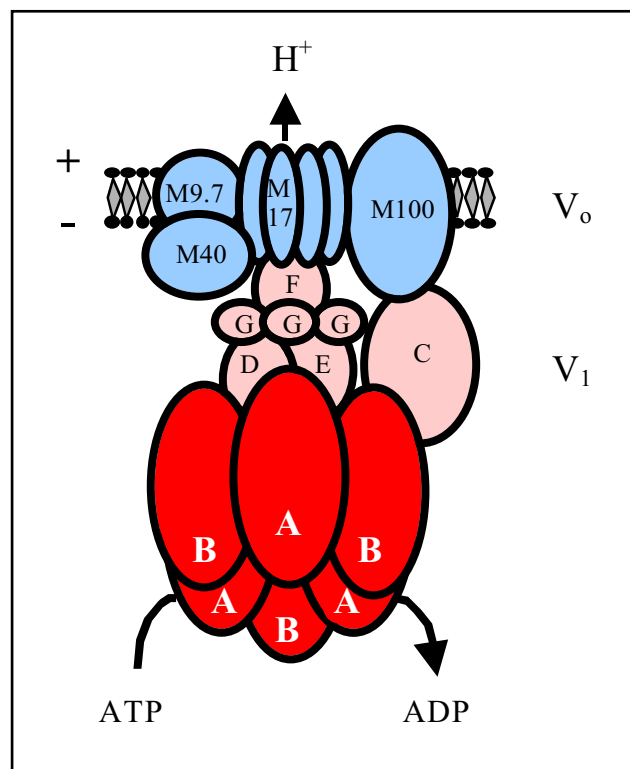


**Figure 8. Diagram of  $H^+$  ATPase.** The  $V_1$  domain catalytic/regulatory subunits is composed of subunits A/B (red) along with connecting subunits C, D, E, F, and G (pink). The  $V_0$  domain (blue) is composed of the  $H^+$  channel forming subunit M17, along with subunits M9.7, M40 and M100. (Modified from Wieczorek *et al.*, 1999).

In the collecting tubules of the kidney cortex, intercalated cells are known to actively transport and secrete hydrogen ions against high concentration gradients, thus modulating the acid-base balance of the body. These intercalated cells show an apical, basolateral, diffuse, or bipolar  $H^+$  ATPase localization that suggests a complex

regulation of expression and localization at the cell surface (Brown *et al.*, 1988a). A subpopulation of intercalated cells, the A-cells, secrete protons into the tubule lumen and always have the H<sup>+</sup> ATPase at their apical pole while the antiporter Cl<sup>-</sup>/HCO<sub>3</sub><sup>-</sup> (AE1) is at their basolateral pole (Alper *et al.*, 1989). In other intercalated cells, the B-cells, the H<sup>+</sup> ATPase can be apical, basolateral, or bipolar while AE1 is not detectable in either plasma membrane domain (Sabolic *et al.*, 1997).

### 3.2.1 NHE-RF Co-localizes with the H<sup>+</sup> ATPase

Previous studies have pinpointed NHE3 and NHE-RF to the proximal tubules in the kidney: Weinman *et al.* (1995) showed that NHE-RF inhibits NHE3 in a cAMP-dependent protein kinase A (PKA) dependent manner in the renal proximal tubule brush border membrane. Biemesderfer *et al.* (1997) showed that NHE3 is localized in proximal tubules by immunohistochemical studies. Thus, one expects NHE-RF to localize to the proximal tubules, while no information was available of NHE-RF in intercalated cells.

In this study, NHE-RF localization was examined in the kidney to test if there is an overlapping pattern with the H<sup>+</sup> ATPase. Hence, the specific, polyclonal antibody (IC270) was employed on fixed cryostat sections. These immunohistochemical studies were performed in collaboration with Drs. Sylvie Breton and Dennis Brown from the Renal Unit at Massachusetts General Hospital, Boston. As expected, the greatest amount of NHE-RF was detected in all proximal tubule segments. Furthermore, NHE-RF was detected in some cells of the cortical collecting ducts and connecting segments (Figure 9A and C). Some cells showed distinct basolateral staining (Figure 9A) while others showed a more diffuse cytoplasmic staining (Figure 9C), and yet others showed apical staining (Figure 9C). Thus, the extent and intracellular location of NHE-RF was variable in these cells. Double incubations using a chicken polyclonal antibody against the E (31kD) subunit of the H<sup>+</sup> ATPase identified these cells as intercalated cells of the collecting tubules in the kidney cortex (Figure 9B and D). Dr. Dennis Brown and colleagues had previously shown that the three major subunits of the cytoplasmic

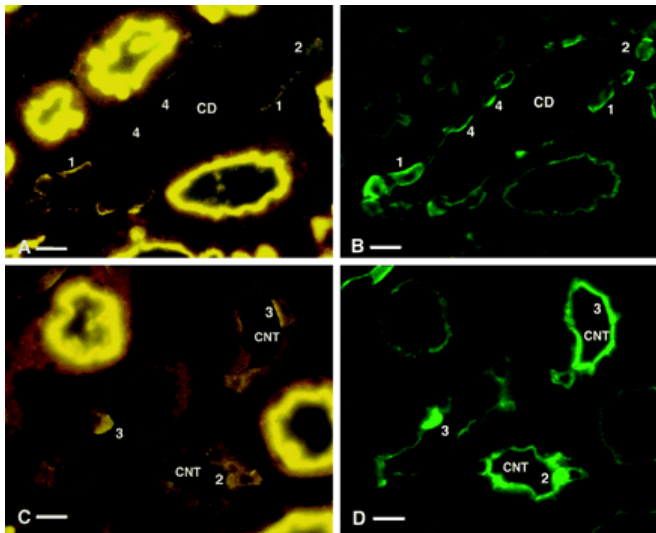


**Figure 9. NHE-RF (A and C) and the E (31kD) Subunit of the H<sup>+</sup> ATPase (B and D) Colocalize in Double Stained Sections of Rat Kidney Cortex.**

The brush border is strongly stained in all proximal tubules. Some cells of the collecting ducts (CD) and connecting segments (CNT) are also stained. Different patterns of NHE-RF staining are detected, and the staining overlaps with that of the H<sup>+</sup> ATPase in intercalated cells. Some cells have basolateral staining (1), some have diffuse cytoplasmic staining (2), some

have apical staining (3) and others have little or no NHE-RF staining but show apical H<sup>+</sup> ATPase staining (4). In connecting segments (CNT), all cells have strong H<sup>+</sup> ATPase staining, as described previously (Brown *et al.*, 1988b), but only a few of these are clearly NHE-RF positive. The staining in A and C, which represent single exposures of the NHE-RF staining, appears yellow because of the use of a highly specific filter combination used for the CY3 fluorophore. CY3 emission is yellow with filter combination used. Bar, 15 $\mu$ m. (From Breton *et al.*, 2000).

domain of this enzyme co-localize in intercalated cells. Consequently, the E subunit is a reliable marker for the entire cytoplasmic domain of the H<sup>+</sup> ATPase and contains the B (56kD) subunit in intercalated cells (Brown *et al.*, 1988b). Here, NHE-RF co-localized with the H<sup>+</sup> ATPase in intercalated cells in these double-stained sections supporting the idea that these two proteins can interact, possibly through the PDZ-domain binding motif. However, some intercalated cells contain the H<sup>+</sup> ATPase but do not express detectable levels of NHE-RF (Figure 9A<sub>4</sub>).

An anti-AE1 antibody that labels only A-cells (Alper *et al.*, 1989) was used in conjunction with the anti-NHE-RF antibody to distinguish between A- and B-intercalated cells. All cells with distinct apical, basolateral or diffuse NHE-RF localization were AE1 negative indicating that these intercalated cells are B-cells (data not shown, see appendix: Breton *et al.*, 2000, Figure 2). In addition, NHE-RF was not detected in A-intercalated cells that are only found in the inner stripe of the outer medulla (data not shown). Thus, NHE-RF is expressed with variable intracellular localization patterns in B-intercalated cells and overlaps with that of the H<sup>+</sup> ATPase in every individual B-cell in the cortical collecting duct and connecting segment.



In proximal tubules, the H<sup>+</sup> ATPase staining was concentrated in a tight subapical band at the base of the brush border. This subapical domain did not contain detectable levels of NHE-RF. As predicted from the location of NHE3 (Biemesderfer *et al.*, 1997; Weinman *et al.*, 1995) and in contrast to the H<sup>+</sup> ATPase, NHE-RF was detected in the brush border. The basolateral domain of proximal tubules showed no detectable levels of NHE-RF (data not shown, see appendix: Breton *et al.*, 2000, Figure 3). It is of interest to note that these cells that show no colocalization of NHE-RF are known to express the carboxy-terminally truncated H<sup>+</sup> ATPase B2 isoform, which lacks the DTAL PDZ-binding motif (Nelson *et al.*, 1992).

The specificity of the obtained staining data was confirmed by preincubating the NHE-RF antibody with the immunogen (GST-NHE-RF fusion protein). Sections were stained in parallel with normal and preabsorbed NHE-RF antibodies. The staining in the proximal tubule as well as in the apical, basolateral and bipolar intercalated cells was abolished upon incubation with preabsorbed NHE-RF antibodies while staining with the normal NHE-RF antibody was reproducible (data not shown, see appendix: Breton *et al.*, 2000, Figure 4). Hence, the staining data obtained of NHE-RF reflect the true localization of NHE-RF.

### **3.2.2 Soluble H<sup>+</sup> ATPase Complexes bind to NHE-RF *In Vitro***

The localization of NHE-RF and the H<sup>+</sup> ATPase support the hypothesis that these two proteins can interact through the PDZ-domain binding motif. To test the physical interaction of these proteins, affinity precipitation experiments were performed in collaboration with Dr. Vladimir Marshansky, a member of Dr. Dennis Brown's laboratory. Equal quantities of GST-NHE-RF and GST alone were bound to Sepharose beads and incubated with an equal amount of renal medullary cytosol to extract potential binding proteins. After extensive washes, the coupled proteins were removed from the beads by boiling and detected by Western blot analysis using specific antibodies directed against the B1 (56kD) and E (31kD) subunits. The results demonstrate that both the B1 and the E subunits of the H<sup>+</sup> ATPase were present in the affinity precipitates. Little or no H<sup>+</sup> ATPase subunits bound to the negative control

GST alone demonstrating the specificity of the NHE-RF/H<sup>+</sup> ATPase association (Figure 10A).

Next, competition experiments were performed to investigate the importance of the B1 subunit PDZ-binding motif for the association with NHE-RF. Carboxy-terminal peptides deriving from the B1 subunit, which contain the motif DTAL (PQDTEADTAL) or from the B2 subunit, which lack the motif DTAL (EFYPRDSAKH) were incubated with the affinity beads (GST-NHE-RF) prior to adding equal amounts of kidney cytosol. The peptide derived from the B1 subunit abrogated the interaction of NHE-RF and the H<sup>+</sup> ATPase completely while the peptide derived the B2 subunit had no effect on the association (Figure 10B). These data suggest that NHE-RF binds directly to the B1 subunit through the PDZ-binding motif. Furthermore, the E subunit precipitates in concert with the B1 subunit supporting earlier studies that suggest this subunit is a reliable marker for the entire cytoplasmic domain of the H<sup>+</sup> ATPase (Brown *et al.*, 1988b).

### 3.2.3 NHE-RF and the H<sup>+</sup> ATPase Associate *In Vivo*

To examine if this association also takes place *in vivo*, co-immunoprecipitation experiments were conducted. However, NHE-RF was first immunoprecipitated to test if the antibody IC270 can be used for these experiments. Once the protocol for immunoprecipitating NHE-RF was established, co-immunoprecipitations of NHE-RF and H<sup>+</sup> ATPase were attempted.

NHE-RF and the immunoglobulin heavy chain migrate at the same level (~50kD) and detection of NHE-RF is obscured when polyclonal rabbit antibodies are employed for immunoprecipitation followed by immunodetection. To overcome this problem a strategy had to be developed to ensure the integrity of the NHE-RF immunoprecipitates. Using biotinylated primary antibodies to probe immunoblots of immunoprecipitates, followed by horseradish peroxidase-conjugated streptavidin results in little or no background staining caused by the immunoglobulin heavy chain and yet does not reduce the sensitivity or specificity of the primary antibody

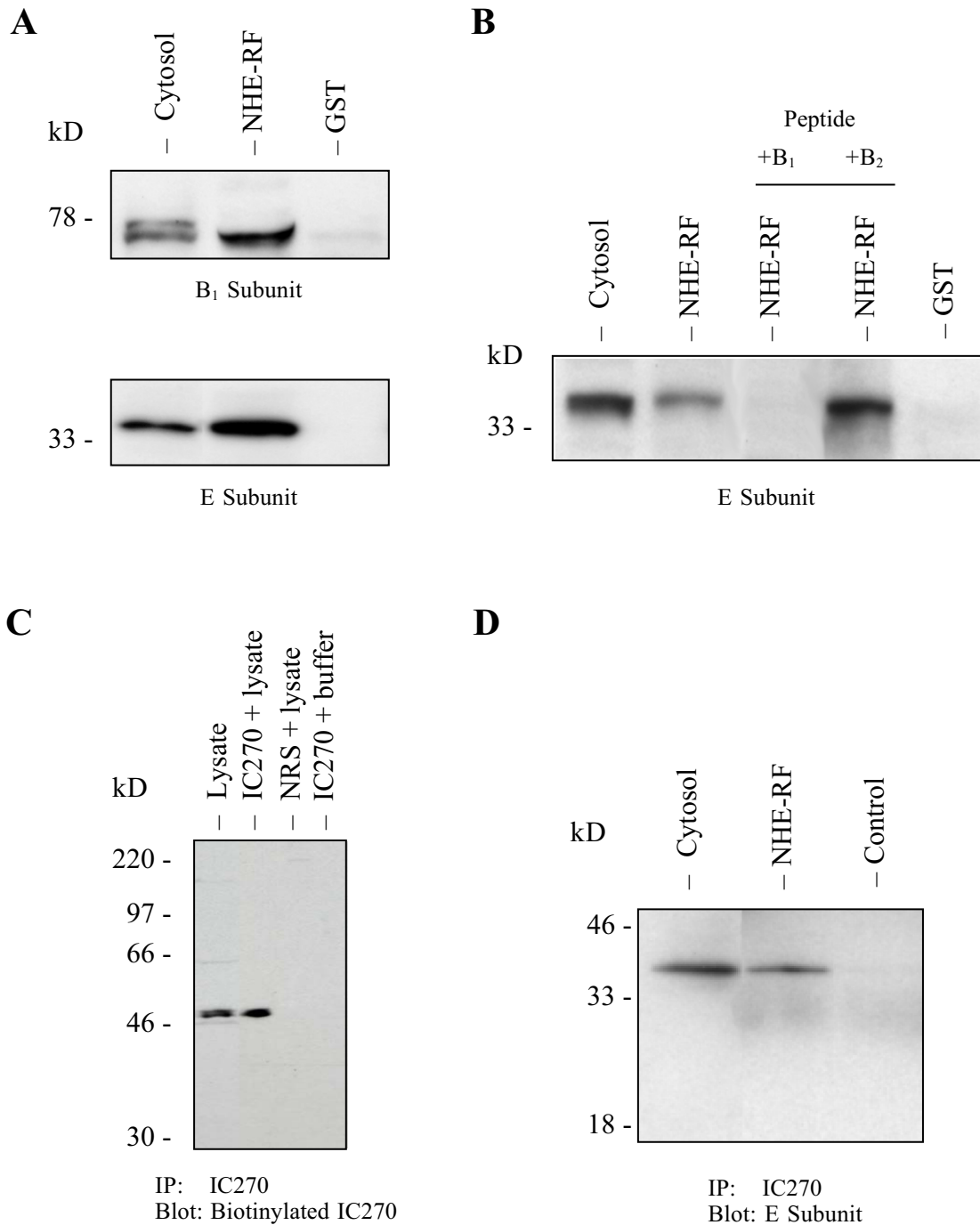


**Figure 10. NHE-RF Binds to the  $H^+$  ATPase *In Vitro* and *In Vivo*.** The B1 and the E subunits of the  $H^+$  ATPase are both captured by GST-NHE-RF beads, but not by beads coupled to GST alone (A). The ability of the GST-NHE-RF to capture the  $H^+$  ATPase (in this case the E subunit) is completely inhibited by the B1 subunit peptide (which contains the DTAL motif) in contrast to the B2 subunit peptide (which lacks the DTAL motif) (B). NHE-RF is immunoprecipitated with the polyclonal antibody IC270. No background staining is detected in the control lanes normal rabbit serum (NRS) with cell lysate and IC270 without cell lysate (IC270 + buffer) using biotinylated IC270 for immunoblotting (C). The E subunit of the  $H^+$  ATPase is co-immunoprecipitated by IC270 but not by preimmune serum. In all of these blots, the E subunit runs slightly higher than the predicted 31kD molecular mass for this subunit. IP, immunoprecipitate. (Adapted from Breton *et al.*, 2000).

(Berryman *et al.*, 1998). Thus, a signal seen at ~50kD of immunoprecipitations with the antibody IC270 is expected to be from the presence of NHE-RF and not from the immunoglobulin. To test this method, cell lysates were incubated with the NHE-RF antibody and protein A that is covalently coupled to an agarose matrix. As controls, lysis buffer alone replaced cell lysate or alternatively, lysate was incubated with a non-relevant antibody (normal rabbit serum or pre-immune serum). This method was successfully employed to show that NHE-RF immunoprecipitates with the antibody IC270 and no background staining is detected in the controls (Figure 10C). Thus, this antibody can be utilized to study protein-protein interactions by co-immunoprecipitation experiments.

To test the physical interaction of NHE-RF and the H<sup>+</sup> ATPase *in vivo*, co-immunoprecipitation experiments were performed in collaboration with Dr. Vladimir Marshansky. Towards this end, cytosol from the rat kidney was again incubated with the NHE-RF specific antibody IC270 bound to protein A, which is covalently coupled to an agarose matrix. Immunoprecipitates were then analyzed with antibodies against the H<sup>+</sup> ATPase. The E subunit of the H<sup>+</sup> ATPase was co-immunoprecipitated from kidney cytosol by the anti-NHE-RF antibody but not in the control where preimmune serum was employed (Figure 10D). These experiments support that NHE-RF and the cytoplasmic domain of the H<sup>+</sup> ATPase bind to each other and give evidence that this interaction takes place *in vivo*.

### 3.3 Examination of NHE-RF in Human Cancer

The fact that *NF2* mutations are only found in approximately 60% of meningiomas suggests that a gene other than the *NF2* gene is involved in the formation of some of these tumors (Louis *et al.*, 1995). Candidate genes encode proteins that are in the same pathway as merlin such as the merlin binding protein NHE-RF. Could NHE-RF, therefore, be inactivated in meningiomas in which merlin is not mutated? To pursue this question, a possible inactivation of the *NHE-RF* gene was tested by molecular genetic analyses. Moreover, the expression and localization of NHE-RF was investigated in meningiomas and tumors deriving from other organs including colon, ovary and breast.

#### 3.3.1 Expression of NHE-RF is Upregulated in a Subset of Breast Cancer Cell Lines

Meningiomas that have no *NF2* mutations were selected to determine whether the merlin binding protein NHE-RF may play a role in the development of these tumors. Mutations in the *NHE-RF* gene were sought by single strand conformation polymorphism (SSCP) in thirty primary meningiomas of which twenty-one express intact merlin. The status of merlin in the other tumors was not clear. Although four polymorphisms were found, none of the tumors had any mutations. These observations imply that mutations in NHE-RF do not play a role in the formation of the tested tumors (data not shown).

The expression of NHE-RF was studied in ten primary meningioma cell lines that express intact merlin. Seven meningioma cell lines that do not express merlin were included in this study for comparison. In addition, a panel of other tumor cell lines obtained from eleven colon carcinomas, four ovarian cancer and eight breast carcinomas was examined for NHE-RF protein expression. Western blot analyses performed with the NHE-RF antibody IC270 did not reveal significant differences between meningioma cell lines that were positive or negative for merlin. Similarly, none of the examined colon and ovarian cancer lines exhibited variations in NHE-RF expression (data not shown).

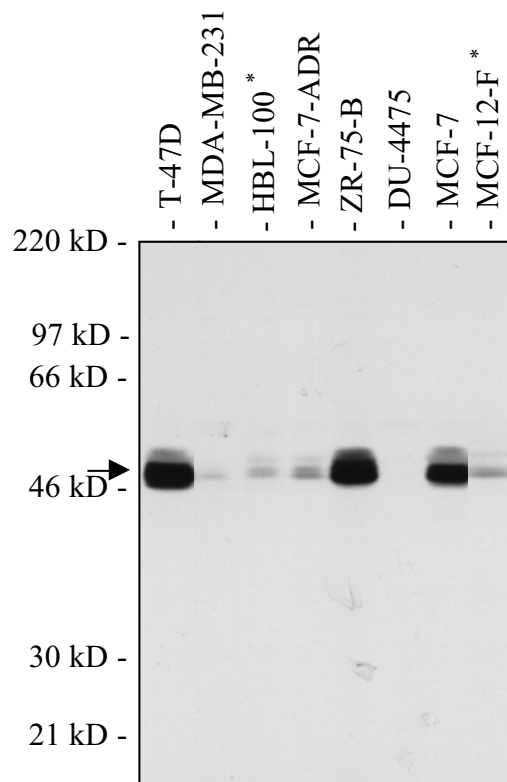


**Figure 11. Western Blot Analysis of Various Mammary Epithelial and Breast Cancer Cell Lines.** Cells were grown to 85-95% confluency in DMEM containing 10% fetal calf serum. Three hundred  $\mu$ g of total cellular protein from each cell line was subjected to 10% SDS-PAGE gel electrophoresis, proteins were transferred to nitrocellulose and probed for NHE-RF with the polyclonal antibody IC270. The star (\*) indicates normal mammary epithelial breast cell lines and the arrow indicates NHE-RF at  $\sim$ 50kD.

Therefore, these cell lines were not further analyzed with respect to NHE-RF mutations or gene expression.

In contrast, three of the eight breast carcinoma cell lines showed an obvious and dramatic increase in NHE-RF expression. As a control, six normal breast epithelial cell lines were analyzed and none of these revealed high levels of expression. Ms. Denise Pinney-Michalowski, a member of the laboratory of Dr. V. Ramesh, conducted Western blot analyses of these cell lines. The intensity of the bands was further analyzed by densitometric scanning of the autorads using transmittance analysis (Fluor-S, Multiimager, BioRad) to compare the expression levels in these cell lines. Results from three independent experiments revealed that the three cancer cell lines, MCF-7, ZR-75-B and T-47-D, had  $9.50 \pm 2.20$  fold higher levels of NHE-RF when compared to the normal mammary lines HBL-100 and MCF-12-F (Figure 11). No expression of NHE-RF was detected in the breast cancer cell lines DU-447-S while moderate levels of expression were seen in the breast cancer cell lines MDA-MB-231 and MCF-7-ADR (a multidrug resistant cell line derived from MCF-7).

To investigate whether upregulation of NHE-RF is also seen at the level of transcription, Northern blot analysis was employed using total RNA from all eight breast cancer lines together with the control breast epithelial cell lines MCF-12-F and HBL-100. A  $4.41 \pm 0.88$  fold increase in NHE-RF RNA was observed in the cell lines MCF-7, ZR-75-B, and T-47-D, compared to the controls MCF-12-F and HBL-100 (Figure 12A). Moreover, the detectable levels of NHE-RF RNA were little to none in the cell lines MDA-MB-231, MCF-7-ADR and DU-447-S. The membranes were re-probed with GAPDH to confirm that the increase in NHE-RF transcript did not reflect variations in loading (Figure 12B). Interestingly, no increase of the related NHE-RF2 RNA was observed in any of the breast cancer lines examined (data not shown). Thus, both mRNA and protein expression of NHE-RF were specifically increased in the three breast cancer cell lines MCF-7, ZR-75-B and T-47-D.

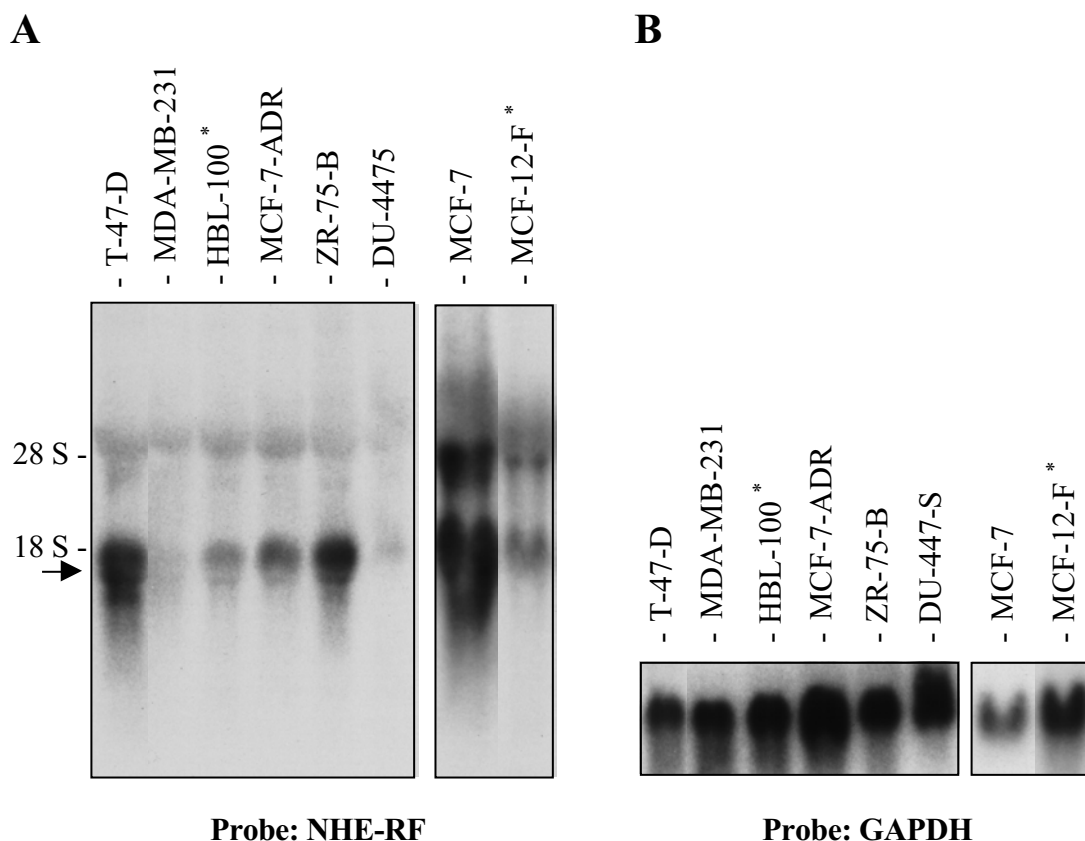


**Figure 12. Northern Blot Analysis of Various Mammary Epithelial and Breast Cancer Cell Lines.** Thirty-five micrograms total RNA from each cell line was subjected to electrophoresis on a 1% agarose-formaldehyde gel and transferred to nitrocellulose. Membranes were hybridized with  $^{32}\text{P}$ -labeled and ultra-purified full-length NHE-RF cDNA (A). As a control for total RNA amount, membranes were stripped and rehybridized with  $^{32}\text{P}$ -labeled and ultra-purified GAPDH cDNA (B). The star (\*) indicates normal mammary epithelial breast cell lines.

### 3.3.2 NHE-RF Expression is Regulated Through the Estrogen Receptor

Next, the mechanism by which NHE-RF expression is upregulated was sought. Determining this mechanism was facilitated by the observation that the three cell lines that show a dramatic increase in the expression of NHE-RF have been reported to be estrogen receptor (ER)- positive (Arteaga et al., 1988). In addition, MDA-MB-231 and MCF-7-ADR, where no elevated expression of NHE-RF was observed, are known to be ER- negative (deFazio et al., 1992; Vickers et al., 1989). These findings suggested that ER could play a regulatory role in NHE-RF expression. To test this hypothesis, both MCF-7 (ER- positive) and MCF-7-ADR (ER- negative) cell lines were depleted of estrogen and examined for expression of NHE-RF mRNA and protein compared with matched, non-estrogen depleted lines. Expression of NHE-RF in estrogen-depleted MCF-7 cells was found to be significantly reduced relative to the MCF-7 control cells by Northern and Western blot analyses (Figure 13A, D, control and 0 h respectively). No difference in the expression of NHE-RF was detected by either Northern blot analysis in MCF-7-ADR cells grown in the presence and absence of estrogen (Figure 13C).

To further examine the estrogen responsiveness of NHE-RF expression, the estrogen depleted MCF-7 and MCF-7-ADR cells were treated with the estrogen analogue  $\beta$ -estradiol, and cells were harvested at various time points. Northern blot analysis revealed that transcription of NHE-RF in MCF-7 cells is upregulated by about two-fold as early as 1 hour after hormone treatment and remains above the basal level (0 h) up to at least 24 h after estrogen induction (Figure 13A). These membranes were also re-probed with GAPDH to confirm that the increase in NHE-RF transcript did not reflect variation in loading (Figure 13B). This phenomenon was not observed in the cell line MCF-7-ADR (Figure 13C). To test whether the specific increase in NHE-RF mRNA is a primary response to  $\beta$ -estradiol, similar experiments were carried out in the presence of the antibiotic cycloheximide. This antibiotic interferes with the translocation step by directly interacting with the translocase enzyme, thus inhibiting protein synthesis in eukaryotes (<http://www.calbiochem.com>). These experiments



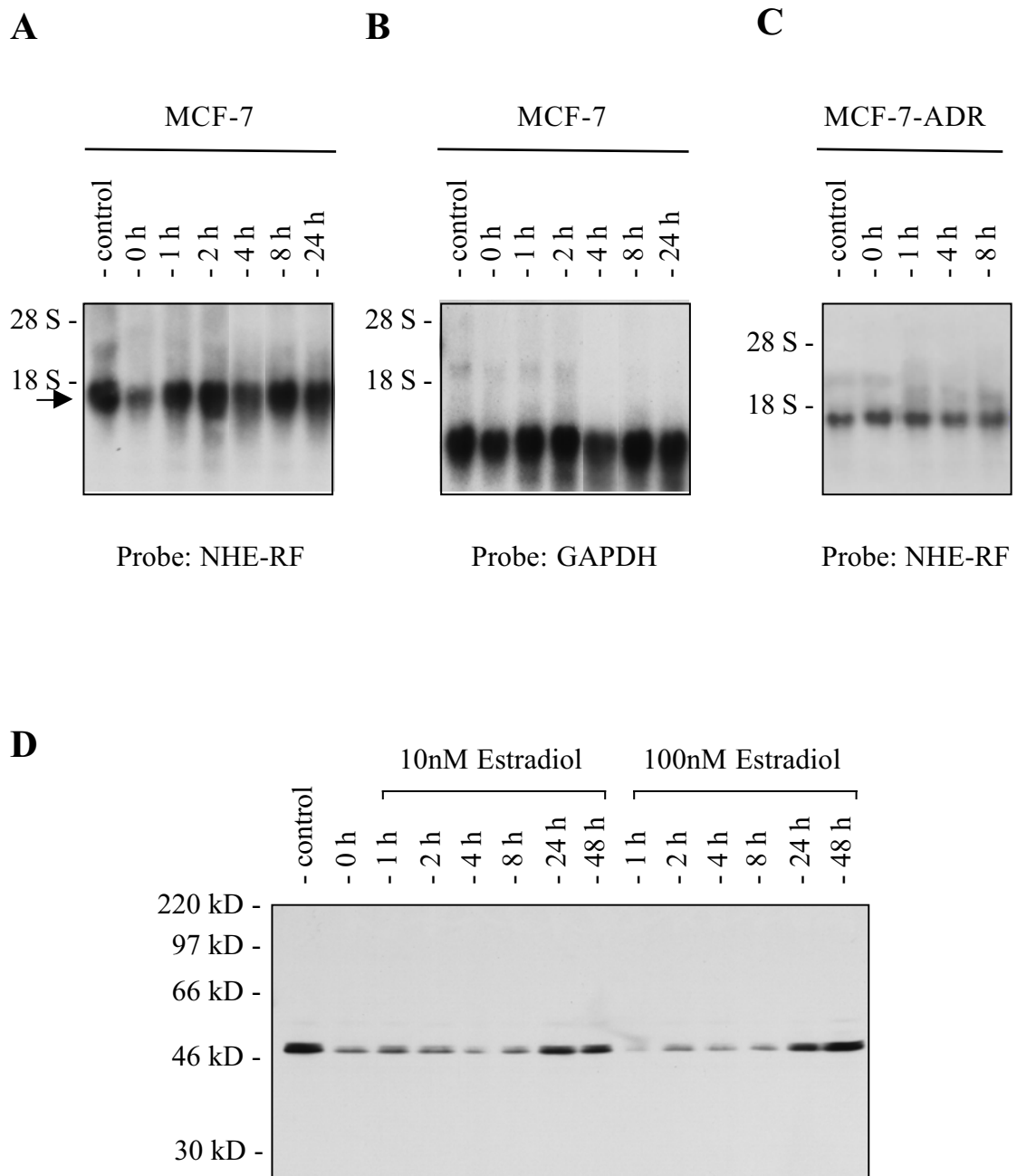


**Figure 13. Expression of NHE-RF is Induced by  $\beta$ -Estradiol in the cell line MCF-7.** Cells were plated and grown under standard conditions (control) or alternatively depleted of estrogen by growing in estrogen-free medium for 3 days. These cells were then fed with estrogen free medium supplemented with  $\beta$ -estradiol and harvested after 1h, 2h, 4h, 8h, 24h and 48h. Northern blot analysis was performed as described in Figure 12 and the membranes were hybridized with  $^{32}$ P labeled full-length NHE-RF cDNA, stripped and rehybridized with  $^{32}$ P-labeled GAPDH cDNA (A). Western blot analysis of the same cells was performed and the membrane was probed with the anti-NHE-RF monoclonal antibody 1D12. Induction of NHE-RF at 10nM and 100nM estradiol are shown (B).

showed that cycloheximide does not block the increase in NHE-RF mRNA in the ER-positive cell line MCF-7 (data not shown). Therefore, the upregulation of NHE-RF is a primary response to estrogen as opposed to being mediated by other proteins that are induced by this hormone.

Western blot analysis was performed for the estrogen depleted and  $\beta$ -estradiol induced cell lines (conducted by Ms. Denise Pinney-Michalowski, a member of the laboratory of Dr. V. Ramesh). This analysis was aimed to examine the effect of this estrogen analogue on NHE-RF protein expression at various time points. A  $4.45 \pm 2.90$  fold increase over the estrogen depleted level (0 h) of NHE-RF was seen in MCF-7 cells treated with 10nM and 100nM  $\beta$ -estradiol for 24 and 48 hours (Figure 13D). Again, no induction of NHE-RF was observed in the ER-negative cell line MCF-7-ADR by Western blot analysis (data not shown) confirming the results of the Northern blot analysis (Figure 13C).

Estrogen is known to increase the number and the length of microvilli at the cell surface of MCF-7 cells 48 hours after treatment (Vic *et al.*, 1982). Furthermore, NHE-RF has been localized to microvilli, the finger-like structures at the surface of a cell (Murthy *et al.*, 1998). Therefore, the localization of NHE-RF was examined by indirect immunofluorescence analysis in control MCF-7 cells, cells depleted of estrogen (0 h), and cells stimulated with  $\beta$ -estradiol (48 h) (conducted by Dr. C. Agosti-Gonzalez). NHE-RF was not detectable in estrogen depleted, non-induced MCF-7 cells (0 h) while cells grown under regular conditions (control: non-depleted and always in the presence of estrogen) showed NHE-RF localization in the few microvilli seen. In contrast, a dramatic increase in NHE-RF was observed in the increased number of microvilli after 48 hours of  $\beta$ -estradiol induction (Figure 14). The ER-negative cell line MCF-7-ADR did not reveal an increase in microvilli formation nor in NHE-RF staining when subjected to the same analysis as its parental counterpart MCF-7 (data not shown). Hence, the localization of NHE-RF to microvilli in MCF-7 cells closely correlates with the effects of estrogen on cell cytoarchitecture and support the upregulation of NHE-RF seen by Northern blot and Western blot analysis.

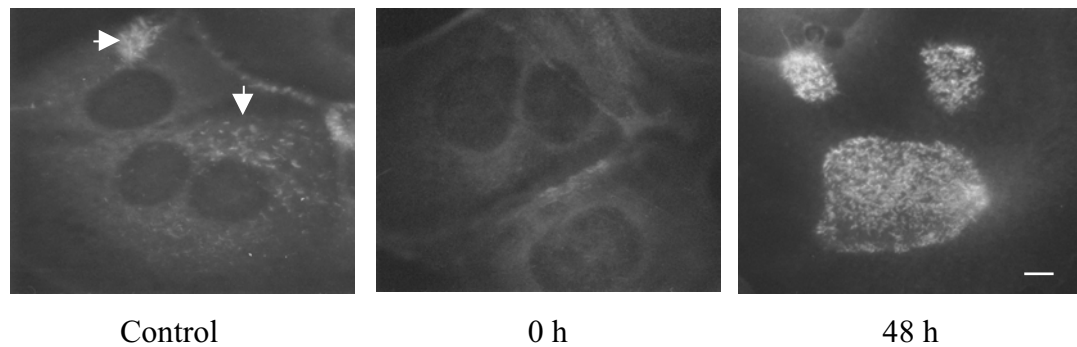


**Figure 14. Visualization of NHE-RF by Immunocytochemistry in  $\beta$ -Estradiol Induced Cells.** Cells were plated and grown under standard conditions (control); depleted of estrogen by growing in estrogen-free medium for 3 days (0 h) and induced with 100nM  $\beta$ -estradiol (48 h). These cells were stained with the affinity eluted anti-NHE-RF antibody IC270. Control cells show localization of NHE-RF in some microvilli (arrows). Localization of NHE-RF is not detected in estrogen depleted and non-induced cells. Stimulation of depleted cells with  $\beta$ -estradiol for 48 h shows a dramatic increase in NHE-RF in the microvilli-rich apical surface of the cells. Bar, 5 $\mu$ m.

### 3.3.3 Expression of NHE-RF in Primary Breast Tumors

To ascertain that estrogen regulation of NHE-RF is also seen *in vivo* in breast cancer, the analysis of NHE-RF expression was extended to primary breast tumor samples in collaboration with Drs. Anat Stemmer-Rachamimov and David Louis from Molecular Neuro-Oncology at Massachusetts General Hospital, Boston. Examination of sections from eighteen infiltrating breast adenocarcinomas showed strong correlation between positive immunostaining for ER and high expression of the NHE-RF protein: over 90% (10/11) of the ER- positive tumors strongly expressed NHE-RF. On the other hand, only 30% (2/7) of the ER- negative tumors showed strong expression of NHE-RF. In ER positive tumors, immunostaining of NHE-RF was observed in most tumor cells, contrasting the adjacent immunonegative stroma. NHE-RF protein is seen as membranous staining, especially prominent at the luminal aspect of the cell (Figure 15A) and as diffuse cytoplasmic staining (Figure 15B). Of the seven ER- negative cancers, five showed very weak to absent NHE-RF staining (Figure 15C). The control cells MCF-7 and MCF-7-ADR showed strong and weak expression, respectively, by immunohistochemistry validating the data obtained in primary breast tumors (Figure 15D1, D2). Controls that included omission of primary antibody were negative (data

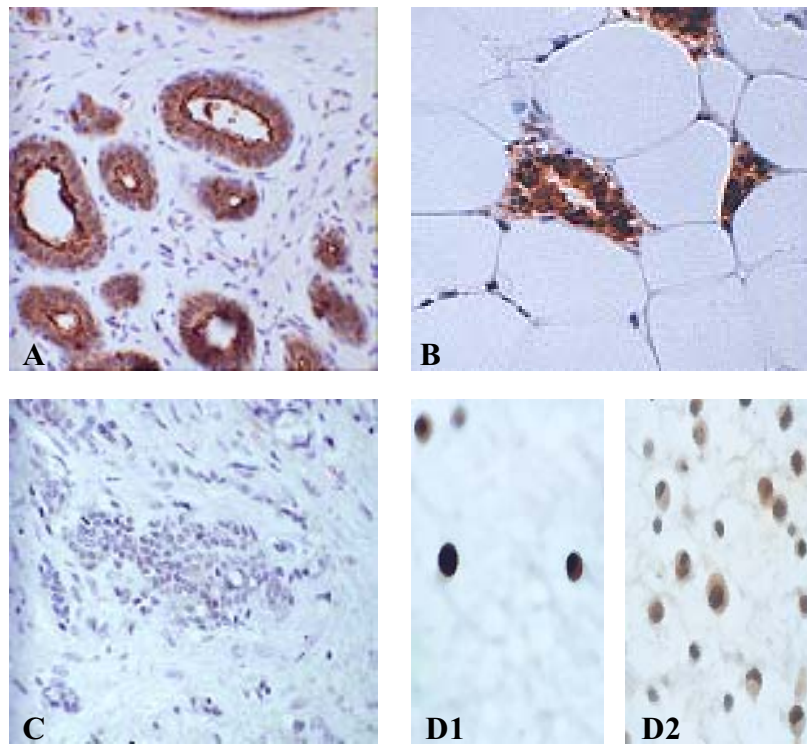


**Figure 15. Expression of NHE-RF in ER-positive and ER-negative breast carcinomas by immunohistochemistry.** NHE-RF is strongly expressed in ER-positive breast carcinomas of different patients: linear membranous pattern (A) or in a diffuse cytoplasmic pattern (B). Lack of expression of NHE-RF in an ER-negative tumor (C). Formalin fixed, paraffin-embedded cell pellets from MCF-7 and MCF-7-ADR cell lines used as positive controls show strong and weak expression of NHE-RF respectively (D1 and D2).

not shown). Together, the results obtained from primary breast tumors show a strong correlation between NHE-RF and ER expression supporting the data obtained in the cell lines. In addition, these results suggest a role for NHE-RF in ER mediated signaling in breast tumors.

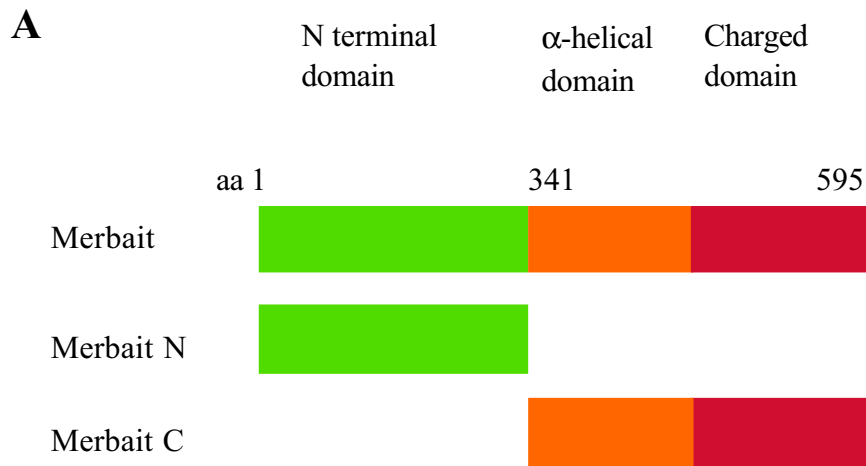
### 3.4 Isolation and Characterization of Novel Merlin Binding Proteins

Although the *NF2* gene was cloned in 1993, limited information about its protein product merlin is available. Clues come from animal models such as mouse and fly as well as from the identification of merlin binding proteins. To further define the role of merlin as a tumor suppressor, additional merlin binding proteins were sought.

#### 3.4.1 Identification of Merlin Binding Proteins by a Yeast Two-Hybrid Screen

A human fetal frontal cortex interaction library was screened with three different (p)merbaits (merbait, merbait N and merbait C) by Dr. A. Murthy (Figure 16A). About  $10^6$  primary transformants were pooled and replated (at a multiplicity of 20) onto galactose *leu 2* selection plates. Thirty-three colonies, which showed galactose-dependent growth and blue color on *leu 2* plates and on 5-bromo-4-chloro-3-indolyl b-D-galactopyranoside medium, respectively, were identified, and plasmids containing the cDNA clones were isolated. Restriction mapping and hybridization experiments revealed that these cDNAs were clustered into three different groups of overlapping clones, representing three different cDNAs as recurrent, independent interactors. The first of these cDNAs, merintC, the human homologue of a regulatory co-factor of the  $\text{Na}^+\text{-H}^+$  exchanger (NHE-RF), has been reported (Murthy *et al.*, 1998).

In this study, the other cDNAs were characterized and provided mixed results. MerintB interacts consistently in the yeast two-hybrid assay with the amino-terminal and full-length merlin constructs (Figure 16B). The sequence analysis of this cDNA had revealed that this is a novel gene and no entries in any databases were found at the time it was isolated. However, recent database searches showed that merintB has been cloned over the course of this work and entries for the human and mouse genes can be found at GenBank/EMBL/DDBJ. The human gene for merintB encodes a 125 amino acid protein and was named “similar to golgi-associated MP1 adapter protein”. The sequence can be found under the accession number XM\_017041. The mouse gene for merintB is 99% identical to its human orthologue and was named “mitogen activated protein binding protein interacting protein (Mapbpip)” or p14. This sequence can be

**B**

Bait	MerintA	MerintB	MerintC (NHE-RF)
Merlin (Merbait)	+	+	+
Merbait N	-	+	+
Merbait C	+	-	-
APP	-	-	-
Bicoid	-	-	-
CDC2	-	-	-
IQ GAP	-	-	-
Neurofibromin (NF1)	-	-	-

**Figure 16. Isolation of Merlin Binding Proteins Using the Yeast-Two Hybrid System.** Schematic diagram of the merlin baits that were used to seek merlin binding proteins (A). Table indicating the specificity of interactions. Controls were tested under the same conditions as merlin baits and do not show any interaction with any of the candidates (B).

found under the accession number NM\_031248. Wunderlich *et al.* (2001) reported that merintB/p14 associates with the cytoplasmic face of late endosomes/lysosomes in a variety of different cell types and that it binds to MP1 (mitogen-activated protein kinase (MAPK) partner 1). In our study, the interaction between merlin and merintB was tested beyond the yeast two-hybrid system by other methods such as affinity

precipitation assays. However, no binding could be detected in these experiments (data not shown) and therefore merintB was not further characterized.

The final cDNA is a ~500 base pair fragment, which is referred to as merintA. MerintA had been tested for associations in yeast strains containing either the amino- (aa 1–341) or the carboxy- (aa 342–595) terminal portion of merlin as bait (conducted by Dr. A. Murthy). Results of these tests indicated that merintA specifically associates with full-length and carboxy-terminal merlin constructs but not with controls such as APP, Bicoid, CDC2, IQ GAP or neurofibromin (NF1) (Figure 16B).

### 3.4.2 DNA Sequence Analysis and Isolation of a Full-length MerintA cDNA

To determine the identity of merintA and for subsequent analyses, the original cDNA was cloned into pcDNA3 (Invitrogen). Towards this end, a restriction digest was performed to release the cDNA out of the vector pJG4-5. This strategy ensures that the sequence obtained has no errors introduced by *Taq* polymerase during polymerase chain reaction (PCR). Furthermore, the hemagglutinin (HA) tag from pJG4-5 could be carried along in fusion with the cDNA, which allows detecting the protein product of merintA HA-tag antibodies. However, this strategy resulted in 270 additional base pairs (or 90 amino acids) of vector sequence from pJG4-5 between the HA-tag and merintA. Sequence analysis revealed that merintA is a novel gene, which has not been described so far. The cDNA of merintA did not have a start codon in the reading frame indicating that the 5' end of this clone was not complete. The original cDNA did have a stop codon in the open reading frame although the poly-A signal was missing. Thus, rapid amplification of cDNA ends (5' RACE) was performed from placenta and peripheral blood mononuclear cells (PBMC) cDNAs to obtain the 5' end of merintA. Clones from two independent PCRs were analyzed to identify the sequence of the merintA cDNA. Additional 36bp were obtained with a start codon and surrounding sequence that is almost completely identical to the Kozak sequence. The combined sequence analysis of the original cDNA from the yeast two-hybrid screen and the 5' RACE revealed a novel gene that encodes a protein of 178 amino acids (Figure 17A). The COILS2 program

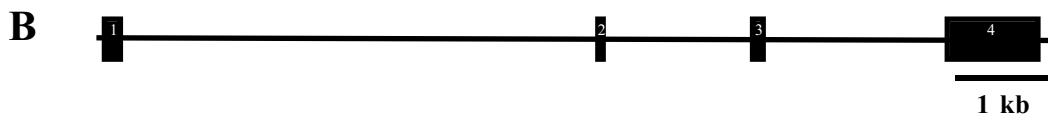


**Figure 17. cDNA Sequence and Genomic Structure of the MerintA Gene.** Nucleotide and derived protein sequences of the human merintA cDNA. The nucleotide sequences of exons 1 and 3 are depicted in red and the nucleotide sequences of exons 2 and 4 are depicted in blue. The predicted Grb2 binding motif is boxed (A). Schematic diagram of the predicted intron and exon segments comprising the merintA gene. Boxes indicate exons and are numbered sequentially from 5' to 3' (B).



(<http://tofu.tamu.edu/Pise/5.a/coils2.html>) predicted a coiled-coil domain between amino acids 109 and 145 of the merintA sequence. Moreover, several glycine and proline residues reside at the amino-terminus of the protein generating a low-complexity region. When the sequence data was first obtained, no matches were found in the databases; however, during the course of this study, further database analyses identified a genomic clone (AC006160) and revealed that the human merintA gene resides at chromosome locus 4p15.3. Furthermore, a comparison of the transcribed and genomic sequences predicts that the merintA gene consists of four exons (Figure 17B). At least eight partial or complete processed pseudogenes at different locations in the human genome can be found. However, these pseudogenes are all degenerated, containing interspersed stop codons, and it is questionable that any of these are expressed. No other expressed genes producing proteins related to merintA have been found to date, making it a novel protein unassociated with any known functional families. Through the course of this study three mRNA sequences, which match that of merintA were deposited at GenBank/EMBL/DDBJ with accession numbers AF317679, AF358829 and AF321617. These entries are 1069bp, 1363bp and 3109bp sequences although the open reading frames are identical among themselves and to merintA differing only in the length of the untranslated regions. Information submitted to GenBank/EMBL/DDBJ for AF317679 suggests that merintA is tumor-related protein while AF358829 indicates that merintA may play some role as a tumor angiogenesis marker. No other information has been reported to date.

Further database analyses identified anonymous, predicted orthologues in mouse (BAB23039), cow (AW357991 and AW (464009), zebrafish (AI942663 and AI884138) and fly (AAF56470) while no orthologues were immediately evident in worm or yeast. MerintA is highly conserved in vertebrates with only 10 residue differences. Six of these are conservative between human and mouse and three of the four non-conservative changes occur in the low complexity amino-terminal region. The zebrafish and fly orthologues are 76 and 43 % identical to the human protein (Figure 18). Thus, merintA is a novel gene that is conserved in various species and encodes a protein of unknown function.

```

1                                                    50
HUMAN MerintA MAAPLGGMFS GQ.PPGP.PQ APPGLPGQAS LLQAAPGAPR PSSSTLVDEL
MOUSE MerintA MAASLGGMFT GQ.PPGP.PP PPPGLPGQAS LLQAAPGAPR PSNSTLVDEL
COW MerintA MAAPLGGMFS GQ.PPGP.PQ PPPGLLGQAS LLQATPGVPR TSNSTLVDEL
FISH MerintA MASSMGGLFP GQQPPGSLPP SGPGGPGQPG LLTGTPG.NR GANNTLVDEL
FLY MerintA ..... .. MASNE SGGGNLMDEF

51                                                    100
HUMAN MerintA ESSFEACFAS LVSQDYVNGT DQEEIIRTGVD QCIQKFLDIA RQTECFFLQK
MOUSE MerintA ESSFEACFAS LVSQDYVNGT DQEEIIRTGVD QCIQKFLDIA RQTECFFLQK
COW MerintA ESSFEACFAS LVSQDYVNGT DQEEIIRTGVD QCIQKFLDIA RQTECFFLQK
FISH MerintA EASFACFAS LVSQDYVNGT DQEEIIRTGVD QCIQKFLDVA RQTECFFLQK
FLY MerintA EEAFQSCLLT LTKQEPNSGT NKEEIDLEVQ KTTNRFIDVA RQMEAFFLQK

101                                                    150
HUMAN MerintA RLQLSVQKPE QVIKEDVSEL RNELQRKDAL VQKHLTKLRH WQQVLEDINV
MOUSE MerintA RLQLSVQKPD QVIKEDVSEL RSELQRKDAL VQKHLTKLRH WQQVLEDINV
COW MerintA RLQLSVQKPE QVIKEDVSEL RNELQRKDAL VQKHLTKLRH WQQVLEDINM
FISH MerintA RLQLSVQKPE QVEKEDASEL KNELQRKEML IQKHLAKIHH WQQVLEDINV
FLY MerintA RFLVSTLKPY MLIKDENQDL SIEIQRKEAL LQKHYNRLEE WKACLSIDIQQ

151                                                    200
HUMAN MerintA Q.HKKPAD.. ...IPQGSIA YLEQASANIP APLKPT.... .....
MOUSE MerintA Q.HKKPAD.. ...MPQGSIA FLEQASANIP APLKQT.... .....
COW MerintA Q.HKKPAD.. ...IPQGSIA YLEQASANIP APMKQT.... .....
FISH MerintA Q.HKKPTE.. ...LPQGPIA FLEQASANLP APMKPN.... .....
FLY MerintA GVHSRPTPPI GSGMLQGGP GMPPMGGTTP RGMMPGMPP GAMQPGGPMQ

201                                                    224
HUMAN MerintA ..... ..
MOUSE MerintA ..... ..
COW MerintA ..... ..
FISH MerintA ..... ..
FLY MerintA PSPHMLQAQQ MQQLRMISRQ MPPK

```

**Figure 18. Alignment on MerintA Orthologues.** The protein sequence of human merintA was aligned with the predicted sequences of mouse, cow, fish and fly merintA using multalin at [http://npsa-pbil.ibcp.fr/cgi-bin/npsa\\_automat.pl?page=/NPSA/npsa\\_multalin.html](http://npsa-pbil.ibcp.fr/cgi-bin/npsa_automat.pl?page=/NPSA/npsa_multalin.html). The complete sequences of the human, mouse, and fly proteins are available at the following GenBank accession numbers: *Homo sapiens* (AAK32724), *Mus musculus* (BAB23039) and *Drosophila melanogaster* (AAF56470). MerintA EST sequences are available for cow and fish: *Bos taurus* (AW357991 and AW464009) and *Danio rerio* (AI942663 and AI884138). A contiguous sequence was assembled from the cow and fish EST sequences and the open reading frame was translated into the respective protein sequence. While the (p)YVNG Grb2 binding motif is conserved in mouse, cow and fish it is of interest to note that it is not present in fly.

### 3.4.3 MerintA is Widely Expressed in Cells and Tissues

To investigate the merintA protein mono- and polyclonal antibodies were generated. Mice were immunized with a GST-merintA fusion protein (aa 13-178). Ms. Nicole Smith, a member of the laboratory of Dr. V. Ramesh fused the spleen of a responding mouse to SP2 cells and the resulting monoclonal antibody was named 7E1. This

antibody recognizes a predominant band at ~24kD (Figure 19A), which is slightly larger than predicted (20kD) from the open reading frame. This 24kD polypeptide disappeared upon preabsorbing the antibody with purified merintA protein. Polyclonal anti-merintA antibodies were generated by immunizing rabbits with keyhole limpet hemocyanin- (KLH) conjugated peptides from the amino-terminal (aa 9-23), central (aa 114-125) and carboxy-terminal (aa 165- 178) regions of merintA. The peptides were synthesized and injected by Research Genetics Inc, Huntsville. Bleeds collected ten weeks after immunization from all animals were tested and gave mixed results. While the bleeds of the animals injected with the amino-terminal and central region of merintA showed little to no response, the carboxy-terminal bleed responded well resulting in the polyclonal antiserum Tim3. The specificity of the antibodies 7E1 and Tim3 was further confirmed by immunoprecipitation experiments. Towards this end, Tim3 was employed to immunoprecipitate merintA and the monoclonal antibody 7E1 recognized the same 24kD protein in the following Western blot analysis (Figure 19B, lane 2). Two important controls ensure specificity of the antibody used to immunoprecipitate and the signal detected by the antibody used for Western blot analysis. Therefore, immunoprecipitation experiments were carried out with Tim3 but the cell lysate was substituted with lysis buffer (Figure 19B, lane 3). No signal was detected in this control indicating that the band detected in the complete reaction represents merintA as opposed to the light chain of Tim3 that approximately co-migrates with merintA during gel electrophoresis. A non-specific antibody (pre-immune serum) was employed as a second control and no signal was detected here, demonstrating that Tim3 specifically immunoprecipitates merintA (Figure 19B, lane 4).

Next, full-length HA-tagged merintA protein was overexpressed in CAD (Cath a-differentiated) cells. Protein lysates were subjected to Western blot analysis and membranes were probed with a HA-tag antibody (12CA5, Roche). This fusion protein migrates slightly slower than endogenous merintA presumably due to the tag. This band is not seen upon transfection of vector alone (Figure 19C). The antibodies 7E1 and Tim3 also recognize the overexpressed protein (data not shown). Thus, specificity of

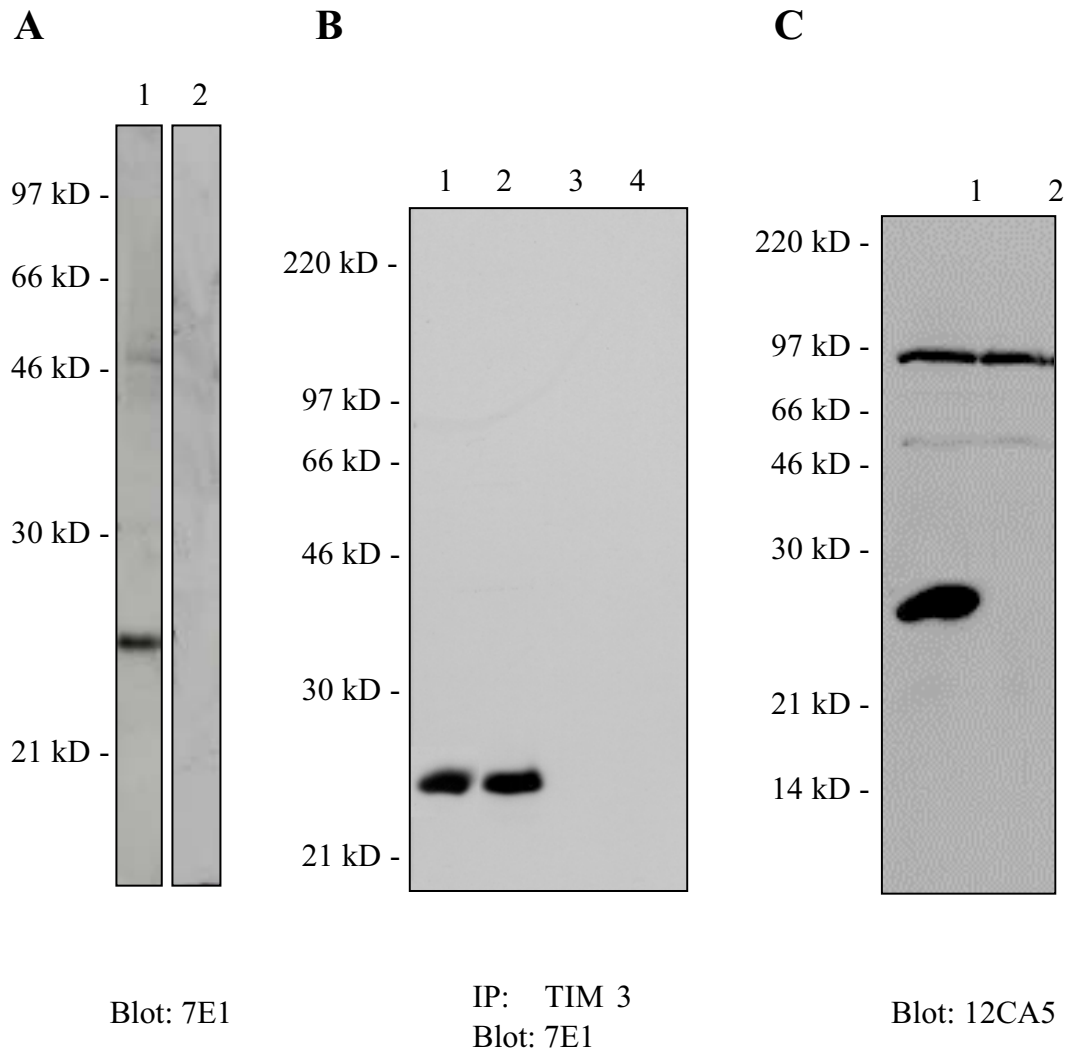


**Figure 19. Characterization of MerintA Antibodies and HA-MerintA.** CAD cell lysates were fractionated on a 12% SDS-polyacrylamide gel and blotted onto nitrocellulose. Strips of this blot were immunoprobed with the monoclonal antibody 7E1 (lane 1) and preabsorbed 7E1 (lane 2). A specific band of 24kD is detected, which represents merintA (A). CAD cell lysates were subjected to immunoprecipitation with the rabbit polyclonal anti-peptide antibody (Tim3). Precipitates were immunoprobed with the monoclonal antibody 7E1. Lane 1 shows a positive control where a total CAD cell lysate was examined. Lane 2 shows the complete reaction where Tim3 immunoprecipitated merintA from the cell lysate. Lane 3 shows a control with the Tim3 antibody but no lysate, and lane 4 shows a control with lysate but a non-specific antibody (B). CAD cell lysates overexpressing HA-tagged merintA (lane 1) and vector alone (lane 2) were immunoprobed with the HA-antibody 12CA5 (C).

the two independent merintA antibodies (Tim3 and 7E1) was confirmed since they detect the same 24kD endogenous protein. Moreover, the antibodies detect the same band as HA-tag antibodies upon overexpression of full-length HA-merintA (A4).

To investigate the length of the merintA transcript as well as developmental and tissue distribution of merintA on the level of RNA, fetal and adult human multiple-

tissue RNA blots (Clontech) were probed with the  $^{32}\text{P}$  labeled merintA cDNA. Multiple transcripts with sizes of ~1, ~1.3, ~3.4 and ~6.3kb were detected in the adult human tissues. Strongest levels of expression were detected in skeletal muscle and heart where all transcripts are expressed. Less expression was seen in brain, placenta, lung, liver, kidney and pancreas. Furthermore, the ~1.3kb transcript was below detectable levels in these tissues (Figure 20A). The same ~1 and ~1.3kb in addition to a ~3.2kb transcript was detected in fetal human tissues. Interestingly, the sizes of these transcripts match those deposited in GenBank indicating that they all translate into the same protein and differ only in the untranslated regions. Again, all transcripts were expressed in all the tested fetal tissues brain, lung, liver and kidney (Figure 20B). Thus, merintA is widely expressed in various tissues and has different transcripts. Here, the 1kb transcript was isolated which results in the expression of the merlin binding protein merintA.

The expression and distribution of endogenous merintA was examined next in various cell lines by Western blot analysis. Analysis of normalized protein lysates indicate that merintA is expressed in many of the tested cell lines including CAD (mouse neural cells), Met5A (mesothelioma), H237 (glioma), 293T (kidney), Cos-7 (kidney), HeLa (adenocarcinoma; cervix) and RD135 (fibroblast). It is of interest to note that merintA is hardly expressed in merlin positive or negative meningioma cell lines (Figure 20C, lane 1 and 2). However, a ~50kD band is detected in these and some other cell lines with 7E1. This species was not further characterized but it may represent a potential alternatively spliced merintA isoform, a strong dimer that resists the denaturing conditions of SDS-PAGE, a closely related protein or an unrelated protein with a conserved epitope. Furthermore, the expression of merintA was examined at different stages of rat development by quantitative Western blot analysis. Interestingly, levels of merintA expression decreased from embryo to newborn and adult (data not shown). These findings suggest that merintA is of general importance during development and might play a significant role in cell proliferation and/or differentiation.

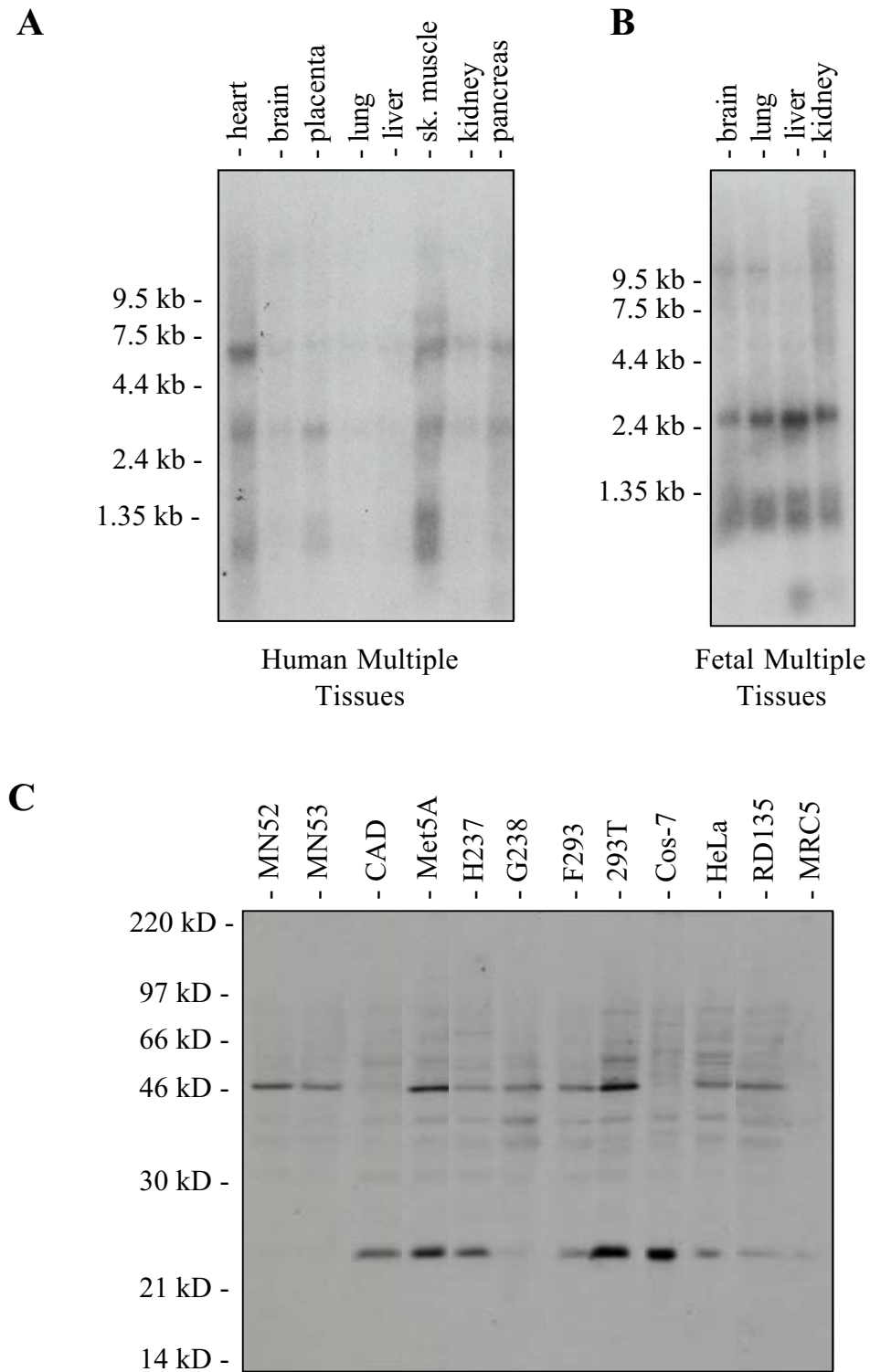


**Figure 20. Expression of MerintA in Different Tissues and Cell Lines.** A multiple tissue poly(A)<sup>+</sup> RNA blot (Clontech) was probed with <sup>32</sup>P- labeled merintA cDNA as recommended by the manufacturer (A). Western blot analysis reveals that merintA is expressed as a 24kD protein. Equal amounts of protein lysates (NP40) were separated on 12% SDS-PAGE and immunoblotted with the monoclonal antibody 7E1 (B).

During the course of this study a number of expressed sequence tags (ESTs) identical in part to merintA were deposited in public databases. These database searches confirm that merintA is expressed in a broad spectrum of tissues and cells which include adrenal gland, aorta, B-cells, brain, breast, cervix, central nervous system, colon, foreskin, gall bladder, germ cell, heart, kidney, lung, ovary, pancreas, parathyroid, prostate, stomach, testis, tonsil and uterus from adult cDNA sources. Strong expression of merintA was also confirmed in the following fetal tissues: whole embryo, bone, brain, breast, cervix, colon, connective tissue, eye, genitourinary tract, kidney, liver, lung, marrow, muscle, ovary, placenta, prostate, skin, spleen, testis, thymus, thyroid and uterus (<http://www.ncbi.nlm.nih.gov/UniGene/clust.cgi?ORG=Hs&CID=33032>). It is also of interest to note that merintA fragments were also isolated from a large number of different tumors originating from organs such as brain, (glioblastoma and neuroblastoma), eye (retinoblastoma), placenta (choriocarcinoma), lung (small cell carcinoma), testis (embryonal carcinoma), uterus, colon, liver (hepatocellular carcinoma) and mammary (gross tissue tumor). In conclusion, the merlin binding protein merintA is ubiquitously expressed in normal and tumor tissues.

#### **3.4.4 Merlin but not Moesin binds to MerintA *In Vitro* and *In Vivo***

To confirm the association between merlin and merintA beyond the yeast two-hybrid system, *in vitro* binding assays were performed. These experiments were conducted prior to isolating the full-length cDNA of merintA and generating antibodies against merintA. However, the results are presented together with *in vivo* binding studies (co-immunoprecipitation) using merintA specific antibodies to demonstrate the interaction of merintA and merlin.

First, GST-merlin was used to precipitate merintA that was expressed in mammalian cells. The HA-tagged merintA expressed in Cos-7 cells encoded amino acids 13-178. Additional 90 amino acids deriving from the vector sequence (pJG4-5) were expressed between the HA-tag and merintA as a fusion protein. Thus, this protein migrates above the 30kD marker, which is slower than the endogenous full-length protein. Cell lysates expressing epitope tagged merintA were tested for their ability to

bind with different segments of merlin expressed as bacterial GST fusion proteins and immobilized on Sepharose beads. The bound protein was detected in immunoblots, using an anti-HA antibody (hybridoma supernatant provided by Dr. Ed Harlow). MerintA bound specifically to the carboxy-terminal and full-length merlin fusion proteins, but did not bind to either the amino-terminus of merlin or to GST alone (Figure 21A). The results further demonstrate that the carboxy-terminal GST fusion protein of merlin isoform 2 captured more merintA than the truncated carboxy-terminal protein common to both isoforms. Less merintA was captured by the carboxy-terminal GST fusion protein of isoform 1 compared to the other carboxy-terminal proteins. These results were confirmed by three independent experiments.

For the reciprocal experiment, merlin isoforms 1 and 2 were expressed as FLAG-tagged proteins in 293T cells, which were then utilized in affinity binding assays with GST-merintA fusion protein. The FLAG-tagged merlin isoform proteins were examined by Western blot analysis with an anti-FLAG antibody (M2, Sigma) prior to the affinity binding assay to ensure equal expression. Cell lysates, expressing approximately the same amount of merlin isoform 1 and 2, were then incubated with GST-merintA or GST alone bound to beads. The proteins that precipitated with the beads were again analyzed by Western blot analysis for the presence of merlin with the M2 antibody. These experiments demonstrated that merlin isoforms expressed in mammalian cells also bind differentially to merintA (data not shown). GST-merintA also captured more merlin isoform 2 than isoform 1. Western blots were stained with Ponceau-S for total proteins before probing with the FLAG-antibody. This staining confirmed that equal amounts of GST fusion proteins and GST alone were bound to the beads in the experiments (data not shown).

To test whether merintA binds exclusively to merlin and not to ERM family members, different segments of moesin, expressed as bacterial GST fusion proteins, were tested as a representative. No binding of merintA to moesin was detected in this assay (Figure 21B). Thus, as was predicted by the two-hybrid analysis, merintA associates with the carboxy-terminal but not with the amino-terminal domain of merlin. Moreover, as predicted by sequence comparison merintA binds specifically to merlin but not to moesin.



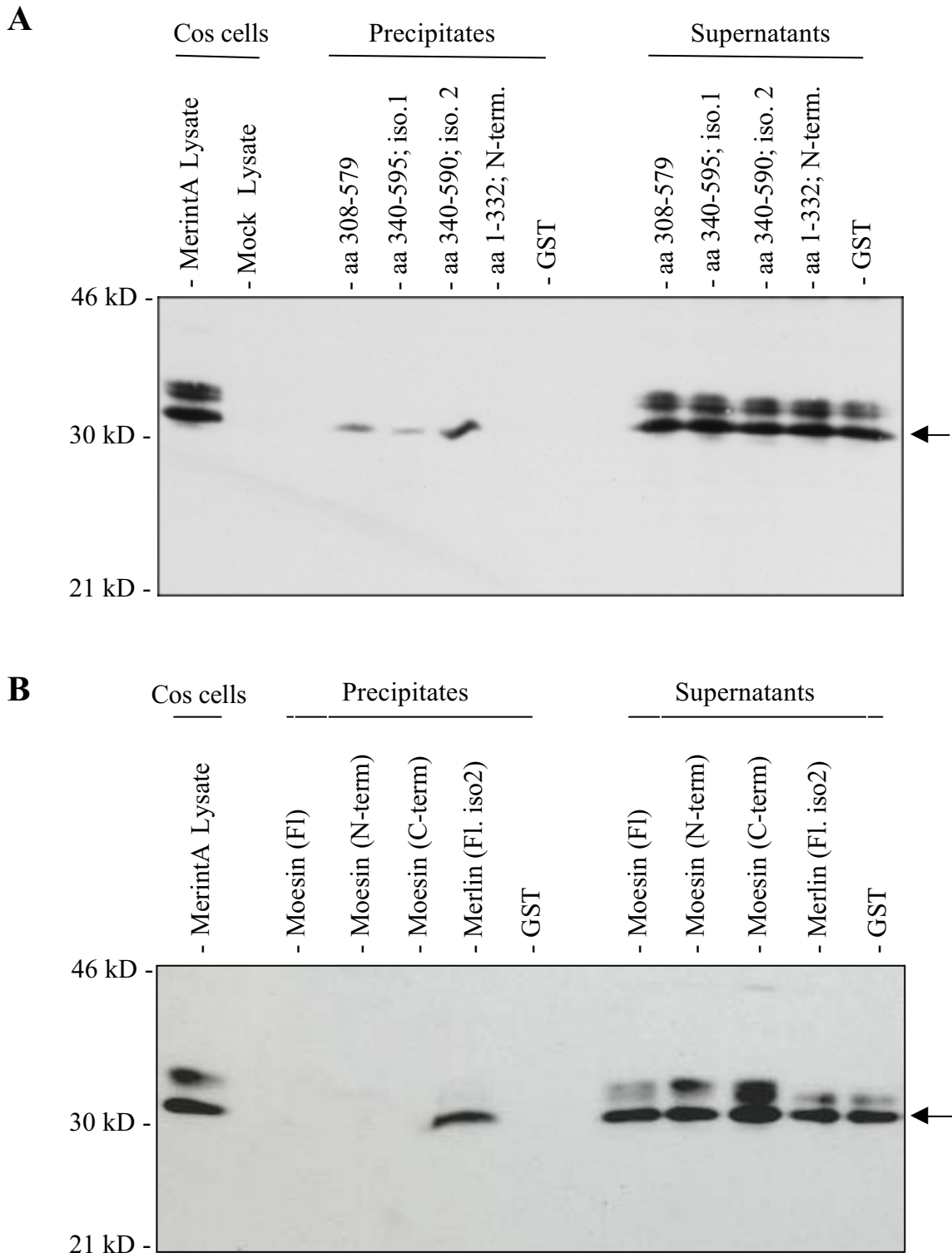


**Figure 21. Binding of MerintA to Merlin but not to Moesin.** NP40 lysates from Cos-7 cells overexpressing HA-merintA were incubated with various GST-merlin fusion proteins immobilized on glutathione Sepharose 4B beads. The beads were washed extensively, and bound proteins were separated on 10% SDS-PAGE and immunoblotted with an anti-HA antibody (A). The same assay was performed as in (A). However, various GST-moesin fusion proteins were tested for binding to merintA. Full-length merlin isoform 2 was used as positive control (B). Note: The HA-tagged merintA expressed in Cos-7 cells encoded amino acids 13-178. Additional 90 amino acids deriving from the vector sequence (pJG4-5) were expressed between the HA-tag and merintA as a fusion protein. Thus, this protein migrates above the 30kD marker, which is slower than the endogenous full-length protein.

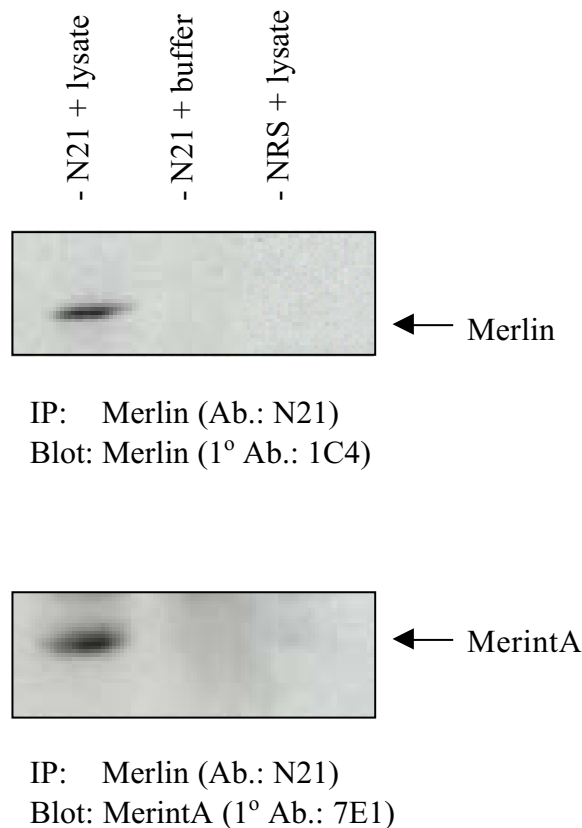


**Figure 22. MerintA Binds to Merlin *in vivo*.** A specific antibody (pAb: N21) was employed to immunoprecipitate merlin from CAD cell lysates followed by fractionation of the immunoprecipitates by 12% SDS-PAGE. Immunoblotting was performed for merlin (mAb 1C4) and merintA (mAb 7E1). Control lanes show N21 used without cell lysate (N21+buffer) and cell lysate employed with a non-specific antibody (NRS: normal rabbit serum).

Finally, co-immunoprecipitation experiments were conducted to test if the association between merlin and merintA also takes place *in vivo*. Towards this end, full-length merlin isoform 2 was overexpressed in CAD cells and cell lysates were incubated with a merlin antibody bound to protein A that is covalently coupled to an agarose matrix. Immunoprecipitates were tested for the presence of merlin as an internal control with a second merlin-specific antibody. In addition, merintA could be detected in these samples in three independent experiments indicating that it co-immunoprecipitated with merlin (Figure 22). Two controls ensure specificity of the antibody used to immunoprecipitate, and the signal detected by the antibody used for Western blot analysis. Immunoprecipitation experiments were carried out with the merlin antibody but the cell lysate was substituted with lysis buffer (Figure 22, lane 2). No signal was detected in this control indicating that the band detected in the complete reaction

represents merintA as opposed to the light chain of immunoprecipitating antibody that approximately co-migrates with merintA during gel electrophoresis. A non-specific antibody (normal rabbit serum) was employed in the second control and again no signal was detected, demonstrating specificity of these co-immunoprecipitation experiments (Figure 22, lane 3). Thus, merintA and merlin interact beyond the yeast-two hybrid system *in vitro* and *in vivo*.

### 3.4.5 MerintA Localization and Co-localization with Merlin

Previously, members of the Ramesh laboratory localized endogenous merlin to submembranous regions with an enrichment in motile regions, such as leading or ruffling edges in human fibroblast and meningioma cells. Merlin was also co-localized with F-actin in these motile regions but did not associate with stress fibers (Gonzalez-Agosti *et al.*, 1996). This localization pattern of merlin has been confirmed by a number of other studies (Deguen *et al.*, 1998; den Bakker *et al.*, 1995; Sainio *et al.*, 1997; Shaw *et al.*, 1998). In addition, the localization of merlin is in agreement with the direct and indirect interactions of merlin with the actin cytoskeleton and integral membrane proteins.

CAD cells were transiently transfected to express full-length HA-tagged merintA (A4) and GFP-merlin isoform 1 or 2 to examine the localization of these proteins. In these cells, merintA specifically localizes to submembranous regions and neurites (Figure 23, B+E). The co-transfection of epitope tagged merintA and GFP-merlin permitted comparison of the distribution of merintA with merlin isoform 1 or 2. This staining revealed that merintA co-localizes precisely with merlin isoform 2 in submembranous regions and neurites (Figure 23). Similar results were obtained in cells that were examined for co-localization of merintA and GFP merlin isoform 1 (data not shown). Furthermore, merintA was transfected alone into CAD cells to test if the observed localization is dependent on GFP-merlin. MerintA showed identical staining patterns in these singly transfected cells compared to the double transfected cells. Again merintA localized to submembranous regions and neurites of CAD cells (data not shown).

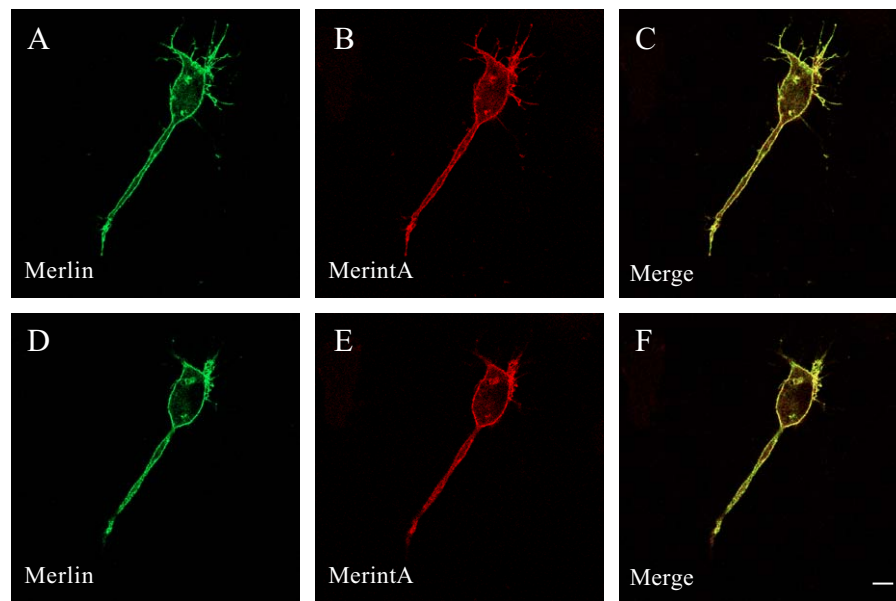


**Figure 23. Localization of GFP-Merlin and HA-tagged MerintA (A4).** GFP-merlin isoform 2 (A and D) was directly visualized in CAD cells that were also stained with 12CA5 (B and E). Merged images (C and F). Merlin co-localizes with merintA in neurites and underneath the plasma membrane. Bar, 10 $\mu$ m.

The localization studies of merlin and merintA resulted in two other observations and both occurred in single (merintA alone) and double transfected cells. First, many of the cells that stained positive showed membrane blebbing as opposed to neighboring cells that did not stain presumably because they did not express epitope tagged merintA and merlin. Cells undergoing apoptosis are characterized by phenotypes such as membrane blebbing as well as condensation of the nuclei, fragmentation of chromatin at nucleosome linkage sites and the formation of apoptotic bodies (Merino *et al.*, 1998). Second, a high percentage of cells that expressed epitope tagged merintA died ~48 hours after transfection. To test if merintA could be involved in programmed cell death, transfected cells were analyzed for nuclear condensation by staining with Hoechst 33342 (Sigma). This fluorescent dye specifically stains the nucleus of cells and allows comparison of cells that express epitope tagged merintA with neighboring cells that do not express these proteins. No condensation of nuclei was observed in these transfected cells that expressed merintA alone or co-expressed merintA and merlin (data not shown). An involvement of merintA or merlin in apoptosis thus appears unlikely.

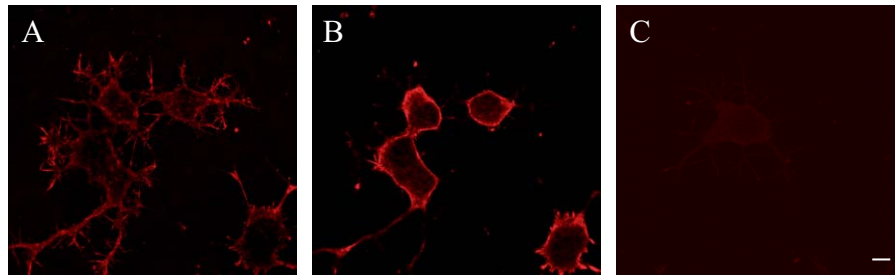


**Figure 24. Endogenous Localization of MerintA.** CAD cells were stained with 7E1 (A and B) and no primary antibody (C). Endogenous merintA localizes in neurites and underneath the plasma membrane. Bar, 10 $\mu$ m.

The localization pattern of exogenous merintA could be confirmed when CAD cells were stained with the monoclonal antibody 7E1 for visualization of the endogenous protein. Again, the protein was localized to submembranous regions and neurites (Figure 24A+B) whereas no specific staining was obtained when the primary antibody was omitted (Figure 24C). In conclusion, merintA co-localizes with merlin in CAD cells and thus fulfills this requirement of a merlin binding protein *in vivo*.

#### 3.4.6 MerintA Associates with the Actin Cytoskeleton

Previously, members of the Ramesh laboratory have co-localized merlin with F-actin and the physical interaction between merlin and actin was characterized in detail during the course of this study (Gonzalez-Agosti *et al.*, 1996; James *et al.*, 2001). Merlin lacks the high-affinity actin-binding site present in the carboxy-terminal end of ERM proteins (Huang *et al.*, 1998). However, it can bind actin either directly through a low-affinity binding site in the carboxy-terminal end of its FERM-domain (residues 178-367) (Xu H. *et al.*, 1998; James *et al.*, 2001), or indirectly via the actin-binding protein  $\beta$ II-spectrin (Scoles *et al.*, 1998).

Since the localization patterns of merintA and merlin are extremely similar, a possible relationship between merintA and actin was examined by immunofluorescence studies. CAD cells expressing HA-merintA were stained with HA-tag antibody 12CA5

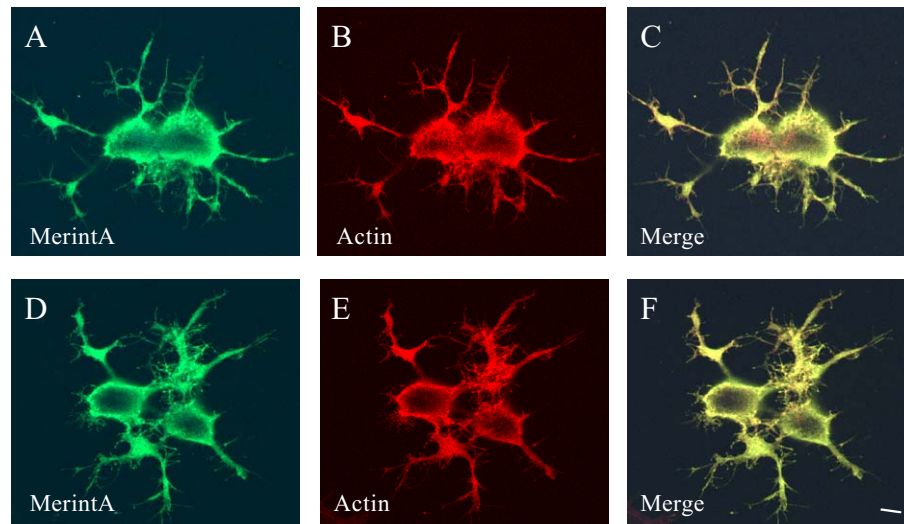


**Figure 25. Localization of HA-tagged MerintA (A4) and Actin.** CAD cells were stained with 12CA5 (A and D) and rhodamine phalloidin (B and E). Merged images (C and F). MerintA co-localizes with actin in neurites and underneath the plasma membrane. Bar, 10 $\mu$ m.

and with rhodamine phalloidin for actin. A strong co-localization of merintA with actin is observed in these cells in neurites and underneath the plasma membrane (Figure 25). These data imply that merintA and actin can associate directly or indirectly.

Merlin is detergent (Triton X-100) insoluble, indicating an ability to interact with the cytoskeleton (Deguen *et al.*, 1998; Stokowski *et al.*, 2000). Here, merintA was tested for an association with the cytoskeleton by similar fractionation experiments. Therefore, FLAG-tagged merlin isoform 2 and HA-tagged merintA were co-expressed in CAD cells. As expected, merlin fractionated in the insoluble moiety. MerintA was analyzed with the monoclonal antibody 7E1 to detect exogenous and endogenous proteins. Both proteins were found in the insoluble/cytoskeletal fraction (Figure 26). These investigations indicate that merintA is associated (directly or indirectly) to the actin cytoskeleton.

The co-localization and co-fractionation of actin and merintA led to the question whether merintA can bind actin directly or whether this association is mediated through other proteins such as merlin. Therefore, purified F-actin and merintA were submitted to high g-forces that cause purified actin filaments to pellet. The results of these

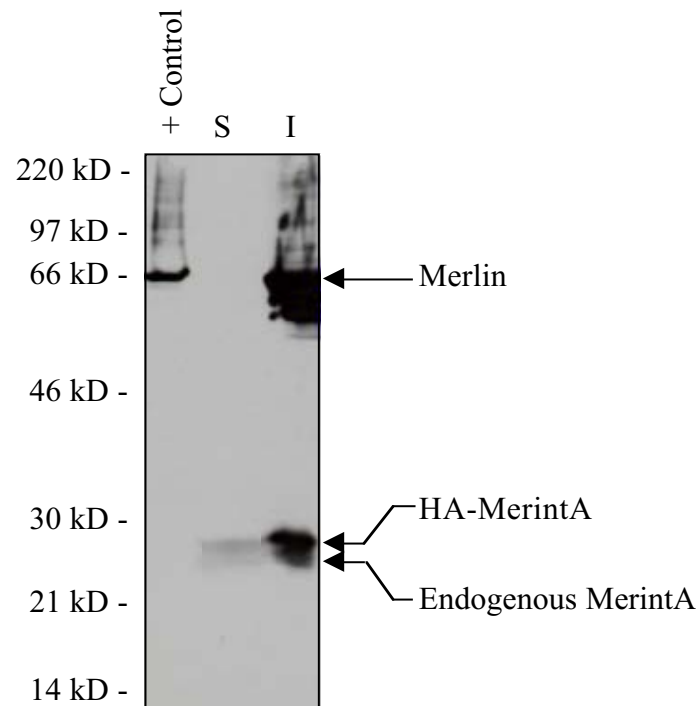


**Figure 26. Analysis of Merlin and MerintA Protein Solubility.** CAD cells were transfected with FLAG-merlin (isoform 2) and HA-merintA (A4) constructs, and cell lysates were recovered 48 hours after transfection. Total amounts of soluble (S) and insoluble (I) protein were separated on 12% SDS-PAGE and immunoblotted for merlin (1C4) and for merintA (7E1). Merlin and merintA localize to the insoluble cytoskeletal fraction.

experiments were inconclusive since merintA showed strong sedimentation in the absence of actin (data not shown). Next, a solid phase binding assay was utilized to test if merintA can bind to actin directly. Here, purified GST-merintA, GST-merlin or GST alone was coated in wells of plates and overlaid with purified F-actin. The samples were analyzed for the presence of actin after extensive washing. A two-fold increase in binding of actin to merintA was detected by ELISA over the background from the negative control (GST alone). In contrast, a five-fold increase in binding to merlin was detected by this assay. These experiments indicate moderate direct binding of merintA with actin.

The association of merintA with the cytoskeleton was further investigated by immuno-electron microscopy. These studies were carried out in collaboration with Drs. Ralph Neujahr and John Hartwig from the Division of Experimental Medicine, at the Brigham and Women's Hospital, Boston. Immunogold staining of CAD cells with the

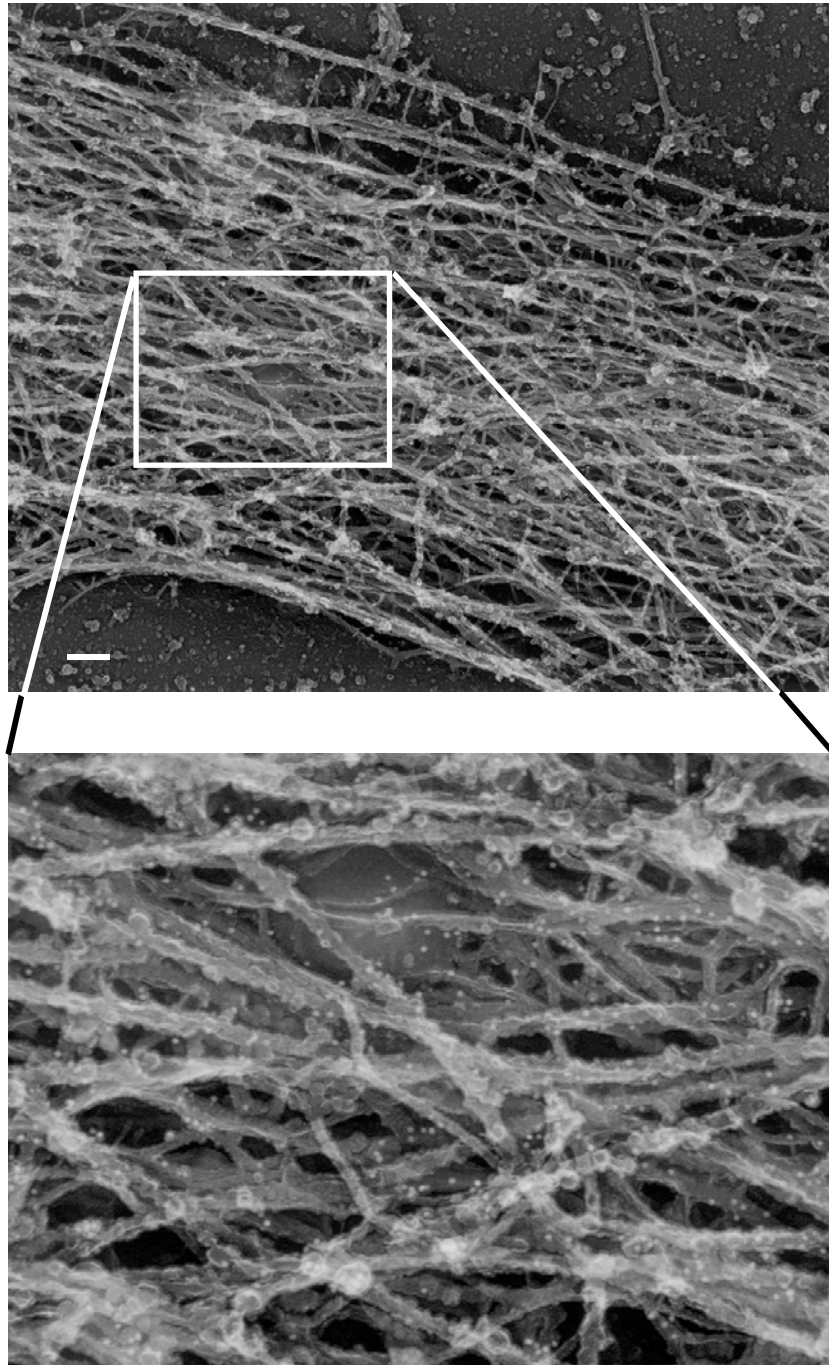


**Figure 27. Localization of MerintA in a Neurite of a CAD Cell Determined by Electron Microscopy.** MerintA was detected in the Triton X-100 insoluble cytoskeleton from a CAD cell using the merintA specific monoclonal antibody 7E1 followed by 10nm colloidal gold particles conjugated to secondary antibodies. Immunogold-labeled specimens were photographed after rapid freezing, freeze-drying, and tantalum-tungsten and carbon coating in a Jeol 1200-EX electron microscope. Bar, 200nm.



monoclonal antibody 7E1 showed that endogenous merintA resides on cortical actin filaments. MerintA is evenly distributed along these filaments and does not localize preferentially to substructures such as branching points or filament ends. Extensive staining of merintA can also be seen along the actin cytoskeleton within neurites (Figure 27). Next, CAD cells were investigated for merintA and merlin co-staining by immunoelectron microscopy. MerintA was again detected with 7E1 followed by 10nm colloidal gold particles conjugated to secondary antibodies while merlin was detected with the polyclonal antibody A19 followed by 5nm gold particles conjugated to secondary antibodies. MerintA and merlin co-localize in the cortex of the cytoskeleton from CAD cells. However, there are areas where distinct merintA and merlin staining, respectively, is seen at this subcellular resolution (Figure 28A). The primary antibodies were omitted in the negative control that shows no gold particles (Figure 28B). This distribution suggests that merintA was targeted to this location either through merlin, through other binding proteins or through independent actin-binding sites. Moreover, these results support a physiological relevance of the interaction between actin, merintA and merlin.

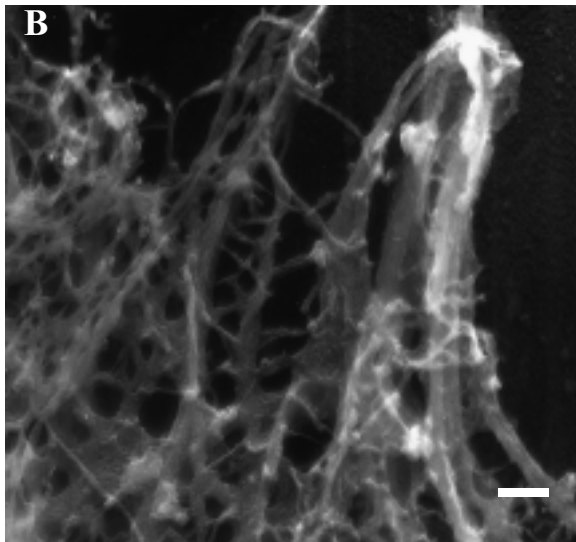
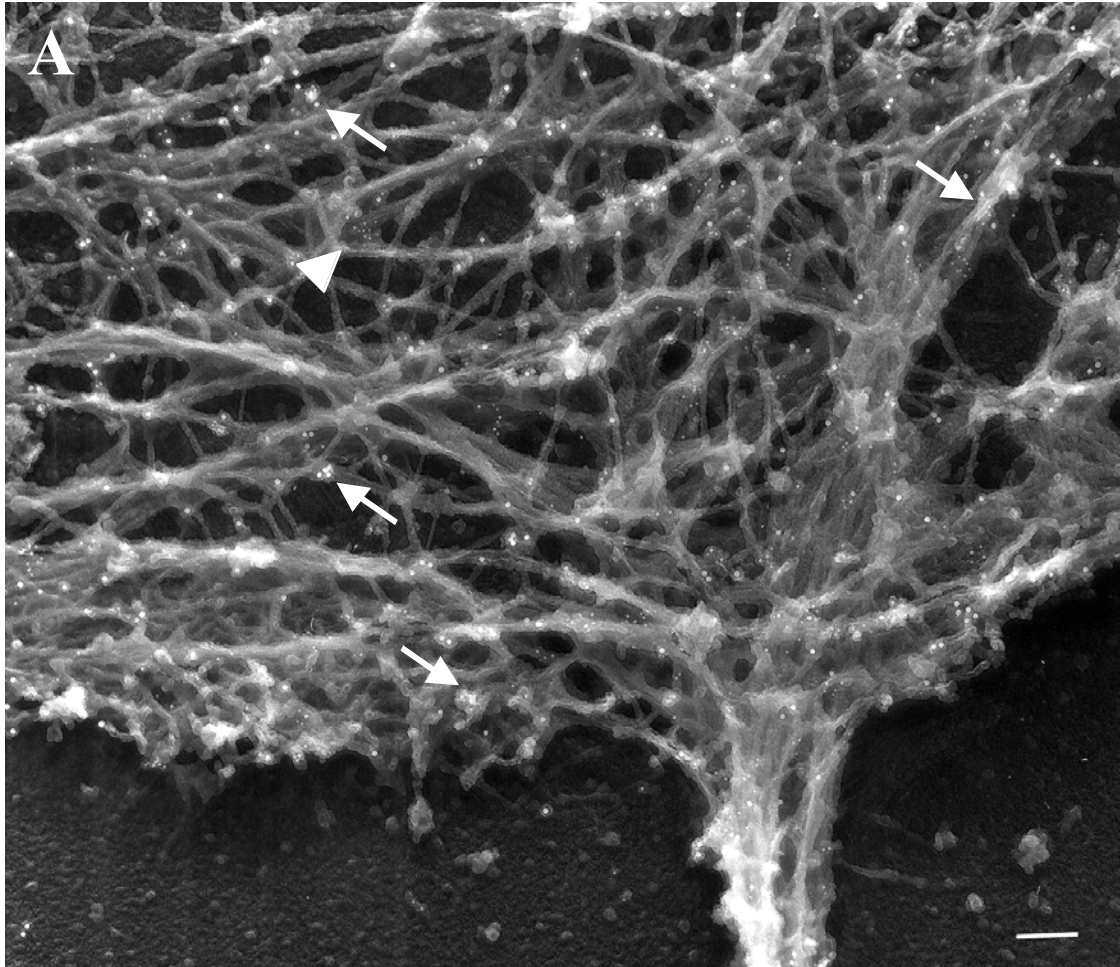


**Figure 28. Co-localization of MerintA and Merlin in the Cortex of a CAD Cell Determined by Electron Microscopy.**

MerintA and Merlin were detected in the Triton X-100 insoluble cytoskeleton from a CAD cell using the merintA specific monoclonal antibody 7E1 and the polyclonal merlin antibody A19 (Santa Cruz) followed by 10nm and 5nm colloidal gold particles conjugated to secondary antibodies. MerintA and merlin co-localize in many areas along the cytoskeleton (arrows). However, some regions show distinct merintA and merlin staining (arrowhead). Bar, 100nm (A). CAD cells were treated as above except for the omission of primary antibodies. No staining can be detected. Bar, 100nm (B).

### 3.4.7 MerintA Binds to Grb2

GenBank database searches did not associate merintA with any known functional protein families. Therefore, other databases were searched extensively to obtain clues of merintA function. Analysis of the merintA sequence for the occurrence of ProSite patterns (<http://ca.expasy.org/tools/scnpsit1.html>) predicted one N-glycosylation site (aa 66-69 NGTD) and three N-myristoylation sites (aa 6-11: GGMFSG; aa 7-12: GMFSGQ; aa 76-81: GVDQCI). The phosphorylation prediction program NetPhos2.0 (<http://www.cbs.dtu.dk/services/NetPhos/>) identified six serine, two threonine and one tyrosine residue (Y64) that could be phosphorylated. The consensus sequences of different protein kinases were scanned against the merintA sequence for potential phosphorylation sites at

<http://www.cbs.dtu.dk/databases/PhosphoBase/predict/predform.html>. The results of this analysis can be found in Table 4 and they predict several potential phosphorylation sites and the kinases including calmodulin-dependent protein kinase II (CaM II), casein kinase I (CK I), casein kinase II (CK II) and protein kinase A (PKA).

Finally, merintA was examined with *Scansite* (<http://cansite.bidmc.harvard.edu>) to predict protein motifs and binding sites. Here, the binding motif for the Src homology 2 (SH2-) domain of the growth factor receptor bound 2 (Grb2) protein was found in a high stringency scan between amino acids 63 and 67 (Y64 of merintA). The consensus sequence of this binding motif is pYV/INX (Schlessinger, 1994) and only 0.13% of all proteins can be found in SwissProt with this motif.

Grb2 is 25kD protein that localizes in submembranous regions and membrane ruffles of the cell (Bar-Sagi *et al.*, 1993). It is composed of one SH2-domain flanked by two Src homology 3 (SH3-) domains. The SH2-domain has been shown to bind to a number of autophosphorylated receptor protein tyrosine kinases (RTKs) and several cytoplasmic proteins, including Shc, SHP-2, Syp and Bcr-Abl, in a tyrosine phosphorylation-dependent manner (Buday, 1999; Li *et al.*, 1994; Pendergast *et al.*, 1993). The SH3-domains on the other hand are known to physically associate with proline-rich proteins including the Ras guanine-nucleotide exchange factor, Sos and

<b>Kinase</b>	<b>Consensus Sequence Sites of MerintA</b>	<b>Potential Phosphorylation</b>
CaM II	R-X-X-S/T-X	S-41 RPSSSTL
CK I *	Sp/Tp-X2-3-S/T-X	T-43 SSSTLVD S-61 SLVSQDY
CK II	X-S/T-X-X-D/E	T-43 SSSTLVD S-50 ELESSFE T-68 VNGTDQE T-75 EIRTGVD
GSK3	X-S/T-X-X-X-Sp	non
MLCK	X-K-K-R-X-X-S-X	non
p34cdc2	X-S/T-P-X-R/K	non
p70s6k	K/R-X-R-X-X-S/T-X	non
PKA	R-X1-2-S/T-X	S-41 RPSSSTL T-91 RQTECF
PKC	X-S/T-X-R/K	non
PKG	(R/K)2-3-X-S/T-X	non

**Table 4. List of Protein Kinases and Consensus Sequences for Potential Phosphorylation Sites of MerintA.** Predicted phosphorylation sites were obtained for merintA at <http://www.cbs.dtu.dk/databases/PhosphoBase/predict/predform.html>. The consensus sequences of individual kinases and potential phosphorylation sites of merintA are shown. (\* Amino-terminal serine/threonine must be prephosphorylated for the potential phosphorylation sites of the protein kinase CKI).

N-WASP (Buday, 1999). For example, the Grb2-Sos complex binds to the autophosphorylated EGF receptor (EGFR) upon EGF stimulation. This complex formation brings the exchange factor Sos into contact with its substrate Ras at the plasma membrane. Thus, Ras is activated through the formation of a ternary complex of EGFR-Sos-Grb2 and a signal is transmitted to other effector molecules such as Rac (Buday, 1999). Although this is a well-characterized signaling pathway, Grb2 is also involved in the activation of many others. While most studies indicate that the tyrosine

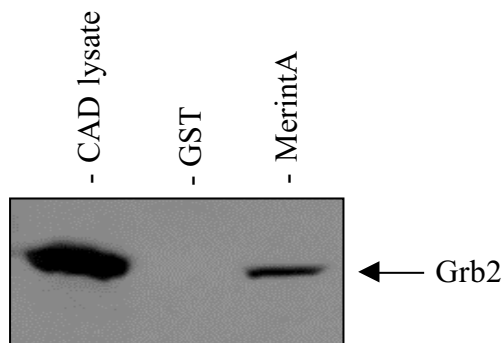


**Figure 29. MerintA Binds Grb2 *In Vitro*.** NP40 lysates from CAD cells were incubated with GST or GST-merintA proteins immobilized on glutathione Sepharose 4B beads. The beads were washed extensively, bound proteins were separated on 12% SDS-PAGE and immunoblotted with an anti-Grb2 (sc-255) antibody.

in the YN/IVX sequence needs to be phosphorylated for the Grb2 SH2-domain to bind, there are also more recent studies that support binding of non-phosphorylated peptide ligands for this SH2-domain (Long *et al.*, 1999; Oliginao *et al.*, 1997).

Here, the interaction of merintA with endogenous Grb2 was tested *in vitro*. Equal quantities of merintA expressed as GST fusion protein or GST alone were bound to glutathione Sepharose beads and incubated with equal amounts of CAD cell lysates. After extensive washes, the coupled proteins were removed from the beads by boiling and were detected by Western blot analysis using an anti-Grb2 (sc-255; Santa Cruz) antibody. The results demonstrate that merintA specifically captured Grb2, which did not bind to the GST control protein (Figure 29). Western blots were stained with Ponceau-S for total proteins before probing with the specific Grb2 antibody. This staining confirmed that equal amounts of GST fusion proteins and GST alone were bound to the beads in the experiments (data not shown).

The interaction between merintA and Grb2 was confirmed by blot overlay assays. His-merintA and BSA were subjected to SDS-PAGE and transferred to nitrocellulose membranes. Ponceau-S staining confirmed equal quantities of the proteins (Figure 30). Membranes were then overlaid with full-length GST-Grb2 followed by Western blot analysis using a GST-antibody. Grb2 bound specifically to merintA, but not to the control protein (Figure 30). These experiments demonstrate that merintA can bind directly to Grb2.

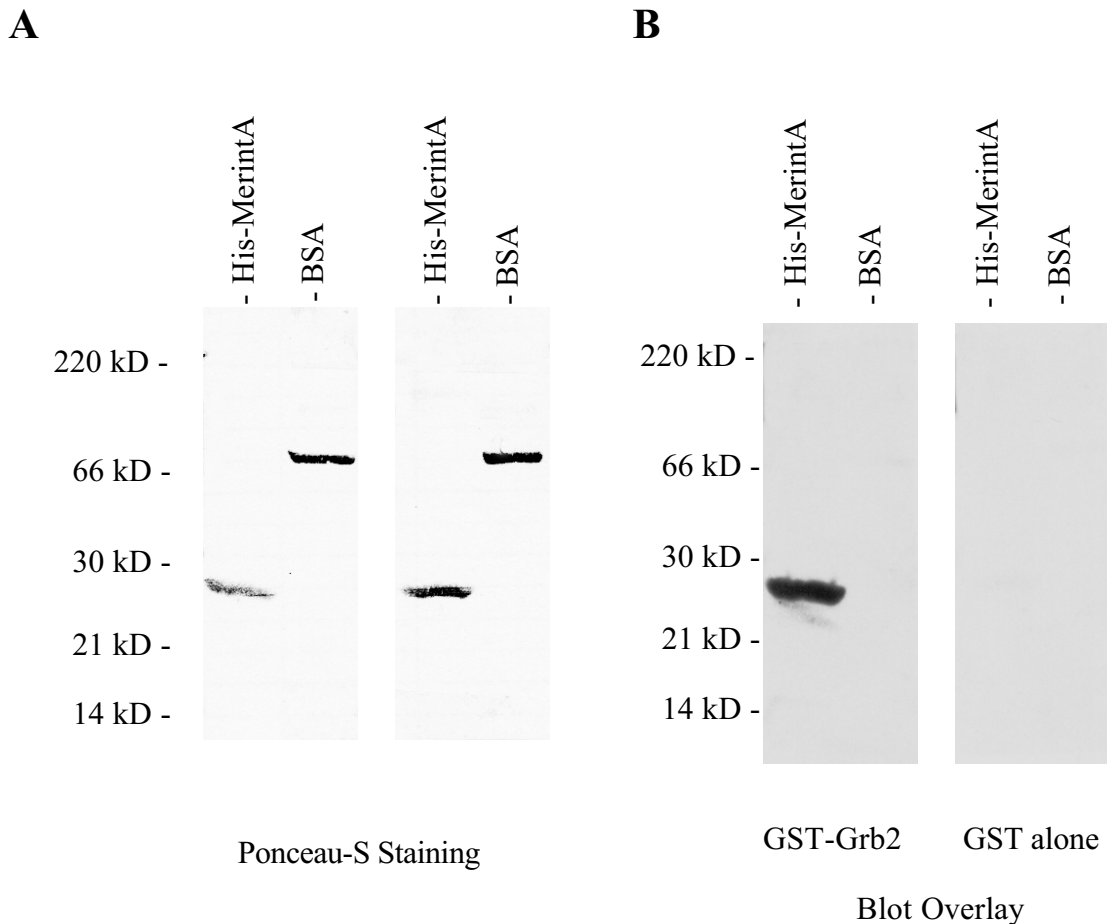


**Figure 30. MerintA Binds Directly to Grb2 *In Vitro*.** His-merintA and BSA were subjected to 12% SDS-PAGE and transferred to nitrocellulose membranes. Ponceau-S staining shows equal amounts of His-merintA and BSA (A). Full-length GST-Grb2 or GST alone was incubated with the membrane and then immunoblotted with an anti-GST (B14) antibody. GST-Grb2 binds specifically and directly to His-merintA (B).

As mentioned above, the tyrosine of the SH2-domain binding motif YV/INX is phosphorylated in many cases in order for Grb2 to bind (Schlessinger, 1994). Therefore, in addition to the fact that merintA has several predicted phosphorylation sites, it was tested whether this protein indeed gets phosphorylated. MerintA is not constitutively tyrosine phosphorylated based on three lines of evidence. First, merintA was immunoprecipitated as in Figure 4 and probed with the anti-phosphotyrosine antibodies 4G10 and pY20 (Upstate Biotechnology and TaKaRa). While the control shows that merintA precipitated, neither antibody cross-reacts with merintA indicating that no tyrosine residues are phosphorylated under these conditions. Alternatively, the tyrosine phosphorylation is below detectable levels (data not shown). Second, cell

lysates were treated with calf intestine phosphatase (CIP) and merintA was analyzed for shifts in mobility by Western blot analysis similar to those experiments shown in Figure 5B. While the positive control NHE-RF showed an obvious shift, no such change was detected for merintA (data not shown). Finally, cells were metabolically labeled with  $^{32}\text{P}$  and merintA was immunoprecipitated as above. Again, merintA precipitated but did not show detectable levels of phosphorylation (data not shown). These results demonstrate that merintA is not constitutively phosphorylated but is still able to bind to Grb2 *in vitro*. One of the next questions that arise is whether merintA becomes transiently phosphorylated upon specific growth factor induction such as EGF or PDGF. This and other questions will need further investigation. In summary, the novel protein merintA is widely expressed, binds and co-localizes specifically with merlin, is associated with the actin cytoskeleton and could be linked to signal transduction pathways in which Grb2 is involved in such as mitogenesis or cytoskeletal reorganization. However, further investigations need to be conducted in order to link the merlin-merintA and/or merintA-Grb2 complex specifically to one of these pathways.

## 4. Discussion

Merlin shares many properties with its family members, the ERM proteins, but it differs from these relatives in having two isoforms with alternative carboxy-termini and in having an established tumor suppressor function. The two major isoforms of *NF2* are expressed at the RNA and protein level in a variety of cell lines examined including *NF2* target cells such as Schwann and meningeal cells (Arakawa *et al.*, 1994, Haase *et al.*, 1994; Pykett *et al.*, 1994, Ramesh V., pers. commun.). Affinity co-electrophoresis experiments performed in the laboratory of Dr. V. Ramesh demonstrated a difference between merlin isoforms with respect to their interdomain interactions and defined the affinities of these interactions (Gonzalez-Agosti *et al.*, 1999). The measured affinities for the self-interaction of merlin isoform 1 and for the merlin-moesin interaction were in the same order of magnitude as the reported affinities for intramolecular associations of radixin (Magendantz *et al.*, 1995). It is believed that the isoform 1 specific carboxy-terminal residues (aa 580-595) are critical for the interdomain binding because the carboxy-terminal halves of merlin containing residues either common to both isoforms (aa 340-579) or isoform 2 (aa 340-590) did not exhibit the self-interaction (Gonzalez-Agosti *et al.*, 1999). The yeast two-hybrid system, blot overlay assays, affinity precipitation assays and co-immunoprecipitation experiments performed in other laboratories confirmed the interdomain interaction of merlin isoform 1 (Gronholm *et al.*, 1999; Huang *et al.*, 1998; Sherman *et al.*, 1997).

### 4.1 Characterization of the Interaction of Merlin Isoform 1 and 2 with NHE-RF

The intramolecular self-associations of the ERM proteins are known to mask the binding sites for other ligands, thus suppressing the association with their membrane partners and the actin cytoskeleton (Bretscher *et al.*, 1999; Tsukita *et al.*, 1997).

Moreover, binding of the ERM proteins to NHE-RF is blocked by the interdomain interaction of the full-length molecules which does not occur in the truncated amino-terminal proteins (Ramesh V., pers. commun.; Reczek *et al.*, 1998). Interdomain interactions, however, are disrupted either by phosphorylation or phospholipids such



as phosphatidylinositol 4-phosphate (PIP) or phosphatidylinositol 4,5-bisphosphate (PIP<sub>2</sub>). These phospholipids bind directly to the amino-terminus of the ERM proteins and expose other ligand binding sites (Heiska *et al.*, 1998; Hirao *et al.*, 1996; Niggli *et al.*, 1995).

These data raised the following questions: Do merlin isoform 1 and 2 have different binding properties towards the ligand NHE-RF based on their different conformations? Do phospholipids affect ligand binding? Indeed the observed head-to-tail association of merlin isoform 1 interferes with the binding to the ligand NHE-RF. In addition, the experiments conducted illustrate a difference in the ability of the two alternatively spliced isoforms of merlin to interact with NHE-RF. The carboxy-terminus of merlin isoform 1 competes with NHE-RF for the amino-terminal binding site. On the other hand, merlin isoform 2 exists in a constitutively open conformation that allows the binding of NHE-RF without being hindered by the intramolecular associations that occur in merlin isoform 1. Merlin expressed in bacteria or in mammalian cells illustrated this phenomenon. The phospholipid PIP<sub>2</sub> enhances the binding properties of this merlin isoform to NHE-RF. Phospholipids might, as in the case of the ERM proteins, bind to merlin to reveal the binding sites for NHE-RF which are masked otherwise. NHE-RF is constitutively phosphorylated and hypophosphorylated NHE-RF shows no difference in binding to merlin isoforms, in contrast to hyperphosphorylated NHE-RF, which binds exclusively to merlin isoform 2. However, in the reciprocal experiment, when GST-NHE-RF was utilized to capture merlin isoform 1 or 2, NHE-RF is not phosphorylated and a clear difference in the amount of merlin binding is seen. Here, more merlin isoform 2 binds to GST-NHE-RF than isoform 1.

The intramolecular interaction of merlin, which is quite dynamic, is of lower affinity than for ezrin (Nguyen *et al.*, 2001). This phenomenon has been established by analyzing both the full-length molecules and the respective domains in solution. The interaction of NHE-RF with the amino-terminus of ezrin can be inhibited by the presence of the carboxy-terminus of ezrin. In contrast, the interaction of NHE-RF with the amino-terminus of merlin is not inhibited by the carboxy-terminus of either ezrin or

merlin (Nguyen *et al.*, 2001). These competitive binding studies provide evidence of the potential dynamic exchange between binding partners even though associations may appear stable in the absence of a competing species. Moreover, these studies suggest selection of proteins between multiple binding partners. Differential binding of NHE-RF to merlin isoforms and different family members may have functional significance *in vivo*. The interaction of merlin with the ERM proteins indicates that these proteins could also regulate the activities of each other.

RhoA-induced phosphorylation of a carboxy-terminal threonine (T558 in moesin) has also been implicated in conformational regulation of the ERM proteins (Matsui *et al.*, 1998; Matsui *et al.*, 1999; Nakamura *et al.*, 1995; Nakamura *et al.*, 1999; Pietromonaco *et al.*, 1998; Simons *et al.*, 1998). This threonine residue is conserved in both isoforms of merlin (T577); however, while the sequence surrounding this amino acid is quite distinct in merlin, it is conserved in all three ERM proteins. This distinct sequence suggests that phosphorylation of this particular threonine has no effect on merlin's conformation and should not influence the binding to ligands such as NHE-RF. Recently, it has been reported that Rho activation has no effect on merlin phosphorylation (Shaw *et al.*, 2001) supporting the idea that this mechanism of action might be unique for the ERM proteins. Nonetheless, further studies are required to understand whether the phosphorylation of this residue is indeed not involved in regulating the intramolecular association of merlin isoform 1 and to determine the role it might play in merlin isoform 2.

Comparing merlin with the related ERM proteins is expected to reveal similarities that are instructive concerning the overall function of these proteins. In addition, differences are predicted that could reveal specific functions of these proteins, such as the tumor suppressor activity of merlin. Both similarities and differences came out of characterizing the interaction of merlin isoform 1 and 2 with NHE-RF. Merlin specific functions could be attributed to the regulation of merlin isoform 2 versus merlin isoform 1 and the ERM proteins. Merlin isoform 2 does not undergo intramolecular head-to-tail associations and exists always in the open state. These interactions with NHE-RF and potentially other merlin binding proteins may occur when the equivalent

sites in merlin isoform 1 and in the ERM proteins are masked due to intramolecular head-to-tail associations (closed state). The full range of merlin interactions with other proteins remains to be delineated (see 4.4 Merlin Binding Proteins). However, it is quite possible that merlin mediates many interactions with multiple partners. Merlin, therefore, could be involved in different signaling pathways, some of which may be shared with the ERM family members. The distinct tumor suppressor role of merlin could lie in the participation in a signaling pathway that is not shared with the ERM proteins and is uniquely important to NF2 target cells such as Schwann and meningeal cells. At this point, it remains unclear which merlin isoform conducts tumor suppressor function since both isoforms are ubiquitously expressed including in the NF2 target cells and no mutations have been found in the isoform defining exons.

## 4.2 NHE-RF Binding Proteins

The interaction of NHE-RF with merlin and the ERM proteins is mediated by the extreme carboxy-terminus of NHE-RF (Murthy *et al.*, 1998; Reczek *et al.*, 1998; Yun *et al.*, 1998). NHE-RF possesses two PDZ-domains that are known to mediate protein-protein interactions, and during the course of this study a number of proteins have been shown to bind to these domains (see below). Proteins binding to the PDZ-1 domain of NHE-RF have the consensus sequence DS/TXL (Hall *et al.*, 1998a), and database searches (GenBank) reveal proteins with this motif at the extreme carboxy-terminus (see Table 3).

The B1 subunit of the H<sup>+</sup> ATPase has the PDZ-binding motif DTAL, which suggests it is a potential binding partner of NHE-RF, and a possible interaction was analyzed between NHE-RF and the H<sup>+</sup> ATPase by localization and binding studies. NHE-RF and the H<sup>+</sup> ATPase physically associate in affinity binding- and co-immunoprecipitation experiments. Competition experiments show that the interaction occurs through the PDZ-binding motif of the H<sup>+</sup> ATPase. Immunolocalization studies of NHE-RF show that the two proteins co-localize in the kidney (in the collecting duct and connecting segment), supporting the relevance of this interaction.

In the collecting duct of the kidney, A-type intercalated cells contain high levels of H<sup>+</sup> ATPase and always have an apical staining pattern for this protein (Alper *et al.*, 1989; Brown *et al.*, 1988a). In B-type intercalated cells, the H<sup>+</sup> ATPase is also highly expressed and it localizes to the apical or the basolateral membrane (Alper *et al.*, 1989; Brown *et al.*, 1988a). These B-cells express ample amounts of NHE-RF in contrast to A-cells. Thus, B-cells represent a distinct cell type with respect to NHE-RF expression just like they do for the Cl<sup>-</sup>/HCO<sub>3</sub><sup>-</sup> exchanger (AE1). A-cells express AE1 with a basolateral staining pattern while this protein is not expressed in B-cells (Alper *et al.*, 1989). The results of the experiments carried out here clearly indicate that the polarity of NHE-RF and the H<sup>+</sup> ATPase is not unidirectional (i.e. exclusively apical) in every cell type.

The mechanism of action by which B-cells generate and maintain H<sup>+</sup> ATPase polarity has not been established but NHE-RF could be involved. Hensin, an

extracellular matrix protein, is involved in generating plasticity of the intercalated cell phenotype *in vitro* (Al-Awqati, 1996; Al-Awqati *et al.*, 1998). Similar to hensen, NHE-RF may play a role in establishing H<sup>+</sup> ATPase polarity. NHE-RF could bind to the cytosolic subunits (V<sub>1</sub> sector), including the B subunit, and recruit this complex to the transmembrane portion (V<sub>0</sub> sector). The diffuse intracellular localization of NHE-RF and the H<sup>+</sup> ATPase in some B intercalated cells supports that NHE-RF might play a role in trafficking. Alternatively, NHE-RF could maintain H<sup>+</sup> ATPase localization through its association with merlin or the ERM proteins, which in turn could anchor this entire complex to the actin cytoskeleton. In fact, phosphorylation of NHE-RF is known to interrupt the physical link between the  $\beta$ 2-adrenergic receptor and the actin cytoskeleton, an interruption which affects the endocytic sorting of this receptor (Cao *et al.*, 1999). Also, the B1 or B2 subunits of the H<sup>+</sup> ATPase are capable of binding actin directly via their amino-terminus (Lee *et al.*, 1999). The H<sup>+</sup> ATPase could, therefore, interact with the actin cytoskeleton directly via a B subunit or indirectly via the NHE-RF-merlin/ERM protein complex.

The concept of NHE-RF stabilizing a formed complex once it has reached its target membrane is supported by other studies. For example, NHE-RF is thought to stabilize the cystic fibrosis transmembrane conductance regulator in the apical plasma membrane (Hall *et al.*, 1998a). Other PDZ proteins appear to be involved in basolateral anchoring and targeting of various receptors in *Caenorhabditis elegans* (Kim, 1997). Disc lost, a *Drosophila* PDZ-domain protein, has been shown to have a dual role in maintaining apical and basolateral epithelial cell polarity (Bhat *et al.*, 1999). Further investigations should establish the relevance of the two mechanisms by which the H<sup>+</sup> ATPase can interact with the actin cytoskeleton, should elucidate their respective roles and should give clues with respect to H<sup>+</sup> ATPase cell polarity.

In proximal tubules, large amounts of NHE-RF are detected; NHE-RF co-localizes with NHE-3 in the apical membrane (Biemesderfer *et al.*, 1997) and in the apical brush border (Brown D. pers. commun.). Interestingly, the B2 subunit of the H<sup>+</sup> ATPase, which lacks the carboxy-terminal DTAL residues, is expressed in these tubule segments (Nelson *et al.*, 1992). Therefore, it is anticipated that in this cell type, the H<sup>+</sup>

ATPase is incapable of binding to NHE-RF. Localization studies reveal that in proximal tubules the H<sup>+</sup> ATPase does not co-localize with NHE-RF. It is unclear why it may be favorable for these cells to express the B2 subunit of the H<sup>+</sup> ATPase that cannot associate with NHE-RF at the apical membrane, but these data support that the DTAL motif is required to mediate the interaction of NHE-RF and the H<sup>+</sup> ATPase.

At least two major cytosolic subunits (B1 and E) associate with NHE-RF in affinity binding assays. Other subunits are expected to bind in a complex through the B1 subunit to NHE-RF although only the B1 and E subunits were tested as markers. Competition experiments confirm that the DTAL PDZ-binding motif of the B1 subunit is responsible for the interaction of the H<sup>+</sup> ATPase and NHE-RF. A peptide derived from the carboxy-terminus of the B1 56kD subunit, in contrast to the B2 isoform, inhibits the interaction of NHE-RF with the H<sup>+</sup> ATPase. All affinity-precipitation experiments were carried out with cytosolic preparations from the inner medulla for various reasons. First, kidney cytosol contains large amounts of free cytosolic H<sup>+</sup> ATPase subunits. Secondly, this kidney region contains high levels of the B1-H<sup>+</sup> ATPase isoform, and finally this region contains no proximal tubules, which express abundant endogenous NHE-RF that could potentially compete with protein binding to the affinity matrix.

In order to attempt co-immunoprecipitation experiments, validation of the only NHE-RF antibody (IC270) available at the time was necessary to confirm that NHE-RF precipitates in the first place. Conventional methods impede this determination because of the interference of the immunoglobulin visualized by secondary antibodies used for Western blot analysis and the antigen NHE-RF at ~50kD. Therefore, IC270 was biotinylated prior to utilizing it in Western blot analyses of immunoprecipitates. Streptavidin binds with high affinity to biotin, and horseradish peroxidase conjugated to streptavidin allows visualizing the immunoprecipitate-biotinylated primary antibody complex. This strategy successfully demonstrated that IC270 immunoprecipitates NHE-RF. Biotinylation of the primary antibody is rapid and can be used with small amounts of the antibody. This method is highly effective for the analysis of immunoprecipitates and protein-protein interactions.

IC270 immunoprecipitates NHE-RF from rat kidney cytosol. Furthermore, the E subunit of the H<sup>+</sup> ATPase co-immunoprecipitates with NHE-RF suggesting that NHE-RF exists indeed in a complex with the cytosolic subunits of the H<sup>+</sup> ATPase. The E subunit is a reliable marker of the assembled cytoplasmic subunits since previous data show that the cytoplasmic domains of the H<sup>+</sup> ATPase exist preassembled in the cytosol (Nelson *et al.*, 1999). These studies confirm the physiological relevance of the interaction between NHE-RF and the H<sup>+</sup> ATPase, and the competition experiments indicate that the interaction is direct and through the DTAL motif at the carboxy-terminus of the H<sup>+</sup> ATPase.

NHE-RF2 also possesses two PDZ-domains similar to NHE-RF, and the PDZ-1 domains are 73% identical between NHE-RF and NHE-RF2. The PDZ-1 domain of NHE-RF2 has also been shown to bind to both the consensus sequence DS/TXL and the carboxy-terminal motif DTRL of the cystic fibrosis transmembrane regulator (CFTR). Hence, it is likely that NHE-RF2 can also bind to the H<sup>+</sup> ATPase, and it would be valuable to investigate whether NHE-RF2 localizes to A-cells where NHE-RF expression is low and conducts analogous functions in these cells. While these two family members have been shown to bind to the same consensus sequence, it is unlikely that other PDZ-domain proteins also bind to this sequence. PDZ-domains were first identified in the post-synaptic density protein (PSD-95), *Drosophila* septate junction protein disc-large (Dlg) and the epithelial tight-junction protein zona occludens-1 (ZO-1) (Cho *et al.*, 1992; Stevenson *et al.*, 1986; Woods *et al.*, 1991; Woods *et al.*, 1993). PSD-95 has been shown to bind to the carboxy-terminal motif SXV (Kornau *et al.*, 1995), and INAD, another *Drosophila* PDZ-domain protein, has been shown to bind to the carboxy-terminal motif XF/Y/WCF (van Huizen *et al.*, 1998). These examples indicate that not all PDZ-domains can bind to the DS/TXL motif but that so far it is specific for the PDZ-1 domain of NHE-RF and NHE-RF2.

During the course of this study a number of proteins have been shown to bind to PDZ-domains of NHE-RF including  $\beta$ 2-adrenergic receptor, CFTR, EPI64, GRK6A, NHE3, P2Y1, PDGFR, PLC $\beta$  1, 2 & 3, Trp 4 & 5 and Yap 65 (for review see Voltz *et al.*, 2001), and most of these proteins have been shown to bind through the PDZ-1

binding motif. This rapidly growing list of proteins that bind NHE-RF and NHE-RF2 generates urgent questions: Are all reported interactions functionally significant or just some? What is the context of significant interactions? Are they regulated in a spatial or temporal manner, or do the receptors and binding partners of NHE-RF compete with each other? An apparent difference in stoichiometry of NHE-RF and candidates that bind the PDZ-domains of NHE-RF has been reported (Reczek *et al.*, 2001). The high levels of NHE-RF suggest that many different proteins can bind to NHE-RF even in one structure of a given cell. This idea is supported by the findings that many different NHE-RF binding proteins associate with NHE-RF in extracts of placental microvilli (Reczek *et al.*, 2001). Thus, it is possible that many of the reported interactions occur in parallel and that NHE-RF may function in different processes and pathways.

In summary, the B1 subunit of the H<sup>+</sup> ATPase is a physiologically relevant binding protein of NHE-RF and may link the H<sup>+</sup> ATPase to the cytoskeleton. The two proteins co-localize in B-intercalated cells but not in A-cells, suggesting a possible function in generating, maintaining or modulating the B-cell phenotype. In contrast, NHE-RF and H<sup>+</sup> ATPase do not co-localize in proximal tubules, which express a truncated B2 subunit of the H<sup>+</sup> ATPase that lacks the PDZ-binding motif DTAL. These studies could be extended to Schwann and meningeal cells to test the relevance of this interaction in the context of NF2.



### 4.3 The Potential Role of NHE-RF in Cancer

NHE-RF is highly expressed in epithelial cells of many tissues, especially in those with numerous microvilli. Prominent NHE-RF expression is also seen in specialized ion transporting cells such as renal proximal tubules, eccrine glands, parietal cells in gastric glands, colonic absorptive cells and ependymal cells (Stemmer-Rachamimov *et al.*, 2001).

#### 4.3.1 NHE-RF Expression is Regulated by Estrogen in Breast Cancer Cells

The expression and localization of NHE-RF were investigated in meningiomas and tumors deriving from other organs including colon, ovary and breast. An enormous upregulation of NHE-RF was found in the breast cancer cell lines MCF-7, ZR-75-B and T-47-D compared to other breast cancer cell lines and normal mammary cell lines. NHE-RF and the related NHE-RF2 appear to share many functions; however, an upregulation of NHE-RF2 was not observed in any of the tested breast cancer cells. Various mechanisms can explain upregulation of genes, in general and some examples are insertional mutations, gene translocations or gene amplification. All cell lines analyzed earlier were subjected to Southern blot analysis to detect gene amplification. These studies, however, gave no evidence for gene amplification (data not shown) and other means of upregulation of NHE-RF had to be considered. The breast cancer cell lines where NHE-RF is upregulated are all positive for the estrogen receptor (ER-). Our study suggests that induction of NHE-RF expression is a primary response to estrogen. Interestingly, during the course of this work, Ediger *et al.* (1999) reported that NHE-RF is under estrogen regulation. Using differential display RNA methods, the authors showed that NHE-RF was under rapid and direct regulation by estrogen in the ER-containing cell line MCF-7. This stimulation appeared selective for estrogen ligands, since no stimulation was detected by other classes of steroid hormones. In addition, the anti-estrogens tamoxifen and ICI 182,780 suppressed stimulation by estrogen. Thus, the results of our study were consistent with those reported by Ediger *et al.* (1999). In addition, our study gathered evidence for the upregulation of NHE-RF in a majority of

ER- positive primary breast tumors, establishing that NHE-RF expression is regulated by estrogen *in vivo*.

#### 4.3.2 The Role of Estrogen and NHE-RF in Breast Cancer

Estrogen stimulation of mammary epithelial cells is considered a key factor in the development of breast cancer. The intracellular, nuclear estrogen receptor (ER) binds estrogen and is then transformed into an active transcription factor that mediates proliferative effects. Two closely related receptor families, ER-  $\alpha$  and ER-  $\beta$ , are known to mediate estrogen stimulated responses, and the expression of ERs is used as an important prognostic marker in breast cancer. Therefore, antiestrogens may be therapeutically effective in ER- positive breast cancers. Patients with ER- negative tumors tend to have a higher recurrence rate compared to patients with ER- positive tumors. ER- negative tumors are also more aggressive, do not respond to antiestrogen treatment in general and result in poor patient survival (Knight *et al.*, 1977; Sigurdsson *et al.*, 1990). Although ER- positive tumors are more likely to respond to hormonal therapy, there is no absolute correlation between ER expression and hormone response (Osborne 1998). Endocrine manipulations have no effect on approximately 40% of patients with ER- positive cancer while approximately 10% of ER- negative tumors respond (Henderson *et al.*, 1997; Nagai *et al.*, 1979). Moreover, ER- positive tumors can convert into refractory tumors and these mechanisms are poorly understood.

In our study, high levels of NHE-RF expression were observed in approximately 30% of the ER- negative breast tumors. Some ER- negative tumors express a variant form of ER with an exon 5 deletion, which is transcriptionally active and capable of inducing the expression of specific genes (Fuqua *et al.*, 1995; Lemieux *et al.*, 1996). The expression of NHE-RF in ER- negative tumors raises the question whether this variant form is present in these tumors. Other mechanisms by which NHE-RF is induced in the ER- negative tumors cannot be ruled out. Several signaling cascades, including epidermal growth factor, insulin like growth factor and MAP- kinase pathways are involved in estrogen signaling (Aronica *et al.*, 1993; Katzenellenbogen,

1996; Korach *et al.*, 1996; Migliaccio *et al.*, 1993; Smith, 1998). These overlapping pathways may partly explain ER- independent upregulation of NHE-RF and explain those breast cancer cells that adapt to or bypass antiestrogen therapy.

Estrogen binds and activates ER, which then binds to estrogen responsive elements (ERE) often located in the 5' flanking region of estrogen responsive genes. Additional investigations are necessary to identify and characterize such EREs in the *NHE-RF* gene. In this context, it is worth noting that the BRCA1 protein is thought to suppress estrogen-dependent transcriptional pathways related to mammary epithelial cell proliferation, and the loss of this ability might contribute to tumorigenesis (Fan *et al.*, 1999). Testing whether BRCA1 has any influence on the induction of NHE-RF by estrogen would be of potential interest.

#### **4.3.3 The Role of NHE-RF in the Organization of Microvilli**

It is well documented that NHE-RF localizes to microvilli of cultured cells (Murthy *et al.*, 1998; Reczek *et al.*, 1997). Estrogen induces cytoskeletal alterations in ER-containing breast cancer cells such as increasing the number and length of microvilli at the cell surface. In fact, MCF-7 cells are uniformly covered with microvilli 2 days after  $\beta$ -estradiol treatment (Coutts *et al.*, 1996; Vic *et al.*, 1982).

It is remarkable to observe the abundance of NHE-RF in microvilli of MCF-7 cells treated with estrogen for 48 hours. Molecular mechanisms behind the organization of these membrane surface structures are not completely understood and remain a focus of study. Overexpression of some cytoskeletal or lipid-binding proteins results in the elongation of microvilli (Arpin *et al.*, 1994; Friederich *et al.*, 1989; Ma *et al.*, 1997). Small GTPases (e.g. Rho and Rac) and the ERM proteins are known to function in cortical actin polymerization (MacKay *et al.*, 1997). Furthermore, ERM proteins are thought to play a key role in the formation of microvilli through cross-linking actin filaments and integral membrane proteins such as CD43, CD44, and ICAM2 (Bretscher *et al.*, 1999). A recent study has shown that overexpression of ERM binding membrane proteins (e.g. CD44) in fibroblasts induces microvillar elongation with the recruitment of the ERM proteins and actin filaments (Yonemura *et al.*, 1999). In light of these

findings, it is tempting to consider the possibility that a cytosolic ERM binding protein such as NHE-RF could be involved in microvillar organization in ER- positive breast cancer cells. Further studies are required to address whether estrogen simply induces the formation of a large number of microvilli and whether they are also elongated. NHE-RF could be involved in the *de novo* formation of microvilli or recruited in concert with the MERM proteins to this location and influence microvilli length.

NHE-RF is a multi-phosphorylated protein, interacts with many different proteins (Reczek *et al.*, 2001) and has roles in the apical surfaces of ion transporting epithelia (Breton *et al.*, 2000). This study demonstrates that estrogen stimulates NHE-RF expression in breast carcinomas, that it binds differentially to merlin isoform 1 and 2 and that it interacts with the H<sup>+</sup> ATPase. Other reports have connected NHE-RF to many other membrane proteins. Consequently, NHE-RF is a multifunctional protein and appears to be a key adaptor within a web of interactions involving membrane proteins/NHE-RF/MERM/F-actin (Figure 31). Cross talk among different signal transduction pathways may be mediated by the interactions of NHE-RF. Moreover, the study of NHE-RF provides new possibilities for future insights into normal and abnormal intracellular signaling. Defining the pathways through which ER mediated signaling is linked to NHE-RF will certainly provide a better knowledge of the role that NHE-RF might play in breast cancer and may enable the development of novel therapeutic intervention for such growth pathways.

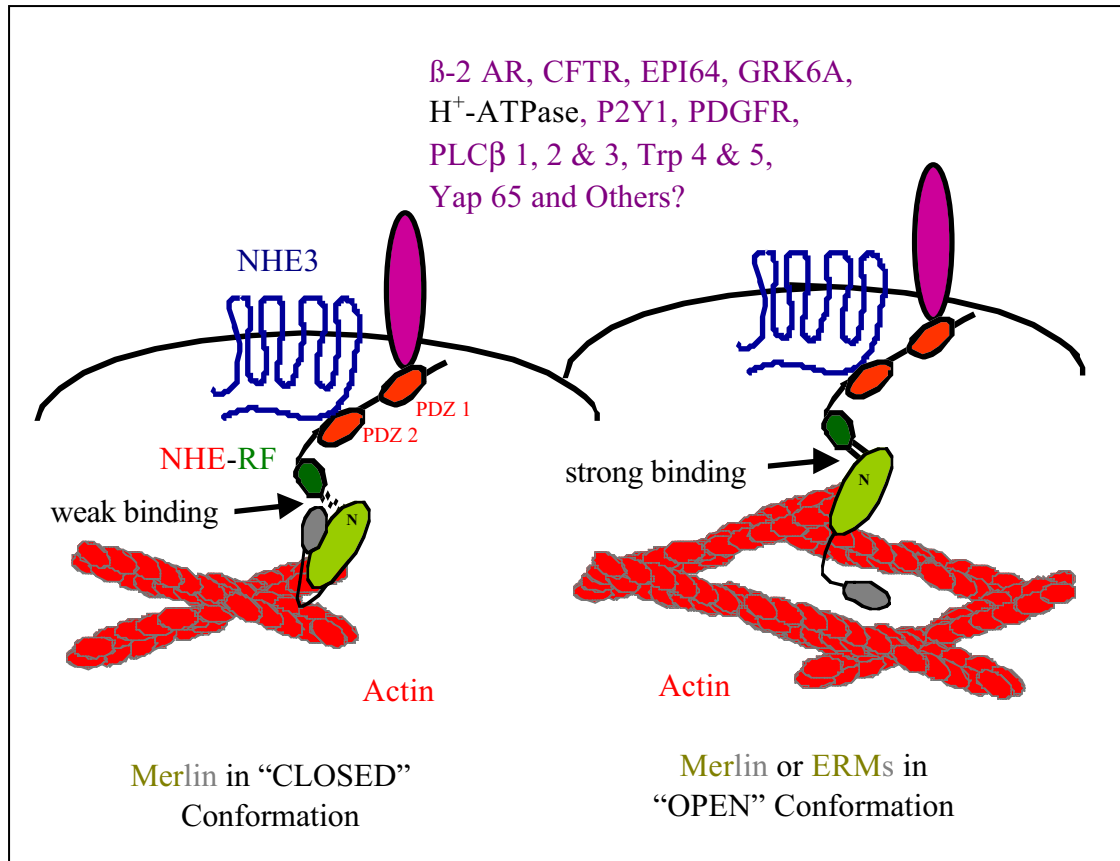


Figure 31. A Model of Merlin, NHE-RF and Their Binding Partners. See text for details.

#### 4.4 Merlin Binding Proteins

The function of merlin is the subject of many studies, and insights into possible roles of merlin have come in part from animal models. Limited information on merlin binding proteins was available at the time this work began. Several cellular proteins have been shown to interact with merlin *in vitro*; however, the identities of these proteins have not been revealed (Takeshima *et al.*, 1994). NHE-RF was one of the first discovered merlin binding proteins which was also shown to bind the ERM proteins (Murthy *et al.*, 1998; Rezcek *et al.*, 1997). Accordingly, it was of great interest to identify and to characterize further merlin binding proteins.

##### 4.4.1 Identification of Merlin Binding Proteins

Prior to this work, the yeast two-hybrid system had been employed in the Molecular Neurogenetics Unit at Massachusetts General Hospital, Boston to identify merlin binding proteins. Three candidates were found, and one of these was NHE-RF (merintC). The two other binding partners, merintA and merintB, were characterized in this study and gave mixed results. MerintB, a novel gene at the time of isolation, interacts consistently in the yeast two-hybrid system; however, affinity binding assays did not confirm that merintB truly binds to merlin. It is not clear why this candidate was identified numerous times in the original yeast two-hybrid screen but merintB might simply be a false positive. On the other hand, a number of reasons might explain why no binding was seen by other methods. Only a partial cDNA was available at the time the interaction was tested. Expressing parts of a protein in mammalian cells might not allow the right conformation that is needed for the interaction. In the affinity binding assay, merlin was expressed as a GST fusion protein and merintB was overexpressed in Cos-7 cells. The reciprocal experiment could be tested to see a possible interaction. It is known that affinity binding assays sometimes work only unidirectionally because important post-translational modification might be missing for the bacterially expressed protein. Hence, GST-merlin used in this assay might lack post-translational modifications that are necessary for this particular interaction.

Nonetheless, the affinity binding assay did not show an interaction of merintB with merlin, and, therefore, merintB was not further analyzed.

#### 4.4.2 The Interaction of MerintA with Merlin

MerintA, on the other hand, has proven to be a new merlin binding protein. Initial affinity binding assays quickly demonstrated that merintA binds to merlin beyond the yeast two-hybrid system, and these findings encouraged further studies. Co-immunoprecipitation experiments, in addition to the yeast two-hybrid system and affinity binding assays, demonstrate that merintA and merlin bind to each other *in vitro* and *in vivo*. Immunofluorescence and electron microscopy studies show a high and significant degree of co-localization between merintA and merlin supporting the relevance of this interaction. Merlin isoform 2 captures more merintA than merlin isoform 1 in the affinity binding assays. These observed binding properties might be different from the preferential binding of NHE-RF to merlin isoform 2. In the case of merintA, the binding might be sequence specific. Unlike full-length merlin isoform 1, the carboxy-terminal domains used in this assay do not undergo intramolecular associations. The preference of merintA to merlin isoform 2 might be caused by the amino acid sequence encoded by exon 16. However, merintA does not bind exclusively to merlin isoform 2. MerintA was originally identified by screening for merlin binding proteins using merlin isoform 1, and affinity binding assays confirm an interaction between merintA and merlin isoform 1. The carboxy-terminus of merlin is less homologous to the ERM proteins than the amino-terminus (Figure 2). As expected, merintA binds specifically to merlin and not to the ERM protein moesin. The specificity of the merintA-merlin interaction illustrates a unique property of merlin, and may provide clues to the tumor suppressor function of merlin, which is not shared with the ERM proteins. In summary, the binding analyses and subcellular localization data indicate that merintA is a physiologically relevant binding partner of merlin.

#### 4.4.3 Characterization of MerintA

Sequence analysis revealed that merintA is a novel gene that has not been characterized to date, and a cDNA was isolated corresponding to the shortest transcript seen by Northern blot analysis. The original transcript isolated from the yeast two-hybrid screen did not have a start codon. 5' rapid amplification of cDNA ends (5'-RACE) was employed to identify a full-length transcript. Sequence analysis of the 5'-RACE products distinguished a start codon with surrounding sequence that roughly fulfills the requirements of the Kozak-sequence. A second ATG encodes the eighth amino acid of merintA although the surrounding sequence of this codon does not fulfill the requirements of the Kozak-sequence. Therefore, it is unlikely that this second ATG is indeed a start codon. The other transcripts seen by Northern blot analysis raise the possibility of alternative splice products. During the course of this study, mRNA sequences have been deposited at GenBank, and they account for most of the other transcripts. Interestingly, all these sequences, including the one isolated here, have the same open reading frame indicating that the full-length sequence was obtained. Further studies are necessary to explore temporal and spatial expression of the various transcripts, which might regulate merintA by the different untranslated regions. One larger transcript, seen only in adult tissues, is unaccounted for, and a different open reading frame is possible.

MerintA is a 178 amino acid protein, which is predicted to be encoded by a four-exon gene on chromosome 4p15.3. The existence of anonymous orthologues in mouse, rat, cow, zebrafish and fly demonstrate that this gene is of general significance. A sequence (AF358829) identical to merintA was also submitted to GenBank in April 2001 and is entitled "novel gene as tumor angiogenesis marker." In the absence of any published information, it is reasonable to assume that merintA might play a role during angiogenesis in general or specifically during tumor angiogenesis. The protein consists of an amino-terminal low-complexity region with several glycines and prolines followed by a coiled-coil domain (aa 109-145). The latter domain is often found in adaptor or structural proteins and is known to mediate protein-protein interactions (Alberts *et al.*, 1994). It would be worthwhile to investigate whether the interaction of merintA and



merlin is mediated through this coiled-coil domain and to identify other proteins that bind to this domain. Analysis of the merintA sequence for the occurrence of ProSite patterns predicted N-myristoylation sites. An appreciable number of eukaryotic proteins are N-myristoylated, which is the covalent addition of myristate (a C14-saturated fatty acid) to their N-terminal residue via an amide linkage (Grand *et al.*, 1989; Towler *et al.*, 1988). Myristoylation of the guanidine nucleotide exchange factor Sos, for example, targets the protein to the membrane and complements activation of the Ras signaling pathway (Aronheim *et al.*, 1994). Possible merintA myristoylation could explain its submembranous localization, and merintA, like Sos, might recruit other proteins to this site.

To analyze merintA further, polyclonal and monoclonal antibodies were generated. Several lines of evidence demonstrate that the antibodies raised against merintA are specific. First, the antibodies cross-react with the exogenous merintA expressed in bacteria or mammalian cells. Second, pre-absorbing the antibody with the purified antigen abolishes the signal, and finally the different polyclonal and monoclonal antibodies recognize the same endogenous protein. These data demonstrate that the antibodies raised are indeed specific and that they are valuable tools for studying merintA. The protein is detected with an apparent size of 24kD by Western blot analysis, slightly larger than the size predicted from its actual sequence. The anomalous migration might be caused by unidentified post-translational modifications. MerintA is not constitutively phosphorylated; however, some phosphorylation sites are predicted based on sequence analysis. On that note, it would be useful to test whether the predicted kinases CaM II, CK I, CK II or PKA can phosphorylate merintA *in vitro* or *in vivo*.

Expression analysis from different human cell lines shows that merintA is seen to varying extents in most of the lines examined. An additional band at ~50kD is also recognized by the monoclonal antibody 7E1 but not by the polyclonal antibodies. This species might represent one of the following: (A) an alternatively spliced merintA isoform deriving from the larger unaccounted transcript mentioned above; (B) a strong dimer that resists the denaturing conditions of SDS-PAGE; (C) a closely related

protein, or (D) an unrelated protein with a similar epitope. The identity of this species has not been determined to date. Interestingly, primary meningioma cell lines that are NF2 positive or negative express the ~50kD protein while merintA (24kD) is expressed almost below detectable levels. In fact, a longer exposure than the one shown in Figure 20 is necessary to detect merintA in meningioma cell lines. On the other hand, the relative amounts of merintA and the ~50kD protein are inverted in CAD and Cos-7 cells. Here, the ~50kD protein is almost below detectable levels while merintA is expressed abundantly. Therefore, CAD cells were used in this study to characterize merintA and its interaction with merlin.

CAD (Cath a-differentiated) cells derive from the cell line Cath a, which was established from a brain tumor that arose in a transgenic mouse carrying wild-type SV40 T antigen under the transcriptional control of the rat tyrosine hydroxylase promoter. Reversible, morphological differentiation in CAD cells can be initiated by removal of serum or exogenously added protein to the medium. Differentiated CAD cells stop proliferating and extend long neurite-like processes (Qi *et al.*, 1997). MerintA and merlin localize in these neurites and underneath the plasma membrane in differentiating CAD cells. Merlin has been localized to lamellipodia or membrane ruffles (Gonzalez-Agosti *et al.*, 1996), but differentiated CAD cells do not exhibit these motile structures. Thus, neither merlin nor merintA was localized to membrane ruffles in CAD cells. However, just like merlin, merintA localizes to membrane ruffles in other cell types that do display these motile structures (data not shown). Examining the localization of merintA in merlin deficient cells and vice versa would be of great interest in order to test whether the localization of one protein is dependent on the other.

CAD cells lack an obvious phenotype upon exogenous expression of merintA. Initial studies suggested that merintA might play a role in apoptosis since a majority of the cells die ~48 hours post-transfection. Membrane blebbing, a characteristic of apoptosis, is observed upon exogenous expression of merintA. However, condensed nuclei, another phenotype of apoptotic cells, are not induced by merintA (data not shown). Hence, the overexpression of merintA could simply be toxic to the cells. Interestingly, merlin also prompts membrane blebbing, cytoplasmic shrinking, cell

rounding, condensed nuclei and cell death, yet this phenotype is not suppressed by co-expressing the apoptosis inhibitors p35 (caspase family inhibitor) and Bcl-2 (Shaw *et al.*, 1998). There is no data supporting that merlin normally plays a role in the regulation of cell death. It is possible that overexpression of merintA sensitizes cells for apoptosis rather than induces apoptosis and that co-expression of merintA and merlin induces apoptosis. Detailed studies using an inducible promoter system to drive expression of merintA and merlin should illuminate on the relationship between cell death induction and the morphogenetic properties observed.

#### 4.4.4 MerintA and the Actin Cytoskeleton

Merlin is an actin binding protein (James *et al.*, 2001), and based on the high degree of co-localization between merlin and merintA, it was predicted that merintA also associates with the actin cytoskeleton. Indeed, co-fractionation, co-localization and electron microscopy demonstrate a connection between merintA and actin. However, these proteins appear to bind to each other indirectly since no robust direct interaction could be seen with various methods that detect the direct binding of merlin to actin. Thus, merlin and other proteins are likely to mediate the merintA-actin association.

Merlin is thought to stabilize F-actin through a lateral association (James *et al.*, 2001) similar to ezrin and moesin (Pestonjamas *et al.*, 1995; Shuster *et al.*, 1995; Tsukita *et al.*, 1999; Yao *et al.*, 1996). MerintA also resides along actin filaments most highly concentrated at cortical actin-rich regions as seen by electron microscopy. MerintA and merlin significantly co-localize at the subcellular resolution achieved by electron microscopy. It seems reasonable to assume that other proteins might be involved in the association of merintA and actin because merintA can be found to some extent along actin filaments in the absence of merlin. MerintA is highly expressed in skeletal muscle and heart. The major function of muscle cells is to perform contractions and the cytoplasm of these cells is full of organized actin filaments among other protein filaments and many mitochondria. Strong expression of merintA in actin rich cells concurs with the fact that merintA is an actin cytoskeleton associated protein.

A large number of germline and somatic mutations have been found in NF2 patients. Mainly inactivating genetic alterations, such as frameshift and nonsense mutations, have been identified, although rare missense mutations have also been discovered. Based on mutational analyses, either isoform of merlin could function as a tumor suppressor since no mutations have been reported in isoform defining exons 16 or 17 (Gusella *et al.*, 1999). Investigations performed with NF2 missense mutations reveal a significant increase in detergent solubility compared to the wild type protein (Stokowski *et al.*, 2000). It is assumed that the ability of mutant merlin to interact with the cytoskeleton is decreased. Localization studies of mutant merlin confirmed an impaired association with actin (Deugen *et al.*, 1998; Stokowski *et al.*, 2000). It would be worthwhile to test whether NF2 missense mutations affect the solubility of merintA and its interaction with merlin.

Originally, the actin cytoskeleton was simply thought to have structural significance for a cell, playing a role in cell shape and motility events such as cell movement, intracellular transport, contractile-ring formation and chromosome movement. However, recent studies demonstrate that the cytoskeleton is of critical importance in the regulation of various other cellular processes including proliferation, contact inhibition, anchorage-independent cell growth and apoptosis (for review see Pawlak *et al.*, 2001). The small GTPases Rho, Rac and Cdc42 regulate the organization of the actin cytoskeleton, and results have implicated the cytoskeleton and ERM proteins in transformation. First, Dbl and Net, Rho guanine nucleotide exchange factors (RhoGEF), and RhoA are involved in cell transformation and require ezrin-mediated cytoskeletal changes (Sahai *et al.*, 1999; Tran Quang *et al.*, 2000). Second, the ERM proteins bind directly with the TSC1 tumor-suppressor hamartin. This physical interaction is necessary for the activation of Rho by serum or lysophosphatidic acid, and it results in the assembly of actin stress fibers and formation of focal adhesions (Lamb *et al.*, 2000). These studies suggest that a Rho-mediated signaling pathway regulates cell adhesion and may constitute a rate-limiting step in tumor formation. They may also represent a paradigm for the action of merlin and merintA in a Rac-mediated signaling pathway, and elucidating these functions will provide fundamental knowledge

of merlin in the pathogenesis of NF2. Further investigations are necessary to define a potential role of merintA and cytoskeleton-mediated transformation.

#### 4.4.5 The Association of MerintA with the Adaptor Protein Grb2

Examination of merintA with *Scansite* predicted the binding motif for the Src homology 2 (SH2-) domain of the growth factor receptor bound 2 (Grb2). The consensus sequence of this binding motif is pYV/INX (Schlessinger, 1994), and merintA has the sequence YVNG between amino acids 63 and 68 (Y64 of merintA). Only 0.13% of all proteins can be found in SwissProt with this motif.

Grb2 was identified by screening a bacterial cDNA expression library with the tyrosine phosphorylated EGF receptor (Lowenstein *et al.*, 1992). Subsequently, many proteins have been identified, and they have been shown to bind to the SH2-domain of Grb2 in a tyrosine phosphorylation dependent manner (for review see Buday, 1999). Thus, Y64 of merintA is predicted to be phosphorylated, in order to mediate the interaction with Grb2 via the SH2-domain. Grb2 is composed of one SH2-domain flanked by two SH3-domains, and these latter domains are known to bind to proline rich proteins. MerintA has an amino-terminal proline rich region that could conceivably interact with a Grb2 SH3-domain in addition to or exclusive of an SH2-domain interaction. The proline rich region of merintA matches the minimal SH3-binding domain consensus-sequence PXXP (Ren *et al.*, 1993), although *Scansite* did not predict an interaction through either SH3-domain of Grb2 and merintA.

Grb2 localizes in submembranous regions and membrane ruffles of the cell (Bar-Sagi *et al.*, 1993), and this intracellular localization supports an interaction between merintA and Grb2. Affinity binding assays demonstrate that merintA and Grb2 can associate. Moreover, blot overlay assays indicate a direct association between full-length GST-Grb2 and His-merintA. MerintA was bacterially expressed in these assays and it is not phosphorylated. Thus, Grb2 can bind to merintA even if Y64 is not phosphorylated. These assays support binding of merintA to Grb2: (A) via the SH2-domain while merintA is not phosphorylated, (B) via either SH3-domain or (C) via both SH2- and SH3-domains.

The data supporting an interaction between merintA and Grb2 open doors for many further questions and it is important to determine the domains responsible for this association. *Scansite* predicted that the SH2-domain of Grb2 binds to (p)YVNG of merintA. Therefore, the phosphorylation status of the merintA residue Y64 needs to be determined. Although merintA is not constitutively phosphorylated, Y64 could be phosphorylated upon certain growth factor stimulation. Hence, it is important to analyze carefully the phosphorylation status of merintA after stimulation with various growth factors and correlate potential phosphorylated merintA with respect to Grb2 binding. Conversely, while most studies indicate that the tyrosine in the YV/INX sequence needs to be phosphorylated for the Grb2 SH2-domain to bind to this consensus sequence, more recent studies support the binding of non-phosphorylated peptide ligands to this SH2-domain (Long *et al.*, 1999; Oliginao *et al.*, 1997). The data obtained from the blot overlay assays support binding of non-phosphorylated merintA to Grb2. If this interaction turns out to be exclusively mediated by non-phosphorylated merintA and the Grb2 SH2-domain, merintA would inhibit Grb2 signaling by competing with other phosphorylated proteins.

Alternatively, the interaction of merintA and Grb2 could be mediated through a SH3-domain of Grb2 and the proline rich domain of merintA, which would also be consistent with non-phosphorylated merintA binding to Grb2. Grb2, containing SH2-loss-of-function point mutations, localizes primarily to membrane ruffles similar to the wild type protein. On the other hand, Grb2, with SH3-loss-of-function point mutations, exhibits diffuse cytoplasmic distribution (Bar-Sagi *et al.*, 1993). Consequently, the localization of Grb2 to membrane ruffles does not require SH2-mediated interactions, and SH3-domains are responsible for the correct targeting to the specific subcellular location. A possible binding of Grb2 to merintA via the SH3-domain could target Grb2 to membrane ruffles and submembranous regions of the cell.

Finally, the interaction of merintA and Grb2 could be mediated through both SH2- and SH3-domains of Grb2. The SH3-domain of Grb2 could bind to the proline rich domain of merintA in a non-phosphorylation dependent manner. In contrast, the SH2-domain might enhance the interaction in a phospho-dependent manner to pYVNG

of merintA. It is well established that the SH2-domain of Grb2 binds to autophosphorylated receptor protein tyrosine kinases (RTKs) such as EGFR or PDGFR (Lowenstein *et al.*, 1992) and mediates EGF signaling pathways (for review see Buday, 1999). The following question remains if the SH2-domain of Grb2 indeed binds to merintA in a phospho-dependent manner. Assuming that merintA, Grb2 and EGFR, for instance, are in the same signaling pathway, how can the SH2-domain of Grb2 bind to EGFR and merintA? Cytoplasmic linker proteins, such as Shc and SHP-2, are known to recruit Grb2 to a number of different receptors in the plasma membrane. The interaction between these linker proteins is also mediated by the SH2-domain of Grb2 (Buday, 1999). However, unlike merintA, Shc and SHP-2 have SH2-domains themselves that bind to membrane-bound tyrosine phosphorylated receptors. Consequently, merintA might compete with the two “linker” proteins Shc and SHP-2, and membrane-bound tyrosine phosphoproteins known to bind directly to Grb2. In this case, merintA would inhibit Grb2 signaling pathways (see Figure 32). This hypothesis is in agreement with the data obtained so far, and would be consistent with the fact that merlin is a tumor- and growth suppressor.

Initial attempts to co-immunoprecipitate the two proteins were not successful. A polyclonal rabbit antibody was used to immunoprecipitate merintA, and an antibody from the same species against Grb2 cannot detect the protein since it co-migrates with the light chain of the merintA antibody (data not shown). A different strategy needs to be sought to identify a possible interaction *in vivo*, and a similar approach to the one used to demonstrate that NHE-RF immunoprecipitates (see Figure 10 C) could be applied. Alternatively, monoclonal antibodies raised in mice are commercially available and could also be used with little or no background staining derived from the binding of the horseradish peroxidase-conjugated secondary antibody (Western blot analysis) to the immunoglobulin used for immunoprecipitation. Furthermore, the reciprocal experiment was performed where Grb2 was successfully immunoprecipitated with a polyclonal rabbit antibody, and immunoprecipitates were subsequently probed with a monoclonal mouse antibody against merintA. Here, the problem of background staining mentioned above was circumvented; however, merintA did not co-immunoprecipitate

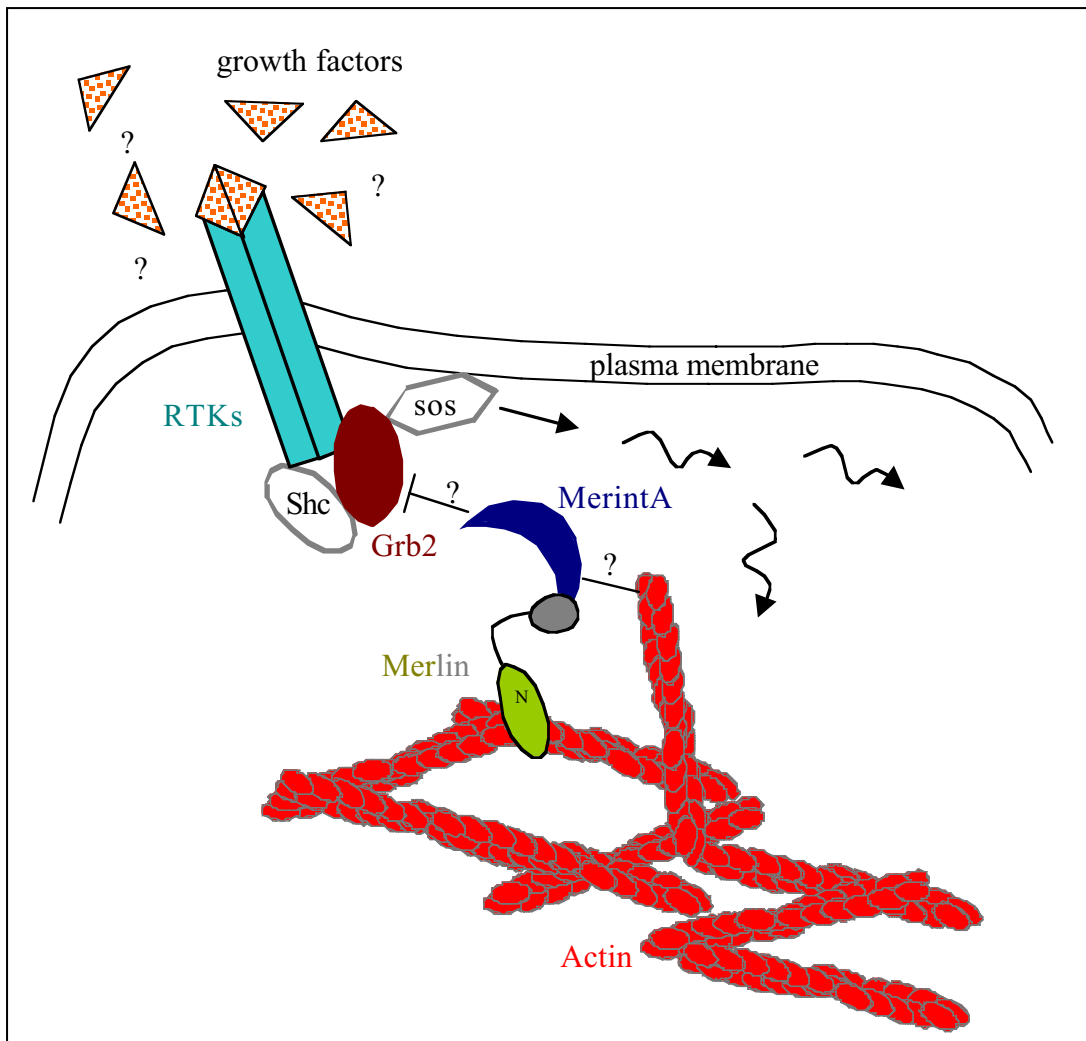


**Figure 32. A Potential Model Connecting Merlin and MerintA to Signaling Pathways through Grb2.** See text for details.

with Grb2 (data not shown). These experiments demonstrate the difficulty of co-immunoprecipitating two proteins. Certain signals might be necessary for the interaction of merintA and Grb2 *in vivo* that are not controlled in the co-immunoprecipitation experiments performed to date. Growth factors such as epidermal growth factor (EGF) and platelet-derived growth factor (PDGF) are candidates that might facilitate this interaction (see below). The data suggest that the interaction observed between merintA and Grb2 is relevant, but further experiments are necessary to draw a conclusion.



Again, the SH2-domain of Grb2 binds to autophosphorylated receptor protein tyrosine kinases (RTKs) such as EGFR or PDGFR (Lowenstein *et al.*, 1992) and the SH3-domains physically associate with proline-rich proteins including the Ras guanine-nucleotide exchange factor, Sos (Buday *et al.*, 1993; Egan *et al.*, 1993). For example, the Grb2-Sos complex binds to the autophosphorylated EGF receptor (EGFR) upon EGF stimulation. This complex formation brings the exchange factor Sos into contact with its substrate Ras at the plasma membrane. Thus, Ras is activated through the formation of a ternary complex of EGFR-Sos-Grb2, and a signal is transmitted to effector molecules and other GTPases such as Rac (Nimnual *et al.*, 1998; Ridley *et al.*, 1992). Rac, on the other hand, has been shown to induce membrane ruffles linking growth factors such as PDGF and EGF to the organization of polymerized actin (Ridley *et al.*, 1992). Merlin localizes to membrane ruffles upon PDGF induction (Ramesh V., pers. commun.) and has been placed in a Rac signaling pathway (Shaw *et al.*, 2001). It is tempting to place merintA into this scenario, but further studies are required to demonstrate its authenticity. Additional investigations might both, distinguish among EGF, PDGF or other growth factor mediated induction and define a role for merintA in such a pathway. Although these are well characterized Grb2 signaling pathways, others are known and may also be influenced by merintA or vice versa. The linkage of merlin-merintA to Grb2 should be further analyzed and should be valuable in terms of understanding the functions of merintA and merlin.

#### 4.5 Possible Biological Functions of Merlin

Studies of merlin and the ERM proteins reveal that some, but not all of the characteristics of merlin are shared with the ERM proteins. Subcellular localization patterns overlap to some extent but are not identical. In contrast to the ERM proteins, merlin has two major isoforms that differ at the extreme carboxy-terminus. And it is isoform 1 that forms head-to-tail associations similar to the ERM proteins. Again, some but not all merlin binding proteins also bind to the ERM proteins. These observations raise the following question: Why do merlin and the ERM proteins share sequence and structural properties? The following three points discuss this question: (A) Merlin and the ERM proteins could be functionally redundant. However, merlin-deficient mice are embryonic lethal (McClatchey *et al.*, 1997), as opposed to moesin-deficient mice that develop normally, are fertile and have no obvious histological abnormalities in any tissues (Doi *et al.*, 1999). In addition, it is merlin that has a known tumor suppressor function. These data contradict functional redundancy. (B) Merlin and the ERM proteins might compete for the same binding partners. The molar ratio of endogenous merlin/ERM proteins was calculated to be between 0.05 and 0.15 in cultured fibroblast and epithelial cells (Maeda *et al.*, 1999). NHE-RF has been shown to bind with higher affinity to ezrin than to merlin *in vitro* (Nguyen *et al.*, 2001). Hence, a merlin-ERM competition does not seem likely based on the molar ratio and the affinity towards NHE-RF. However, a recent study suggests that merlin acts as a molecular switch. When merlin is phosphorylated, it is growth permissive and exists in a complex with ezrin, moesin and CD44 (transmembrane HA receptor). In contrast, merlin's growth-inhibitory activity was suggested to depend on a dephosphorylated, specific and exclusive interaction with the cytoplasmic tail of CD44 (Morrison *et al.*, 2001). Thus, the affinities for their ligands may-be higher for the ERM proteins than for merlin, but these might also change temporally giving an advantage to merlin, which is less abundant and may have lower affinities for ligands. Further studies are necessary to conclude if the shared sequence is reflected in competition for the same ligands. (C) It is possible that the similarities of the family members mirror analogous mechanisms and functions in specific pathways. It is reasonable to hypothesize that merlin and ERM

proteins function in small GTP-binding protein-dependent signaling pathways. While merlin could be involved in a small GTPase dependent pathway that regulates cell growth, cell proliferation and/or cell death, other family members could be responsible for regulating another small GTPase with different outputs. Understanding the pathway(s) unique to merlin remains a challenge that will certainly give clues to the tumor suppressor function of merlin.

This work manifests both similarities and differences between merlin and the ERM proteins. Merlin isoform 1 behaves similar to the ERM proteins with respect to binding to the ligand NHE-RF and enhanced binding to NHE-RF in the presence of phospholipids such as PIP<sub>2</sub>. In contrast, merintA binds specifically to merlin and not to the ERM proteins suggesting that the characterization of this protein might lead to the identification of merlin specific functions. The function of merintA is still under investigation; however, the possible connection to Grb2 signaling pathways might illuminate on the function of merintA and the tumor suppressor function of merlin. Although many binding proteins have been identified during the past few years, a critical question still remains. How can a cell orchestrate interactions with different proteins in a way that allows specific signals to be translated into specific responses? Answering this question in the context of Schwann and meningeal cells will give an increased understanding of Neurofibromatosis 2 in the future.

## 5. Summary

Neurofibromatosis 2 (NF2) is a dominantly inherited disorder that is characterized by the occurrence of vestibular schwannomas, meningiomas and other nervous system tumors. Both the familial tumors of NF2, and equivalent sporadic tumors in the general population, are caused by inactivation of a tumor suppressor gene located on chromosome band 22q12. By a positional cloning strategy, the *NF2* gene has been isolated and the identity of this tumor suppressor has been discovered. The *NF2* gene has two major isoforms with altered the carboxy-termini, and the *NF2* gene product has been named merlin (**m**oesin, **e**zrin and **r**adixin **l**ike **p**rotein) because of its striking similarity to ezrin, radixin and moesin (ERM). Regulation of the merlin and ERM proteins (MERM) involves intramolecular and intermolecular head-to-tail associations between family members. However, in the case of merlin, only the carboxy-terminus of merlin isoform 1 is able to associate with its amino-terminal domain in a head-to-tail fashion whereas the carboxy-terminus of isoform 2 lacks this ability. The next step is to further analyze the normal function of merlin and its role as a growth regulator. Towards this end the MERM binding protein, NHE-RF, was further characterized and other merlin binding proteins were sought.

First, the effect of merlin's self-association on binding to NHE-RF was examined. Merlin isoform 2 captured more NHE-RF than merlin isoform 1 in affinity binding assays, suggesting that in full-length merlin isoform 1, the NHE-RF binding site is masked because of the self-interactions of merlin. Treatment with a phospholipid (PIP<sub>2</sub>) known to decrease self-association of ERMs enhanced the binding of merlin isoform 1 to NHE-RF. Thus, although isoform 1 resembles the ERM proteins, which transition between inactive (closed) and active (open) states, isoform 2 is distinct, existing only in the active (open) state.

Next, interactions between NHE-RF and potential binding proteins were investigated. It had been shown that the PDZ1-domain of NHE-RF binds to the amino acid motif DS/TXL. The B1 (56kD) subunit of the vacuolar H<sup>+</sup> ATPase has the carboxy-terminal DTAL amino acid motif suggesting a possible association with NHE-RF. This B1 isoform is amplified in intercalated cells in collecting tubules of the kidney.

These cells play a role in distal urinary acid-base transport. In contrast, proximal tubules of the kidney express the B2 isoform that lacks the carboxy-terminal PDZ1 binding motif. Both the B1 subunit and the E subunit of the H<sup>+</sup> ATPase are affinity precipitated by NHE-RF and this interaction was inhibited by a peptide derived from the carboxy-terminus of the B1 but not the B2 isoform. Furthermore, it is known that the B and E subunits associate *in vivo* as part of the cytoplasmic V<sub>1</sub> portion of the H<sup>+</sup> ATPase, and here the E subunit was co-immunoprecipitated from rat kidney cytosol with NHE-RF antibodies. NHE-RF co-localized with H<sup>+</sup> ATPase in either the apical or the basolateral region of B-type intercalated cells, whereas NHE-RF staining was undetectable in A-intercalated cells. This co-localization of NHE-RF and H<sup>+</sup> ATPase suggests a role in generating, maintaining or modulating the variable H<sup>+</sup> ATPase localization that characterizes the B-cell phenotype.

During the analysis of NHE-RF expression in various tumor lines, a significant upregulation of NHE-RF expression was observed in the ER- positive breast carcinoma cell lines MCF-7, ZR-75-B and T-47-D. The induction of NHE-RF by  $\beta$ -estradiol in estrogen depleted MCF-7 cells was explored, and a dramatic induction of NHE-RF expression was observed both at the RNA and protein levels. In addition, the expression of NHE-RF was examined by immunohistochemistry in primary breast tumors, and it was observed that 90% of the analyzed ER-positive tumors express high levels of NHE-RF. As NHE-RF appears to be a multifunctional adaptor protein involved in many cellular signaling pathways, it is likely that its regulation through estrogen plays a role in breast neoplasia.

To isolate further merlin binding proteins, a yeast two-hybrid screen of a frontal cortex library had been conducted and revealed that a novel protein (merintA) interacts directly with merlin. The carboxy-terminus of merlin binds specifically to merintA in yeast two-hybrid as well as in affinity binding assays. These experiments did not demonstrate an interaction with the ERM proteins. Moreover, merintA and merlin can be co-immunoprecipitated as a complex. The gene for human merintA lies on chromosome 4 where the predicted four exons encode a 178 amino acid protein with the Grb2 binding motif (p)YVNG. Anonymous orthologues of merintA are expressed in

mouse, fish and fly. In addition, expression analyses show that merintA is widely distributed in tissues and cell lines. MerintA co-localizes with merlin and F-actin in cultured cells as determined by immunofluorescence and electron microscopy. In addition, merintA associates with merlin to the actin cytoskeleton. Affinity binding assays and blot overlay assays demonstrate that merintA binds to Grb2 directly. These findings reveal that merintA is a specific and relevant merlin binding protein and could link merlin to Grb2 signaling pathways that might reveal clues to the tumor suppressor function of merlin.

## **6. Acknowledgements**

Many reasons make me very thankful for having had the opportunity of writing my “Dissertation” with Dr. Vijaya Ramesh as a mentor. Dr. Ramesh not only gave me a dynamic topic to investigate, but also guided me through this project with her constructive feedback.

It was very encouraging to work with the NF2 Group including Ms. Roberta Beauchamp, Dr. Charo Gonzalez-Agosti, Ms. Nile Hull, Dr. Marianne James, Ms. Nitasha Manchanda, Dr. Ming Fen-Lee, Ms. Denise Pinney-Michalowski and Ms. Nicole Smith. Everybody contributed to a great environment to work in and participated in many discussions that were helpful for this project.

A Gottlieb Daimler and Karl Benz Predoctoral Fellowship supported this work.

Also, I would like to thank Prof. Dr. Karl Heinz Scheidtmann for being my co-mentor from the Rheinische Friedrich-Wilhelms-Universität in Bonn and enabling me to pursue this research project in Boston.

Finally, I would like to thank Dr. James Gusella for being my co-mentor and for his continuous support and supervision of this project.

## 7. References

1. **Al-Awqati, Q.** 1996. Plasticity in epithelial polarity of renal intercalated cells: targeting of the H<sup>+</sup> ATPase and band 3. *Am J Physiol* **270**:C1571-80.
2. **Al-Awqati, Q., S. Vijayakumar, C. Hikita, J. Chen, and J. Takito.** 1998. Phenotypic plasticity in the intercalated cell: the hensin pathway. *Am J Physiol* **275**:F183-90.
3. **Alberts, B., D. Bray, J. Lewis, M. Raff, K. Roberts, and J. Watson.** 1994. *Molecular biology of the cell.* Garland Publishing Inc. :New York & London.
4. **Alper, S. L., J. Natale, S. Gluck, H. F. Lodish, and D. Brown.** 1989. Subtypes of intercalated cells in rat kidney collecting duct defined by antibodies against erythroid band 3 and renal vacuolar H<sup>+</sup> ATPase. *Proc Natl Acad Sci U S A* **86**:5429-33.
5. **Amieva, M. R., K. K. Wilgenbus, and H. Furthmayr.** 1994. Radixin is a component of hepatocyte microvilli in situ. *Exp Cell Res* **210**:140-4.
6. **Arakawa, H., N. Hayashi, H. Nagase, M. Ogawa, and Y. Nakamura.** 1994. Alternative splicing of the NF2 gene and its mutation analysis of breast and colorectal cancers. *Hum Mol Genet* **3**:565-8.
7. **Aronheim, A., D. Engelberg, N. Li, N. al-Alawi, J. Schlessinger, and M. Karin.** 1994. Membrane targeting of the nucleotide exchange factor Sos is sufficient for activating the Ras signaling pathway. *Cell* **78**:949-61.
8. **Aronica, S. M., and B. S. Katzenellenbogen.** 1993. Stimulation of estrogen receptor-mediated transcription and alteration in the phosphorylation state of the rat uterine estrogen receptor by estrogen, cyclic adenosine monophosphate, and insulin-like growth factor-I. *Mol Endocrinol* **7**:743-52.
9. **Arpin, M., E. Friederich, M. Algrain, F. Vernel, and D. Louvard.** 1994. Functional differences between L- and T-plastin isoforms. *J Cell Biol* **127**:1995-2008.
10. **Arteaga, C. L., A. K. Tandon, D. D. Von Hoff, and C. K. Osborne.** 1988. Transforming growth factor beta: potential autocrine growth inhibitor of estrogen receptor-negative human breast cancer cells. *Cancer Res* **48**:3898-904.
11. **Ballester, R., D. Marchuk, M. Boguski, A. Saulino, R. Letcher, M. Wigler, and F. Collins.** 1990. The NF1 locus encodes a protein functionally related to mammalian GAP and yeast IRA proteins. *Cell* **63**:851-9.
12. **Bar-Sagi, D., D. Rotin, A. Batzer, V. Mandiyan, and J. Schlessinger.** 1993. SH3 domains direct cellular localization of signaling molecules. *Cell* **74**:83-91.
13. **Basu, T. N., D. H. Gutmann, J. A. Fletcher, T. W. Glover, F. S. Collins, and J. Downward.** 1992. Aberrant regulation of ras proteins in malignant tumour cells from type 1 neurofibromatosis patients. *Nature* **356**:713-5.
14. **Beauchamp, R. L., A. Banwell, P. McNamara, M. Jacobsen, E. Higgins, H. Northrup, P. Short, K. Sims, L. Ozelius, and V. Ramesh.** 1998. Exon scanning of the entire TSC2 gene for germline mutations in 40 unrelated patients with tuberous sclerosis. *Hum Mutat* **12**:408-16.
15. **Berryman, M., and A. Bretscher.** 1998. A simple method for the detection of antigens in immunoprecipitates. *Mol Biol Cell (Supplemental ASCB Annual Meeting Abstracts Issue)* **9**:476a.
16. **Berryman, M., Z. Franck, and A. Bretscher.** 1993. Ezrin is concentrated in the apical microvilli of a wide variety of epithelial cells whereas moesin is found primarily in endothelial cells. *J Cell Sci* **105**:1025-43.



17. **Berryman, M., R. Gary, and A. Bretscher.** 1995. Ezrin oligomers are major cytoskeletal components of placental microvilli: a proposal for their involvement in cortical morphogenesis. *J Cell Biol* **131**:1231-42.
18. **Bhat, M. A., S. Izaddoost, Y. Lu, K. O. Cho, K. W. Choi, and H. J. Bellen.** 1999. Discs Lost, a novel multi-PDZ domain protein, establishes and maintains epithelial polarity. *Cell* **96**:833-45.
19. **Bianchi, A. B., T. Hara, V. Ramesh, J. Gao, A. J. Klein-Szanto, F. Morin, A. G. Menon, J. A. Trofatter, J. F. Gusella, B. R. Seizinger, and *et al.*** 1994. Mutations in transcript isoforms of the neurofibromatosis 2 gene in multiple human tumour types. *Nat Genet* **6**:185-92.
20. **Bianchi, A. B., S. I. Mitsunaga, J. Q. Cheng, W. M. Klein, S. C. Jhanwar, B. Seizinger, N. Kley, A. J. Klein-Szanto, and J. R. Testa.** 1995. High frequency of inactivating mutations in the neurofibromatosis type 2 gene (NF2) in primary malignant mesotheliomas. *Proc Natl Acad Sci U S A* **92**:10854-8.
21. **Biemesderfer, D., P. A. Rutherford, T. Nagy, J. H. Pizzonia, A. K. Abu-Alfa, and P. S. Aronson.** 1997. Monoclonal antibodies for high-resolution localization of NHE3 in adult and neonatal rat kidney. *Am J Physiol* **273**:F289-99.
22. **Bijlsma, E. K., R. Brouwer-Mladin, D. A. Bosch, A. Westerveld, and T. J. Hulsebos.** 1992. Molecular characterization of chromosome 22 deletions in schwannomas. *Genes Chromosomes Cancer* **5**:201-5.
23. **Borowsky, M. L., and R. O. Hynes.** 1998. Layilin, a novel talin-binding transmembrane protein homologous with C- type lectins, is localized in membrane ruffles. *J Cell Biol* **143**:429-42.
24. **Breton, S., T. Wiederhold, V. Marshansky, N. N. Nsumu, V. Ramesh, and D. Brown.** 2000. The B1 subunit of the H<sup>+</sup> ATPase is a PDZ domain-binding protein. Colocalization with NHE-RF in renal B-intercalated cells. *J Biol Chem* **275**:18219-24.
25. **Bretscher, A.** 1999. Regulation of cortical structure by the ezrin-radixin-moesin protein family. *Curr Opin Cell Biol* **11**:109-16.
26. **Bretscher, A., R. Gary, and M. Berryman.** 1995. Soluble ezrin purified from placenta exists as stable monomers and elongated dimers with masked C-terminal ezrin-radixin-moesin association domains. *Biochemistry* **34**:16830-7.
27. **Brown, D., S. Hirsch, and S. Bluck.** 1988a. An H<sup>+</sup> ATPase in opposite plasma membrane domains in kidney epithelial cell subpopulations. *Nature* **331**:622-4.
28. **Brown, D., S. Hirsch, and S. Gluck.** 1988b. Localization of a proton-pumping ATPase in rat kidney. *J Clin Invest* **82**:2114-26.
29. **Brown, D., J. Lydon, M. McLaughlin, A. Stuart-Tilley, R. Tyszkowski, and S. Alper.** 1996. Antigen retrieval in cryostat tissue sections and cultured cells by treatment with sodium dodecyl sulfate (SDS). *Histochem Cell Biol* **105**:261-7.
30. **Buchberg, A. M., L. S. Cleveland, N. A. Jenkins, and N. G. Copeland.** 1990. Sequence homology shared by neurofibromatosis type-1 gene and IRA-1 and IRA-2 negative regulators of the RAS cyclic AMP pathway. *Nature* **347**:291-4.
31. **Buday, L.** 1999. Membrane-targeting of signalling molecules by SH2/SH3 domain-containing adaptor proteins. *Biochim Biophys Acta* **1422**:187-204.
32. **Buday, L., and J. Downward.** 1993. Epidermal growth factor regulates p21ras through the formation of a complex of receptor, Grb2 adapter protein, and Sos nucleotide exchange factor. *Cell* **73**:611-20.

33. **Cao1, T. T., H. W. Deacon, D. Reczek, A. Bretscher, and M. von Zastrow.** 1999. A kinase-regulated PDZ-domain interaction controls endocytic sorting of the beta2-adrenergic receptor. *Nature* **401**:286-90.
34. **Cawthon, R. M., R. Weiss, G. F. Xu, D. Viskochil, M. Culver, J. Stevens, M. Robertson, D. Dunn, R. Gesteland, P. O'Connell, and *et al.*** 1990. A major segment of the neurofibromatosis type 1 gene: cDNA sequence, genomic structure, and point mutations. *Cell* **62**:193-201.
35. **Cho, K. O., C. A. Hunt, and M. B. Kennedy.** 1992. The rat brain postsynaptic density fraction contains a homolog of the *Drosophila* discs-large tumor suppressor protein. *Neuron* **9**:929-42.
36. **Coutts, A. S., J. R. Davie, H. Dotzlaw, and L. C. Murphy.** 1996. Estrogen regulation of nuclear matrix-intermediate filament proteins in human breast cancer cells. *J Cell Biochem* **63**:174-84.
37. **Couturier, J., O. Delattre, M. Kujas, J. Philippon, M. Peter, G. Rouleau, A. Aurias, and G. Thomas.** 1990. Assessment of chromosome 22 anomalies in neuroinomas by combined karyotype and RFLP analyses. *Cancer Genet Cytogenet* **45**:55-62.
38. **DeClue, J. E., A. G. Papageorge, J. A. Fletcher, S. R. Diehl, N. Ratner, W. C. Vass, and D. R. Lowy.** 1992. Abnormal regulation of mammalian p21ras contributes to malignant tumor growth in von Recklinghausen (type 1) neurofibromatosis. *Cell* **69**:265-73.
39. **deFazio, A., Y. E. Chiew, C. Donoghue, C. S. Lee, and R. L. Sutherland.** 1992. Effect of sodium butyrate on estrogen receptor and epidermal growth factor receptor gene expression in human breast cancer cell lines. *J Biol Chem* **267**:18008-12.
40. **Deguen, B., P. Merel, L. Goutebroze, M. Giovannini, H. Reggio, M. Arpin, and G. Thomas.** 1998. Impaired interaction of naturally occurring mutant NF2 protein with actin-based cytoskeleton and membrane. *Hum Mol Genet* **7**:217-26.
41. **den Bakker, M. A., K. J. Vissers, A. C. Molijn, J. M. Kros, E. C. Zwarthoff, and T. H. van der Kwast.** 1999. Expression of the neurofibromatosis type 2 gene in human tissues. *J Histochem Cytochem* **47**:1471-80.
42. **Doi, Y., M. Itoh, S. Yonemura, S. Ishihara, H. Takano, T. Noda, and S. Tsukita.** 1999. Normal development of mice and unimpaired cell adhesion/cell motility/actin-based cytoskeleton without compensatory up-regulation of ezrin or radixin in moesin gene knockout. *J Biol Chem* **274**:2315-21.
43. **Ediger, T. R., W. L. Kraus, E. J. Weinman, and B. S. Katzenellenbogen.** 1999. Estrogen receptor regulation of the Na<sup>+</sup>/H<sup>+</sup> exchange regulatory factor. *Endocrinology* **140**:2976-82.
44. **Egan, S. E., B. W. Giddings, M. W. Brooks, L. Buday, A. M. Sizeland, and R. A. Weinberg.** 1993. Association of Sos Ras exchange protein with Grb2 is implicated in tyrosine kinase signal transduction and transformation. *Nature* **363**:45-51.
45. **Evans, D. G., S. M. Huson, D. Donnai, W. Neary, V. Blair, D. Teare, V. Newton, T. Strachan, R. Ramsden, and R. Harris.** 1992. A genetic study of type 2 neurofibromatosis in the United Kingdom. I. Prevalence, mutation rate, fitness, and confirmation of maternal transmission effect on severity. *J Med Genet* **29**:841-6.
46. **Fan, S., J. Wang, R. Yuan, Y. Ma, Q. Meng, M. R. Erdos, R. G. Pestell, F. Yuan, K. J. Auborn, I. D. Goldberg, and E. M. Rosen.** 1999. BRCA1 inhibition of estrogen receptor signaling in transfected cells. *Science* **284**:1354-6.
47. **Fiedler, W., U. Claussen, H. J. Ludecke, G. Senger, B. Horsthemke, A. Geurts Van Kessel, W. Goertzen, and R. Fahsold.** 1991. New markers for the neurofibromatosis-2 region generated by microdissection of chromosome 22. *Genomics* **10**:786-91.

48. **Fontaine, B., M. P. Hanson, J. P. VonSattel, R. L. Martuza, and J. F. Gusella.** 1991a. Loss of chromosome 22 alleles in human sporadic spinal schwannomas. *Ann Neurol* **29**:183-6.
49. **Fontaine, B., M. Sanson, O. Delattre, A. G. Menon, G. A. Rouleau, B. R. Seizinger, A. F. Jewell, M. P. Hanson, A. Aurias, R. L. Martuza, and *et al.*** 1991b. Parental origin of chromosome 22 loss in sporadic and NF2 neuromas. *Genomics* **10**:280-3.
50. **Franck, Z., R. Gary, and A. Bretscher.** 1993. Moesin, like ezrin, colocalizes with actin in the cortical cytoskeleton in cultured cells, but its expression is more variable. *J Cell Sci* **105**:219-31.
51. **Friederich, E., C. Huet, M. Arpin, and D. Louvard.** 1989. Villin induces microvilli growth and actin redistribution in transfected fibroblasts. *Cell* **59**:461-75.
52. **Fuqua, S. A., and D. M. Wolf.** 1995. Molecular aspects of estrogen receptor variants in breast cancer. *Breast Cancer Res Treat* **35**:233-41.
53. **Gary, R., and A. Bretscher.** 1995. Ezrin self-association involves binding of an N-terminal domain to a normally masked C-terminal domain that includes the F-actin binding site. *Mol Biol Cell* **6**:1061-75.
54. **Gilmore, A. P., and K. Burridge.** 1996. Regulation of vinculin binding to talin and actin by phosphatidyl- inositol-4-5-bisphosphate. *Nature* **381**:531-5.
55. **Gonzalez-Agosti, C., T. Wiederhold, M. E. Herndon, J. Gusella, and V. Ramesh.** 1999. Interdomain interaction of merlin isoforms and its influence on intermolecular binding to NHERF. *J Biol Chem* **274**:34438-42.
56. **Gonzalez-Agosti, C., L. Xu, D. Pinney, R. Beauchamp, W. Hobbs, J. Gusella, and V. Ramesh.** 1996. The merlin tumor suppressor localizes preferentially in membrane ruffles. *Oncogene* **13**:1239-47.
57. **Goslin, K., E. Birgbauer, G. Banker, and F. Solomon.** 1989. The role of cytoskeleton in organizing growth cones: a microfilament- associated growth cone component depends upon microtubules for its localization. *J Cell Biol* **109**:1621-31.
58. **Goutebroze, L., E. Brault, C. Muchardt, J. Camonis, and G. Thomas.** 2000. Cloning and characterization of SCHIP-1, a novel protein interacting specifically with spliced isoforms and naturally occurring mutant NF2 proteins. *Mol Cell Biol* **20**:1699-712.
59. **Grand, R. J.** 1989. Acylation of viral and eukaryotic proteins. *Biochem J* **258**:625-38.
60. **Gronholm, M., M. Sainio, F. Zhao, L. Heiska, A. Vaheri, and O. Carpen.** 1999. Homotypic and heterotypic interaction of the neurofibromatosis 2 tumor suppressor protein merlin and the ERM protein ezrin. *J Cell Sci* **112**:895-904.
61. **Gu, M. X., J. D. York, I. Warshawsky, and P. W. Majerus.** 1991. Identification, cloning, and expression of a cytosolic megakaryocyte protein-tyrosine-phosphatase with sequence homology to cytoskeletal protein 4.1. *Proc Natl Acad Sci U S A* **88**:5867-71.
62. **Gusella, J. F., V. Ramesh, M. MacCollin, and L. B. Jacoby.** 1999. Merlin: the neurofibromatosis 2 tumor suppressor. *Biochim Biophys Acta* **1423**:M29-36.
63. **Gusella, J. F., V. Ramesh, M. MacCollin, and L. B. Jacoby.** 1996. Neurofibromatosis 2: loss of merlin's protective spell. *Curr Opin Genet Dev* **6**:87-92.
64. **Gyuris, J., E. Golemis, H. Chertkov, and R. Brent.** 1993. Cdi1, a human G1 and S phase protein phosphatase that associates with Cdk2. *Cell* **75**:791-803.

65. **Hall, R. A., L. S. Ostedgaard, R. T. Premont, J. T. Blitzer, N. Rahman, M. J. Welsh, and R. J. Lefkowitz.** 1998a. A C-terminal motif found in the beta2-adrenergic receptor, P2Y1 receptor and cystic fibrosis transmembrane conductance regulator determines binding to the Na<sup>+</sup>/H<sup>+</sup> exchanger regulatory factor family of PDZ proteins. *Proc Natl Acad Sci U S A* **95**:8496-501.
66. **Haase, V. H., J. A. Trofatter, M. MacCollin, E. Tarttelin, J. F. Gusella, and V. Ramesh.** 1994. The murine NF2 homologue encodes a highly conserved merlin protein with alternative forms. *Hum Mol Genet* **3**:407-11.
67. **Hall, R. A., R. T. Premont, C. W. Chow, J. T. Blitzer, J. A. Pitcher, A. Claing, R. H. Stoffel, L. S. Barak, S. Shenolikar, E. J. Weinman, S. Grinstein, and R. J. Lefkowitz.** 1998b. The beta2-adrenergic receptor interacts with the Na<sup>+</sup>/H<sup>+</sup>-exchanger regulatory factor to control Na<sup>+</sup>/H<sup>+</sup> exchange. *Nature* **392**:626-30.
68. **Halliday, A. L., R. A. Sobel, and R. L. Martuza.** 1991. Benign spinal nerve sheath tumors: their occurrence sporadically and in neurofibromatosis types 1 and 2. *J Neurosurg* **74**:248-53.
69. **Hartwig, J. H.** 1992. Mechanisms of actin rearrangements mediating platelet activation. *J Cell Biol* **118**:1421-42.
70. **Heiska, L., K. Alfthan, M. Gronholm, P. Vilja, A. Vaheri, and O. Carpen.** 1998. Association of ezrin with intercellular adhesion molecule-1 and -2 (ICAM-1 and ICAM-2). Regulation by phosphatidylinositol 4, 5- biphosphate. *J Biol Chem* **273**:21893-900.
71. **Henderson, B. E., L. Bernstein, and R. Ross.** 1997. Etiology of cancer: hormonal factors. *Cancer: principles and practice of oncology*, ed 5. Philadelphia, Lippincott-Raven. .
72. **Henry, M. D., C. Gonzalez Agosti, and F. Solomon.** 1995. Molecular dissection of radixin: distinct and interdependent functions of the amino- and carboxy-terminal domains. *J Cell Biol* **129**:1007-22.
73. **Hewett, J., C. Gonzalez-Agosti, D. Slater, P. Ziefer, S. Li, D. Bergeron, D. J. Jacoby, L. J. Ozelius, V. Ramesh, and X. O. Breakefield.** 2000. Mutant torsinA, responsible for early-onset torsion dystonia, forms membrane inclusions in cultured neural cells. *Hum Mol Genet* **9**:1403-13.
74. **Hirao, M., N. Sato, T. Kondo, S. Yonemura, M. Monden, T. Sasaki, Y. Takai, and S. Tsukita.** 1996. Regulation mechanism of ERM (ezrin/radixin/moesin) protein/plasma membrane association: possible involvement of phosphatidylinositol turnover and Rho-dependent signaling pathway. *J Cell Biol* **135**:37-51.
75. **Huang, L., E. Ichimaru, K. Pestonjamas, X. Cui, H. Nakamura, G. Y. Lo, F. I. Lin, E. J. Luna, and H. Furthmayr.** 1998. Merlin differs from moesin in binding to F-actin and in its intra- and intermolecular interactions. *Biochem Biophys Res Commun* **248**:548-53.
76. **Huson, S. M.** 1994. Neurofibromatosis: historical perspective, classification and diagnostic criteria. *The neurofibromatoses: a pathogenetic and clinical overview* :1-22, Chapman& Hall Medical: London.
77. **Huynh, D. P., T. M. Tran, T. Nechiporuk, and S. M. Pulst.** 1996. Expression of neurofibromatosis 2 transcript and gene product during mouse fetal development. *Cell Growth Differ* **7**:1551-61.
78. **Ikeda, K., Y. Saeki, C. Gonzalez-Agosti, V. Ramesh, and E. A. Chiocca.** 1999. Inhibition of NF2-negative and NF2-positive primary human meningioma cell proliferation by overexpression of merlin due to vector-mediated gene transfer. *J Neurosurg* **91**:85-92.
79. **James, M. F., N. Manchanda, C. Gonzalez-Agosti, J. H. Hartwig, and V. Ramesh.** 2001. The neurofibromatosis 2 protein product merlin selectively binds F- actin but not G-actin, and stabilizes the filaments through a lateral association. *Biochem J* **356**:377-86.

80. **Jannatipour, M., P. Dion, S. Khan, H. Jindal, X. Fan, J. Laganriere, A. H. Chishti, and G. A. Rouleau.** 2001. Schwannomin isoform-1 interacts with syntenin via PDZ domains. *J Biol Chem* **29**:29.
81. **Kaiser-Kupfer, M. I., V. Freidlin, M. B. Datiles, P. A. Edwards, J. L. Sherman, D. Parry, L. M. McCain, and R. Eldridge.** 1989. The association of posterior capsular lens opacities with bilateral acoustic neuromas in patients with neurofibromatosis type 2. *Arch Ophthalmol* **107**:541-4.
82. **Katzenellenbogen, B. S.** 1996. Estrogen receptors: bioactivities and interactions with cell signaling pathways. *Biol Reprod* **54**:287-93.
83. **Kim, S. K.** 1997. Polarized signaling: basolateral receptor localization in epithelial cells by PDZ-containing proteins. *Curr Opin Cell Biol* **9**:853-9.
84. **Knight, W. A., R. B. Livingston, E. J. Gregory, and W. L. McGuire.** 1977. Estrogen receptor as an independent prognostic factor for early recurrence in breast cancer. *Cancer Res* **37**:4669-71.
85. **Knudson, A. G., Jr.** 1971. Mutation and cancer: statistical study of retinoblastoma. *Proc Natl Acad Sci U S A* **68**:820-3.
86. **Korach, K. S., J. F. Couse, S. W. Curtis, T. F. Washburn, J. Lindzey, K. S. Kimbro, E. M. Eddy, S. Migliaccio, S. M. Snedeker, D. B. Lubahn, D. W. Schomberg, and E. P. Smith.** 1996. Estrogen receptor gene disruption: molecular characterization and experimental and clinical phenotypes. *Recent Prog Horm Res* **51**:159-86.
87. **Kornau, H. C., L. T. Schenker, M. B. Kennedy, and P. H. Seeburg.** 1995. Domain interaction between NMDA receptor subunits and the postsynaptic density protein PSD-95. *Science* **269**:1737-40.
88. **Laemmli, U. K.** 1970. Cleavage of structural proteins during the assembly of the head of bacteriophage T4. *Nature* **227**:680-5.
89. **Lamb, R. F., C. Roy, T. J. Diefenbach, H. V. Vinters, M. W. Johnson, D. G. Jay, and A. Hall.** 2000. The TSC1 tumour suppressor hamartin regulates cell adhesion through ERM proteins and the GTPase Rho. *Nat Cell Biol* **2**:281-7.
90. **Lee, B. S., S. L. Gluck, and L. S. Holliday.** 1999. Interaction between vacuolar H<sup>+</sup> ATPase and microfilaments during osteoclast activation. *J Biol Chem* **274**:29164-71.
91. **Legg, J. W., and C. M. Isacke.** 1998. Identification and functional analysis of the ezrin-binding site in the hyaluronan receptor, CD44. *Curr Biol* **8**:705-8.
92. **Lemieux, P., and S. Fuqua.** 1996. The role of the estrogen receptor in tumor progression. *J Steroid Biochem Mol Biol* **56**:87-91.
93. **Li, W., R. Nishimura, A. Kashishian, A. G. Batzer, W. J. Kim, J. A. Cooper, and J. Schlessinger.** 1994. A new function for a phosphotyrosine phosphatase: linking Grb2-Sos to a receptor tyrosine kinase. *Mol Cell Biol* **14**:509-17.
94. **Long, Y. Q., Z. J. Yao, J. H. Voigt, F. D. Lung, J. H. Luo, T. R. Burke, Jr., C. R. King, D. Yang, and P. P. Roller.** 1999. Structural requirements for Tyr in the consensus sequence Y-E-N of a novel nonphosphorylated inhibitor to the Grb2-SH2 domain. *Biochem Biophys Res Commun* **264**:902-8.
95. **Louis, D. N., V. Ramesh, and J. F. Gusella.** 1995. Neuropathology and molecular genetics of neurofibromatosis 2 and related tumors. *Brain Pathol* **5**:163-72.
96. **Lowenstein, E. J., R. J. Daly, A. G. Batzer, W. Li, B. Margolis, R. Lammers, A. Ullrich, E. Y. Skolnik, D. Bar-Sagi, and J. Schlessinger.** 1992. The SH2 and SH3 domain-containing protein Grb2 links receptor tyrosine kinases to ras signaling. *Cell* **70**:431-42.

97. **Lutchman, M., and G. A. Rouleau.** 1995. The neurofibromatosis type 2 gene product, schwannomin, suppresses growth of NIH 3T3 cells. *Cancer Res* **55**:2270-4.
98. **Ma, A. D., L. F. Brass, and C. S. Abrams.** 1997. Pleckstrin associates with plasma membranes and induces the formation of membrane projections: requirements for phosphorylation and the NH<sub>2</sub>-terminal PH domain. *J Cell Biol* **136**:1071-9.
99. **Mackay, D. J., F. Esch, H. Furthmayr, and A. Hall.** 1997. Rho- and rac-dependent assembly of focal adhesion complexes and actin filaments in permeabilized fibroblasts: an essential role for ezrin/radixin/moesin proteins. *J Cell Biol* **138**:927-38.
100. **Maeda, M., T. Matsui, M. Imamura, and S. Tsukita.** 1999. Expression level, subcellular distribution and rho-GDI binding affinity of merlin in comparison with Ezrin/Radixin/Moesin proteins. *Oncogene* **18**:4788-97.
101. **Magendantz, M., M. D. Henry, A. Lander, and F. Solomon.** 1995. Interdomain interactions of radixin in vitro. *J Biol Chem* **270**:25324-7.
102. **Martuza, R. L., and R. Eldridge.** 1988. Neurofibromatosis 2 (bilateral acoustic neurofibromatosis). *N Engl J Med* **318**:684-8.
103. **Matsui, T., M. Maeda, Y. Doi, S. Yonemura, M. Amano, K. Kaibuchi, and S. Tsukita.** 1998. Rho-kinase phosphorylates COOH-terminal threonines of ezrin/radixin/moesin (ERM) proteins and regulates their head-to-tail association. *J Cell Biol* **140**:647-57.
104. **Matsui, T., S. Yonemura, and S. Tsukita.** 1999. Activation of ERM proteins in vivo by Rho involves phosphatidylinositol 4-phosphate 5-kinase and not ROCK kinases. *Curr Biol* **9**:1259-62.
105. **McClatchey, A. I., I. Saotome, V. Ramesh, J. F. Gusella, and T. Jacks.** 1997. The Nf2 tumor suppressor gene product is essential for extraembryonic development immediately prior to gastrulation. *Genes Dev* **11**:1253-65.
106. **McLean, L. A., J. Roscoe, N. K. Jorgensen, F. A. Gorin, and P. M. Cala.** 2000. Malignant gliomas display altered pH regulation by NHE1 compared with nontransformed astrocytes. *Am J Physiol Cell Physiol* **278**:C676-88.
107. **Merino, J. J., and M. I. Cordero-Campana.** 1998. [Molecular bases of the programmed cell death process: implications of tumor suppressor protein p53 and other proteins in the control of cell cycle. Mechanisms of apoptotic action. Review]. *Invest Clin* **39**:323-58.
108. **Migliaccio, A., M. Pagano, and F. Auricchio.** 1993. Immediate and transient stimulation of protein tyrosine phosphorylation by estradiol in MCF-7 cells. *Oncogene* **8**:2183-91.
109. **Morrison, H., L. S. Sherman, J. Legg, F. Banine, C. Isacke, C. A. Haipek, D. H. Gutmann, H. Ponta, and P. Herrlich.** 2001. The NF2 tumor suppressor gene product, merlin, mediates contact inhibition of growth through interactions with CD44. *Genes Dev* **15**:968-80.
110. **Mulvihill, J. J., D. M. Parry, J. L. Sherman, A. Pikus, M. I. Kaiser-Kupfer, and R. Eldridge.** 1990. NIH conference. Neurofibromatosis 1 (Recklinghausen disease) and neurofibromatosis 2 (bilateral acoustic neurofibromatosis). An update. *Ann Intern Med* **113**:39-52.
111. **Murthy, A., C. Gonzalez-Agosti, E. Cordero, D. Pinney, C. Candia, F. Solomon, J. Gusella, and V. Ramesh.** 1998. NHE-RF, a regulatory cofactor for Na<sup>+</sup>-H<sup>+</sup> exchange, is a common interactor for merlin and ERM (MERM) proteins. *J Biol Chem* **273**:1273-6.
112. **Nagai, R., M. Kataoka, S. Kobayashi, K. Ishihara, N. Tobioka, K. Nakashima, M. Naruse, K. Saito, and S. Sakuma.** 1979. Estrogen and progesterone receptors in human breast cancer with concomitant assay of plasma 17beta-estradiol, progesterone, and prolactin levels. *Cancer Res* **39**:1834-40.

113. **Nakamura, F., M. R. Amieva, and H. Furthmayr.** 1995. Phosphorylation of threonine 558 in the carboxyl-terminal actin-binding domain of moesin by thrombin activation of human platelets. *J Biol Chem* **270**:31377-85.
114. **Nakamura, F., L. Huang, K. Pestonjamas, E. J. Luna, and H. Furthmayr.** 1999. Regulation of F-actin binding to platelet moesin in vitro by both phosphorylation of threonine 558 and polyphosphatidylinositides. *Mol Biol Cell* **10**:2669-85.
115. **Narod, S. A., D. M. Parry, J. Parboosingh, G. M. Lenoir, M. Rutledge, G. Fischer, R. Eldridge, R. L. Martuza, M. Frontali, J. Haines, and *et al.*** 1992. Neurofibromatosis type 2 appears to be a genetically homogeneous disease. *Am J Hum Genet* **51**:486-96.
116. **Neill, G. W., and M. R. Crompton.** 2001. Binding of the merlin-I product of the neurofibromatosis type 2 tumour suppressor gene to a novel site in beta-fodrin is regulated by association between merlin domains. *Biochem J* **358**:727-35.
117. **Nelson, N., and W. R. Harvey.** 1999. Vacuolar and plasma membrane proton-adenosinetriphosphatases. *Physiol Rev* **79**:361-85.
118. **Nelson, R. D., X. L. Guo, K. Masood, D. Brown, M. Kalkbrenner, and S. Gluck.** 1992. Selectively amplified expression of an isoform of the vacuolar H<sup>+</sup> ATPase 56-kilodalton subunit in renal intercalated cells. *Proc Natl Acad Sci U S A* **89**:3541-5.
119. **Nguyen, R., D. Reczek, and A. Bretscher.** 2001. Hierarchy of merlin and ezrin N- and C-terminal domain interactions in homo- and heterotypic associations and their relationship to binding of scaffolding proteins EBP50 and E3KARP. *J Biol Chem* **276**:7621-9.
120. **Niggli, V., C. Andreoli, C. Roy, and P. Mangeat.** 1995. Identification of a phosphatidylinositol-4,5-bisphosphate-binding domain in the N-terminal region of ezrin. *FEBS Lett* **376**:172-6.
121. **Nimnual, A. S., B. A. Yatsula, and D. Bar-Sagi.** 1998. Coupling of Ras and Rac guanosine triphosphatases through the Ras exchanger Sos. *Science* **279**:560-3.
122. **Obremski, V. J., A. M. Hall, and C. Fernandez-Valle.** 1998. Merlin, the neurofibromatosis type 2 gene product, and beta1 integrin associate in isolated and differentiating Schwann cells. *J Neurobiol* **37**:487-501.
123. **Oligino, L., F. D. Lung, L. Sastry, J. Bigelow, T. Cao, M. Curran, T. R. Burke, Jr., S. Wang, D. Krag, P. P. Roller, and C. R. King.** 1997. Nonphosphorylated peptide ligands for the Grb2 Src homology 2 domain. *J Biol Chem* **272**:29046-52.
124. **Osborne, C. K.** 1998. Steroid hormone receptors in breast cancer management. *Breast Cancer Res Treat* **51**:227-38.
125. **Pawlak, G., and D. M. Helfman.** 2001. Cytoskeletal changes in cell transformation and tumorigenesis. *Curr Opin Genet Dev* **11**:41-7.
126. **Pearson, M. A., D. Reczek, A. Bretscher, and P. A. Karplus.** 2000. Structure of the ERM protein moesin reveals the FERM domain fold masked by an extended actin binding tail domain. *Cell* **101**:259-70.
127. **Pendergast, A. M., L. A. Quilliam, L. D. Cripe, C. H. Bassing, Z. Dai, N. Li, A. Batzer, K. M. Rabun, C. J. Der, J. Schlessinger, and *et al.*** 1993. BCR-ABL-induced oncogenesis is mediated by direct interaction with the SH2 domain of the GRB-2 adaptor protein. *Cell* **75**:175-85.
128. **Pestonjamas, K., M. R. Amieva, C. P. Strassel, W. M. Nauseef, H. Furthmayr, and E. J. Luna.** 1995. Moesin, ezrin, and p205 are actin-binding proteins associated with neutrophil plasma membranes. *Mol Biol Cell* **6**:247-59.
129. **Pietromonaco, S. F., P. C. Simons, A. Altman, and L. Elias.** 1998. Protein kinase C-theta phosphorylation of moesin in the actin-binding sequence. *J Biol Chem* **273**:7594-603.

130. **Pulst, S. M., G. A. Rouleau, C. Marineau, P. Fain, and J. P. Sieb.** 1993. Familial meningioma is not allelic to neurofibromatosis 2. *Neurology* **43**:2096-8.
131. **Pykett, M. J., M. Murphy, P. R. Harnish, and D. L. George.** 1994. The neurofibromatosis 2 (NF2) tumor suppressor gene encodes multiple alternatively spliced transcripts. *Hum Mol Genet* **3**:559-64.
132. **Qi, Y., J. K. Wang, M. McMillian, and D. M. Chikaraishi.** 1997. Characterization of a CNS cell line, CAD, in which morphological differentiation is initiated by serum deprivation. *J Neurosci* **17**:1217-25.
133. **Raghuhand, N., X. He, R. van Sluis, B. Mahoney, B. Baggett, C. W. Taylor, G. Paine-Murrieta, D. Roe, Z. M. Bhujwala, and R. J. Gillies.** 1999. Enhancement of chemotherapy by manipulation of tumour pH. *Br J Cancer* **80**:1005-11.
134. **Ramesh, V., M. M. Shaffer, J. M. Allaire, V. E. Shih, and J. F. Gusella.** 1986. Investigation of gyrate atrophy using a cDNA clone for human ornithine aminotransferase. *Dna* **5**:493-501.
135. **Reczek, D., M. Berryman, and A. Bretscher.** 1997. Identification of EBP50: A PDZ-containing phosphoprotein that associates with members of the ezrin-radixin-moesin family. *J Cell Biol* **139**:169-79.
136. **Reczek, D., and A. Bretscher.** 1998. The carboxyl-terminal region of EBP50 binds to a site in the amino-terminal domain of ezrin that is masked in the dormant molecule. *J Biol Chem* **273**:18452-8.
137. **Reczek, D., and A. Bretscher.** 2001. Identification of EPI64, a TBC/rabGAP domain-containing microvillar protein that binds to the first PDZ domain of EBP50 and E3KARP. *J Cell Biol* **153**:191-206.
138. **Ren, R., B. J. Mayer, P. Cicchetti, and D. Baltimore.** 1993. Identification of a ten-amino acid proline-rich SH3 binding site. *Science* **259**:1157-61.
139. **Reshkin, S. J., A. Bellizzi, S. Caldeira, V. Albarani, I. Malanchi, M. Poignee, M. Alunni-Fabbroni, V. Casavola, and M. Tommasino.** 2000. Na<sup>+</sup>-H<sup>+</sup> exchanger-dependent intracellular alkalinization is an early event in malignant transformation and plays an essential role in the development of subsequent transformation-associated phenotypes. *Faseb J* **14**:2185-97.
140. **Riccardi, V. M.** 1981. Von Recklinghausen neurofibromatosis. *N Engl J Med* **305**:1617-27.
141. **Ridley, A. J., H. F. Paterson, C. L. Johnston, D. Diekmann, and A. Hall.** 1992. The small GTP-binding protein rac regulates growth factor-induced membrane ruffling. *Cell* **70**:401-10.
142. **Rouleau, G. A., P. Merel, M. Lutchman, M. Sanson, J. Zucman, C. Marineau, K. Hoang-Xuan, S. Demczuk, C. Desmaze, B. Plougastel, and *et al.*** 1993. Alteration in a new gene encoding a putative membrane-organizing protein causes neuro-fibromatosis type 2. *Nature* **363**:515-21.
143. **Rouleau, G. A., B. R. Seizinger, W. Wartecki, J. L. Haines, D. W. Superneau, R. L. Martuza, and J. F. Gusella.** 1990. Flanking markers bracket the neurofibromatosis type 2 (NF2) gene on chromosome 22. *Am J Hum Genet* **46**:323-8.
144. **Rouleau, G. A., W. Wartecki, J. L. Haines, W. J. Hobbs, J. A. Trofatter, B. R. Seizinger, R. L. Martuza, D. W. Superneau, P. M. Conneally, and J. F. Gusella.** 1987. Genetic linkage of bilateral acoustic neurofibromatosis to a DNA marker on chromosome 22. *Nature* **329**:246-8.
145. **Russell, D. S., and R. J.L.** 1989. Pathology of tumours of the nervous system. Williams & Wilkings: Baltimore :55.



146. **Rustgi, A. K., L. Xu, D. Pinney, C. Sterner, R. Beauchamp, S. Schmidt, J. F. Gusella, and V. Ramesh.** 1995. Neurofibromatosis 2 gene in human colorectal cancer. *Cancer Genet Cytogenet* **84**:24-6.
147. **Sabolic, I., D. Brown, S. L. Gluck, and S. L. Alper.** 1997. Regulation of AE1 anion exchanger and H<sup>+</sup> ATPase in rat cortex by acute metabolic acidosis and alkalosis. *Kidney Int* **51**:125-37.
148. **Sahai, E., T. Ishizaki, S. Narumiya, and R. Treisman.** 1999. Transformation mediated by RhoA requires activity of ROCK kinases. *Curr Biol* **9**:136-45.
149. **Sainio, M., F. Zhao, L. Heiska, O. Turunen, M. den Bakker, E. Zwarthoff, M. Lutchman, G. A. Rouleau, J. Jaaskelainen, A. Vaheri, and O. Carpen.** 1997. Neurofibromatosis 2 tumor suppressor protein colocalizes with ezrin and CD44 and associates with actin-containing cytoskeleton. *J Cell Sci* **110**:2249-60.
150. **Sanger, F., S. Nicklen, and A. R. Coulson.** 1977. DNA sequencing with chain-terminating inhibitors. *Proc Natl Acad Sci U S A* **74**:5463-7.
151. **Sato, N., N. Funayama, A. Nagafuchi, S. Yonemura, and S. Tsukita.** 1992. A gene family consisting of ezrin, radixin and moesin. Its specific localization at actin filament/plasma membrane association sites. *J Cell Sci* **103**:131-43.
152. **Schiffer, D.** 1993. *Brain Tumors. Pathology and biological correlates.* Springer-Verlag. Berlin.
153. **Schlessinger, J.** 1994. SH2/SH3 signaling proteins. *Curr Opin Genet Dev* **4**:25-30.
154. **Schmucker, B., Y. Tang, and M. Kressel.** 1999. Novel alternatively spliced isoforms of the neurofibromatosis type 2 tumor suppressor are targeted to the nucleus and cytoplasmic granules. *Hum Mol Genet* **8**:1561-70.
155. **Scoles, D. R., D. P. Huynh, M. S. Chen, S. P. Burke, D. H. Gutmann, and S. M. Pulst.** 2000. The neurofibromatosis 2 tumor suppressor protein interacts with hepatocyte growth factor-regulated tyrosine kinase substrate. *Hum Mol Genet* **9**:1567-74.
156. **Scoles, D. R., D. P. Huynh, P. A. Morcos, E. R. Coulsell, N. G. Robinson, F. Tamanoi, and S. M. Pulst.** 1998. Neurofibromatosis 2 tumour suppressor schwannomin interacts with betaII- spectrin. *Nat Genet* **18**:354-9.
157. **Seizinger, B. R., S. de la Monte, L. Atkins, J. F. Gusella, and R. L. Martuza.** 1987a. Molecular genetic approach to human meningioma: loss of genes on chromosome 22. *Proc Natl Acad Sci U S A* **84**:5419-23.
158. **Seizinger, B. R., R. L. Martuza, and J. F. Gusella.** 1986. Loss of genes on chromosome 22 in tumorigenesis of human acoustic neuroma. *Nature* **322**:644-7.
159. **Seizinger, B. R., G. Rouleau, L. J. Ozelius, A. H. Lane, P. St George-Hyslop, S. Huson, J. F. Gusella, and R. L. Martuza.** 1987b. Common pathogenetic mechanism for three tumor types in bilateral acoustic neurofibromatosis. *Science* **236**:317-9.
160. **Sekido, Y., H. I. Pass, S. Bader, D. J. Mew, M. F. Christman, A. F. Gazdar, and J. D. Minna.** 1995. Neurofibromatosis type 2 (NF2) gene is somatically mutated in mesothelioma but not in lung cancer. *Cancer Res* **55**:1227-31151.
161. **Serrador, J. M., M. Nieto, J. L. Alonso-Lebrero, M. A. del Pozo, J. Calvo, H. Furthmayr, R. Schwartz-Albiez, F. Lozano, R. Gonzalez-Amaro, P. Sanchez-Mateos, and F. Sanchez-Madrid.** 1998. CD43 interacts with moesin and ezrin and regulates its redistribution to the uropods of T lymphocytes at the cell-cell contacts. *Blood* **91**:4632-44.
162. **Shaw, R. J., A. I. McClatchey, and T. Jacks.** 1998. Localization and functional domains of the neurofibromatosis type II tumor suppressor, merlin. *Cell Growth Differ* **9**:287-96.

163. **Shaw, R. J., J. G. Paez, M. Curto, A. Yaktine, W. M. Pruitt, I. Saotome, J. P. O'Bryan, V. Gupta, N. Ratner, C. J. Der, T. Jacks, and A. I. McClatchey.** 2001. The Nf2 tumor suppressor, merlin, functions in Rac-dependent signaling. *Dev Cell* **1**:63-72.
164. **Sherman, L., H. M. Xu, R. T. Geist, S. Saporito-Irwin, N. Howells, H. Ponta, P. Herrlich, and D. H. Gutmann.** 1997. Interdomain binding mediates tumor growth suppression by the NF2 gene product. *Oncogene* **15**:2505-9.
165. **Short, M. P., T. L. Martuza, and S. M. Huson.** 1994. Neurofibromatosis 2: Clinical features, genetic counseling and management issues. I: The neurofibromatoses: a pathogenetic and clinical overview, Huson S.M., Hughes T.A.C. (eds.). Chapman & Hall Medical: London :1-22.
166. **Shuster, C. B., and I. M. Herman.** 1995. Indirect association of ezrin with F-actin: isoform specificity and calcium sensitivity. *J Cell Biol* **128**:837-48.
167. **Sieb, J. P., S. M. Pulst, and A. Buch.** 1992. Familial CNS tumors. *J Neurol* **239**:343-4.
168. **Sigurdsson, H., B. Baldetorp, A. Borg, M. Dalberg, M. Ferno, D. Killander, and H. Olsson.** 1990. Indicators of prognosis in node-negative breast cancer. *N Engl J Med* **322**:1045-53.
169. **Simons, P. C., S. F. Pietromonaco, D. Reczek, A. Bretscher, and L. Elias.** 1998. C-terminal threonine phosphorylation activates ERM proteins to link the cell's cortical lipid bilayer to the cytoskeleton. *Biochem Biophys Res Commun* **253**:561-5.
170. **Smith, A. L., P. J. Mitchell, J. Shipley, B. A. Gusterson, M. V. Rogers, and M. R. Crompton.** 1995. Pez: a novel human cDNA encoding protein tyrosine phosphatase- and ezrin-like domains. *Biochem Biophys Res Commun* **209**:959-65.
171. **Smith, C. L.** 1998. Cross-talk between peptide growth factor and estrogen receptor signaling pathways. *Biol Reprod* **58**:627-32.
172. **Stemmer-Rachamimov, A. O., C. Gonzalez-Agosti, L. Xu, J. A. Burwick, R. Beauchamp, D. Pinney, D. N. Louis, and V. Ramesh.** 1997a. Expression of NF2-encoded merlin and related ERM family proteins in the human central nervous system. *J Neuropathol Exp Neurol* **56**:735-42.
173. **Stemmer-Rachamimov, A. O., T. Wiederhold, G. P. Nielsen, M. James, D. Pinney-Michalowski, J. E. Roy, W. A. Cohen, V. Ramesh, and D. N. Louis.** 2001. NHE-RF, a merlin-interacting protein, is primarily expressed in luminal epithelia, proliferative endometrium, and estrogen receptor-positive breast carcinomas. *Am J Pathol* **158**:57-62.
174. **Stemmer-Rachamimov, A. O., L. Xu, C. Gonzalez-Agosti, J. A. Burwick, D. Pinney, R. Beauchamp, L. B. Jacoby, J. F. Gusella, V. Ramesh, and D. N. Louis.** 1997b. Universal absence of merlin, but not other ERM family members, in schwannomas. *Am J Pathol* **151**:1649-54.
175. **Stevenson, B. R., J. D. Siliciano, M. S. Mooseker, and D. A. Goodenough.** 1986. Identification of ZO-1: a high molecular weight polypeptide associated with the tight junction (zonula occludens) in a variety of epithelia. *J Cell Biol* **103**:755-66.
176. **Stokowski, R. P., and D. R. Cox.** 2000. Functional analysis of the neurofibromatosis type 2 protein by means of disease-causing point mutations. *Am J Hum Genet* **66**:873-91.
177. **Takahashi, K., T. Sasaki, A. Mammoto, K. Takaishi, T. Kameyama, S. Tsukita, and Y. Takai.** 1997. Direct interaction of the Rho GDP dissociation inhibitor with ezrin/radixin/moesin initiates the activation of the Rho small G protein. *J Biol Chem* **272**:23371-5.
178. **Takeshima, H., I. Izawa, P. S. Lee, N. Safdar, V. A. Levin, and H. Saya.** 1994. Detection of cellular proteins that interact with the NF2 tumor suppressor gene product. *Oncogene* **9**:2135-44.

179. **Towler, D. A., J. I. Gordon, S. P. Adams, and L. Glaser.** 1988. The biology and enzymology of eukaryotic protein acylation. *Annu Rev Biochem* **57**:69-99.
180. **Tran Quang, C., A. Gautreau, M. Arpin, and R. Treisman.** 2000. Ezrin function is required for ROCK-mediated fibroblast transformation by the Net and Dbl oncogenes. *Embo J* **19**:4565-76.
181. **Tran, Y. K., O. Bogler, K. M. Gorse, I. Wieland, M. R. Green, and I. F. Newsham.** 1999. A novel member of the NF2/ERM/4.1 superfamily with growth suppressing properties in lung cancer. *Cancer Res* **59**:35-43.
182. **Trofatter, J. A., M. M. MacCollin, J. L. Rutter, J. R. Murrell, M. P. Duyao, D. M. Parry, R. Eldridge, N. Kley, A. G. Menon, K. Pulaski, and *et al.*** 1993. A novel moesin-, ezrin-, radixin-like gene is a candidate for the neurofibromatosis 2 tumor suppressor. *Cell* **72**:791-800.
183. **Tsukita, S., K. Oishi, N. Sato, J. Sagara, and A. Kawai.** 1994. ERM family members as molecular linkers between the cell surface glycoprotein CD44 and actin-based cytoskeletons. *J Cell Biol* **126**:391-401.
184. **Tsukita, S., and S. Yonemura.** 1997. ERM proteins: head-to-tail regulation of actin-plasma membrane interaction. *Trends Biochem Sci* **22**:53-8.
185. **Tsukita, S., and S. Yonemura.** 1999. Cortical actin organization: lessons from ERM (ezrin/radixin/moesin) proteins. *J Biol Chem* **274**:34507-10.
186. **Turunen, O., T. Wahlstrom, and A. Vaheri.** 1994. Ezrin has a COOH-terminal actin-binding site that is conserved in the ezrin protein family. *J Cell Biol* **126**:1445-53.
187. **van Huizen, R., K. Miller, D. M. Chen, Y. Li, Z. C. Lai, R. W. Raab, W. S. Stark, R. D. Shortridge, and M. Li.** 1998. Two distantly positioned PDZ domains mediate multivalent INAD- phospholipase C interactions essential for G protein-coupled signaling. *Embo J* **17**:2285-97.
188. **van Slegtenhorst, M., M. Nellist, B. Nagelkerken, J. Cheadle, R. Snell, A. van den Ouweland, A. Reuser, J. Sampson, D. Halley, and P. van der Sluijs.** 1998. Interaction between hamartin and tuberlin, the TSC1 and TSC2 gene products. *Hum Mol Genet* **7**:1053-7.
189. **Vic, P., F. Vignon, D. Derocq, and H. Rochefort.** 1982. Effect of estradiol on the ultrastructure of the MCF7 human breast cancer cells in culture. *Cancer Res* **42**:667-73.
190. **Vickers, P. J., M. J. Dufresne, and K. H. Cowan.** 1989. Relation between cytochrome P450IA1 expression and estrogen receptor content of human breast cancer cells. *Mol Endocrinol* **3**:157-64.
191. **Viskochil, D., A. M. Buchberg, G. Xu, R. M. Cawthon, J. Stevens, R. K. Wolff, M. Culver, J. C. Carey, N. G. Copeland, N. A. Jenkins, and *et al.*** 1990. Deletions and a translocation interrupt a cloned gene at the neurofibromatosis type 1 locus. *Cell* **62**:187-92.
192. **Voltz, J. W., E. J. Weinman, and S. Shenolikar.** 2001. Expanding the role of NHERF, a PDZ-domain containing protein adapter, to growth regulation. *Oncogene* **20**:6309-14.
193. **Wallace, M. R., D. A. Marchuk, L. B. Andersen, R. Letcher, H. M. Odeh, A. M. Saulino, J. W. Fountain, A. Brereton, J. Nicholson, A. L. Mitchell, and *et al.*** 1990. Type 1 neurofibromatosis gene: identification of a large transcript disrupted in three NF1 patients. *Science* **249**:181-6.
194. **Weinman, E. J., D. Steplock, Y. Wang, and S. Shenolikar.** 1995. Characterization of a protein cofactor that mediates protein kinase A regulation of the renal brush border membrane Na(+)-H+ exchanger. *J Clin Invest* **95**:2143-9.
195. **Wellenreuther, R., J. A. Kraus, D. Lenartz, A. G. Menon, J. Schramm, D. N. Louis, V. Ramesh, J. F. Gusella, O. D. Wiestler, and A. von Deimling.** 1995. Analysis of the neurofibromatosis 2 gene reveals molecular variants of meningioma. *Am J Pathol* **146**:827-32.

196. **Wertelecki, W., G. A. Rouleau, D. W. Superneau, L. W. Forehand, J. P. Williams, J. L. Haines, and J. F. Gusella.** 1988. Neurofibromatosis 2: clinical and DNA linkage studies of a large kindred. *N Engl J Med* **319**:278-83.
197. **Wieczorek, H., D. Brown, S. Grinstein, J. Ehrenfeld, and W. R. Harvey.** 1999. Animal plasma membrane energization by proton-motive V-ATPases. *Bioessays* **21**:637-48.
198. **Winckler, B., C. Gonzalez Agosti, M. Magendantz, and F. Solomon.** 1994. Analysis of a cortical cytoskeletal structure: a role for ezrin-radixin-moesin (ERM proteins) in the marginal band of chicken erythrocytes. *J Cell Sci* **107**:2523-34.
199. **Wolff, R. K., K. A. Frazer, R. K. Jackler, M. J. Lanser, L. H. Pitts, and D. R. Cox.** 1992. Analysis of chromosome 22 deletions in neurofibromatosis type 2-related tumors. *Am J Hum Genet* **51**:478-85.
200. **Woods, D. F., and P. J. Bryant.** 1991. The discs-large tumor suppressor gene of *Drosophila* encodes a guanylate kinase homolog localized at septate junctions. *Cell* **66**:451-64.
201. **Woods, D. F., and P. J. Bryant.** 1993. ZO-1, DlgA and PSD-95/SAP90: homologous proteins in tight, septate and synaptic cell junctions. *Mech Dev* **44**:85-9.
202. **Wunderlich, W., I. Fialka, D. Teis, A. Alpi, A. Pfeifer, R. G. Parton, F. Lottspeich, and L. A. Huber.** 2001. A novel 14-kilodalton protein interacts with the mitogen-activated protein kinase scaffold mp1 on a late endosomal/lysosomal compartment. *J Cell Biol* **152**:765-76.
203. **Xu, G. F., P. O'Connell, D. Viskochil, R. Cawthon, M. Robertson, M. Culver, D. Dunn, J. Stevens, R. Gesteland, R. White, and *et al.*** 1990. The neurofibromatosis type 1 gene encodes a protein related to GAP. *Cell* **62**:599-608.
204. **Xu, H. M., and D. H. Gutmann.** 1998. Merlin differentially associates with the microtubule and actin cytoskeleton. *J Neurosci Res* **51**:403-15.
205. **Xu, L., C. Gonzalez-Agosti, R. Beauchamp, D. Pinney, C. Sterner, and V. Ramesh.** 1998. Analysis of molecular domains of epitope-tagged merlin isoforms in Cos-7 cells and primary rat Schwann cells. *Exp Cell Res* **238**:231-40.
206. **Yang, Q., and N. K. Tonks.** 1991. Isolation of a cDNA clone encoding a human protein-tyrosine phosphatase with homology to the cytoskeletal-associated proteins band 4.1, ezrin, and talin. *Proc Natl Acad Sci U S A* **88**:5949-53.
207. **Yao, X., L. Cheng, and J. G. Forte.** 1996. Biochemical characterization of ezrin-actin interaction. *J Biol Chem* **271**:7224-9.
208. **Yonemura, S., and S. Tsukita.** 1999. Direct involvement of ezrin/radixin/moesin (ERM)-binding membrane proteins in the organization of microvilli in collaboration with activated ERM proteins. *J Cell Biol* **145**:1497-509.
209. **Yun, C. H., G. Lamprecht, D. V. Forster, and A. Sidor.** 1998. NHE3 kinase A regulatory protein E3KARP binds the epithelial brush border Na<sup>+</sup>-H<sup>+</sup> exchanger NHE3 and the cytoskeletal protein ezrin. *J Biol Chem* **273**:25856-63.

## 8. Appendix

### List of Publications

- **Wiederhold, T., *et al.*** Identification of merintA: A novel cytoskeletal protein that associates with merlin. Manuscript in preparation.
- **Stemmer-Rachamimov, A. O., T. Wiederhold, G. P. Nielsen, M. James, D. Pinney-Michalowski, J. E. Roy, W. A. Cohen, V. Ramesh, and D. N. Louis.** 2001. NHE-RF, a merlin-interacting protein, is primarily expressed in luminal epithelia, proliferative endometrium, and estrogen receptor-positive breast carcinomas. *Am J Pathol* **158**:57-62.
- **Breton, S., T. Wiederhold, V. Marshansky, N. N. Nsumu, V. Ramesh, and D. Brown.** 2000. The B1 subunit of the H<sup>+</sup> ATPase is a PDZ domain-binding protein. Co-localization with NHE-RF in renal B-intercalated cells. *J Biol Chem* **275**:18219-24.
- **Gonzalez-Agosti, C., T. Wiederhold, M. E. Herndon, J. Gusella, and V. Ramesh.** 1999. Interdomain interaction of merlin isoforms and its influence on intermolecular binding to NHE-RF. *J Biol Chem* **274**:34438-42.

### List of Published Abstracts

- **Wiederhold, T., M. James, N. Hull, N. Smith, J.F. Gusella, V. Ramesh.** 2000. Isolation and Characterization of a Novel Interactor for Merlin. 40<sup>th</sup> American Society for Cell Biology Annual Meeting.
- **Wiederhold, T., S. Breton, D. Brown, J.F. Gusella, V. Ramesh.** 2000. The NF2 Tumor Suppressor Merlin and its Interactions. NNFF International Consortium for the Molecular Biology of NF1 and NF2.
- **Wiederhold, T., M. James, A. Stemmer-Rachamimov, D. Pinney, R. Levenson, J. Roy, C. Gonzalez-Agosti, J. Gusella, D. Louis, V. Ramesh.** 1999. The MERM Interactor NHE-RF is Upregulated and Displays a Response through Estrogen in Breast Cancer. 39<sup>th</sup> American Society for Cell Biology Annual Meeting.
- **Breton, S., T. Wiederhold, V. Marshansky, V. Ramesh, D. Brown.** 1999. The PDZ-Domain Protein NHE-RF Interacts with the B1 Subunit of the H<sup>+</sup> ATPase, and Co-localizes with Proton Pumps in Type B Intercalated Cells. American Society of Nephrology Meeting.
- **Gonzalez-Agosti, C., T. Wiederhold, M.E. Herndon, J.F. Gusella and V. Ramesh.** 1998. Homotypic and Heterotypic Interaction of Merlin and the ERM Proteins Differences Between Isoform 1 and 2 of Merlin. 38<sup>th</sup> American Society for Cell Biology Annual Meeting.

**Erklärung**

Hiermit versichere ich, dass ich diese Dissertation selbständig verfasst habe und nur die angegebenen Quellen und Hilfsmittel benutzt habe. Ferner erkläre ich, dass die vorliegende Arbeit an keiner anderen Hochschule als Dissertation eingereicht wurde.

Boston, im Dezember 2001

Thorsten Wiederhold

## Interdomain Interaction of Merlin Isoforms and Its Influence on Intermolecular Binding to NHE-RF\*

(Received for publication, June 18, 1999, and in revised form, August 12, 1999)

Charo Gonzalez-Agosti‡, Thorsten Wiederhold‡, Mary E. Herndon§, James Gusella‡, and Vijaya Ramesh‡¶

From the ‡Molecular Neurogenetics Unit, Massachusetts General Hospital, Charlestown, Massachusetts 02129 and the §Beth Israel Deaconess Medical Center, Harvard Medical School, Boston, Massachusetts 02215

**Merlin, the neurofibromatosis 2 tumor suppressor protein, has two major isoforms with alternate C termini and is related to the ERM (ezrin, radixin, moesin) proteins. Regulation of the ERMs involves intramolecular and/or intermolecular head-to-tail associations between family members. We have determined whether merlin undergoes similar interactions, and our findings indicate that the C terminus of merlin isoform 1 is able to associate with its N-terminal domain in a head-to-tail fashion. However, the C terminus of isoform 2 lacks this property. Similarly, the N terminus of merlin can also associate with C terminus of moesin. We have also explored the effect of merlin self-association on binding to the regulatory cofactor of Na<sup>+</sup>-H<sup>+</sup> exchanger (NHE-RF), an interacting protein for merlin and the ERMs. Merlin isoform 2 captures more NHE-RF than merlin isoform 1 in affinity binding assays, suggesting that in full-length merlin isoform 1, the NHE-RF binding site is masked because of the self-interactions of merlin. Treatment with a phospholipid known to decrease self-association of ERMs enhances the binding of merlin isoform 1 to NHE-RF. Thus, although isoform 1 resembles the ERM proteins, which transition between inactive (closed) and active (open) states, isoform 2 is distinct, existing only in the active (open) state and presumably constitutively more available for interaction with other protein partners.**

Merlin is the tumor suppressor protein deficient in neurofibromatosis 2 (NF2),<sup>1</sup> a dominantly inherited disorder characterized by bilateral vestibular schwannomas and other brain tumors (1, 2). Merlin has a striking similarity in sequence and structure with ezrin, radixin, and moesin, commonly referred to as the ERM proteins. The ERM proteins share ~78% amino acid identity with each other, and all three are 45–47% identical to merlin (3). Like the ERM proteins and protein 4.1, merlin possesses a FERM (protein 4.1, ezrin, radixin, moesin) domain (~270 amino acids defining membership in the protein

4.1 superfamily) in its N-terminal half, followed by a long  $\alpha$ -helical segment and a charged C-terminal domain (4). The NF2 gene comprises 17 exons with alternative splicing of the penultimate exon producing two major merlin isoforms. Isoform 1 is a 595-amino acid protein produced from exons 1–15 and exon 17. Isoform 2 results from the presence of the alternatively spliced exon 16, which alters the C terminus of the protein to produce a 590-amino acid protein identical to isoform 1 over the first 579 residues (5–7). Mutational analysis has revealed a wide variety of mutations in the germline and tumors of NF2 patients as well as in sporadic schwannomas and meningiomas, confirming merlin's tumor suppressor function (8).

ERM proteins act as linkers between integral membrane proteins and the actin cytoskeleton (9). Proteins identified as ligands for ERM proteins include CD44, CD43, ICAM1, ICAM2, and actin (9–13). We and others have recently identified the human homologue of a regulatory cofactor for Na<sup>+</sup>-H<sup>+</sup> exchanger (NHE-RF) as a novel interactor for the conserved N terminus of merlin and ERM proteins (14, 15). In addition to interacting with many binding partners, the ERM proteins are capable of forming homo- and heterotypic associations between family members (16, 17). Indeed, several recent studies performed on the regulation of ERM proteins suggest that the availability of ERM domains to binding partners is controlled by self-association of the N-terminal and C-terminal regions (13, 18, 19). Thus the ERM proteins can exist in the "closed" state, where the N- and C-terminal regions undergo an intramolecular interaction, masking the respective ligand-binding site. This closed state can be converted to the "open" state in which intramolecular interaction is disrupted by a variety of cellular signals, including Rho-mediated signaling and the phospholipid PIP<sub>2</sub>. *In vitro* binding studies performed with merlin isoforms suggested that the C terminus of isoform 1 can interact with its N terminus, and the C terminus of isoform 2 lacked this property (20). Homotypic interaction of merlin isoform 1 and heterotypic interaction between merlin and the ERM proteins have also been reported recently by yeast two hybrid and blot overlay assays (21, 22).

In view of the importance of self-association in regulation of the ERM proteins, we have used affinity co-electrophoresis (ACE) assays to explore the capacity of the two major merlin isoforms to self-associate and to interact with a representative ERM protein. The uniqueness of this assay is the ability to determine the dissociation constants of the observed interactions. Although, like the ERMs, the C terminus of merlin isoform 1 interacts in a head-to-tail fashion with its N-terminal domain, the C terminus of isoform 2 lacks this property. The N terminus of merlin is also able to associate heterotypically with the C terminus of moesin. Furthermore, in affinity binding experiments we observe that full-length merlin isoform 2 is

\* This work was supported by National Institutes of Health Grant NS24279 and by funds from Neurofibromatosis Inc. (Massachusetts Chapter). The costs of publication of this article were defrayed in part by the payment of page charges. This article must therefore be hereby marked "advertisement" in accordance with 18 U.S.C. Section 1734 solely to indicate this fact.

¶ To whom correspondence should be addressed: Molecular Neurogenetics Unit, Massachusetts General Hospital, Bldg. 149, 13th St., Charlestown, MA 02129. Tel.: 617-724-9733; Fax: 617-726-5736. E-mail: Ramesh@helix.mgh.harvard.edu.

<sup>1</sup> The abbreviations used are: NF2, neurofibromatosis 2; NHE-RF, regulatory cofactor of Na<sup>+</sup>-H<sup>+</sup> exchanger; ACE, affinity co-electrophoresis; PIP<sub>2</sub>, phosphatidylinositol 4,5-bisphosphate; GST, glutathione S-transferase; aa, amino acid(s); GSH, glutathione; PAGE, polyacrylamide gel electrophoresis.

able to capture greater quantities of NHE-RF than full-length merlin isoform 1, consistent with the notion that the ligand binding is suppressed by the self-interaction of merlin isoform 1. In addition, the interaction between merlin isoform 1 and NHE-RF is enhanced in the presence of the phosphoinositide  $PIP_2$ . Thus, merlin isoform 1 behaves like the ERM proteins in its interdomain interaction and its regulation by phospholipids, but merlin isoform 2 does not exhibit this property and is always available for interaction with other ligands. The different regulation of inter- and intramolecular domain interactions of the isoforms of merlin could play an essential role in its tumor suppressor function.

#### EXPERIMENTAL PROCEDURES

**Expression Constructs**—Full-length isoform 1 (aa 1–595), full-length isoform 2 (aa 1–590), N-terminal (aa 1–332), and C-terminal (isoform 1 aa 340–595; isoform 2 aa 340–590; common to both isoforms aa 340–579) portions of merlin were expressed as glutathione *S*-transferase (GST) fusion proteins in pGEX2T. Also, full-length moesin (aa 1–577), N-terminal (aa 1–332), and C-terminal (aa 307–577) portions of moesin were expressed as GST fusion proteins in pGEX4T1. Similarly, full-length NHE-RF (aa 1–338) was expressed as a GST fusion protein. Expression and purification of the GST fusion proteins were performed as described previously for merlin (23) and using standard methods for moesin and NHE-RF. In addition, full-length merlin isoform 1 and 2 were cloned into the mammalian expression vector pcDNA 3 engineered to have a FLAG tag at the N terminus. These constructs were transiently expressed in Cos-7 cells as described previously (24).

**Antibodies**—The polyclonal anti-merlin antibody (N21) and the polyclonal anti-GST antibody have been described previously (23, 25). A rabbit polyclonal antibody IC270 was raised against the GST-NHE-RF fusion protein (aa 270–358). The anti-FLAG antibody M2 was commercially obtained (Kodak, IBI).

**Affinity Co-electrophoresis**—For affinity co-electrophoresis (ACE), purified GST fusion protein products of merlin and moesin were thrombin cleaved. ACE gels were prepared using 1% low melting point agarose in 125 mM potassium acetate, 50 mM Hepes, pH 7.5, and carried out as described (25, 26). Gels were run at 60 volts for 4 h, and the proteins were then transferred to nitrocellulose by capillary action and analyzed by immunoblotting using an affinity eluted N terminus-specific anti-merlin antibody (N21) at a dilution of 1:100 and protein A conjugated to  $^{125}I$ . Retardation coefficients were calculated as described previously (27). Dissociation constants were calculated from nonlinear, least squares fitting of plots of corrected retardation coefficient versus concentration of retarding protein (27, 28). Data were then fit, using a nonlinear least squares approach (Kaleidagraph, Synergy Software), to the equation  $r = R_{\infty}/[1 + (K_d/[P_{tot}])]$ , where  $r$  = retardation coefficient and  $[P_{tot}]$  = protein concentration in a given lane of an ACE gel. The variables that were fit simultaneously were  $K_d$ , the dissociation constant, and  $R_{\infty}$ , the maximum value of  $R$ . Data from two independent experiments were used for calculating dissociation constants, and the  $K_d$  value is shown with S.E.

**Affinity Precipitation Assays**—ZR-75-B cells were lysed in Brij lysis buffer (50 mM Tris, 150 mM NaCl, 1 mM EDTA, pH 8.0, 30% glycerol, 1% Brij 96) containing a 1 $\times$  protease inhibitor mixture (Roche Molecular Biochemicals), and the lysate was incubated with 600 pmol of GST-merlin immobilized on glutathione (GSH)-Sepharose 4B beads. The beads were washed extensively with phosphate-buffered saline containing Pefabloc, resuspended in Laemmli loading buffer, subjected to 10% SDS-PAGE, and immunoblotted with IC270 antiserum (1:1000). In some experiments, GST-merlin immobilized on beads was incubated with ZR-75-B lysate along with 50  $\mu$ M/ml phosphatidyl serine or  $PIP_2$  (Sigma). Each phospholipid was dissolved in distilled water to a final concentration of 1 mg/ml and sonicated three times each for 10 s.

Cos-7 cells expressing merlin isoforms 1 and 2 as FLAG-tagged proteins were lysed in Nonidet P-40 lysis buffer (150 mM NaCl, 50 mM Tris, pH 8.0, 0.5% Nonidet P-40) containing a 1 $\times$  protease inhibitor mixture as described above. The lysates were incubated with 600 pmol of GST-NHE-RF full-length fusion protein or GST protein alone coupled to GSH-Sepharose 4B beads. The beads were washed as described above, and the separated proteins were immunoblotted with the anti-FLAG antibody M2.

#### RESULTS

**Interdomain Interaction of Merlin Isoforms**—To determine whether merlin as an ERM family member is capable of self-

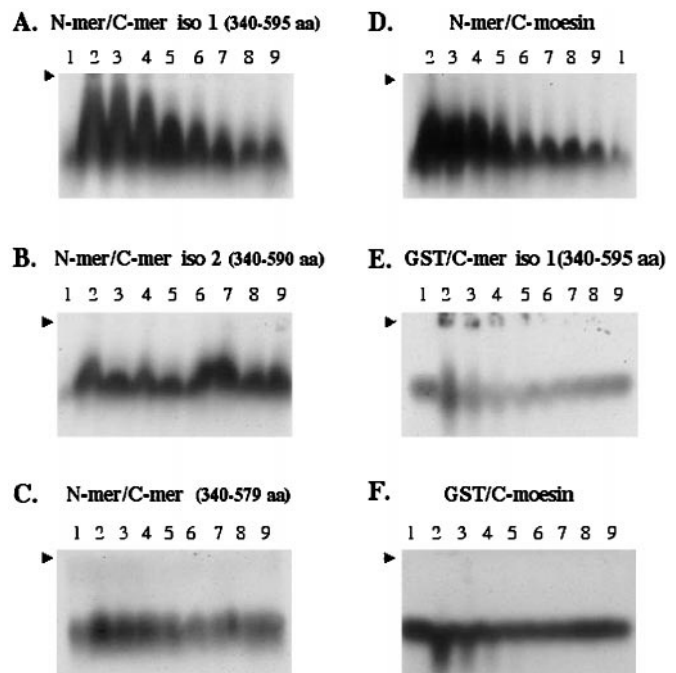


**FIG. 1. Affinity co-electrophoresis of N- and C-domain of merlin (homotypic) and N-domain of merlin and C-domain of moesin (heterotypic).** Thrombin-cleaved GST fusion protein of merlin N-domain (125 nM) was loaded into a long gel slot perpendicular to the direction of electrophoresis. Thrombin-cleaved GST fusion proteins of merlin C-domains isoform 1 (A), isoform 2 (B), domain common to both isoforms (C), or moesin (D) were loaded at 0, 750, 375, 188, 94, 47, 24, 12, and 6  $\mu$ M (lanes 1–9, respectively) into multiple wells parallel to the direction of electrophoresis. After electrophoresis, during which time the migrating front of N-domain transversed the zones containing the C-domain, the contents of the gels were transferred to nitrocellulose and visualized by immunoblotting with an antibody against the N-domain of merlin. In E and F, electrophoresis was carried out as in A–D, except the purified GST protein was used as a control in place of the N-domain of merlin in the long slot, and C-domain of merlin isoform 1 (E) or C-domain of moesin (F) was loaded into the multiple wells. The migration of the control protein was detected using a specific antibody against GST. The arrowhead represents the origin where the C termini of various proteins were loaded.

association and to ascertain whether the two major isoforms of merlin differ from each other in this property, we used the technique of ACE. Using this technique we were able to demonstrate direct binding between the N- and C termini of merlin isoforms in solution and to measure the strength of the binding. Briefly, the thrombin cleaved N- (aa 1–332) and C-terminal (iso 1, aa 340–595 or iso 2, aa 340–590) polypeptides were subjected to affinity electrophoresis in 1% agarose gel in physiological buffer. The N terminus of merlin (at 125 nM) was loaded into a long transverse slot. The C terminus of either isoform 1 or 2 of merlin was cast (in agarose) into nine rectangular wells at concentrations ranging from 750 to 0 nM. The anode was placed so that the more rapidly migrating N-domain passes through the zones containing the C-domain during most of the electrophoresis run. The mobility of the N-domain was then detected by transferring the proteins to nitrocellulose and probing with an N-terminal-specific antibody. Fig. 1A demonstrates the interaction of the N terminus of merlin with the C terminus of merlin isoform 1, where migrating N-domain encountered the C-domain. The migration of the former was retarded in a manner that varied directly with the concentration of the latter. In contrast, the migration of the N-domain of merlin was not retarded by the C-domain of merlin isoform 2 over the same range of concentrations (Fig. 1B).

Because we were able to demonstrate a difference in self-association between the two isoforms of merlin that differ from



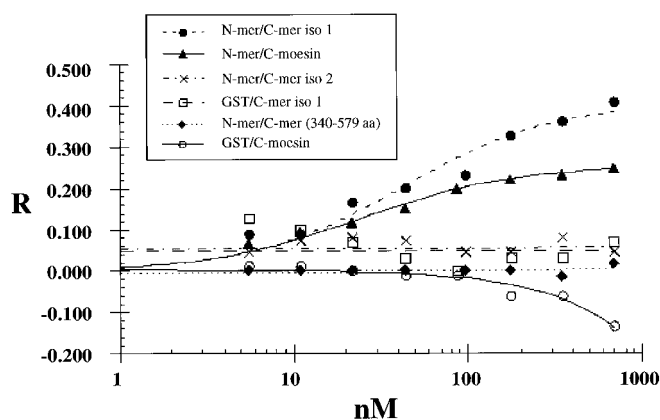


FIG. 2. Analysis of binding of the homotypic interaction of merlin isoforms and heterotypic interaction of merlin to moesin by affinity co-electrophoresis. Six representative ACE gels were used for these analyses. For each gel, retardation coefficients ( $R$ ) were determined for all protein concentration tested for the C termini. Dissociation constants were measurable for N-mer/C-mer iso 1 and N-mer/C-moesin gels by fitting the data to the equation  $r = R_{\infty}/[1 + (K_{d,app}/[\text{protein}_{tot}])]$  (see "Experimental Procedures"). The remaining gels showed no detectable binding. Data for these gels could not be fit to the equation above and are instead represented as linear fits.

each other only at the extreme C terminus, we further sought to determine whether the C-domain of merlin lacking both exons 16 and 17 is capable of self-interaction. To address this question we performed the same type of experiment described above except the C-domain of merlin spanned the common region aa 340–579. The results shown in Fig. 1C indicate that the migration of the N terminus was not retarded by this C-domain. These data suggest that the domain responsible for the self-association of the N terminus of merlin to the C terminus of merlin isoform 1 includes, at least in part, the last 16 amino acids (aa 580–595) specific to this isoform.

To evaluate whether merlin can interact in a heterotypic fashion with other ERM family members, we performed ACE experiments where the N-domain of merlin was used as the faster migrating protein passing through the zones containing the C-domain of moesin (aa 305–557). Fig. 1D shows the interaction of merlin and moesin by the retardation of migration of the N terminus of merlin. The migration of purified GST used as a control protein was not affected by the merlin C-domain isoform 1 and moesin C-domain over the same range of concentrations (Fig. 1, E and F). From measurements of mobility retardation in Fig. 1 (A–F), we can calculate the dissociation constant for the interaction of the N- and C-terminal polypeptides of merlin isoforms 1 and 2 (homotypic) and for the interaction of merlin to moesin (heterotypic). To avoid problems arising from the saturation of the films, ImageQuant software (Molecular Dynamics) was used to determine the true midpoint of each of the bands (28). Fig. 2 shows the analyses of the six representative experiments. For every gel, retardation coefficients ( $R$ ) were determined for each C-terminal protein concentration tested. Dissociation constants were measurable for N-merlin interaction with the C-merlin isoform 1 and N-merlin interaction with the C-moesin by fitting the data to the equation  $r = R_{\infty}/[1 + (K_{d,app}/[\text{protein}_{tot}])]$  (see "Experimental Procedures"). Merlin isoform 1 can self-interact with a  $K_d$  of 49.0  $\pm$  6.45 nM, whereas merlin interacts with moesin with a  $K_d$  of  $28.5 \pm 6.5$  nM. By contrast, no binding was measurable with merlin isoform 2 and control proteins.

**NHE-RF Binds Differentially to Merlin Isoforms**—We recently identified NHE-RF, a regulatory factor for the  $\text{Na}^+\text{-H}^+$  exchanger isoform 3 (NHE3), as an interacting protein for merlin in a two-hybrid screen and demonstrated that NHE-RF

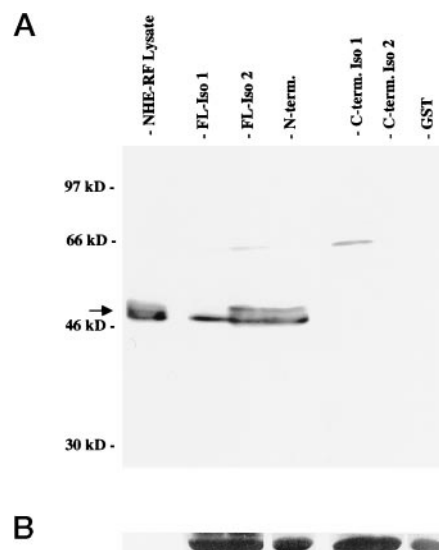


FIG. 3. Binding of NHE-RF to merlin isoforms. Lysate from ZR-75-B cells were incubated with various GST-merlin fusion proteins immobilized on GSH-Sepharose 4B beads. The beads were extensively washed, and bound proteins were separated on 10% SDS-PAGE and immunoblotted with an anti-NHE-RF antibody (IC270 serum). The arrow indicates NHE-RF at  $\sim 50$  kDa (A). *FL-iso 1*, full-length isoform 1; *FL-iso 2*, full-length isoform 2. B shows equal amounts of GST-merlin fusion proteins bound to the beads detected by Ponceau S staining.

can bind to merlin, moesin, and radixin via their conserved N-terminal regions (14). It is well documented that the binding of ERM proteins to their ligands is suppressed in the native full-length protein (13, 18, 19), a phenomenon explained by the interdomain interactions of the ERM proteins that could compete with the ligand binding (29). We therefore investigated whether NHE-RF displays differential binding with isoforms 1 and 2 of merlin by performing affinity precipitation experiments. Briefly, equal quantities of merlin full-length isoforms 1 and 2, N-domain, C-domain of both isoforms 1 and 2, expressed as GST fusion proteins, were bound to Sepharose beads and incubated with equal amount of ZR-75-B cell lysates. After extensive washes, the coupled proteins were removed from the beads by boiling and were detected on Western blots using a specific polyclonal antibody against NHE-RF. The results shown in Fig. 3 demonstrate that the N-domain and full-length isoform 2 of merlin exhibit a greater affinity for NHE-RF than merlin isoform 1. As expected NHE-RF did not bind to either the C-domain of both isoforms of merlin or the GST control protein. These results were further confirmed by at least three independent experiments.

To confirm the differential binding of merlin isoforms to NHE-RF, affinity binding assays were performed utilizing merlin isoforms expressed as FLAG-tagged proteins in Cos-7 cells and GST fusion protein of NHE-RF. The expression of FLAG-tagged merlin isoforms in Cos-7 cells were examined with an anti-FLAG antibody (M2) and found to be equally expressed (Fig. 4, lanes 1 and 2). Cos-7 cell lysates expressing approximately the same amount of the isoforms were incubated with 600 pmol of GST-NHE-RF beads. The bound proteins were separated on a 7.5% SDS-PAGE and probed with M2 antibody (Fig. 4). Merlin isoforms expressed in mammalian cells also revealed a differential binding to NHE-RF, and the analysis of the supernatants that were not bound to the beads clearly showed that NHE-RF beads capture 3–5-fold more merlin isoform 2 than isoform 1 in duplicate set of experiments. These data are consistent with the ACE results supporting that merlin isoform 2 exists constitutively in an open conformation that allows its ligand, NHE-RF, to interact without being hindered by the interdomain interaction that occurs in merlin isoform 1.

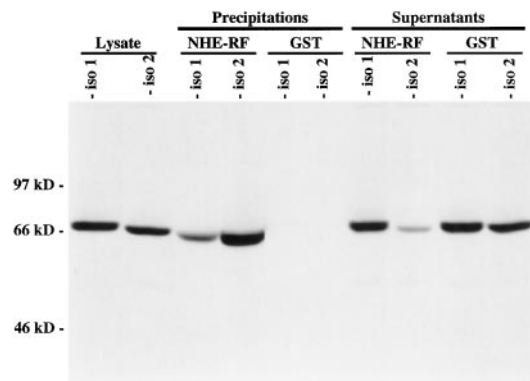


FIG. 4. **Binding of merlin isoforms 1 and 2 to NHE-RF.** Cos-7 cell lysates expressing either FLAG-tagged merlin isoform 1 or merlin isoform 2 were incubated with NHE-RF-GST fusion protein or GST protein expressed alone (control) immobilized on GSH-Sepharose 4B beads. The beads were extensively washed, and bound proteins were separated on 7.5% SDS-PAGE and immunoblotted with the anti-FLAG monoclonal antibody M2. Lysates from Cos-7 cells expressing merlin isoforms are shown for protein expression level in transfected cells. The supernatants that were not bound to the beads are shown to point out that NHE-RF beads capture more merlin isoform 2 than merlin isoform 1.

*Phospholipids Enhance the Binding of NHE-RF to Merlin Isoform 1*—Phosphatidylinositol 4-phosphate and PIP<sub>2</sub> enhance the interaction of ERM proteins to its ligands CD44, ICAM-1, and ICAM-2 (13, 18). ERM proteins bind to phosphatidylinositol 4-phosphate and PIP<sub>2</sub> (30), and it is believed that this binding evokes conformational changes in these proteins in a manner similar to the regulation of vinculin activity by PIP<sub>2</sub> (31). We therefore examined whether PIP<sub>2</sub> influences the binding of NHE-RF to merlin isoforms. For this, PIP<sub>2</sub> or phosphatidyl serine was included in the affinity precipitation assays. In the presence of PIP<sub>2</sub>, the amount of NHE-RF bound to merlin isoform 1 significantly increased (Fig. 5). The intensity of the bands was further analyzed by densitometric scanning of the autorads using transmittance analysis (Fluor-S, Multiimager, Bio-Rad). Results from three independent experiments revealed a 3-fold increase ( $3.10 \pm 1.04$ ) in binding of NHE-RF to merlin isoform 1 in the presence of PIP<sub>2</sub>. The binding of NHE-RF to either the N-domain of merlin or merlin isoform 2 ( $1.07 \pm 0.45$ ) was not influenced by PIP<sub>2</sub> (Fig. 5). The control phospholipid phosphatidyl serine did not enhance the NHE-RF binding to merlin isoform 1 (Fig. 5).

#### DISCUSSION

Despite an overall structural similarity to the ERM proteins, merlin differs from these relatives in having two isoforms with alternative C termini and in having a demonstrated tumor suppressor function. Both isoforms are expressed at the RNA and protein level in a variety of cell lines examined including NF2 target cells such as Schwann and meningeal cells (Refs. 6 and 7 and our unpublished data).<sup>2</sup> Work from other laboratories has demonstrated the interdomain interaction of merlin using yeast two hybrid, blot overlay, co-immunoprecipitation, and *in vitro* binding assays (20–22). Employing the technique of ACE, we not only demonstrate the difference between merlin isoforms in their interdomain interaction but also define the affinities of these interactions. The affinities that we have observed for merlin self-interaction and for the interaction of merlin with moesin are quite comparable with that reported for radixin using similar analysis (25). Because the C-terminal construct of merlin containing the common region (aa 340–579) did not exhibit the self-interaction, we believe that the isoform 1-specific C-terminal residues (aa 580–595) are critical for the

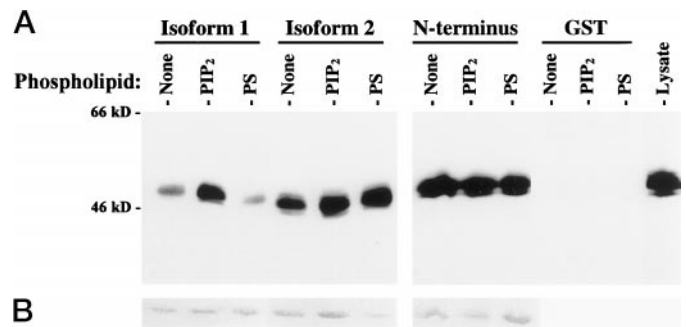


FIG. 5. **PIP<sub>2</sub> enhances binding of NHE-RF to merlin isoform 1.** GST-merlin fusion proteins or GST alone were bound to GSH-Sepharose 4B beads and incubated with ZR-75-B cell lysates. In addition, 50  $\mu$ g/ml PIP<sub>2</sub> or 50  $\mu$ g/ml phosphatidyl serine (PS) was added to the beads with the cell lysates. The eluted proteins were detected by Western blot analysis using IC270 serum (A). B shows Ponceau S staining of GST-merlin fusion proteins bound to the beads.

interdomain binding. This is in agreement with a previous report suggesting that extreme C-terminal protein sequences encoded by exon 17 is critical for the interdomain interaction (20).

It is well established that the interaction of ERM proteins with their membrane partners, as well as with the actin cytoskeleton, is suppressed in the full-length molecule, a phenomenon explained by intramolecular self-association that masks the binding sites for other ligands (32, 33). In the presence of phospholipids such as phosphatidylinositol 4-phosphate or PIP<sub>2</sub>, the interdomain interaction is disrupted, thus exposing the ligand binding sites (13, 18). Interdomain interaction also blocks the binding of full-length ezrin and radixin to NHE-RF compared with their N termini (29).<sup>2</sup> In our earlier studies (14), we failed to note a similar difference in binding to NHE-RF between the full-length merlin isoform 1 and the N-domain of merlin (aa 1–332). This apparent discrepancy could be explained by the fact that the previous studies were designed to answer qualitatively whether merlin binds to NHE-RF. However, the present studies were done in a quantitative fashion to address the differences in binding between the two isoforms of merlin. Our results demonstrate that the binding of merlin isoform 1 to its ligand NHE-RF is suppressed in the full-length molecule, and in the presence of PIP<sub>2</sub> this suppression is relieved. Merlin isoforms expressed in mammalian cells show the same difference in their binding to NHE-RF as the bacterially expressed proteins. The fact that merlin isoforms expressed in mammalian cells show differential binding to NHE-RF suggests that this may have functional significance *in vivo*.

The studies performed here illustrate the differences in the ability of the two alternatively spliced isoforms of merlin to interact with NHE-RF and further show that a phospholipid such as PIP<sub>2</sub> can regulate the interaction of merlin isoform 1 to NHE-RF. Thus these results document that merlin isoform 1 behaves in a manner similar to its ERM relatives, whereas merlin isoform 2 behaves distinctly and binds to NHE-RF more efficiently. Similarly, betaII-spectrin, a C-terminal interactor of merlin, has been shown to interact to a greater extent with the C terminus of merlin isoform 2 than with the C terminus of isoform 1 (34). Phosphorylation of a critical Thr residue at the C terminus of the ERM proteins has been implicated in stabilizing the open conformation of these proteins (19). This Thr residue is conserved in both isoforms of merlin; however, further studies are required to understand whether the phosphorylation of this residue is involved in regulating the intramolecular interaction of merlin isoform 1 and what role it might play in the function of merlin isoform 2.

<sup>2</sup> Solomon, F., personal communication.

Both NHE-RF and the related NHE-RF2 possess two PDZ domains known to mediate protein-protein interactions. The interaction of NHE-RF and NHE-RF2 with merlin and the ERMs is not mediated by the PDZ domains (14, 29, 35). However, the PDZ domains of both NHE-RF and NHE-RF2 can interact with several other membrane proteins, such as Na<sup>+</sup>-H<sup>+</sup> exchanger isoform 3, the  $\beta_2$ -adrenergic receptor, the purinergic P2Y1 receptor, and the cystic fibrosis transmembrane conductance regulator, which functions as a Cl<sup>-</sup> channel (35, 36). Thus, NHE-RF and NHE-RF2 appear to act as multifunctional adaptor proteins that may link merlin and the ERM proteins to different ion channels and receptors, providing many new possibilities for effects on intracellular signaling. Because merlin isoform 2 exists always in the open state, its interaction with NHE-RF and potentially with other merlin interactors may in fact occur when the equivalent sites in merlin isoform 1 and in the ERM proteins are masked in the closed state.

The strategy of comparing merlin with the related ERM proteins can be expected to produce similarities that are instructive concerning the overall function of these types of proteins and differences that could reveal the special tumor suppressor activity of merlin. In this study, we have observed both. The behavior of merlin isoform 1 with respect to interdomain interactions suggests that its regulation is similar to the regulation of ERM protein interactions. Moreover, the interaction of merlin with the ERM proteins suggests that these proteins could also be involved in mutual regulation of each other's activities. Although the full range of merlin interactions with other proteins remains to be delineated, it is likely that merlin sits within a web of interactions comprising multiple partners and signaling pathways, some of which are shared with the ERM family members. Interestingly, studies of the *Drosophila* homologue of merlin suggest that its growth suppression properties reside within the conserved N-terminal domain of the protein (37). Thus, the distinct tumor suppressor role of merlin could lie either in the distinct regulation of isoform 2, which differs from that of isoform 1 and the ERM proteins, or in the participation of merlin but not the ERM proteins in a signaling pathway that is uniquely important to NF2 target cells such as Schwann and meningeal cells.

**Acknowledgments**—We thank Dr. Frank Solomon for valuable discussions. We also thank Drs. Margaret Magendantz and Etchell Cordero for advice on the ACE experiments. The technical expertise of Denise Pinney and Cecilia Candia is gratefully acknowledged. We thank the members of our laboratory for helpful comments on the manuscript.

#### REFERENCES

- Martuza, R. L., and Eldridge, R. (1988) *N. Engl. J. Med.* **318**, 684–688
- Kaiser-Kupfer, M. I., Freidlin, V., Datiles, M. B., Edwards, P. A., Sherman, J. L., Parry, D., McCain, L. M., and Eldridge, R. (1989) *Arch. Ophthalmol.* **107**, 541–544
- Trofatter, J. A., MacCollin, M. M., Rutter, J. L., Murrell, J. R., Duyao, M. P., Parry, D. M., Eldridge, R., Kley, N., Menon, A. G., Pulaski, K., Haase, V. H., Ambrose, C. M., Munroe, D., Bove, C., Haines, J. L., Martuza, R. L., MacDonald, M. E., Seizinger, B. R., Short, M. P., Buckler, A. J., and Gusella, J. F. (1993) *Cell* **72**, 791–800
- Chishti, A. H., Kim, A. C., Marfatia, S. M. et al. (1998) *Trends Biochem. Sci.* **23**, 281–282
- Haase, V. H., Trofatter, J. A., McCollin, M., Tarttelin, E., Gusella, J. F., and Ramesh, V. (1994) *Hum. Mol. Genet.* **3**, 407–411
- Arakawa, H., Hayashi, N., Nagase, H., Ogawa, M., and Nakamura, Y. (1994) *Hum. Mol. Genet.* **3**, 565–568
- Pykett, M. J., Murphy, M., Harnish, P. R., and George, D. L. (1994) *Hum. Mol. Genet.* **3**, 559–564
- Gusella, J. F., Ramesh, V., McCollin, M., and Jacoby, L. B. (1996) *Curr. Opin. Genet. Dev.* **6**, 87–92
- Tsukita, S., Oishi, K., Sato, N., Sagara, J., Kawai, A., and Tsukita, S. (1994) *J. Cell Biol.* **126**, 391–401
- Turunen, O., Wahlström, T., and Vaheri, A. (1994) *J. Cell Biol.* **126**, 1445–1453
- Pestonjams, K., Amieva, M. R., Strassel, C. P., Nauseef, W. M., Furthmayr, H., and Luna, E. J. (1995) *Mol. Biol. Cell* **6**, 247–259
- Yonemura, S., Hirao, M., Doi, Y., Takahashi, N., Kondo, T., and Tsukita, S. (1998) *J. Cell Biol.* **140**, 885–895
- Heiska, L., Alifhan, K., Gronholm, M., Vilja, P., Vaheri, A., and Carpen, O. (1998) *J. Biol. Chem.* **273**, 21893–21900
- Murthy, A., Gonzalez-Agosti, C., Cordero, E., Pinney, D., Candia, C., Solomon, F., Gusella, J., and Ramesh, V. (1998) *J. Biol. Chem.* **273**, 1273–1276
- Reczek, D., Berryman, M., and Bretscher, A. (1997) *J. Cell Biol.* **139**, 169–179
- Gary, R., and Bretscher, A. (1993) *Proc. Natl. Acad. Sci. U. S. A.* **90**, 10846–10850
- Berryman, M., Gary, R., and Bretscher, A. (1995) *J. Cell Biol.* **131**, 1231–1242
- Hirao, M., Sato, N., Kondo, T., Yonemura, S., Monden, M., Sasaki, T., Takai, Y., Tsukita, S., and Tsukita, S. (1996) *J. Cell Biol.* **135**, 37–51
- Matsui, T., Maeda, M., Doi, Y., Yonemura, S., Amano, M., Kaibuchi, K., Tsukita, S., and Tsukita, S. (1998) *J. Cell Biol.* **140**, 647–657
- Sherman, L., Xu, H. M., Geist, R. T., Saporito-Irwin, S., Howells, N., Ponta, H., Herrlich, P., and Gutmann, D. H. (1997) *Oncogene* **15**, 2505–2509
- Gronholm, M., Sainio, M., Zhao, F., Heiska, L., Vaheri, A., and Carpen, O. (1999) *J. Cell Sci.* **112**, 895–904
- Huang, L., Ichimaru, E., Pestonjams, K., Cui, X., Nakamura, H., Lo, G. Y. H., Lin, F. I. K., Luna, E. J., and Furthmayr, H. (1998) *Biochem. Biophys. Res. Commun.* **248**, 548–553
- Gonzalez-Agosti, C., Xu, L., Pinney, D., Beauchamp, R., Hobbs, W., Gusella, J., and Ramesh, V. (1996) *Oncogene* **13**, 1239–1247
- Xu, L., Gonzalez-Agosti, C., Beauchamp, R., Pinney, D., Sterner, C., and Ramesh, V. (1998) *Exp. Cell. Res.* **238**, 231–240
- Magendantz, M., Henry, M. D., Lander, A., and Solomon, F. (1995) *J. Biol. Chem.* **270**, 25324–25327
- Herndon, M. E., and Lander, A. D. (1997) in *A Laboratory Guide to Glycoconjugate Analysis* (Jackson, P. L., and Gallagher, J. T., eds) pp. 379–398 Birkhauser Verlag AG, Basel, Switzerland
- Lim, W. A., Sauer, R. T., and Lander, A. D. (1991) *Methods Enzymol.* **208**, 196–212
- SanAntonio, J. D., Slover, J., Lawler, J., Karnovsky, M. J., and Lander, A. D. (1993) *Biochemistry* **32**, 4746–4755
- Reczek, D., and Bretscher, A. (1998) *J. Biol. Chem.* **273**, 18452–18458
- Niggli, V., Andreoli, C., Roy, C., and Manget, P. (1995) *FEBS Lett.* **376**, 172–176
- Gilmore, A. P., and Burridge, K. (1996) *Nature* **381**, 531–535
- Tsukita, S., Yonemura, S., and Tsukita, S. (1997) *Trends Biochem. Sci.* **22**, 53–58
- Bretscher, A. (1999) *Curr. Opin. Cell Biol.* **11**, 109–116
- Scoles, D. R., Huynh, D. P., Morcos, P. A., Coursell, E. R., Robinson, N. G. G., Tamanoi, F., and Pulst, S. M. (1998) *Nat. Genet.* **18**, 354–359
- Yun, C. H., Lamprecht, G., Foster, D. V., and Sidor, A. (1998) *J. Biol. Chem.* **273**, 25856–25863
- Hall, R. A., Ostedgaard, L. S., Premont, R. T., Blitzer, J. T., Rahman, N., Welsh, M. J., and Lefkowitz, R. J. (1998) *Proc. Natl. Acad. Sci. U. S. A.* **95**, 8496–501
- Lajeunesse, D. R., McCartney, B. M., and Fehon, R. G. (1998) *J. Cell Biol.* **141**, 1589–1599

# The B1 Subunit of the H<sup>+</sup>ATPase Is a PDZ Domain-binding Protein

COLOCALIZATION WITH NHE-RF IN RENAL B-INTERCALATED CELLS\*

Received for publication, December 13, 1999, and in revised form, March 2, 2000  
Published, JBC Papers in Press, March 30, 2000, DOI 10.1074/jbc.M909857199

Sylvie Breton<sup>‡§¶</sup>, Thorsten Wiederhold<sup>||\*\*</sup>, Vladimir Marshansky<sup>‡</sup>, Ndona N. Nsumu<sup>‡</sup>,  
Vijaya Ramesh<sup>§||</sup>, and Dennis Brown<sup>‡ ††</sup>

From the <sup>‡</sup>Renal Unit and Program in Membrane Biology and the <sup>||</sup>Molecular Neurogenetics Unit,  
Massachusetts General Hospital East, Charlestown, Massachusetts 02129 and the Departments of  
<sup>‡‡</sup>Pathology and <sup>§</sup>Medicine, Harvard Medical School, Boston, Massachusetts 02114

The 56-kDa B1 subunit of the vacuolar H<sup>+</sup>ATPase has a C-terminal DTAL amino acid motif typical of PDZ-binding proteins that associate with the PDZ protein, NHE-RF (Na<sup>+</sup>/H<sup>+</sup> exchanger regulatory factor). This B1 isoform is amplified in renal intercalated cells, which play a role in distal urinary acid-base transport. In contrast, proximal tubules express the B2 isoform that lacks the C-terminal PDZ-binding motif. Both the B1 56-kDa subunit and the 31-kDa (E) subunit of the H<sup>+</sup>ATPase are pulled down by glutathione S-transferase NHE-RF bound to GSH-Sepharose beads. These subunits associate *in vivo* as part of the cytoplasmic V1 portion of the H<sup>+</sup>ATPase, and the E subunit was co-immunoprecipitated from rat kidney cytosol with NHE-RF antibodies. The interaction of H<sup>+</sup>ATPase subunits with NHE-RF was inhibited by a peptide derived from the C terminus of the B1 but not the B2 isoform. NHE-RF colocalized with H<sup>+</sup>ATPase in either the apical or the basolateral region of B-type intercalated cells, whereas NHE-RF staining was undetectable in A-intercalated cells. In proximal tubules, NHE-RF was located in the apical brush border. In contrast, H<sup>+</sup>ATPase was concentrated in a distinct membrane domain at the base of the brush border, from which NHE-RF was absent, consistent with the expression of the truncated B2 subunit isoform in this tubule segment. The colocalization of NHE-RF and H<sup>+</sup>ATPase in B- but not A-intercalated cells suggests a role in generating, maintaining, or modulating the variable H<sup>+</sup>ATPase polarity that characterizes the B-cell phenotype.

after the initial three members of the family (PSD-95, *Drosophila* discs large protein, and ZO-1), PDZ proteins contain 80–100-amino acid stretches that allow them to interact with other proteins that have a four amino acid PDZ-binding cassette, usually at the extreme C terminus of the cytoplasmic domain (2). One such PDZ-binding cassette is the amino acid sequence D(S/T)XL. Thus, putative PDZ-binding proteins can be identified by screening their amino acid sequence for these consensus cassettes. Among the many proteins identified so far are the cystic fibrosis transmembrane conductance regulator (3), the  $\beta_2$ -adrenergic receptor (4), neuronal nitric-oxide synthase (5), GLUT1 (6), and some potassium channels (7–9). One PDZ protein to which the cystic fibrosis transmembrane conductance regulator (10), the  $\beta_2$ -adrenergic receptor, and P2Y1 receptor (4) bind is the Na<sup>+</sup>/H<sup>+</sup> exchanger regulatory factor, NHE-RF, originally identified in rabbit kidney as a soluble factor that participates in the regulation of the NHE-3 Na<sup>+</sup>/H<sup>+</sup> exchanger at the apical pole of proximal tubule epithelial cells (11, 12). NHE-RF also binds to the ERM family of actin-binding proteins via its C terminus outside the PDZ-binding motif (13, 14), thus potentially linking many ion channel and receptors to the actin cytoskeleton. Furthermore, NHE-RF has been reported to interact with the Na<sup>+</sup>/HCO<sub>3</sub><sup>-</sup> co-transporter, a basolateral protein in proximal tubules (15).

The B1 (56-kDa) subunit of the vacuolar proton-pumping ATPase (H<sup>+</sup>ATPase) has a C-terminal DTAL motif, which suggests that it is a candidate PDZ-binding protein. This subunit of the H<sup>+</sup>ATPase is expressed in several tissues, but it is strongly amplified in specialized proton-translocating intercalated cells in the kidney (16), as well as similar cells in the epididymis (17). In contrast, a highly homologous 56-kDa isoform, the B2 isoform, is expressed in the kidney proximal tubule, but it has a C-terminal truncation and lacks the terminal PDZ-binding cassette (16). Most if not all of the PDZ-binding proteins so far reported are transmembrane proteins, but the B1 H<sup>+</sup>ATPase subunit is part of the V1 portion of the holo-enzyme and has no membrane spanning domain. It is tethered to the membrane by interaction with other subunits of the enzyme, some of which span the lipid bilayer (18). Furthermore, multi-subunit complexes consisting of the cytoplasmic portion of the H<sup>+</sup>ATPase can exist as free, cytosolic entities (18).

In kidney cortex, intercalated cells show a complex regulation of H<sup>+</sup>ATPase expression at the cell surface (19), and subpopulations of these cells with apical, basolateral, diffuse, or even bipolar H<sup>+</sup>ATPase localization can be detected by immunocytochemistry (20). A-cells always have H<sup>+</sup>ATPase at their apical pole and the Cl<sup>-</sup>/HCO<sub>3</sub><sup>-</sup> exchanger AE1 at their basolateral pole (21). These cells secrete protons into the tubule lumen. B-cells have no detectable AE1 in either plasma mem-

Membrane transport proteins are directed toward and inserted into specific cell surface domains by an elaborate series of sorting mechanisms (1). A relatively recent development in understanding how some of these proteins are concentrated into functionally differentiated regions of the plasma membrane has been the discovery of the so-called PDZ domain family of proteins and associated PDZ-binding proteins. Named

\* This work was supported by National Institutes of Health Grants DK38452 (to S. B.), DK42956 (to D. B.), and NS24279 (to V. R.) and by a U.S. Army grant (to V. R.). The costs of publication of this article were defrayed in part by the payment of page charges. This article must therefore be hereby marked "advertisement" in accordance with 18 U.S.C. Section 1734 solely to indicate this fact.

¶ Supported by a Massachusetts General Hospital Claflin Distinguished Fellowship. To whom correspondence should be addressed: Renal Unit and Program in Membrane Biology, Massachusetts General Hospital East, 149 13<sup>th</sup> St., Charlestown, MA 02129. Tel.: 617-726-5785; Fax: 617-726-5669; E-mail: sbreton@receptor.mgh.harvard.edu.

\*\* Supported by a Gottlieb Daimler and Karl Benzs Predoctoral Fellowship.

brane domain, but the H<sup>+</sup>ATPase can be apical, basolateral, or bipolar in these AE1-negative cells. Cells with basolateral H<sup>+</sup>ATPase are bicarbonate-secreting cells. Although systemic acidosis results in more intercalated cells having apical H<sup>+</sup>ATPase, and alkalosis shifts more cells to a basolateral pattern of localization (22, 23), the cell biological mechanisms underlying these dramatic shifts in the polarized expression of a membrane protein remain unknown *in situ*. In this report, we show that the 56-kDa B1 subunit of the proton pump is a PDZ-binding protein that can associate with NHE-RF and that NHE-RF colocalizes with the H<sup>+</sup>ATPase in all B-intercalated cells, wherever the pump is located within any individual cell. We propose that the interaction of this subunit of the proton pump with NHE-RF could be responsible for the anchoring and/or targeting of membrane-associated H<sup>+</sup>ATPase molecules in this cell type. NHE-RF was barely detectable in A-type intercalated cells. In contrast, NHE-RF was abundant in the proximal tubule brush border, but its intracellular location was clearly distinct from that of the H<sup>+</sup>ATPase in these cells.

#### EXPERIMENTAL PROCEDURES

**Animals**—Male Harlan Sprague-Dawley rats were anesthetized with sodium pentobarbital (Nembutal, 0.1 ml of a 50 mg/ml solution/100 g of body weight), and kidneys were fixed by perfusion through the abdominal aorta with a fixative containing 4% paraformaldehyde, 10 mM sodium periodate, 70 mM lysine (PLP), and 5% sucrose as described previously (24, 25). After 5 min of perfusion, kidneys were removed, sliced, and fixed by immersion for a further 6 h before rinsing and storage in PBS<sup>1</sup> (10 mM sodium phosphate buffer containing 0.9% NaCl, pH 7.4). For preparation of 4- $\mu$ m sections, tissues were cryoprotected in 30% sucrose before sectioning with a Reichert Frigocut microtome using disposable knives.

**Immunostaining**—Tissue sections picked up on Fisher Superfrost Plus slides (Fisher Scientific) were rinsed for 10 min in PBS and then treated with 1% SDS for 5 min. This step augments antigenicity of many proteins in frozen sections of PLP-fixed tissues, as described previously (26). After three more rinses (5 min each) in PBS to remove the SDS, sections were incubated for 20 min in PBS/1% bovine serum albumin to block nonspecific background staining. Primary anti-NHE-RF antibody (affinity purified rabbit polyclonal antibody IC270 raised against GST-NHE-RF fusion protein amino acids 270–358) was applied for 2 h at room temperature at a dilution of 1:4. This antibody has been characterized previously (27). After washing twice for 5 min in high salt PBS (PBS containing 2.7% NaCl) to reduce nonspecific staining and one further washing for 5 min in normal PBS, secondary anti-rabbit antibodies (diluted 1:800) coupled to CY3 (Jackson Immunologicals) were applied for 60 min. After further washing as above, sections were mounted in Vectashield anti-fading solution (Vector Labs., Burlingame, CA), diluted 1:1 in 0.1 M Tris-HCl, pH 8.0.

Some sections were double-stained with anti-H<sup>+</sup>ATPase antibodies to identify the cells that were positive for NHE-RF in the collecting duct. After application of the anti-NHE-RF antibody followed by secondary antibody coupled to CY3, an affinity purified chicken polyclonal antibody against the 31-kDa E subunit of the H<sup>+</sup>ATPase (a marker of A- and B-intercalated cells, diluted 1:40) was applied for 2 h, followed by a donkey anti-chicken IgG coupled to FITC, diluted 1:200 (Jackson Immunologicals). Sections were mounted in Vectashield diluted 1:1 in 0.1 M Tris-HCl, pH 8.0.

Some sections were double stained using a rabbit anti-AE1 Cl<sup>-</sup>/HCO<sub>3</sub><sup>-</sup> exchanger antibody that has been previously characterized (28). Because this antibody is also raised in rabbit, an amplification procedure was used to allow staining of sections with two primary antibodies raised in the same species. Briefly, the first primary, anti-AE1, was applied at a dilution of 1:32,000, a concentration that is too low to be detected by conventional application of a fluorescent secondary antibody, as determined in preliminary experiments. The dilute AE1 antibody was detected using a tyramide amplification kit (NEN Life Science Products) with tyramide-CY3 as a fluorescent reagent, according to the manufacturer's instructions. The sections were then incubated conventionally with anti-NHE-RF and secondary goat anti-rabbit FITC as

described above. No cross-reactivity between the two sets of reagents was detectable under these conditions. Sections were photographed in color on Kodak Ektachrome 400 Elite film exposed at 2500 ASA using a Nikon Eclipse 800 epifluorescence microscope equipped with specific CY3 and FITC filter combinations. Using the specific CY3 filter combination and analog photography, CY3 emission appears yellow (see Fig. 1, A and C). Some micrographs were prepared from digital images captured from the Nikon Eclipse 800 using a Hamamatsu Orca digital camera. Pseudocolored images were merged using IP Lab Spectrum software (Scanalytics Inc, Vienna). In these images, CY3 fluorescence appears red, and FITC is green (see Fig. 2). Control incubations were performed in which the primary NHE-RF antibody was incubated with the GST-NHE-RF fusion protein (at a final concentration of 0.2 mg/ml) for 1 h at room temperature prior to applying the antibody to the sections.

**Preparation of Rat Kidney Inner Stripe Cytosol**—Kidneys of anesthetized rats were perfused with cold PBS for 1–2 min to remove blood, and the inner stripe was separated under a dissecting microscope. Pieces of inner stripe (0.4 g) were homogenized in 2 ml of homogenization buffer (0.25 M sucrose, 1 mM EDTA, 10 mM Tris-HCl, pH 7.4, with Complete<sup>TM</sup>, Roche Molecular Biochemicals, mixture of protease inhibitors) using a Wheaton glass potter fitted with a Teflon pestle (20 complete strokes). Rat kidney inner stripe cytosol was prepared by centrifugation of the homogenate for 1 h at 100,000  $\times$  g (41,000 rpm) using a Beckman, TL-100 Ultracentrifuge equipped with a TLA 55 rotor. Protein concentration of cytosol was measured with the Pierce BCA protein assay reagent using albumin as a standard.

**Affinity Precipitation and Peptide Competition Assay**—Pull-down experiments were performed essentially as described previously (27) with minor modifications. Briefly, rat kidney inner stripe cytosol (0.4 mg of total protein) was incubated overnight at 4 °C with 600 pmol of GST-NHERF or GST alone as a control immobilized on GSH-Sepharose 4B beads. For the peptide competition assay, peptides B1 (PQDTEADTAL) and B2 (EFYPRDSAKH) were dissolved in distilled water, and 300  $\mu$ g of peptide were preincubated with the GST-NHE-RF beads for 1 h at 4 °C. Cytosol containing 300  $\mu$ g of peptide was then added to the beads, and the mixture was incubated overnight at 4 °C. The beads were then washed extensively with phosphate-buffered saline containing Pefabloc and resuspended in Laemmli sample buffer for SDS-PAGE.

**Immunoprecipitation Assay**—Rat kidney cytosol was prepared as for the pull-down assay, except that cytosol from the entire cortex and outer medulla was used to ensure that adequate amounts of NHE-RF were present in the preparation. NHE-RF was immunoprecipitated from 500  $\mu$ l (2.8 mg of total protein) of precleared (by preincubation with protein A-agarose beads alone) cytosol using 10  $\mu$ l of anti-NHE-RF antiserum (IC270 serum or IC270 preimmune serum) and 50  $\mu$ l of protein A-agarose beads (Roche Molecular Biochemicals). Immunoprecipitates were washed extensively with PBS and eluted by boiling in SDS sample buffer (as for the pull-down assay). The immunoprecipitates were run on SDS-PAGE and blotted using a monoclonal anti-E subunit antibody (E11) as described below.

**SDS-PAGE and Western Blot Analysis**—Electrophoresis was performed using 12% SDS-Tris-glycine-PAGE gels. Proteins were transferred to polyvinylidene difluoride membranes and analyzed by Western blotting. The following antibodies were used as detailed in the figure legends: affinity-purified chicken polyclonal anti-E H<sup>+</sup>ATPase subunit (1:1,000) and affinity-purified rabbit polyclonal anti-B1 H<sup>+</sup>ATPase subunit (1:1,000), raised against the bovine subunits, and a monoclonal anti-E subunit antibody (E11) kindly provided by Dr. Steven Gluck (University of Florida, Gainesville). Images were scanned and analyzed with NIH Image (version 1.62) software.

#### RESULTS

**Localization of NHE-RF in the Kidney**—NHE-RF was localized in the kidney on PLP-fixed cryostat sections that had been treated with SDS. As expected from the reported distribution of NHE-3 (29), by far the greatest amount of NHE-RF was found in proximal tubules. The entire brush border was strongly stained in all proximal tubule segments (Fig. 1, A and C). In addition, however, staining was seen in some cells of the cortical collecting ducts and connecting segments (Fig. 1, A and C). The extent and intracellular location of this staining was variable, with some cells showing distinct basolateral staining (Fig. 1A), others showing a more diffuse cytoplasmic staining (Fig. 1C), and yet others showing apical staining (Fig. 1C). These cells were identified as intercalated cells by double incubations

<sup>1</sup> The abbreviations used are: PBS, phosphate-buffered saline; GST, glutathione S-transferase; FITC, fluorescein isothiocyanate; PAGE, polyacrylamide gel electrophoresis.

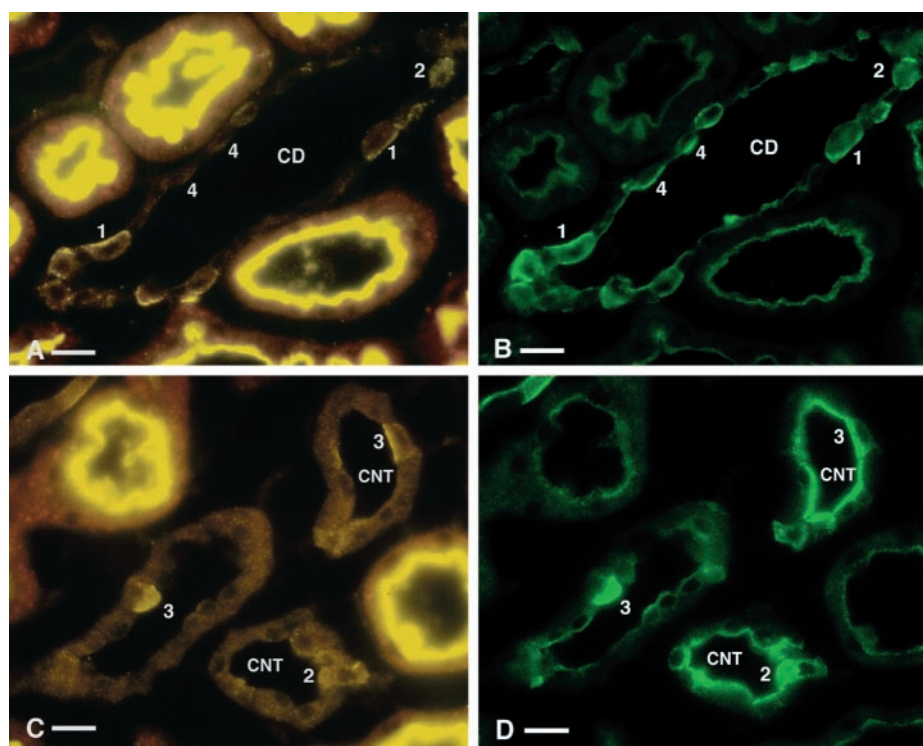


FIG. 1. Sections of rat kidney cortex double stained for NHE-RF (A and C) and the 31-kDa subunit of the  $H^+$ ATPase (B and D). The brush border is strongly stained in all proximal tubules. Some cells of the collecting ducts (CD) and connecting segments (CNT) are also stained. Different patterns of NHE-RF staining are detected, and the staining overlaps with that of the  $H^+$ ATPase in intercalated cells. Some cells have basolateral staining (1), some have diffuse cytoplasmic staining (2), some have apical staining (3), and others have little or no NHE-RF staining but show apical  $H^+$ ATPase staining (4). In connecting tubules (CNT), all cells have strong  $H^+$ ATPase staining, as described previously (30), but only a few of these are clearly NHE-RF-positive. The staining in A and C, which represent single exposures of the NHE-RF staining, appears yellow because of the use of a highly specific filter combination used for the Cy3 fluorophore. Cy3 emission is yellow when the correct filter combination is used. Bar, 15  $\mu$ m.

using a chicken polyclonal antibody against the 31-kDa (E) subunit of the  $H^+$ ATPase (Fig. 1, B and D). We have previously shown that the three major subunits of the cytoplasmic domain of this enzyme colocalize in intercalated cells (30). Thus, the E subunit is a reliable marker for the entire cytoplasmic domain of the  $H^+$ ATPase, which also contains the 56 kDa subunit. In these double-stained sections, the NHE-RF staining colocalized with the  $H^+$ ATPase staining in intercalated cells, whereas connecting tubule cells that also contain the  $H^+$ ATPase do not express detectable levels of NHE-RF (Fig. 1, C and D). However, in some intercalated cells, apical  $H^+$ ATPase staining was seen with no detectable NHE-RF staining (Fig. 1A). Principal cells in some tubule segments showed a faint, finely granular staining in the cytoplasm that was much less intense than in the adjacent intercalated cells.

To distinguish between A- and B-intercalated cells, anti-AE1 antibodies, which label only A-cells (21), were used in conjunction with anti-NHE-RF antibodies. All cells with distinct apical, diffuse, or basolateral NHE-RF staining were negative for AE1 (Fig. 2). Furthermore, only A-intercalated cells are found in the inner stripe of the outer medulla, and these cells showed no detectable staining with the NHE-RF antibody (not shown). Thus, NHE-RF is most highly expressed in B-intercalated cells, and its variable intracellular localization pattern overlaps with that of the  $H^+$ ATPase in each individual B-cell in the cortical collecting duct and connecting segment.

In proximal tubules, NHE-RF was present in the brush border (Fig. 3), as predicted from previous studies that showed abundant NHE-3 in this location (11, 29). However, the  $H^+$ ATPase staining was, as we have previously described (30), the most concentrated in a tight subapical band at the base of the brush border. This subapical domain, showing intense

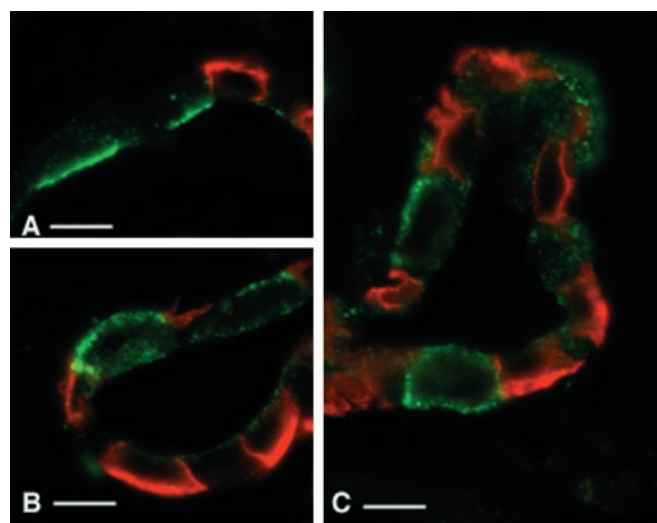


FIG. 2. Double staining of rat kidney cortex collecting ducts with antibodies against NHE-RF (green) and AE1 (red). The red AE1 staining is basolateral in all A-intercalated cells. These cells do not stain for NHE-RF. In A, two cells with apical NHE-RF staining are found alongside an A-intercalated cell with basolateral AE1 staining. In B, two cells with basolateral NHE-RF staining are found in the same tubule as A-intercalated cells with basolateral AE1. Other cells are negative for both antigens. C shows a collecting duct with a mixture of AE1 positive/NHE-RF negative A-intercalated cells and NHE-RF positive/AE1-negative B-intercalated cells. A small amount of punctate NHE-RF staining is seen in cells that are probably principal cells. In these merged digital images, Cy3 staining is pseudocolored red to allow it to be more readily distinguished from the adjacent green FITC staining. Bar, 10  $\mu$ m.

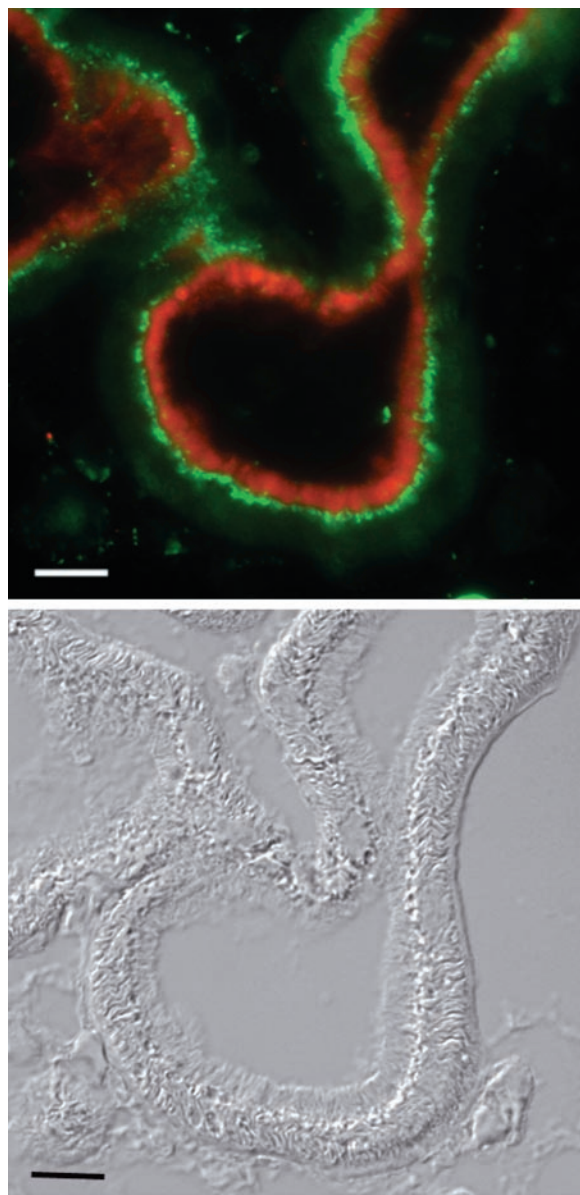


FIG. 3. Proximal tubule from rat kidney cortex showing the distribution of NHE-RF (red) on the brush border microvilli, and the  $H^+$ ATPase (31-kDa subunit; green) on submicrovillar vesicles and invaginations. The two proteins are not co-localized in this S3 tubule segment. A differential interference contrast image is shown in the lower panel for orientation purposes. Bar, 10  $\mu$ m.

$H^+$ ATPase staining in the S3 segment, did not contain detectable levels of NHE-RF (Fig. 3). This is consistent with the known expression of the C-terminally truncated B2 isoform of the 56-kDa subunit in these cells, which lacks the DTAL PDZ-binding motif (16). NHE-RF was not detected in the basolateral domain of proximal tubules.

To determine the specificity of labeling with anti-NHE-RF antibodies in kidney cortex, parallel incubations were performed with normal anti-NHE-RF antibody and with antibody that had been preincubated with 0.2 mg/ml of the GST-NHE-RF fusion protein that was used as an immunogen. The results show that the proximal tubule staining, as well as the apical, basolateral, and bipolar intercalated cell staining were completely abolished by preincubation with the immunizing fusion protein (Fig. 4).

**Binding of Soluble  $H^+$ ATPase Complexes to a GST-NHE-RF Affinity Matrix**—Sepharose beads to which a GST-NHE-RF fusion protein was bound were used as an affinity matrix to

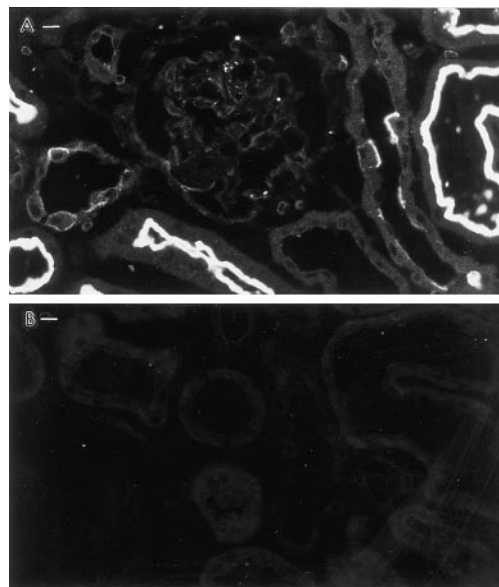


FIG. 4. Control for the specificity of NHE-RF staining in rat renal cortex. Under normal incubation conditions (A), NHE-RF stains the brush border of proximal tubules, as well as intercalated cells in variable patterns (apical, basolateral, and bipolar). This staining is completely inhibited by preincubation of the NHE-RF antibody with the immunizing GST-NHE-RF fusion protein (B). Bar, 10  $\mu$ m.

extract potential binding proteins from renal medullary cytosol. A cytosolic preparation from the inner medulla was used for these experiments because (a) kidney cytosol contains large amounts of free cytosolic  $H^+$ ATPase subunits (Fig. 5A, Cytosol), (b) this kidney region contains high levels of the B1- $H^+$ ATPase isoform, located in A-type intercalated cells, and (c) this region contains no proximal tubules, which express abundant endogenous NHE-RF that could potentially compete with protein binding to the affinity matrix. Under these conditions, Western blots of the affinity-purified material bound to the beads showed that both the B1 and the E subunits of the  $H^+$ ATPase were present (Fig. 5A). Control experiments using the matrix with GST alone showed little or no  $H^+$ ATPase subunit antigenicity associated with the beads in the absence of NHE-RF, indicating the specificity of the association. The binding of  $H^+$ ATPase to the NHE-RF-GST affinity matrix was completely inhibited by incubation of the beads with an 11-amino acid C-terminal peptide derived from the B1  $H^+$ ATPase subunit, which contains the C-terminal motif DTAL (PQD-TEADTAL). However, binding was not inhibited by preincubation with a peptide containing the 11 C-terminal amino acids of the B2 56-kDa subunit isoform (EFYPRDSAKH), which does not contain the PDZ-binding motif (Fig. 5B).

**Co-immunoprecipitation of NHE-RF and the  $H^+$ ATPase**—to strengthen the evidence for an *in vivo* interaction between NHE-RF and the  $H^+$ ATPase, evidence for co-immunoprecipitation of the two proteins from rat kidney cytosol was sought. As shown in Fig. 5C, the E subunit of the  $H^+$ ATPase was co-immunoprecipitated from kidney cytosol by the anti-NHE-RF antibody but not by preimmune serum.

#### DISCUSSION

The present data show that the 56-kDa B1 subunit isoform of the  $H^+$ ATPase is a PDZ-binding protein that allows association of the cytosolic (V1) portion of the  $H^+$ ATPase with NHE-RF, a PDZ protein that is expressed in the kidney. Immunolocalization indicates that in the collecting duct and connecting segment, this association occurs in a specialized subtype of intercalated cell, the B-cell, which has a highly variable pattern of intracellular localization of the  $H^+$ ATPase (19–21, 23). Other

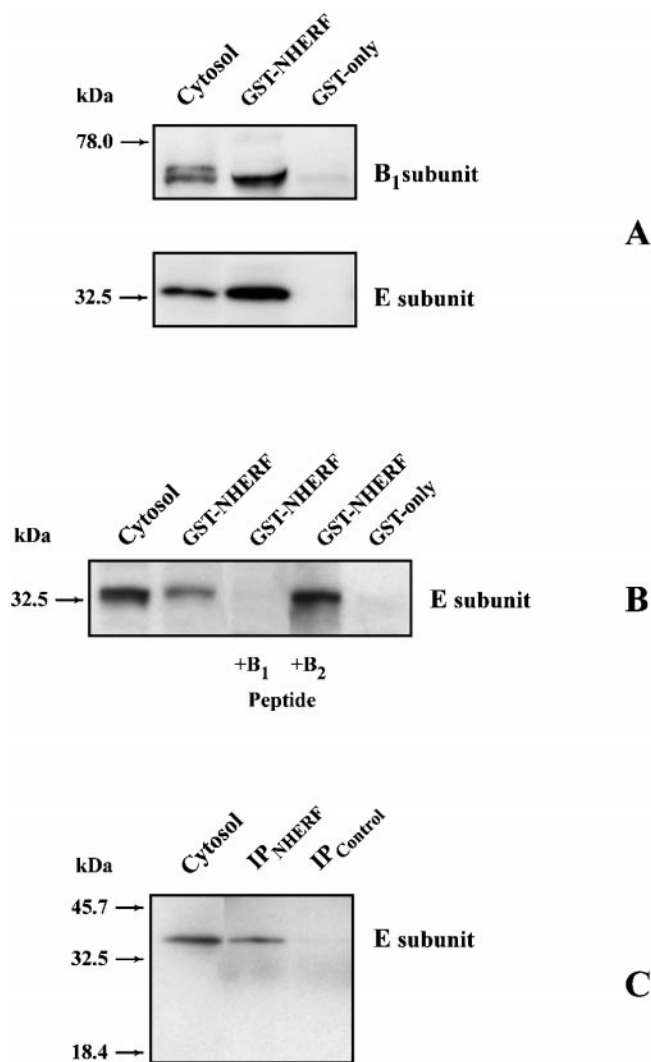


**FIG. 5. Results of the GST-NHE-RF pull down assay and co-immunoprecipitation.** A shows that both the B1 and the E H<sup>+</sup>ATPase subunits are pulled down by GST-NHERF beads, but not by beads coupled to GST alone. B shows that the ability of the GST-NHERF beads to pull down the H<sup>+</sup>ATPase (in this case the E subunit) is completely inhibited by a peptide derived from the B1 H<sup>+</sup>ATPase subunit (which contains the DTAL motif) but is not competed away by the B2 subunit peptide. C shows that the E subunit of the H<sup>+</sup>ATPase is co-immunoprecipitated by anti-NHE-RF antibodies but not by pre-immune serum. In all of these blots, the E subunit runs slightly higher than the predicted 31-kDa molecular mass for this subunit. IP, immunoprecipitate.

collecting duct cell types, including principal cells and A-intercalated cells, showed a very low level of staining. The greatest amount of NHE-RF staining was observed, as expected in proximal tubules, but some thin limbs of Henle in the medulla were also strongly stained (not shown).

Especially intriguing is the failure to detect NHE-RF in A-type intercalated cells, which also contain high levels of the B1-H<sup>+</sup>ATPase subunit but which always have an apical staining for this protein, either on the plasma membrane or on numerous subapical vesicles. Thus, NHE-RF expression is amplified in the AE1-negative B-cell population, in which the pattern of H<sup>+</sup>ATPase localization is widely variable. This result suggests that the B-cell represents a distinct cell type with respect to NHE-RF expression and that NHE-RF could be involved in generating and/or maintaining apical and basolateral H<sup>+</sup>ATPase polarity in B-cells. Because A-cells, which insert H<sup>+</sup>ATPase uniquely into the apical domain, contain little or no detectable NHE-RF, we conclude that NHE-RF is in some

way involved in the ability of B-cells to display plasticity of membrane H<sup>+</sup>ATPase insertion. This could occur via the association of NHE-RF with merlin and/or ezrin, members of the ERM (ezrin, radixin, moesin) family of actin binding proteins, which bind to the C-terminal of NHE-RF (27, 31). Other factors, including an extracellular matrix protein named hensin, have also been implicated in generating the plasticity of the intercalated cell phenotype at least *in vitro* (19, 32). An additional interesting finding is that both the B1 and B2 subunits of the H<sup>+</sup>ATPase are capable of binding actin directly via their N-terminal domains (33). Thus, it is possible that the H<sup>+</sup>ATPase interacts with the actin cytoskeleton both directly and indirectly (via NHE-RF). The respective roles and the regulation of these two mechanisms of interaction now need to be evaluated in different cell types. Indeed, phosphorylation of NHE-RF has been shown to disrupt the indirect interaction of the  $\beta_2$ -adrenergic receptor with the actin cytoskeleton and to affect the endocytic sorting of this receptor (34).

Although antibodies against all of the H<sup>+</sup>ATPase subunits were not utilized in this study, at least two major cytosolic subunits associated with the NHE-RF-GST beads in an affinity binding assay, and the E (31 kDa) subunit of the H<sup>+</sup>ATPase was co-immunoprecipitated from rat kidney cytosol by anti-NHE-RF antibodies. Because of interference from the rabbit-derived polyclonal NHE-RF IgG used for immunoprecipitation, we were unable to determine whether the 56-kDa H<sup>+</sup>ATPase subunit was also co-immunoprecipitated from these samples. In addition, our data show that a peptide derived from the C terminus of the B1 56-kDa subunit isoform, but not from the B2 isoform, inhibits interaction of the H<sup>+</sup>ATPase with NHE-RF. Coupled with previous data showing that preassembled H<sup>+</sup>ATPase cytoplasmic domains exist in the cytosol (18), our data suggest that the cytosolic portion of the H<sup>+</sup>ATPase can bind NHE-RF via a specific interaction with the C-terminal DTAL motif that is unique to the B1 subunit. Furthermore, our data provide some evidence that the interaction occurs via the C-terminal domain of the 56-kDa subunit, because the rest of the protein sequence of these two isoforms is similar except for a short N-terminal sequence difference (16, 35). It is likely that when this 56-kDa subunit is assembled in a membrane together with the transmembrane portion of the H<sup>+</sup>ATPase (the V<sub>o</sub> sector), the entire H<sup>+</sup>ATPase assembly could thereby be coupled to NHE-RF and thus be anchored into a selected membrane domain. However, it is interesting that this domain can be either the apical or the basolateral domain in the B-intercalated cell. It has been stated recently that NHE-RF expression is restricted to the apical domain of epithelial cells (36), but this is clearly not the case in B-intercalated cells. Thus, NHE-RF may not determine the polarity of H<sup>+</sup>ATPase expression *per se*, but NHE-RF might stabilize the complex once it has reached its target membrane. In other cell types, NHE-RF appears to stabilize the cystic fibrosis transmembrane conductance regulator in the apical plasma membrane (3), whereas in *Caenorhabditis elegans*, PDZ proteins have been proposed to be involved in basolateral anchoring and/or targeting of a TGF- $\beta$  homolog (37). Recently, a *Drosophila* PDZ protein, discs lost, was also reported to have a dual role in maintaining apical and basolateral epithelial cell polarity (38). However, the diffuse, intracellular pattern of NHE-RF and H<sup>+</sup>ATPase localization seen in some B-intercalated cells raises the possibility that NHE-RF might participate in the trafficking or targeting of the H<sup>+</sup>ATPase. Whether PDZ proteins are involved in anchoring, targeting, or both processes remains to be determined, but our results clearly indicate that this process is not unidirectional (*i.e.* exclusively apical) in every cell type.

In the proximal tubule, NHE-RF is abundant and is colocal-



ized with NHE-3 in the apical brush border (data not shown). This scaffolding interaction is probably responsible for maintaining NHE-3 at a high concentration in the apical membrane (29). The B subunit of the H<sup>+</sup>ATPase that is expressed in this tubule segment lacks the C-terminal DTAL and should be incapable of interacting with PDZ domain proteins (16). Immunofluorescence shows that the H<sup>+</sup>ATPase is not colocalized with NHE-RF at the apical pole of proximal tubules. Because H<sup>+</sup>ATPase is involved in the extensive apical membrane endocytosis and recycling that occurs in proximal tubules (1), it may be advantageous for this cell type to express an isoform of the H<sup>+</sup>ATPase B subunit that cannot interact with NHE-RF at the apical membrane. Such an interaction would anchor the H<sup>+</sup>ATPase in the plasma membrane by cross-linking to the NHE-3/NHE-RF complex and might hinder the endocytotic recycling of this protein, leading to failure of the endosomal acidification process and defective recycling of apical membrane proteins.

We have previously reported that the 56-kDa B1 subunit of the H<sup>+</sup>ATPase is present on endosomes in the other collecting duct cell type, the principal cell (39). These endosomes are involved in recycling the water channel AQP2, they do not acidify their lumen, and they lack other subunits of the H<sup>+</sup>ATPase (39). We postulated that the 56-kDa subunit might be a promiscuous subunit that could associate with the membranes of these endosomes via another, as yet unidentified mechanism. This mechanism can now be envisaged to occur via the PDZ-binding domain, although principal cells were only weakly stained with the anti-NHE-RF antibody. Thus, it is possible that in principal cells, a different PDZ protein such as the NHE-RF related NHE-RF2 (3) might be associated with the 56-kDa H<sup>+</sup>ATPase B1 subunit.

In summary, we have shown that the B1 subunit isoform of the H<sup>+</sup>ATPase is a PDZ-binding protein that associates with NHE-RF and may therefore be responsible for linking the H<sup>+</sup>ATPase to the cytoskeleton in these cells. The two proteins are colocalized in B-intercalated cells but not in A-cells, suggesting a role in generating, maintaining, or modulating the B-cell phenotype. NHE-RF and H<sup>+</sup>ATPase are not colocalized in proximal tubules, which express a truncated B2 subunit isoform of the H<sup>+</sup>ATPase that lacks the PDZ-binding domain.

## REFERENCES

1. Brown, D., and Stow, J. L. (1996) *Physiol. Rev.* **76**, 245–297
2. Fanning, A. S., and Anderson, J. M. (1998) *Curr. Top. Microbiol. Immunol.* **228**, 209–233
3. Hall, R. A., Ostedgaard, L. S., Premont, R. T., Blitzer, J. T., Rahman, N., Welsh, M. J., and Lefkowitz, R. J. (1998) *Proc. Natl. Acad. Sci. U. S. A.* **95**, 8496–8501
4. Hall, R. A., Premont, R. T., Chow, C. W., Blitzer, J. T., Pitcher, J. A., Claing, A., Stoffel, R. H., Barak, L. S., Shenolikar, S., Weinman, E. J., Grinstein, S., and Lefkowitz, R. J. (1998) *Nature* **392**, 626–630
5. Brennan, J. E., Christopherson, K. S., Craven, S. E., McGee, A. W., and Bredt, D. S. (1996) *J. Neurosci.* **16**, 7407–7415
6. Bunn, R. C., Jensen, M. A., and Reed, B. C. (1999) *Mol. Biol. Cell* **10**, 819–832
7. Kim, E., Niethammer, M., Rothschild, A., Jan, Y. N., and Sheng, M. (1995) *Nature* **378**, 85–88
8. Inanobe, A., Yoshimoto, Y., Horio, Y., Morishige, K. I., Hibino, H., Matsumoto, S., Tokunaga, Y., Maeda, T., Hata, Y., Takai, Y., and Kurachi, Y. (1999) *J. Neurosci.* **19**, 1006–1017
9. Burke, N. A., Takimoto, K., Li, D., Han, W., Watkins, S. C., and Levitan, E. S. (1999) *J. Gen. Physiol.* **113**, 71–80
10. Wang, S., Raab, R. W., Schatz, P. J., Guggino, W. B., and Li, M. (1998) *FEBS Lett.* **427**, 103–108
11. Weinman, E. J., Steplock, D., Wang, Y., and Shenolikar, S. (1995) *J. Clin. Invest.* **95**, 2143–2149
12. Weinman, E. J., Steplock, D., Tate, K., Hall, R. A., Spurney, R. F., and Shenolikar, S. (1998) *J. Clin. Invest.* **101**, 2199–2206
13. Reczek, D., Berryman, M., and Bretscher, A. (1997) *J. Cell Biol.* **139**, 169–179
14. Murthy, A., Gonzalez-Agosti, C., Cordero, E., Pinney, D., Candia, C., Solomon, F., Gusella, J., and Ramesh, V. (1998) *J. Biol. Chem.* **273**, 1273–1276
15. Bernardo, A. A., Kear, F. T., Santos, A. V., Ma, J., Steplock, D., Robey, R. B., and Weinman, E. J. (1999) *J. Clin. Invest.* **104**, 195–201
16. Nelson, R. D., Guo, X. L., Masood, K., Brown, D., Kalkbrenner, M., and Gluck, S. (1992) *Proc. Natl. Acad. Sci. U. S. A.* **89**, 3541–3545
17. Breton, S., Smith, P. J., Lui, B., and Brown, D. (1996) *Nat. Med.* **2**, 470–472
18. Nelson, N., and Harvey, W. R. (1999) *Physiol. Rev.* **79**, 361–385
19. Al-Awqati, Q. (1996) *Am. J. Physiol.* **270**, C1571–C1580
20. Brown, D., Hirsch, S., and Gluck, S. (1988) *Nature* **331**, 622–624
21. Alper, S. L., Natale, J., Gluck, S., Lodish, H. F., and Brown, D. (1989) *Proc. Natl. Acad. Sci. U. S. A.* **86**, 5429–5433
22. Sabolic, I., Brown, D., Gluck, S. L., and Alper, S. L. (1997) *Kidney Int.* **51**, 125–137
23. Purcell, H., Bastani, B., Harris, K. P., Hemken, P., Klahr, S., and Gluck, S. (1991) *Am. J. Physiol.* **261**, F365–F376
24. McLean, I. W., and Nakane, P. K. (1974) *J. Histochem. Cytochem.* **22**, 1077–1083
25. Breton, S., Alper, S. L., Gluck, S. L., Sly, W. S., Barker, J. E., and Brown, D. (1995) *Am. J. Physiol.* **269**, F761–F774
26. Brown, D., Lydon, J., McLaughlin, M., Stuart-Tilley, A., Tyszkowski, R., and Alper, S. (1996) *Histochem. Cell Biol.* **105**, 261–267
27. Gonzalez-Agosti, C., Wiederhold, T., Herndon, M. E., Gusella, J., and Ramesh, V. (1999) *J. Biol. Chem.* **274**, 34438–34442
28. Alper, S. L., Stuart-Tilley, A. K., Biemesderfer, D., Shmukler, B. E., and Brown, D. (1997) *Am. J. Physiol.* **273**, F601–F614
29. Biemesderfer, D., Rutherford, P. A., Nagy, T., Pizzonia, J. H., Abu-Alfa, A. K., and Aronson, P. S. (1997) *Am. J. Physiol.* **273**, F289–F299
30. Brown, D., Hirsch, S., and Gluck, S. (1988) *J. Clin. Invest.* **82**, 2114–2126
31. Yun, C.-H. C., Lamprecht, G., Forster, D. V., and Sidor, A. (1998) *J. Biol. Chem.* **273**, 25856–25863
32. Al-Awqati, Q., Vijayakumar, S., Hikita, C., Chen, J., and Takito, J. (1998) *Am. J. Physiol.* **275**, F183–F190
33. Lee, B. S., Gluck, S. L., and Holliday, L. S. (1999) *J. Biol. Chem.* **274**, 29164–29171
34. Cao, T. T., Deacon, H. W., Reczek, D., Bretscher, A., and von Zastrow, M. (1999) *Nature* **401**, 286–290
35. Puopolo, K., Kumamoto, C., Adachi, I., Magner, R., and Forgac, M. (1992) *J. Biol. Chem.* **267**, 3696–3706
36. Fanning, A. S., and Anderson, J. M. (1999) *Curr. Opin. Cell Biol.* **11**, 432–439
37. Kim, S. K. (1997) *Curr. Opin. Cell Biol.* **9**, 853–859
38. Bhat, M. A., Izaddoost, S., Lu, Y., Cho, K. O., Choi, K. W., and Bellen, H. J. (1999) *Cell* **96**, 833–845
39. Sabolic, I., Wuari, F., Shi, L. B., Verkman, A. S., Ausiello, D. A., Gluck, S., and Brown, D. (1992) *J. Cell Biol.* **119**, 111–122

# NHE-RF, a Merlin-Interacting Protein, Is Primarily Expressed in Luminal Epithelia, Proliferative Endometrium, and Estrogen Receptor-Positive Breast Carcinomas

Anat O. Stemmer-Rachamimov,\*  
Thorsten Wiederhold,<sup>†</sup> G. Petur Nielsen,\*  
Marianne James,<sup>†</sup> Denise Pinney-Michalowski,<sup>†</sup>  
Jennifer E. Roy,\* Wendy A. Cohen,\*  
Vijaya Ramesh,<sup>†</sup> and David N. Louis\*

*From the Molecular Neuro-Oncology Laboratory\* and Molecular Neurogenetics Unit,<sup>†</sup> Departments of Pathology, Neurosurgery, Neurology and Genetics, Massachusetts General Hospital and Harvard Medical School, Boston, Massachusetts*

**NHE-RF, a regulatory cofactor for NHE (Na<sup>+</sup>-H<sup>+</sup> exchanger) type 3, interacts with ion transporters and receptors through its PDZ domains and with the MERM proteins (merlin, ezrin, radixin and moesin) via its carboxyl terminus. Thus, NHE-RF may act as a multifunctional adaptor protein and play a role in the assembly of signal transduction complexes, linking ion channels and receptors to the actin cytoskeleton. NHE-RF expression is up-regulated in response to estrogen in estrogen receptor-positive breast carcinoma cell lines, suggesting that it may be involved in estrogen signaling. To further understand NHE-RF function and its possible role in estrogen signaling, we analyzed NHE-RF expression in normal human tissues, including cycling endometrium, and in breast carcinomas, tissues in which estrogen plays an important role in regulating cell growth and proliferation. NHE-RF is expressed in many epithelia, especially in cells specialized in ion transport or absorption, and is often localized to apical (luminal) membranes. NHE-RF expression varies markedly in proliferative versus secretory endometrium, with high expression in proliferative (estrogen-stimulated) endometrium. Furthermore, estrogen receptor status and NHE-RF expression correlate closely in breast carcinoma specimens. These findings support a role for NHE-RF in estrogen signaling. (Am J Pathol 2001, 158:57–62)**

NHE-RF (Na<sup>+</sup>-H<sup>+</sup> exchanger regulatory factor), a cytoplasmic phosphoprotein, was originally identified in the rabbit renal brush border as a cofactor required for cAMP/protein kinase A-mediated inhibition of NHE (Na<sup>+</sup>-H<sup>+</sup> exchanger) type 3.<sup>1</sup> The human homologue was

identified from human placenta and has also been referred to as EBP50 (ezrin binding protein).<sup>2</sup> NHE-RF is a 358-amino-acid protein with two homologous PDZ domains, which mediate protein-protein interactions. A related protein, NHE-RF2 (also known as E3KARP), was isolated from small intestine and renal brush border and shares 51% identity with NHE-RF, primarily in the PDZ domains.<sup>3</sup> PDZ-containing proteins are often localized at the plasma membrane and appear to promote the assembly of membrane-bound macromolecular complexes (transduction complexes), into which target molecules are recruited. Many PDZ domain-containing-proteins are involved in cell signaling.<sup>4–6</sup>

NHE-RF interacts, via its PDZ domains, with a variety of ion transport proteins such as the cystic fibrosis transmembrane regulator, the sodium bicarbonate cotransporter, as well as with membrane receptors such as the  $\beta$ 2 adrenergic and the purinergic P2Y1. Recently, we and others have shown that NHE-RF directly interacts with merlin, the NF2 (neurofibromatosis 2)-encoded tumor suppressor protein, and with ezrin, radixin, and moesin (MERM proteins), which are involved in cytoskeletal reorganization and signal transduction.<sup>7</sup> The MERM binding region is a non-PDZ site in the C-terminus.<sup>8</sup> Thus, NHE-RF may also be involved in the assembly of transduction complexes that link membrane receptors and transporters with intracellular signaling components.

Interestingly, NHE-RF expression is up-regulated in response to estrogen in estrogen receptor (ER)-positive breast carcinoma cell lines (see Ref. 9 and unpublished data). NHE-RF expression in these cells is mediated by the estrogen receptor and suppressed by antiestrogens.<sup>9</sup> These findings suggest a role for NHE-RF in the estrogen signal transduction cascade in estrogen-responsive tissues. To gain more insight into the physiological relevance of NHE-RF, we performed a comprehensive expression study of the protein in normal adult

---

Supported by National Institutes of Health grant NS24279 and a U.S. Army grant. T. W. was supported by a Gottlieb Daimler and Karl Benz predoctoral fellowship.

Accepted for publication September 20, 2000.

Address reprint requests to David N. Louis, MD, Department of Pathology, Massachusetts General Hospital, WRN 3, 55 Fruit St., Boston, MA 02114. E-mail: louis@helix.mgh.harvard.edu.

human tissues. To evaluate the relationship between estrogen and NHE-RF expression in normal and malignant estrogen-responsive tissues, we also examined NHE-RF expression in cycling endometrium, as well as in ER-positive and ER-negative breast carcinomas.

## **Materials and Methods**

### *Tissues*

Formalin-fixed, paraffin-embedded sections of normal adult human organs from surgical specimens and autopsies were obtained from the Department of Pathology at Massachusetts General Hospital. We examined two to five samples from each paraffin-embedded organ. Organs examined included: brain and spinal cord, peripheral nerve, pituitary gland, placenta, kidney, skin, muscle, endometrium, breast, esophagus, stomach, small and large intestines, liver, spleen, pancreas, salivary glands, thyroid, tonsils, heart, and lungs. To evaluate the possible association between estrogen and NHE-RF expression in normal tissues, we examined multiple samples of proliferative and secretory endometrium. To assess the possible association between estrogen receptor status and NHE-RF expression in breast carcinomas, we studied eighteen invasive breast carcinomas for which estrogen receptor status has been previously determined by immunohistochemistry.

### *Cell Lines*

Breast cancer cell lines MCF-7, ZR-75-B, T-47D, MCF-7-ADR, and MDA-MB-231 were obtained from the Massachusetts General Hospital Cancer Center, and normal breast epithelial cell lines HBL-100 and MCF-12-F were obtained from ATCC. Cell lines were maintained in DMEM with 10% fetal calf serum.

### *Antibodies*

The polyclonal IC270 antibody is directed at the GST-NHE-RF fusion protein and has been characterized elsewhere.<sup>10,11</sup> A commercial antibody (Estrogen Receptor, Clone 1D5, DAKO, Carpinteria, CA) was used to evaluate estrogen receptor status; this antibody recognizes both the  $\alpha$  and  $\beta$  forms of the receptor.

### *Western Blot Analysis*

Protein lysates were prepared from cells in phosphate buffered saline (PBS) containing 2% sodium dodecyl sulfate (SDS) and a cocktail of protease inhibitors (Boehringer Mannheim, Indianapolis, IN). Protein concentrations were measured using the DC protein assay system (Bio-Rad, Melville, NY). Three hundred  $\mu$ g of total cellular protein were subjected to SDS-polyacrylamide gel electrophoresis and transferred to nitrocellulose membranes (Bio-Rad). Blots were then probed with the NHE-RF antibody IC270 (affinity eluted 1:50). Proteins were visualized

with anti-rabbit horseradish peroxidase-conjugated secondary antibody and the ECL chemiluminescence system (Amersham Inc, Arlington Heights, IL). Signal intensity was quantified by densitometric scanning of autoradiographs using transmittance analysis (Fluor-S, Multiimager, Bio-Rad).

### *Immunohistochemistry*

Immunohistochemistry for NHE-RF was performed using IC270. Formalin-fixed, paraffin-embedded, 8- $\mu$ m-thick sections were deparaffinized, rehydrated, immersed in 0.5% H<sub>2</sub>O<sub>2</sub>/methanol for 20 minutes, and rehydrated in graded ethanols. For antigen retrieval, sections were microwaved in 0.01 mol/L sodium citrate buffer (pH 6.0) for 15 minutes. Sections were then blocked in 10% normal goat serum and 5% milk in 1% bovine serum albumin (BSA) in PBS, followed by incubation with primary antibody overnight at 4°C. Incubation with biotinylated goat anti-rabbit antibody (Vector Laboratories, Burlingame, CA) for 30 minutes at room temperature was followed by the standard avidin-biotin-complex (ABC) process (Vectastain Elite ABC kit, Vector). Diaminobenzidine (DAB) was used as a chromogen, followed by counterstaining with hematoxylin. Positive controls included paraffin-embedded human placenta sections as well as formalin fixed, paraffin-embedded cell pellets from MCF-7 and MCF-7-ADR cell lines, which express high levels or low levels of NHE-RF, respectively, as shown in Western blot analysis (see below). For negative controls, the primary antibody was omitted and prior immunostaining with pre-absorbed serum did not reveal any specific reactivity.<sup>12</sup> To control for possible effects of fixation and antigen retrieval, frozen sections of human placenta were also immunostained.

Immunohistochemistry for estrogen receptors was performed according to standard procedures. Briefly, antigen retrieval was achieved by microwaving the sections in Tris buffer (pH 10) for 10 minutes. Sections were blocked with 10% normal horse serum and incubated with ER antibodies (1:100 dilution) overnight at 4°C. Sections were incubated with secondary antibodies at room temperature for 45 minutes followed by the ABC reaction, visualization with DAB and counterstaining with hematoxylin.

## **Results**

### *Western Blotting and Immunohistochemistry for NHE-RF in Cell Lines*

Quantitative Western blot analysis, performed three times, confirmed that three estrogen receptor-positive breast cancer cell lines, MCF-7, ZR-75-B, and T-47D, had  $9.50 \pm 2.20$ -fold higher levels of NHE-RF when compared to the normal mammary lines HBL-100 and MCF-12-F (Figure 1). Expression of NHE-RF was expressed at only low levels in the estrogen receptor-negative breast cancer lines MCF-7-ADR and MDA-MB-231 and was not detectable in the breast cancer cell line DU4475. Immunocytochemical staining of cell pellets from MCF-7 and

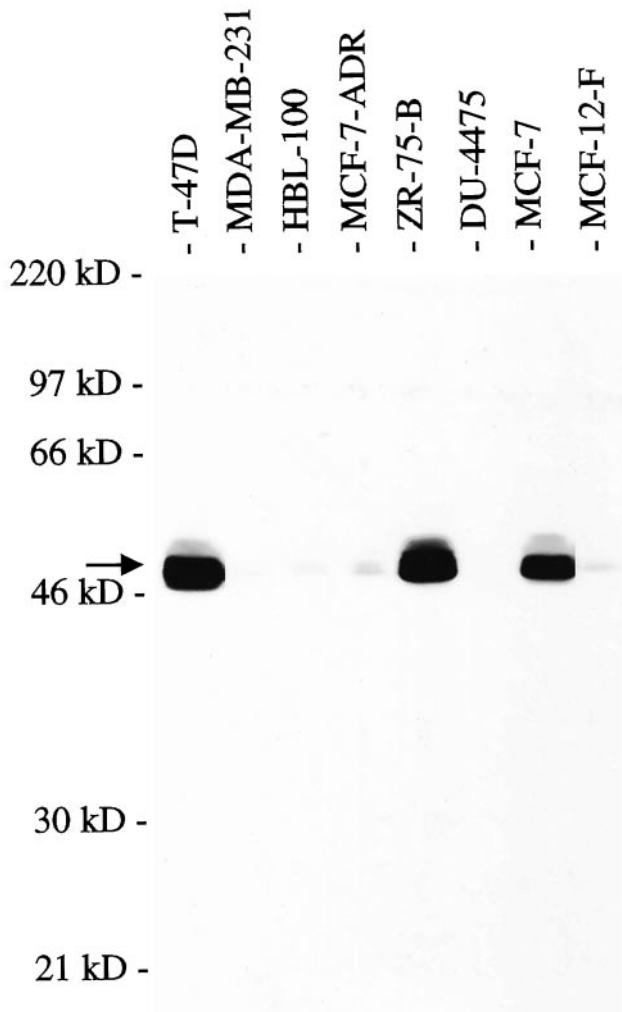


**Figure 1.** Western blot analysis, using affinity eluted IC270 antibody at 1:50 dilution, of mammary epithelial and breast cancer cell lines showing high NHE-RF expression in the ER-positive cell lines T-47D, ZR-75-B, and MCF-7. The **arrow** indicates NHE-RF at 50 kd.

MCF-7-ADR with the IC270 antibody showed strong expression only in MCF-7, the ER-positive cell line (Figure 2A).

### *Immunohistochemistry for NHE-RF Expression in Normal Adult Tissues*

NHE-RF is expressed in many tissues but has a highly selective cellular and subcellular distribution. Intense NHE-RF expression was seen in epithelial cells of many organ systems, especially in cells that perform an absorptive function, possess microvilli, or are involved in ion transport. Immunohistochemistry of paraffin-embedded sections of placenta demonstrated a characteristic pattern of NHE-RF expression, with prominent expression in the syncytiotrophoblast, the outer cell layer of placental villi, and its brush border, whereas the villous mesenchyme was immunonegative. Frozen sections of placenta showed the same pattern of immunostaining. All negative controls showed no staining.

As previously demonstrated using immunofluorescence,<sup>12</sup> strong expression of NHE-RF was seen in the

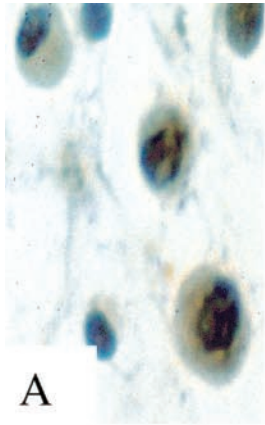
renal proximal tubules with prominent staining of the luminal cell membrane and the microvillous brush border (Figure 2B). The parietal epithelium lining Bowman's capsule of the renal glomeruli also showed prominent positivity, while the mesangium and glomerular endothelium were immunonegative and the distal tubules and collecting tubules had only weak cytoplasmic staining.

A highly selective pattern of expression of NHE-RF was also seen in the gastro-intestinal system. In the stomach, fundic glands showed strong expression in parietal cells, whereas chief cells, mucin-secreting cells, and surface epithelium were immunonegative. In the small bowel, the protein is abundant at the apical surface of absorptive cells and in microvilli extending from the cell surface, but is absent in intercalated goblet cells. Similarly, in the large bowel, absorptive cells of the surface epithelium and colonic crypts show strong membranous staining of the luminal border, but adjacent intercalated goblet cells were immunonegative (Figure 2C).

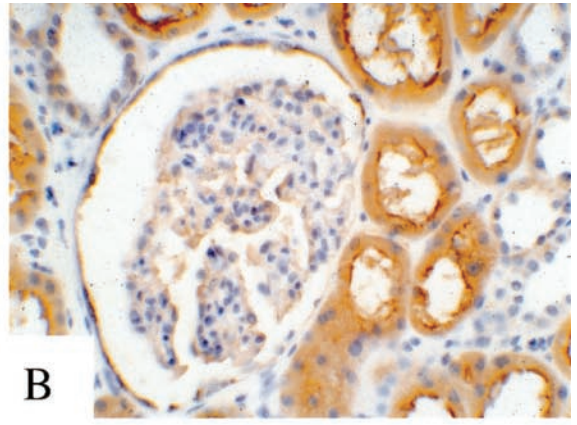
Stratified squamous epithelium in the esophagus, skin, and tonsils showed only weak to moderate cytoplasmic staining, more pronounced in the deep layers. Eccrine glands in the skin, however, showed cytoplasmic immunostaining with strong apical membranous expression, highlighting intercalated canaliculi. In contrast, the underlying myoepithelial cells were immunonegative. Other skin adnexa, such as the pilar unit, showed weak diffuse cytoplasmic staining. In the salivary glands, NHE-RF was weakly expressed in the cytoplasm of serous acinar cells, but there was prominent linear luminal membranous immunostaining. The mucinous acinar cells of the salivary glands were immunonegative. Similarly, acinar cells of the pancreas showed weak cytoplasmic staining and luminal linear immunopositivity, while cells of the islands of Langerhans were immunonegative. In the anterior pituitary, selected cells were moderately immunopositive. The posterior pituitary was immunonegative, as was the thyroid gland. In the breast, ductal and acinar epithelia were immunopositive, with apical membranous staining of the acinar epithelial cells (Figure 2D).

Skeletal muscle and myocardium were immunonegative for NHE-RF, while smooth muscle, particularly vascular smooth muscle, showed moderate immunopositivity in most tissues. In the lung, bronchial epithelium was only weakly positive and alveolar pneumocytes were immunonegative. In the liver, hepatocytes and Kupffer cells showed no expression of NHE-RF and only weak to moderate expression was seen in ductal epithelium. Focal, moderate positivity was seen in the white pulp of the spleen and in scattered lymphocytes in germinal centers of lymph nodes.

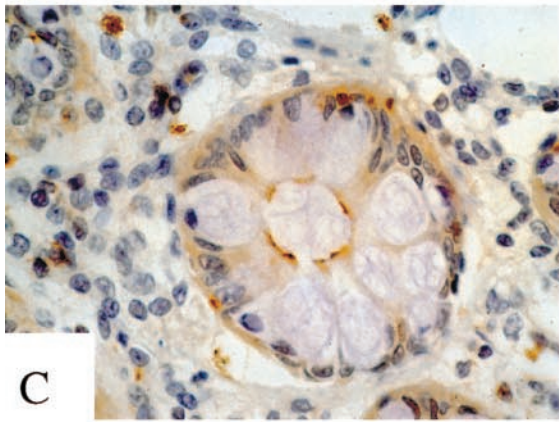
In the brain and spinal cord, neurons and resting glia did not express NHE-RF. Strong expression of NHE-RF, however, was observed in glial processes in areas of chronic reactive gliosis, such as subpial region, or in proliferating Bergmann glia in the cerebellum. Marked NHE-RF expression was also observed at the apical membranes of ependymal cells. Interestingly, this pattern of expression was altered in buried ependymal cells found just below the ventricular surface, in which NHE-RF was seen as an area of strong cytoplasmic immunopos-



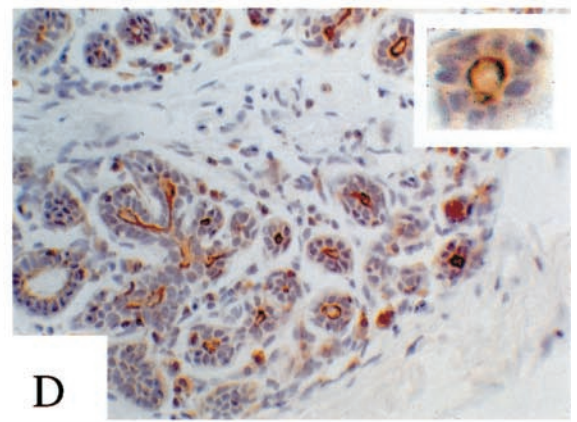
A



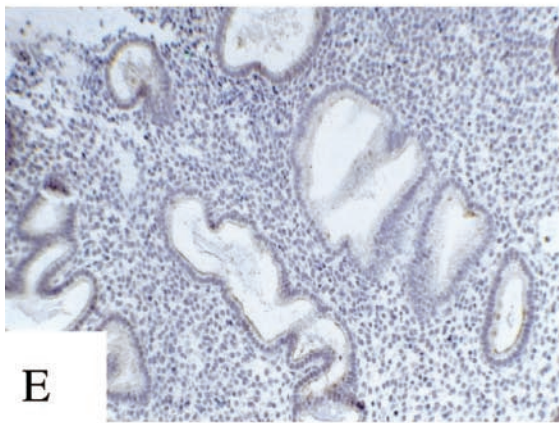
B



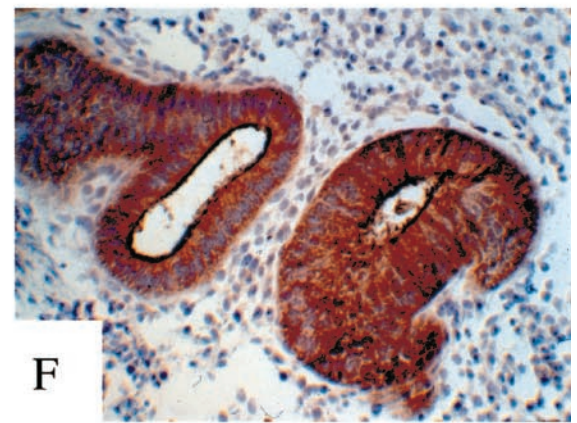
C



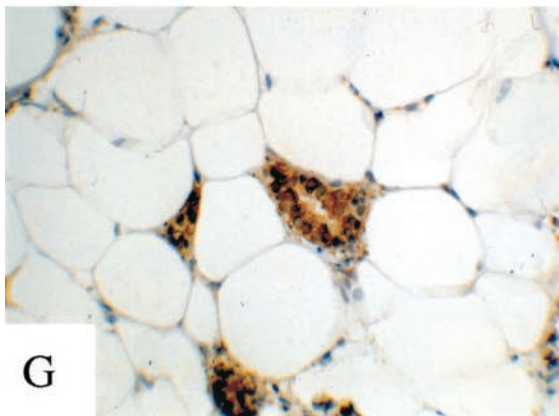
D



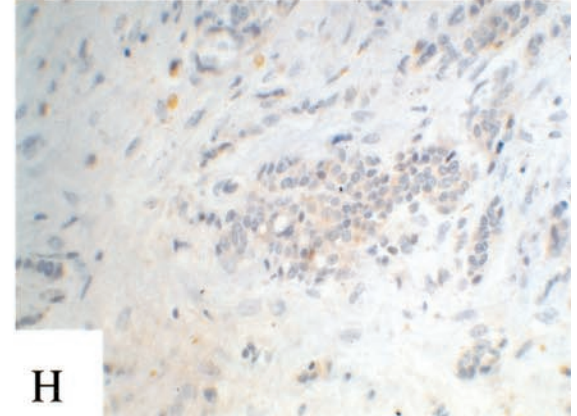
E



F



G



H

**Table 1.** NHE-RF and ER Expression in 18 Primary Breast Carcinomas

Tumor sample	NHE-RF IHC	ER status
BC1	+++	Positive
BC3	+++	Positive
BC5	+++	Positive
BC9	+++	Positive
BC10	+++	Positive
BC11	+++	Positive
BC4	++	Positive
BC7	++	Positive
BC12	++	Positive
BC14	++	Positive
BC8	-	Positive
BC6	++	Negative
BC15	++	Negative
BC2	-	Negative
BC13	-	Negative
BC16	-	Negative
BC17	-	Negative
BC18	-	Negative

NHE-RF immunostaining intensity: +++, strong staining; ++, moderate staining; -, no or minimal staining. When positive, nearly all cells were positive.

itivity without polarized apical or membranous staining. Arachnoid cells were immunonegative, as were Schwann cells in peripheral nerves.

### *Immunohistochemistry for NHE-RF Expression in Endometrium*

Proliferative endometrium showed strong expression of NHE-RF in the cytoplasm and luminal membrane of glandular epithelium as well as in scattered stromal cells (Figure 2F). NHE-RF was expressed in essentially all epithelial cells in the proliferative endometrium samples. In contrast, there was only weak expression of NHE-RF in the glandular epithelium of secretory endometrium and adjacent stroma (Figure 2E).

### *Immunohistochemistry for NHE-RF Expression in Primary Breast Tumors*

Examination of sections from 18 infiltrating breast adenocarcinomas showed strong correlation between positive immunostaining for ER and high expression of the NHE-RF protein: 10 of 11 (>90%) of the ER-positive tumors strongly expressed NHE-RF. On the contrary, 5 of 7 ER-negative tumors did not express NHE-RF (Figure 2, G-H, and Table 1). In those tumors that were NHE-RF immunopositive, staining was observed in nearly all tumor cells, contrasting with the adjacent immunonegative stroma. NHE-RF positivity was present as membranous staining, especially at the luminal aspects of cells, and as diffuse cytoplasmic staining.

## **Discussion**

NHE-RF is highly expressed in epithelia of many tissues, particularly in cells with numerous microvilli, and is often concentrated at the luminal membrane. Prominent NHE-RF expression is seen in cells specialized in ion transport: renal proximal tubules, eccrine glands, colonic absorptive cells, parietal cells in gastric glands and ependymal cells. These findings support the proposed role of NHE-RF as a regulator of membrane protein transporters, and confirm Northern blot data showing high NHE-RF mRNA levels in human tissues containing polarized epithelia such as the mammary gland, kidney, small intestines and salivary gland.<sup>9</sup>

The association between estrogen stimulation and NHE-RF expression in normal endometrium and in breast carcinomas suggests that NHE-RF must be a multifunctional protein, with additional roles to those of ion transport. Specific and early induction of NHE-RF mRNA by estrogen has been observed in breast carcinoma cells.<sup>9</sup> The present observations extend the correlation between ER status and NHE-RF expression in breast cancer to primary human tumors, and raise the possibility that NHE-RF may play a role in estrogen-mediated cell growth. The proliferative effects of the estrogen are mediated through ER, an intracellular nuclear receptor that, when bound to estrogen, is transformed into an active transcription factor and regulates the expression of a variety of genes. Antiestrogens may therefore be therapeutically effective in ER-positive breast cancers. ER-negative tumors, however, are more aggressive tumors, associated with early recurrence and poor patient survival, and do not generally respond to antiestrogen treatment. However, about 40% of patients with ER-positive cancer do not respond to endocrine manipulations, and about 10% of ER-negative tumors respond.<sup>13,14</sup> The factors that lead to the conversion of an ER-positive, responsive breast cancer into a hormone-refractory tumor are poorly understood, and encourage further study of mechanisms of ER-mediated cell growth.

Estrogens induce cytoskeletal changes in ER-positive breast cancer cells that include an increase in the number and size of microvilli,<sup>15,16</sup> as well as increased expression of cytokeratins associated with the nuclear matrix-intermediate filament system.<sup>17</sup> Interestingly, alterations of the nuclear matrix-intermediate filament system, an extensive network that connects the plasma membrane and cytoskeleton with the nuclear membrane and nuclear matrix, can mediate changes in gene expression.<sup>18,19</sup> NHE-RF, an early response gene to estrogen stimulation, may therefore play a role in the assembly of an estrogen transduction complex by linking the actin cytoskeleton to an anchored membrane protein. NHE-RF could bind a transduction complex via interaction with MERM proteins at a C-terminal, non-PDZ site, and to a membrane protein via one of the PDZ

**Figure 2.** NHE-RF expression in normal and neoplastic tissues immunostained with IC270 antibody. **A:** NHE-RF expression in breast carcinoma cell lines: low expression in estrogen receptor (ER) negative MCF-7-ADR (left); strong expression in ER positive MCF-7 cells (right). **B-F:** NHE-RF expression in normal tissues. **B,** strong membranous expression of NHE-RF in proximal tubular epithelium and parietal epithelial cells of Bowman's capsule; **C,** NHE-RF expression in apical surface of absorptive cells in colonic glands; goblet cells are immunonegative; **D,** strong expression of NHE-RF in luminal membrane of ducts and acini in the breast; **E,** low NHE-RF expression in secretory endometrium; **F,** high expression of NHE-RF in proliferative endometrium. **G-H:** Expression of NHE-RF in breast carcinomas. **G,** high expression of NHE-RF in ER-positive breast carcinoma; **H,** ER-negative breast carcinoma immunonegative for NHE-RF.

domains. NHE-RF may also be involved in cross-talk among signal transduction pathways. Several signaling cascades, including epidermal growth factor and tyrosine kinase/MAP-kinase pathways, are involved in estrogen signaling;<sup>20–23</sup> such overlapping pathways may partly explain how breast cancer cells adapt to and bypass estrogen receptors blocked by antiestrogen therapy. It is possible that an alternative pathway for estrogen signaling in ER-negative breast carcinomas might involve NHE-RF expression, via ER-independent up-regulation, which could explain the 30% of ER-negative tumors expressing NHE-RF in our series.

These studies suggest that NHE-RF acts as a multi-functional protein and has potential roles in the apical surfaces of ion transporting epithelium as well as in estrogen-mediated growth control. The data encourage further study of NHE-RF in breast carcinomas to increase understanding of the growth control mechanisms in these hormonally-regulated tumors, and to develop novel means to interfere therapeutically in such growth pathways.

## References

1. Weinman EJ, Steplock D, Wang Y, Shenolikar S: Characterization of a protein cofactor that mediates protein kinase A regulation of the renal brush border membrane Na(+)-H+ exchanger. *J Clin Invest* 1995, 95:2143–2149
2. Reczek D, Berryman M, Bretscher A: Identification of EBP50: A PDZ-containing phosphoprotein that associates with members of the ezrin-radixin-moesin family. *J Cell Biol* 1997, 139:169–179
3. Yun CH, Oh S, Zizak M, Steplock D, Tsao S, Tse CM, Weinman EJ, Donowitz M: cAMP-mediated inhibition of the epithelial brush border Na+ /H+ exchanger, NHE3, requires an associated regulatory protein. *Proc Natl Acad Sci USA* 1997, 94:3010–3015 [published erratum appears in *Proc Natl Acad Sci USA* 1997, 94:10006]
4. Doyle DA, Lee A, Lewis J, Kim E, Sheng M, MacKinnon R: Crystal structures of a complexed and peptide-free membrane protein-binding domain: molecular basis of peptide recognition by PDZ. *Cell* 1996, 85:1067–1076
5. Morais Cabral JH, Petosa C, Sutcliffe MJ, Raza S, Byron O, Poy F, Marfatia SM, Chishti AH, Liddington RC: Crystal structure of a PDZ domain. *Nature* 1996, 382:649–652
6. Fanning AS, Anderson JM: Protein-protein interactions: PDZ domain networks. *Curr Biol* 1996, 6:1385–1388
7. Murthy A, Gonzalez-Agosti C, Cordero E, Pinney D, Candia C, Solomon F, Gusella J, Ramesh V: NHE-RF, a regulatory cofactor for Na(+)-H+ exchange, is a common interactor for merlin and ERM (MERM) proteins. *J Biol Chem* 1998, 273:1273–1276
8. Reczek D, Bretscher A: The carboxyl-terminal region of EBP50 binds to a site in the amino-terminal domain of ezrin that is masked in the dormant molecule. *J Biol Chem* 1998, 273:18452–18458
9. Ediger TR, Kraus WL, Weinman EJ, Katzenellenbogen BS: Estrogen receptor regulation of the Na+ /H+ exchange regulatory factor. *Endocrinology* 1999, 140:2976–2982
10. Gonzalez-Agosti C, Wiederhold T, Herndon ME, Gusella J, Ramesh V: Interdomain interaction of merlin isoforms and its influence on intermolecular binding to NHE-RF. *J Biol Chem* 1999, 274:34438–34442
11. Gonzalez-Agosti C, Xu L, Pinney D, Beauchamp R, Hobbs W, Gusella J, Ramesh V: The merlin tumor suppressor localizes preferentially in membrane ruffles. *Oncogene* 1996, 13:1239–1247
12. Breton S, Wiederhold T, Marshansky V, Nsumu NN, Ramesh V, Brown D: The B1 subunit of the H+ ATPase is a PDZ-domain binding protein: Colocalization with NHE-RF in renal B-intercalated cells. *J Biol Chem* 2000, 275:18219–18224
13. Nagai R, Kataoka M, Kobayashi S, Ishihara K, Tobioka N, Nakashima K, Naruse M, Saito K, Sakuma S: Estrogen and progesterone receptors in human breast cancer with concomitant assay of plasma 17beta-estradiol, progesterone, and prolactin levels. *Cancer Res* 1979, 39:1834–1840
14. Henderson BE, Bernstein L, Ross R: Etiology of cancer: hormonal factors. *Cancer: Principles and Practice of Oncology*, ed 5. Philadelphia, Lippincott-Raven, 1997
15. Vic P, Vignon F, Derocq D, Rochefort H: Effect of estradiol on the ultrastructure of the MCF7 human breast cancer cells in culture. *Cancer Res* 1982, 42:667–673
16. Antakly T, Pelletier G, Zeytinoglu F, Labrie F: Changes of cell morphology and prolactin secretion induced by 2-Br-alpha-ergocryptine, estradiol, and thyrotropin-releasing hormone in rat anterior pituitary cells in culture. *J Cell Biol* 1980, 86:377–387
17. Coutts AS, Davie JR, Dotzlaw H, Murphy LC: Estrogen regulation of nuclear matrix-intermediate filament proteins in human breast cancer cells. *J Cell Biochem* 1996, 63:174–184
18. Blum JL, Wicha MS: Role of the cytoskeleton in laminin induced mammary gene expression. *J Cell Physiol* 1988, 135:13–22
19. Seely KA, Aggeler J: Modulation of milk protein synthesis through alteration of the cytoskeleton in mouse mammary epithelial cells cultured on a reconstituted basement membrane. *J Cell Physiol* 1991, 146:117–130
20. Katzenellenbogen BS: Estrogen receptors: bioactivities and interactions with cell signaling pathways. *Biol Reprod* 1996, 54:287–293
21. Smith CL: Cross-talk between peptide growth factor and estrogen receptor signaling pathways. *Biol Reprod* 1998, 58:627–632
22. Aronica SM, Katzenellenbogen BS: Stimulation of estrogen receptor-mediated transcription and alteration in the phosphorylation state of the rat uterine estrogen receptor by estrogen, cyclic adenosine monophosphate, and insulin-like growth factor-I. *Mol Endocrinol* 1993, 7:743–752
23. Migliaccio A, Pagano M, Auricchio F: Immediate and transient stimulation of protein tyrosine phosphorylation by estradiol in MCF-7 cells. *Oncogene* 1993, 8:2183–2191